

Bicycle Rider Control

Observations, Modeling & Experiments

PROEFSCHRIFT

ter verkrijging van de graad van doctor
aan de Technische Universiteit Delft,
op gezag van de Rector Magnificus prof. ir. K.C.A.M. Luyben,
voorzitter van het College voor Promoties,
in het openbaar te verdedigen
op dinsdag 18 september 2012 om 15.00 uur
door

Johannes Dionisius Gerardus KOOIJMAN

werktuigkundig ingenieur
geboren te Dubai, Verenigde Arabische Emiraten.

Dit proefschrift is goedgekeurd door de promotor:

Prof. dr. ir. D.J. Rixen

Copromotor: Dr. ir. A.L. Schwab

Samenstelling promotiecommissie:

Rector Magnificus	voorzitter
Prof. dr. ir. D.J. Rixen	Technische Universiteit Delft, promotor
Dr. ir. A.L. Schwab	Technische Universiteit Delft, copromotor
Prof. dr. R. Babuska	Technische Universiteit Delft
Prof. dr. D.J.N. Limebeer	University of Oxford
Prof. dr. M. Hubbard	University of California
Dr. ir. M.M. van Paassen	Technische Universiteit Delft
Dr. ir. J.P. Meijaard	Olton Engineering Consultancy
Prof. dr. F.C.T. van der Helm	Technische Universiteit Delft, reservelid

ISBN 978-94-91104-09-1

Copyright © 2012 by J.D.G. Kooijman

All rights reserved. No part of the material protected by this copyright notice may be reproduced or utilized in any form or by any means, electronic or mechanical, including photocopying, recording or by any information storage and retrieval system, without the prior permission of the author.

Cover: Peter de Lange & Wouter Veldman

Typeset by the author with the L^AT_EX Documentation System.

Author email: jodikooijman@gmail.com

Bicycle rider control: observations, modeling and experiments

The safety bicycle, a fantastic vehicle, is over 100 years old and is perfectly suited for its intended use of human powered locomotion. However, consumers are demanding changes to this ordinary bicycle. Not only is the ordinary bicycle being turned into a hybrid electric pedal assist bicycle, but consumers for example also wish to travel further, faster and with less effort, for which the more aerodynamic position of the recumbent bicycle is suited. Others wish to take the bicycle on multi-modal commuter trips, requiring a collapsible bicycle as the bicycle needs to be folded into a small manageable package for storage purposes. Some users wish to transport extra luggage (multiple children, or large parcels), for which cargo bicycles have been designed, and a growing group of elderly consumers simply want to keep cycling, requiring a bicycle specifically designed for the needs of the elderly. Experience shows, however, that these newly developed bicycle models currently have handling qualities that are different from those of the ordinary bicycle.

Bicycle design has thus come to the crossroads, where developers can either continue on down another evolutionary process to optimize these new designs, similar to that of the development of the ordinary bicycle where 60 years of evolution was required to go from the Draisine walking machine to the safety bicycle, or they can take a more engineered and structured route, adopting modern engineering tools to model bicycle and rider dynamics and control. This second route is preferable not only with respect to the amount of time that can be expected to be required to develop a well handling design for each of the different concepts, but also as it enables the complete design space to be evaluated. Furthermore, the recent benchmarking of the Whipple bicycle model for the balance and steer of a bicycle is an opening enabling the accurate modeling of a bicycle and making this second route very viable. However the route also requires a rider model in order to be successful, but at present, very little is known about the bicycle rider. Therefore there is a need to develop a bicycle rider model.

The focus of this thesis is on bicycle rider modeling, where the following topics are covered: a review of the literature on rider models for single track vehicles (bicycles and

motorcycles), rider control observations, investigations into controllability of the system with a passive rider model, and bicycle self-stability theory and experiments.

The literature study shows that many authors have investigated and modeled the bicycle. The most widely used model is the three degree of freedom (steer, roll and forward speed) Whipple bicycle model which has been benchmarked and experimentally validated. On the other hand, no bicycle rider models exist that have been experimentally validated. Furthermore, although most people can ride a bicycle, the actions performed to ride the bicycle are still highly debated. Proposed rider models vary from ones having riders rigidly attached to the bicycle frame, to models where the upper body can steer, lean and move laterally. Most authors propose continuous rider control models, often based on McRuer's cross-over model and based on the neuromuscular dynamics of the rider. The optimal control method is also often used to model the rider but usually for the purpose of optimizing the vehicle performance. Here it is assumed that the rider acts as an optimal controller with limitations and optimizes some performance criterion such as minimizing the required time to complete the maneuver or the required control effort.

For motorcycles some handling quality indices have been developed for standard maneuvers, but this is not the case for bicycles. All handling quality work that has been performed for bicycles has been experimental in nature, and all the authors have performed their own specific experiments allowing only for qualitative comparisons. Only one bicycle handling quality metric has been proposed but it has not been experimentally validated yet.

Two observation experiments were performed in the present work to investigate the rider control actions during normal cycling. First a measurement bicycle was developed with which the steer angle, roll rate and forward speed were measured and which had a camera placed on a boom in front of the rider connected to the rear frame and aimed at the rider. The bicycle was ridden around town in traffic and under controlled circumstances on a large treadmill. The video analysis showed that the rider only leans his upper body as a result of pedaling. This qualitative result was quantitatively verified in a second experiment on the treadmill with motion capture of the bicycle and rider. Principal component analysis was performed on the recorded motion capture data and it was found that the upper-body motion is linked to the pedaling motion.

Other major results of the rider observation experiments include that the rider performs steering actions to stabilize the bicycle and that the size of the steering action is inversely proportional to the speed that the bicycle is moving at, and at high speeds the steering motion is performed in the pedaling frequency. At very low speed the knees of the rider are seen to move laterally relative to the bicycle plane of symmetry but not the upper-body.

The motion capture observation experiment was performed with two different styles of bicycle, with very different handling qualities: the first, a city style bicycle; the second, a more sporty model. The rider's posture on the two bicycles differs significantly: on the city style bicycle the rider sits upright with arms bent at the elbow, whilst on the sporty

style bicycle the upper body leans forward and the arms are straight. The riders were seen to perform different motions in these two postures. For the upright posture the rider steers by only moving his arms whilst in the forward leaned stretched arms posture the rider moves the arms by rotating the upper-body.

In the absence of a rider model the difference that these two postures have on the open loop stability of a bicycle was investigated by extending the Whipple bicycle model to include mechanisms for modeling passive rider motions and investigating the open loop dynamics. The passive rider models can influence the open loop stability substantially. Compared with the rigid rider the passive leaned forward straight arms posture rider does not alter the open loop dynamics drastically. On the other hand, the passive rider model with upright posture and bent arms eliminates the self stability of the system altogether. However, for both rider postures the system is controllable at all forward speeds.

Due to the absence of a bicycle rider model, bicycle handling cannot be predicted. However, it is suspected, but not yet proven, that the ease with which a bicycle can be ridden is correlated with the self-stability of the uncontrolled bicycle. Previously there has been near universal acceptance that either the spin angular momentum (gyroscopic effect), or trail of the front wheel, or both are necessary for self-stability. However, in this thesis it is shown that neither is necessary and that a bicycle can be built without gyros and with no trail that is self stable. It is not denied that gyroscopic effect and trail can contribute to self-stability, however other parameters are also important, especially the front-assembly mass distribution. Of the necessary mathematical conditions for self-stability emerging from the stability analysis of the Whipple bicycle model, one has been found which can be physically interpreted: a self-stable bicycle must steer into the fall.

With no definitive bicycle rider model available at the moment, future work could be directed towards determining and validating rider models through, for example, system identification techniques. Of particular interest are model identification experiments with riders on real bicycles performed on the open road, eliminating the undesired side-effects of riding on a treadmill or simulator. Optimal control models together with measurements of rider control performed for both stabilizing and tracking control could give insight into the optimizing behavior of a bicycle rider. The combined stabilizing and tracking task that a bicycle rider must perform at low speeds also encourages the investigation of rider models of a discrete nature. Investigating low speed and start / stop rider control is also a topic to be investigated in the light of the rising accident statistics for elderly riders. This combined with the recent trend to electrify the bicycle, also encourages future work to be performed on adding active dynamics enhancing devices to a bicycle. However, the theoretical exploration of the available design space can also lead to passively enhancing the bicycle dynamics, enabling super stable design configurations and configurations previously assumed to be un-rideable such as rear wheel steered bicycles.

Fiets besturing: observaties, modellering en experimenten

De fiets is een uitstekend vervoermiddel. Het huidige model is al meer dan 100 jaar oud en voldoet prima aan de eisen van mens aangedreven locomotie. Er is echter een verschuiving in de markt gaande waardoor er veranderingen aan de welbekende oer-Hollandse fiets worden vereist. Niet alleen wordt de fiets steeds vaker uitgerust met elektrische trapondersteuning, maar consumenten willen bijvoorbeeld ook op eigen kracht verder, sneller en met minder moeite kunnen fietsen. De aerodynamische houding van een ligfiets is hier bijvoorbeeld zeer geschikt voor. Andere gebruikers willen de fiets juist voornamelijk voor het woon-werkverkeer gebruiken in combinatie met een ander vervoermiddel zoals de trein, waarvoor een vouwfiets nodig is om ruimte te besparen bij het opbergen. Er zijn ook gebruikers die extra veel personen (meerdere kinderen) of bagage (grote pakketten) willen transporteren, daarvoor is de bakfiets ontwikkeld. Daarnaast zijn er speciale fietsen ontwikkeld voor de snel groeiende groep senioren die steeds langer actief wil blijven. Uit rijproeven blijkt dat al deze nieuwe fietsmodellen andere rijeigenschappen hebben dan die van de oer-Hollandse fiets.

Het fietsontwerp staat dus voor een tweesprong. Vergelijkbaar met hoe de huidige Hollandse fiets tot stand kwam, een 60 jaar durende ontwikkeling van Draisine loopfiets, via de hoge bi tot de het huidige ontwerp, kunnen ontwikkelaars het evolutie pad af blijven wandelen om tot een optimaal ontwerp te komen. Een andere insteek is een meer analytisch gestructureerde, op techniek georiënteerde route. Daarbij kan gebruik worden gemaakt van moderne technische gereedschappen om de dynamica en besturing van de fiets en berijder te modelleren. Deze tweede route verdient de voorkeur, niet alleen in verband met de te verwachten hoeveelheid tijd die nodig zal zijn om tot een ontwerp te komen met de juiste rijeigenschappen voor al deze concepten, maar ook omdat het de mogelijkheid biedt om de complete ontwerp ruimte te evalueren. Aangezien het Whipple-fietsmodel voor het balanceren en sturen van een fiets recentelijk is gevalideerd kan de fiets nauwkeurig worden gemodelleerd en daarmee is deze tweede route zeer levensvatbaar geworden. Deze route heeft nog wel een model van de bestuurder nodig om succesvol te kunnen zijn, er is echter nog maar weinig bekend over de bestuurder.

Het is dus zaak om een model van de fietser te ontwikkelen.

In dit proefschrift komen de volgende onderwerpen aan bod waarbij de focus ligt op de modellering van de fietser: Een literatuuroverzicht van rijdermodellen voor enkelspoor voertuigen (fietsen en motorfietsen), fietser-besturing observaties, onderzoek naar de bestuurbaarheid van een fiets met een model van een passievefietser, en fiets-zelfstabiliteit theorie en experimenten.

Uit het literatuuronderzoek blijkt dat veel auteurs de fiets hebben onderzocht en gemodelleerd. Het meest gebruikelijke model is het drie graden van vrijheid (stuur, rol en voorwaartse snelheid) Whipple-fietsmodel dat zowel gebenchmarked als experimenteel gevalideerd is. Er zijn echter geen experimenteel gevalideerde fietsermodellen. Bovendien is er veel onenigheid over welke acties de fietser uitvoert tijdens het fietsen, terwijl de meeste mensen toch kunnen fietsen. Hierdoor zijn uiteenlopende fietsermodellen voorgesteld, variërend van modellen waar de fietser als star lichaam gefixeerd aan de fiets wordt beschouwd, tot modellen waar het bovenlichaam kan sturen, leunen en lateraal kan verplaatsen. De meeste auteurs stellen voor dat de fietser bestuurt als een continue regelaar, vaak gebruikmakend van een soort “cross over” model gebaseerd op neuromusculaire dynamica. De optimal control methode wordt ook vaak gebruikt om de berijder te modelleren, hierin wordt aangenomen dat de mens als (sub)optimale regelaar werkt en een aspect probeert te minimaliseren, zoals de tijd die nodig is om een manoeuvre uit te voeren of de grootte van de regel inspanning.

Hoewel voor motorfietsen een aantal rijeigenschap indices zijn ontwikkeld is dit niet het geval voor fietsen. Al het rijeigenschap onderzoek dat voor het fietsen is gedaan is experimenteel van aard, en alle auteurs hebben hun eigen specifieke draai aan de experimenten gegeven waardoor onderling enkel kwalitatieve vergelijkingen mogelijk zijn. Er is slechts één metriek voorgesteld voor fiets rijeigenschappen en deze is nog niet experimenteel gevalideerd.

Tijdens dit onderzoek zijn twee observatie experimenten uitgevoerd om de besturingsacties van de fietser tijdens het normaal fietsen te bestuderen. Er is een meetfiets ontwikkeld waarmee de stuurhoek, rol hoeksnelheid en voorwaartse snelheid zijn gemeten. Door middel van een camera die op een spriet was geplaatst voorop de fiets en gericht was naar de rijder, zijn de bewegingen van de fietser ten opzichte van het frame opgenomen. Met de fiets werd door Delft gereden tussen het normale verkeer, maar ook binnen op een grote lopende band onder gecontroleerde omstandigheden. Uit de videoanalyse bleek dat de fietser slechts leunt als gevolg van het trappen. Dit kwalitatief resultaat is kwantitatief gevalideerd met behulp van het tweede experiment op de lopende band en motion capture apparatuur. Door de gemeten data met principal component analysis te analyseren is vastgesteld dat de beweging van het bovenlichaam is gekoppeld aan de trapbeweging.

Andere belangrijke uitkomsten van de observatie experimenten zijn dat de fietser stuuracties uitvoert om de fiets te stabiliseren. De grootte van deze stuuracties zijn omgekeerd evenredig met de voorwaartse snelheid, en bij hoge snelheid worden de stuuracties uitgevoerd in de trapfrequentie. Bij een hele lage snelheid is te zien dat niet het

bovenlichaam van de fietser, maar de knieën van de fietser lateraal bewegen ten opzichte van het frame.

Twee verschillende fietsen met compleet andere rijeigenschappen zijn gebruikt tijdens de motion capture experimenten. Er is een significant verschil in de houding van de rijder tussen de twee fietsen. De eerste fiets is een typische heren stadsfiets waar de rijder rechtop zit met de armen gebogen bij de ellebogen. De tweede fiets is een sportief model, waarbij de rijder voorwaarts leunt en zijn de armen recht houdt. De rijders voeren andere bewegingen uit op de twee verschillende fietsen. In de rechtop houding met gebogen armen stuurt de rijder door enkel zijn armen te bewegen terwijl in het geval van de voorwaartsgeleunde-rechtearmen houding de handen bewogen worden door het bovenlichaam te roteren.

Bij gebrek aan een model van de fietser, is de invloed van de twee houdingen op de open lus stabiliteit van de fiets onderzocht door het Whipple-fietsmodel uit te breiden met mechanismes waarmee passieve rijder bewegingen kunnen worden gemodelleerd en de open lus stabiliteit onderzocht. Het blijkt dat deze passieve rijder modellen de open lus stabiliteit wezenlijk kunnen veranderen. In vergelijking met het starlichaam model verandert het passieve voorwaartsgeleund-rechtearmen-model vrij weinig aan de open lus dynamica. Anderzijds is het zo dat bij het passieverijder-model met een rechtop houding en gebogen armen de zelfstabiliteit volledig verdwijnt. Echter voor beide rijderhoudingen is het systeem regelbaar bij alle snelheden.

Door het gebrek aan een model van de fietser, kunnen de fiets rijeigenschappen niet worden voorspeld. Het vermoeden is echter dat het gemak waarmee een fiets kan worden bestuurd, gecorreleerd is met de mate van zelfstabiliteit van de ongestuurde fiets. Het is bijna universeel geaccepteerd dat, of het draaiend impulsmoment (gyroscopisch effect), of de naloop van het voorwiel, of beide, noodzakelijk zijn voor zelfstabiliteit. Maar in dit proefschrift wordt bewezen dat geen van deze voorwaarden noodzakelijk zijn en dat een zelfstabiele fiets gebouwd kan worden zonder gyro's en zonder naloop. Het wordt niet ontkend dat het gyroscopisch effect en de naloop kunnen bijdragen aan de zelfstabiliteit, andere parameters zijn echter ook erg belangrijk, in het bijzonder de massa verdeling van het voor-frame. Van de set wiskundige condities die voortvloeien uit het Whipple fietsmodel noodzakelijk voor zelfstabiliteit is er één die fysisch geïnterpreteerd kan worden: een zelfstabiele fiets moet sturen in de richting van het omvallen.

Het ontbreken van een gevalideerd model van de fietser leidt tot de aanbeveling om vervolgonderzoek te richten op het bepalen en valideren van een bestuurder model door bijvoorbeeld gebruik te maken van systeem identificatie technieken. Vooral interessant zijn fietser identificatie experimenten uitgevoerd op de openbare weg met echte fietsen om de ongewenste neveneffecten van het fietsen op een lopende band of met een simulator te vermijden. Optimal control modellen in combinatie met metingen van bestuurder acties uitgevoerd voor zowel stabilisatie- als volgtaken zouden inzicht kunnen geven in het optimalisatie gedrag van de fietser. De gecombineerde stabilisatie- en volgtak die een fietser moet uitvoeren bij lage snelheid stimuleert ook onderzoek naar bestuurder modellen met een discreet karakter. Met het oog op de dramatische ongeval-

lenstatistieken voor oudere fietsers, is bestuurder gedrag bij het op- en afstappen ook een onderwerp om te onderzoeken. De combinatie met de recente trend om de fiets te elektrificeren nodigt ook uit om onderzoek te doen naar het toevoegen van actieve, dynamica verbeterende, systemen voor op de fiets. Ook de exploratie van de theoretische ontwerpruimte zou kunnen leiden tot het verbeteren van de fiets dynamica op een passieve manier. Super stabiele ontwerp configuraties en configuraties die eerder werden aangenomen als onberijdbaar, zoals achterwiel bestuurd fietsen, zouden mogelijk kunnen worden.

Summary	i
Samenvatting	v
1 Introduction	1
1.1 Research Context	1
1.2 Thesis Objective	2
1.3 Original Contributions	2
1.4 Thesis Outline	4
2 A Review of Bicycle and Motorcycle Rider Control	5
2.1 Introduction	5
2.2 Dynamics of Single Track Vehicles, Modeling and Experiments	5
2.3 Rider Modeling	8
2.3.1 Rider Control Observations	9
2.3.2 Theoretical Controller Design	16
2.3.3 Experimental Validation of Controller Design	29
2.3.4 Rider Modeling Discussion and Conclusions	38
2.4 Handling Qualities and Maneuverability	39
2.4.1 Handling Qualities for Accident Avoidance: Safety	41
2.4.2 Handling Qualities for Normal Riding	45
2.4.3 Handling Qualities for Racing	47
2.4.4 Handling Qualities Discussion and Conclusions	49
2.5 Discussion and Conclusions	50

3	Bicycle Rider Observations During Normal Cycling	53
3.1	Introduction	53
3.2	Publication I: Bicycle Rider Observations	54
3.3	Publication II: Rider Motion Identification	57
3.4	Conclusions	61
4	Stability and Control of Bicycles with Passive Rider Models	63
4.1	Introduction	63
4.2	Publication III: Physical Properties of a Bicycle and Rider	64
4.3	Publication IV: Dynamics of Bicycles with Passive Rider Models	67
4.4	Conclusions	69
5	Experimental Validation of Bicycle Dynamics	71
5.1	Introduction	71
5.2	Publication V: Lateral Dynamics of a Bicycle on a Treadmill	73
5.2.1	Conclusions	76
5.3	Publication VI: Self-Stable Bicycle without Gyro or Trail	76
5.3.1	Review of the Whipple Bicycle Model	78
5.3.2	From Theoretical Two-Mass-Skate (TMS) Bicycle to Experimental TMS Bicycle	82
5.3.3	Experimental Two-Mass-Skate (TMS) Bicycle Construction	86
5.3.4	Verification of the Produced Experimental TMS Bicycle	91
5.3.5	Experimental Procedure and Results	94
5.3.6	The Experiment, General Observations and Experiences	100
5.3.7	Conclusions	105
5.4	General Conclusions	106
6	Conclusions and Recommendations for Further Research	107
6.1	Conclusions	107
6.2	Recommendations for Future Work	108
	Bibliography	111
	Publication I	127
	Publication II	137
	Publication III	159
	Publication IV	171

Publication V	189
Publication VI	197
Acknowledgements	203
Curriculum Vitae	205

CHAPTER 1

Introduction

1.1 Research Context

Bicycling has become one of the most dangerous modes of transport in the Netherlands [163]. During the period of study, 2004 – 2009, there was a steady 3.6% decrease in the number of deaths due to traffic accidents, from 881 deaths in 2004 to 720 in 2009. The safety improvement was not found for cyclists. The number of cyclist deaths did not decrease but remained constant during this period at roughly 185, accounting for a quarter of all traffic related deaths in 2009. Most of the deaths in the cycling category occurred as a result of an accident between a cyclist and a motorized vehicle, only 15 deaths occurred as a result of single party cycling accidents.

The number of serious injuries as a result of traffic accidents (all modes) alarmingly has increased from roughly 15,400 serious injuries during 2006 to over 18,500 in 2009. Even more alarming is that more than 50% of these serious injuries were incurred in an accident without a motorized vehicle (bicycles and pedestrians only). Furthermore 10,810 serious injuries, roughly 58% of all serious injuries, were cyclists, of which the vast majority (9,240 in 2009) occurred in single party accidents.

Decreasing the number of bicycling accidents and the seriousness of the accidents has therefore become a priority for the Dutch government. Possible methods include: improving road infrastructure and roadside furniture; changing traffic laws; adding passive and active safety features to the bicycle, rider and other road vehicles; (refresh) rider training and riding courses specifically tailored for groups such as young children, teenagers and the elderly (the elderly are a significant group which stands to benefit from improved safety [163]); adjusting the bicycle's handling qualities to be better suited to the rider. This latter method implies improving the rider–bicycle system to reduce the number of accidents. Considering that the vast majority of the cycling accidents

are single vehicle accidents, improving the rider–bicycle system could yield a significant reduction in accidents.

Handling qualities can be viewed as vehicle performance indicators. The handling qualities of a bicycle reflect on control aspects related to the use of the bicycle during cycling, where good handling qualities indicate easy use by the rider. The bicycle handling qualities therefore are related to both the bicycle and the rider. To be able to predict bicycle handling qualities therefore requires models of both the bicycle and rider. There are validated models of the bicycle, but no validated models of the rider exist at present.

The field of bicycle handling qualities is still in its infancy. The same is true for the other single track vehicle, the motorcycle. In other fields, most notably the field of aircraft flight dynamics, this is not the case. Enormous interest was generated for aircraft handling qualities, also called flying qualities, due to the serious safety issues that badly flying aircraft present [24, 159]. There are however some important and fundamental differences between modeling the pilot–aircraft and rider–bicycle interactions, making a direct implementation of aircraft handling qualities in the field of cycling unlikely: in cycling the rider is not only the controller but the rider also contributes significantly to the mechanical system (up to 90% of the mass of the complete bicycle–rider system); the rider has two significant control mechanisms to steer the bicycle: turning the handlebar to steer the bicycle, similar to the manner in which a pilot controls an aircraft by moving the control stick, and the application of a lateral lean (roll) torque to steer the bicycle. These differences make the rider–bicycle interaction challenging and require different modeling and simulation approaches.

1.2 Thesis Objective

The major purpose of this thesis is:

To get a step closer to being able to determine a-priori the handling qualities of bicycles and thereby enable the development of better, safer and out of the ordinary bicycles.

The Whipple bicycle model is capable of accurately predicting the behavior of the motion of the bicycle at low and medium speeds for normal bicycles in ideal situations [81]. The goal of this thesis has two aspects. First is the modeling of the rider: how to model a rider such that the bicycle with rider model describes bicycling. Secondly the robustness of the Whipple bicycle model: determine if the model is also usable when not all of the assumptions are met.

1.3 Original Contributions

This dissertation consists of a literature review on bicycle and motorcycle control and an overview of the work performed in six peer reviewed publications that are listed below and

can be found at the back of this thesis. The publications are referred to as *Publication I*, *Publication II*, *Publication III*, *Publication IV*, *Publication V* and *Publication VI* in the text. Some results of the publications, as well as some further research have been presented at international conferences by myself [77, 78, 98] and by my co-authors [131, 79, 100, 101, 130, 129, 99, 80]. The publications [98, 102, 132, 75] were published in peer-reviewed journals.

- I Kooijman, J. D. G., Moore, J. K., and Schwab, A. L. (2009). Some observations on human control of a bicycle. In *Proceedings of the ASME 2009 International Design Engineering Technical Conferences & Computers and Information in Engineering Conference*, number DETC2009-86959, DETC2009, Aug 30 – Sep 2, 2009, San Diego, CA.
- II Moore, J. K., Kooijman, J. D. G., Schwab, A. L., and Hubbard, M. (2011). Rider motion identification during normal bicycling by means of principal component analysis. *Multibody System Dynamics*, 25 (2) : 225–244.
- III Moore, J. K., Kooijman, J. D. G., Hubbard, M., and Schwab, A. L. (2009). A method for estimating physical properties of a combined bicycle and rider. In *Proceedings of the ASME 2009 International Design Engineering Technical Conferences & Computers and Information in Engineering Conference*, number DETC2009-86947, DETC2009, Aug 30 – Sep 2, 2009, San Diego, CA.
- IV Schwab, A. L., Meijaard, J. P. and Kooijman, J. D. G. (2012). Lateral dynamics of a bicycle with passive rider model: stability and controllability. *Vehicle System Dynamics*, 50 (8) : 1209—1224.
- V Kooijman, J. D. G. and Schwab A. L. (2009). Experimental validation of the lateral dynamics of a bicycle on a treadmill. In *Proceedings of the ASME 2009 International Design Engineering Technical Conferences & Computers and Information in Engineering Conference*, DETC2009-86965, DETC2009, Aug 30 – Sep 2, 2009, San Diego, CA.
- VI Kooijman, J. D. G., Meijaard, J. P., Papadopoulos, J. M., Ruina, A., and Schwab, A. L. (2011). A bicycle can be self-stable without gyroscopic or caster effects. *Science*, 332 (6027) : 339–342.

The developments of the research reported in this thesis are:

- An experimental testing method for investigating bicycle rider control under controlled circumstances in the form of a bicycle on a large treadmill (*Publication I*, *Publication II* & *Publication V*).
- The validity of the Whipple bicycle model for describing the lateral dynamics of a bicycle on a treadmill was experimentally validated (*Publication V*)
- An instrumented measurement bicycle was developed to measure bicycle and rider

motions with which observation experiments were carried out on the open road and on the treadmill. (*Publication I*)

- The quantification of bicycle rider motions using motion capture equipment and Principal Component Analysis and the visualization thereof. (*Publication II*)
- A practical and easy method for determining the physical parameters for modeling a bicycle and rider (*Publication III*).
- Two proposed passive rider models and their effect on the stability and controllability of the complete system (*Publication IV*).
- A bicycle was designed and built with which experiments were performed to investigate the robustness of the Whipple bicycle model with respect to wheel to ground contact and the effect of play at the joints (*Publication VI*).

1.4 Thesis Outline

Each chapter of this thesis tackles a specific research question. Chapter 2 reviews the state of the art on bicycle and motorcycle dynamics and control, modeling and experiments. It also reviews the work done on metrics for comparing bicycles and motorcycles and rider control tasks.

While many authors have proposed control models, almost none have actually observed what a rider actually does on a bicycle. Therefore Chapter 3 describes and discusses bicycle–rider observation experiments that were performed with a measurement bicycle on the open road and on a treadmill and motion capture experiments on a treadmill. This gives insight into how a bicycle rider could be modeled for modeling stabilizing behavior.

Understanding the influence of adding a rider and an extra degree of freedom to the Whipple bicycle model and its effect on the bicycle-rider system stability and controllability is the goal of Chapter 4. First a method for modeling the complete bicycle and rigid rider system is developed, and then the stability and controllability for different passive rider models added to the Whipple bicycle model is investigated.

To what extent can the Whipple bicycle model be used for predicting behavior of bicycles when the wheel-road contact assumptions are not really met is the topic of Chapter 5. First the lateral dynamics of a bicycle on a treadmill are investigated and compared with the corresponding Whipple bicycle model, next for an extreme out of the ordinary bicycle, the admissibility of the Whipple bicycle model is experimentally investigated. The thesis ends with the conclusion of the findings and open ends in Chapter 6.

CHAPTER 2

A Review of Bicycle and Motorcycle Rider Control

2.1 Introduction

This chapter aims to provide a review of research efforts that have gone into handling quality aspects and control of bicycles and motorcycles. The chapter is split into three parts: vehicle dynamics, rider control and handling qualities. It starts by briefly summarizing the most important work on the modeling of the dynamics of single track vehicles and the experimental validation thereof in section 2.2. Rider control, section 2.3, starts by recounting vehicle specific experimental rider control observations before focusing on single track rider control models. The rider control section ends with a review of the experimental validation of many of the rider control models. In the final section 2.4 handling qualities and in particular handling qualities in relation to three vehicle roles: safety, normal riding and racing are reviewed. Definitions of concepts such as maneuverability and handling qualities are reviewed in this section.

2.2 Dynamics of Single Track Vehicles, Modeling and Experiments

There have been a number of review papers on the subject of the dynamics of single-track-vehicles. Notably Meijaard *et al.* [94] carry out a comprehensive review on all those that investigated bicycle dynamics. Sharp [139] recently reviewed the dynamics and control of bicycles and earlier on motorcycle steering behavior [135]. In this thesis we will only present some of the highlights.

The actual physical development of the bicycle was an evolutionary process as described in [59] and shown in Figure 2.1. Starting as a walking machine with vertical steering axis in the early nineteenth century, the bicycle transitioned through a period as a high-wheeler for greater speed but less braking stability, to the standard ‘safety’ bicycle

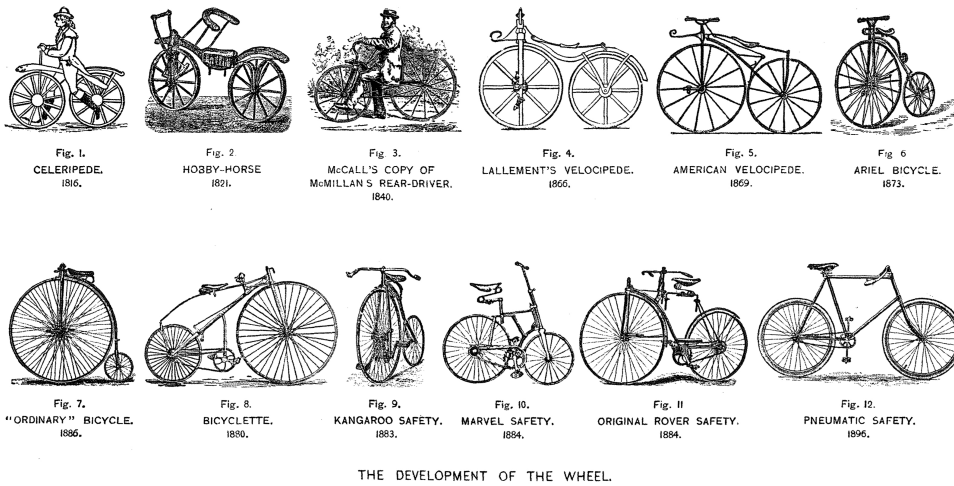


Figure 2.1: *The evolution of the bicycle from velocipede to safety bicycle, from 'The Aeronautical Annual 1896' [93]*

by the end of the nineteenth century with nearly the same geometry as the bicycles of today. This evolutionary process took many years and was based on a system of trial and error. Since 1900 the bicycle has been optimized further, however most of these optimizations were cosmetic.

As early as 1869 [116] it was already noted that a bicycle and rider in forward motion balance by steering towards a fall. By 1899 Carvallo [17] and Whipple [164], independently of one another, were the first to develop the equations of motion for a bicycle with which they could predict instability modes. In the following one hundred years over fifty other authors independently modeled the bicycle until in 2007 Meijaard *et al.* [94] benchmarked Whipple's bicycle model and compared them all.

The first to develop the equations of motion for a motorcycle was Döhring [35] in 1953. He also carried out experiments with a motorcycle to validate his model. His model was essentially the same as that of Whipple [164] and did not take tires or suspension into account. The first to investigate the motorcycle's stability using a proper tire model was Sharp [134]. Since then practically all research into single track vehicle dynamics and modeling has been focussed on motorcycles and was reviewed by Popov *et al.* [114].

The most significant (complete) multi-year, multi researcher scientific program focussed on single track vehicle stability and control was carried out in the early 1970s by the Cornell Aeronautical Laboratory (later renamed Calspan). Much of the work on bicycles however was carried out for the Schwinn Bicycle Company and has only just become publicly available. The work consisted of both modeling and experimentally measuring bicycles and motorcycles (with tires) [123, 117] and their control [122, 120]

and the comparison of experimental maneuvers with time series simulations with the computer. This was quite a feat considering the (analogue) computer system technology available at the time. Some of the results of the Calspan experimental work on bicycle tires [123] which was done to develop their tire models has been doubted by some with respect to their camber thrust coefficients, but 40 years on their work is still the only complete bicycle tire data set available.

Most experimental work for measuring bicycle and motorcycle parameters has been performed in a similar manner to Döhring; using torsional pendulums to measure moments of inertia [123, 39, 115, 81]. Roland & Massing [123] at Calspan developed an interesting method for applying a known lateral (perturbation) force to the bicycle: a calibrated fireworks style rocket attached to the bicycle! They concluded though that this method was not ideal as it did not cause significant lateral dynamics. Instead the bicycle rolled and steered slightly to one side which caused a large (and undesired) yaw motion, but did not dynamically excite the roll and steer. For the recording of data during experiments an ingenious boom system was used at Calspan to relay the measured signals of the wired sensors on the bicycle via cables to large (bulky) ticker-tape recorders that were placed in a chase car. This method was also used by Eaton [39] to carry out experiments to validate the motorcycle model developed by Sharp [134] and theoretical rider control and motorcycle handling work by Weir [160]. With modern electronics this has become much easier. Kooijman *et al.* [81] placed all the required measuring equipment (power supply, sensors, digital to analogue converter and laptop computer) on the bicycle to experimentally validate the benchmark bicycle model for a range of speeds.

Recent experimental investigations into the benchmarked bicycle model include Stevens [142] who used a variable geometry bicycle to validate the model for a wide variety of bicycle geometries. Tak *et al.* [143] investigated both theoretically and experimentally the effect of various parameters on the stability of a bicycle while Moore *et al.* [99] comprehensively measured the parameters of six common bicycles to compare their uncontrolled stability based on the linearized equations of motion. In order to carry out rider control experiments on a treadmill Kooijman & Schwab [79] experimentally investigated the dynamics of the bicycle on the same treadmill to validate that no significant slip takes place at the wheel-treadmill contact.

Recently and based on the work in [94], [75] showed both theoretically and experimentally that the long cited myths, essential for bicycle self stability: trail and gyroscopic effect of the front wheel, are neither required nor necessary for bicycle self stability. They also showed that a third set of parameters, the mass and mass moments of inertia, can be used just as effectively for stabilizing and destabilizing a bicycle. This discovery radically changes the available design space for self stable bicycles. For example, in the same work they discuss (theoretically) how a self stable rear-wheel-steered bicycle could be made.

2.3 Rider Modeling

How rider control is modeled depends on the control actions carried out by actual riders and which of these rider control outputs are expected to be of influence according to the author. For example if the rider's motion is considered negligible i.e. the rider does not move relative to the vehicle, then the rider is often modeled as a single rigid body that is rigidly connected to the rear frame [164]. On the other hand if the rider is perceived to move laterally the rider is often modeled as a two piece body. The lower part is then usually rigidly attached to the rear frame and the upper part is modeled as an inverted pendulum and between the two a spring and damper is sometimes placed [5, 7, 133, 50]. For some applications such as recumbent bicycles the lower body motions are considered important and thus the upper legs and lower legs are modeled as moving separately whilst the upper body is fixed to the rear frame [22]. Finally some authors have tried to make more accurate statements about the rider's control actions by applying multi-body approaches, including full muscle-skeleton models [64, 144].

A second important aspect is the type of steer control that a rider performs; angle (position) or torque (force) control. For automobiles it has generally been accepted that the driver performs position (angle) control [54, 113]. However, recent research has shown that stiffness control is implemented by the driver in throttle control (using the ankle) and that the impedance can also vary for steering control [1, 2]. The automobile driver performs large rotational motions of the steering wheel during normal driving situations. This is not the case on bicycles and motorcycles, where the handlebar is only turned through a very small angle. Furthermore, to enter a corner counter-steer, the turning of the handlebar in the opposite direction to the desired direction, is initially applied to the steering assembly for all single track vehicles. It is therefore of interest to know whether the rider uses steer torque or angle control, or maybe something in between such as impedance (steer-stiffness) control.

The third important aspect in rider modeling is the control task. Authors distinguish between stabilizing control and path following control. Stabilizing control is generally implemented when the goal is to understand the machine to be controlled, i.e. the effort required to keep the machine from falling over. Path following control is implemented when the goal is to follow a set course. There are generally two path following approaches: the first is compensatory, where the current position is compared with the pre-determined desired position and the control output adjusted accordingly to compensate for a miss-match. The second path following control approach looks ahead (preview). By applying some form of weighting function a required control output based on the oncoming path and the current location is determined. Preview control has been implemented in lap time optimization [28] but also for more general purposes [137], to compare different control algorithms, vehicles, or both such as with the optimal maneuver method. This section will first review those that have investigated rider control through observations, before reviewing proposed theoretical rider models. The section will close with the experimental validation of rider models and closing discussions.

2.3.1 Rider Control Observations

Many authors have observed which rider actions or motions actually take place. Most have done so in a qualitative manner, without actually measuring any parameters. A smaller group has performed quantitative observations of which the majority of authors have focussed on motorcycle riding.

Qualitative analysis of rider control

The inventor of the bicycle, Karl von Drais in 1820 was already well aware of the counter steer mechanism used to balance a Draisine (velocipede) [53]¹:

“Alsdann mache man, mittelst leichten Aufsetzens der Füße, große, aber Anfangs langsame Schritte in paralleler Richtung mit den Rädern, und halte die Absätze dabei nicht einwärts, daß man nicht mit denselben unter das hintere Rad komme, und wann man nachher in dem Schuß ist, und aus Versehen die Balance etwas verloren hat, kann man sich gewöhnlich mit den Füßen helfen, oder durch das Leiten, wenn man ein Bischen gegen die Richtung leitet, auf welche der Schwerpunkt des Ganzen sich neigte, und wenn man eine Schwenkung machen will, richte man unmittelbar vorher den Schwerpunkt etwas auf die innere Seite und lenke gleich darauf hin” — (Drais [53], 1820, Page 375.)

“Then one makes, by means of lightly putting the feet to the ground, big but initially slow steps in the direction parallel to the wheels, and keeps the heels not inward, in order that one does not come with them under the rear wheel, and when one has later got some speed, and has lost by accident the balance a bit, one can usually help oneself with the feet, or by steering if one steers a little towards the direction in which the centre of gravity of the whole leans, and if one wants to take a turn, one directs the centre of gravity immediately before a little to the inside and steers right after that to that side.” — (Translation by J.P. Meijaard, 2011)

Prior to the invention of the safety bicycle (≈ 1890), balance by rider steering control had also been described by many others [59]. In 1869 Rankine [116] already described how a leaned forward-moving high wheel bicycle is primarily righted by the lateral acceleration of the support line due to steering. To balance a bicycle that initially is falling to the left, it is steered to the left, causing the wheels to move on curved paths to the left. These leftward curved paths lead to a leftward acceleration of the support line and thereby bring the support back under the center of mass. Rankine also compared bicycle balance to that of the motion of an ice skater who, similar to a bicycle, cannot exert a lateral force without rolling over due to the single line of contact. To maneuver, riders manipulate

¹This and many other interesting facts about Drais are discussed in Hans-Erhard Lessing's book [84].

this falling: to turn right they first counter-steer left, inducing a lean to the right, and then later steer right in the direction of the induced fall. Rankine illustrated this in Figure 5 on page 153 [116].

Since then many other authors have qualitatively investigated bicycle stability and control. One of the first to investigate the rider's actions was Wilson-Jones [168] who investigated motorcycle corner entrance. He installed a torque indicator on the handlebar to indicate if a lean torque, also known as a roll steer torque was applied. The force applied to the handlebar by the rider can be decomposed in forces perpendicular to the steering axis and a force parallel to it. The torque generated as a result of the force parallel to the steer axis is called the roll-steer torque. Note that due to muscle stiffening a rider does not have to lean to apply a roll-steer torque. Wilson found that the rider applies a lean torque on the handlebar in the direction of the desired roll when entering the corner, and that the rider simultaneously applies a negative torque to steer the handlebar, where a negative torque is a moment applied that opposes the direction of steering (counter-steer). Furthermore he found that the rider applies a positive steer moment (in the desired direction) in the corner. Exiting corners is achieved by applying a lean torque on the handlebar to roll the bike towards the upright, and that the steer torque is increased further to decrease the radius of curvature of the bike, increasing the centripetal acceleration and thereby righting the bicycle.

The qualitative analysis of rider control actions is an essential element in the bicycle training program for children with (mental) disabilities developed by Richard Klein and colleagues [7, 150]. The program has bicycles with different levels of stability augmentation and which have slower dynamics than normal bicycles. The children that participate in the program generally have slower neuromuscular sensorial feedback loops. The slower dynamics of these bicycles enables the children to learn the non-minimum phase control (turn left to go right) by giving them more time to feel and adjust to the tipping bicycle and to learn to apply the (correct amount of) counter steer. Each rider progresses through a number of bicycles where each new bicycle has less stability augmentation and feels more like a "normal" bicycle. The first bicycles that each rider uses have so much static stability (very large tyre crown radius) that the rider has to actively "lean" into the corner for the bicycle to follow suit. The "teacher" observes whether the rider is leaning in the correct direction when riding in a curve i.e. leaning into the curve not out of it such as they would if they were relying on an extra support like when using a tricycle or trainer wheels (or a very large tire crown radius). When this is the case the pupil progresses to the next bicycle with less augmentation.

Quantitative analysis of rider control

The authors that have measured rider control have done so mostly for motorcycles [39, 117, 120, 118, 4, 115, 68, 32, 176, 112, 30, 64, 41], but only a few investigated bicycle rider control [140, 123, 122, 124, 36]. To quantitatively analyze rider control, vehicle and rider states are measured, the most widely measured vehicle states are the

Research Question	Authors
Control in general	Aoki [4], Katayama <i>et al.</i> [68], Bocciolone <i>et al.</i> [13], Rice <i>et al.</i> [119] [120], Prem and Good [115], Rice [120] [118], Prem and Good [115], Evertse [41]
Experience	
Physiological limits	Yokomori <i>et al.</i> [176], Cossalter <i>et al.</i> [30], Pierini <i>et al.</i> [112]
Bicycle rider control	Van Lunteren <i>et al.</i> [154] [141], Doyle [36], Kooijman <i>et al.</i> [78] [102]

Table 2.1: *Research questions that have been quantitatively investigated by authors.*

steer angle and steer torque (many authors). More elaborate (complete system) state measurements have been carried by Rice [117, 119, 118] and Aoki [4] with motorcycles and Roland [124, 122, 123] for bicycles, who measured rider lean, steer torque, steer angle, roll angle², yaw rate and lateral acceleration. Eaton [39] measured steer angle, steer torque, roll angle and roll rate, but not the rider lean, in order to validate Weir's rider model [160]. Katayama *et al.* [68] measured steer torque and built a device for measuring rider upper body lean, yaw and pitch angle and the rider's lower body lateral motion which they used to validate a motorcycle control model. Rider lean has generally been measured using a rod with one end attached to the rear of the rider's torso near the arms, and the other end to an angular potentiometer based near the saddle. Steering torque has been measured in a number of ways, mostly by incorporating strain gauges. More recently Evertse [41] measured all the forces applied by the rider on the motorcycle by measuring the forces along and perpendicular to the steering axis on the handle bars, the force applied in the lateral direction on the tank, and in the vertical direction on the pegs and saddle (left and right side). With these measurements he calculated rider roll-steer torques and rider lean torque.

Most research has been initiated with a specific scientific question in mind and they can be grouped as: rider control in general; rider experience; rider physiological limits; bicycle rider control. Table 2.1 gives a brief overview.

²Most authors talk about the three orthogonal rotations of the rear frame of a single track vehicle as roll; the rotation about the longitudinal axis, yaw; the rotation about the vertical axis, and pitch; the rotation about the lateral axis. When a rider is taken into account, the rider is often modeled as two bodies, being; a lower body is rigidly attached to the vehicle rear frame and an upper body which can rotate about the longitudinal axis of the rear frame. The angle that the upper body makes with respect to the rear frame is called the lean angle or rider lean angle. Sometimes the rider upper body is also able to rotate about the lateral axis of the rear frame, this is called rider pitch. When the rider is rigidly connected as a single body to the vehicle such as is the case for the benchmark bicycle [94], there is no (rider) lean or rider pitch. However, to confuse the matter, the authors then often talk about lean instead of roll. Thus the lean is the absolute roll angle that the rider and vehicle make with respect to the vertical axis.

Rider control in general Authors have investigated the number of control inputs, their magnitudes, and phases and compared them to the vehicle state outputs to understand the type of control that is applied by riders.

Transfer functions for rider lean and steer torque control have been experimentally investigated by Aoki [4] who did this with four heavy motorcycles at moderate to high speeds in four tests (steer pulse, lane change, entering a curve and slalom). First the rider control was investigated at various speeds, then for the different motorcycles and finally for the different maneuvers. Based on the yaw velocity transfer function, Aoki concluded that only steer torque has to be considered as an input to the system. Aoki therefore concluded that motorcycle rider control can be treated as a single input system. Similarly, Katayama *et al.* [68] found, by carrying out single lane change experiments at 60 km/h with 12 expert riders fitted with a device to measure the rider upper body lean and lower body's lateral shift, both measured relative to the frame, and a steer torque sensor, that steering torque is dominant. However Katayama found that also lower body torque (as the result of a lateral shift) assists and that upper body torque (rider lean) is such that the upper body is kept vertical and does not really contribute to the control. Katayama hypothesizes that keeping the upper body upright is probably only performed as a comfort measure by the rider.

An instrumented motorcycle together with an inverse 6 DOF Stewart platform to measure the state of the motorcycle and the relative motion of the rider was made by Bocciolone *et al.* [13]. With this setup they demonstrated that not only does the rider lean, but also shifts inwards (into the curve) on the saddle during tight maneuvers. They hypothesize that this however is because the rider prefers a more upright position during tight maneuvers.

Rice [119] on the other hand found that riders only lean during transient situations (such as during the lane change); once the vehicle is in steady state the upper body returns to the motorcycle's plane of symmetry.

Differences in rider control actions for successfully and unsuccessfully completed maneuvers were investigated by Rice and Kunkel [120] and Prem and Good [115]. They carried out lane change experiments with both experienced and novice riders and found that there are no discernable differences between the magnitude of the steer or lean control for successful and unsuccessful runs for the same rider. This indicates that timing, or phase differences, are likely to be the most significant factor for determining whether a lane change will be successful or not.

Rider experience These studies are aimed at finding differences in rider control actions amongst riders with different levels of experience.

For two experimental maneuvers Rice found different rider lean control strategies amongst the different rider groups. In the single lane change maneuver [120] all riders (novice, medium and experienced) initiated the maneuver by applying a steer torque. However, he found significant differences amongst the rider groups with regard to leaning action. The novice riders appear to use only upper body lean as a reactive rather than

deliberate control, unlike more experienced riders. With the second experiment: entering a constant radius turn [118], Rice found that novice riders only use steer torque control to initiate the turn while experienced riders use their upper body to get the motorcycle in the desired lean before they apply a steer torque in the desired direction. It was recently shown with multi-body software by Balletti *et al.* [9] that this type of control, where the rider uses upper body lean to roll the bike in the desired direction and then applies a steer torque, allows a quicker and more precise maneuver at a given speed.

Prem and Good [115] also carried out a single (emergency) lane change and a constant radius curve test to investigate differences between novice and experienced riders. They concluded that skilled riders have a shorter reaction time, achieve larger maximum steer angles, and apply a reverse steer angle for a shorter period of time than the less skilled riders. They also concluded that short reaction time is important for the success of the maneuver. Interestingly, and as could be expected, the less skilled rider group showed more inter-rider variability than the experienced rider group.

Evertse [41] investigated the difference in riding “styles” between novice, expert and racing motorcycle riders for a 90° corner and a single lane change maneuver. He, similar to Prem and Good, found that there was less inter-rider variability for the expert and racing riders than for the novice riders. Furthermore for both transient maneuvers he found that novice riders apply large roll-steer torques to initiate a corner whilst expert and racing riders do not. From the lane change maneuvers Evertse concluded that the difference between novice and experienced riders is that the novice riders are unable to apply sufficient steer torque at higher speeds. He also found that the shape of the applied steering torque becomes more homogenous across the groups at higher speeds as both novice and expert riders resort to applying a pulse torque to initiate the lane change and another pulse to exit the maneuver. This suggests that force control is taking place. This is likely to be caused by the large inertial force of the front wheel that has to be overcome to change the direction of the front frame at higher speeds as described by the handling quality index by Cossalter & Sadauckas [32] (see section 2.4.2 and table 2.5). The size of the required force is so large that the rider can no longer accurately control the position of the handlebar and thus applies a more “bang-bang” type of force control.

Rider physiological limits Physiological limits are human limitations such as the time required to sense a change in a state (time delay), the maximum force a rider can apply, the maximum speed a limb can move at and its maximum acceleration. Rider physiological limits have been investigated in order to limit values for rider model controller feedback gains etc.

Yokomori *et al.* [176] carried out straight line experiments with an instrumented motorcycle to study low speed control. They measured steer angle and motorcycle roll and rider lean angular rates. The riders either had hands on or off the motorcycle during the experiments at multiple speeds between 3 km/h and 25 km/h. The experiments were carried out by only two riders - one experienced and one novice. The time delay

between the rider lean angle and the motorcycle roll angle was investigated and despite the large standard deviation, a slight general trend of decreasing lean and roll angles for increasing speed was found. The power spectra was also investigated and found that these remain constant up to approximately 1 Hz and then fall off.

Cossalter *et al.* [30] carried out experiments on a simulator setup [31] with 5 test subjects (with various riding experience) in order to investigate the effect of rider impedance on motorcycle stability. Only the steer and roll actuators of the simulator were used to carry out two experiments, one to measure the effect of a passive rider on steer motion, the other on lean motion. To investigate the passive steer behavior they applied a stepped sine with constant amplitude of 4 degrees for a frequency range of 0.5 to 8.5 Hz to the handlebar of the simulator and measured the steer torque. They then used the data to identify mass, spring and damper constants by curve fitting of the experimental frequency response function (FRF) to the FRF of two multi-body models. The first model has links for the upper and lower arms and the torso whilst in the second the arms are modeled by spring-dampers only. The torso rotates about a fixed axis in both. The results compare well with those of literature ([64]) showing a peak at 2 Hz and an increase of response at about 6 Hz, which they suspect may influence wobble instability. For the passive lean behavior they experimentally determined the frequency response function of the head, chest and waist by placing 3 accelerometers on the test subject to measure the lateral accelerations. They found that the passive rider roll response shows a peak at about 1 Hz and then drops off, similar to what Yokomori *et al.* [176] found. They note that the rider's motion relative to the motorcycle tends to minimize the rider's lateral acceleration.

To investigate the maximum effect that rider lean can have on the motion of a motorcycle, Pierini *et al.* [112] investigated the maximum acceleration and the maximum displacement that riders could move their upper body on a motorcycle. They investigated how 5 riders, leaned left then right before coming back to the upright position as fast as they could and as extreme as they could in a single motion. The experiments were carried out on two stationary upright motorcycles and each rider repeated the experiment 6 times. The motions were recorded using motion capture equipment with 16 markers placed on the upper body of the rider. With the measured data they found that the seating position affects the maximum values of acceleration and displacement of riders center of gravity. They also found two different styles among the riders for which the maximum values in terms of rider lateral acceleration and displacement were quite different. Therefore they concluded that even defining the riders physiological limits is difficult.

Bicycle rider control While most authors have investigated motorcycle control due to the increased safety risks involved, a few have investigated bicycle rider control.

In the late 1960s and early seventies Van Lunteren & Stassen [154] were interested in modeling the human control actions, and chose to do this using a bicycle simulator. They had modeled the rider under normal circumstances and validated the model by

system identification techniques as discussed in section 2.3.2 on page 19. Even though the correctness of their simulator dynamics was debated, they used it to determine the effect that 4 different drugs have on human control behavior for stabilizing a bicycle (simulator). Two drugs, secobarbital natrium (Seconal Sodium) and aethyl alcohol (Vodka), showed a marked effect, increasing the time delays between the input and output of riders and strongly acting on the remnants, increasing the upper body motion and decreasing the handle bar action. The two other drugs tested: chlordiazepoxydi hydrochloridum (Librium) and perphenazinum (Trilafon) did not have a marked effect on the riders' control actions. Interestingly they noticed that the time delay of the handlebar action was always about one and a half times that of the upper body action (handlebar control was found to have a time delay of 150 ms and 100 ms for upper body control) suggesting that the upper body control is governed by hierarchically lower centers of the central nervous system than those which are involved in the control of the handlebar action.

Stassen [141] also performed experiments where they restrained the upper body of the rider (similar to Eaton [39]) and experiments where the upper body was free to move. By comparing the two they concluded that rider body motions are important in normal bicycle riding, however "perhaps they are not consciously intended as a contribution in the stabilization of the bicycle", but rather are intended to control the rider's head position and orientation in space.

Almost two decades later (1988) Doyle [36] investigated bicycle rider control to understand to what extent motor skills necessarily involve higher functions of the cerebral cortex. Doyle investigated balance control during normal cycling for two situations: firstly on a normal bicycle, and secondly on a bicycle where self-stability factors had been removed (destabilized bicycle). The roll angle and steering angle were recorded on both bicycles.

To get such a bicycle with no self-stability factors he followed Jones' [66] reasoning for an "unrideable bike" and constructed a machine that had the front frame stabilizing factors removed - a vertical head angle and no trail, no gyroscopic effect (counter rotating wheel) and no mass offset from the steer axis (counterweight added). Doyle reasoned that "without these all movements of the front wheel come exclusively from the human control system". More specifically he reasoned that it eliminates the lean to steer coupling, thus on the destabilized bicycle body movements have no effect on the overall motion (the system becomes a single (steer) input system).

By comparing steer and roll angle, rate and accelerations for entering and exiting a circular path at about 13 km/h for the normal bicycle Doyle found that there was a 120 ms lag between the roll and steer action. Indicating that steering follows rolling. Doyle was not sure if the control is achieved through control of the riders arms or through the bicycle's self stability and coupled upper body motion. Therefore he continued with experiments on the destabilized bicycle.

The experiments with the destabilized bicycle were carried out at about 7 km/h. The riders were told to simply stabilize the bicycle and not to track a path. To assist in

this the riders were blindfolded, yet all riders tended to remove any turns automatically so that the general direction of the start was maintained. The recorded data showed a 0.2 Hz signal and a 1 Hz signal present in the roll angle. The steering signals follow the roll signals with a mean 12 0ms delay. In particular the steering acceleration signal follows the roll acceleration signal. Thus Doyle concluded that the basic rider control mechanism feeds the roll acceleration back, multiplied by some constant (gain), as an angle independent force at the handlebar. Interestingly the recorded data indicate that the rider “pumps” energy into the system regardless of the control requirements, which Doyle suggests is to increase the system output values such that they go above a threshold below which the rider cannot detect the value. He concluded that:

Because the system delay in the roll rate is so short it is evident that the output from the vestibular system must go almost directly to the controlling muscles making little or no demand on higher cortical processes for this part of the system.

Two decades after the research by Doyle, understanding what rider control actions are performed, in particular for stabilizing without a significant tracking task but also during normal cycling, was explored by Kooijman *et al.* [78]. They used an instrumented bicycle and carried out initial experiments on the open road amongst traffic. Extracting good data from these trials proved rather difficult due to all the external factors that were influencing the control such as wind, (speed)bumps, traffic, etc. Therefore they also carried out their experiments under controlled conditions (indoor) on a large treadmill (3×5 m). The bicycle was ridden by two averagely skilled riders at various speeds, each rider was given enough time to adjust to riding on the treadmill before the measurements started. Three riding cases were considered: normal bicycling, towing and normal bicycling with lateral perturbations. These latter experiments were carried out to identify the effect of the pedaling motion and the effect of upper body motion on the control. The bicycle was equipped with a camera system facing the rider and connected to the rear frame, making it possible to qualitatively investigate rider motion on the bicycle. They concluded that very little upper-body lean occurs and that stabilization is done by steering control actions only. However, they also found a second control action at very low forward speed: knee movement. Moreover they note that all control actions, except for those at very low forward speeds, are performed at the pedaling frequency, and that the amplitude of the steering motion is inversely proportional to the forward speed. Moore *et al.* [102] then repeated the treadmill experiments with a motion capture system and quantitatively confirmed the qualitative conclusions from [78].

2.3.2 Theoretical Controller Design

In order to understand and predict the stability and handling of a bicycle–rider system, a model for the complete cycling system is required. In other words a model of both the bicycle and rider is required. The bicycle is well described by the Whipple model

Type of Model	Stabilizing	Path following
Classical Control	van Lunteren <i>et al.</i> [154], [152], [151], van Zytveld [155], Ruijs & Pacejka [126]*, Yokomori <i>et al.</i> [175]*, Åström <i>et al.</i> [7]	Roland <i>et al.</i> [123], [122], [124], van Lunteren & Stassen [153], Weir [160]*, Rice [118]*, Prem & Good [115]*, Nagai [106], Katayama <i>et al.</i> [68]*, Levandowski <i>et al.</i> [85]*, [174]*, Tanaka & Murakami [146], Hess <i>et al.</i> [61]
LQR / LGQ Optimal Control	Schwab <i>et al.</i> [131], Connors & Hubbard [22]	Katayama <i>et al.</i> [68]*, Sharp [136]*, [137]*, [138], [139], Cossalter <i>et al.</i> [27]* [28]*, Bertolazzi <i>et al.</i> [11]*
H_∞ Optimal Control	Mammar <i>et al.</i> [87]*, Nishimura <i>et al.</i> [107]*, Thanh & Parnichkun [147]	
Intermittent Control	Doyle [36]	
Intuitive Control	Schwab <i>et al.</i> [131]	
Neural Networks		Cook [23]
Fuzzy Logic		Fujii <i>et al.</i> [45]*, Chen & Dao [19], [20], [21], Levandowski <i>et al.</i> [85]*
Inverse Dynamics		Getz [47], [48], [49]
Forward Dynamics	Cook [23]	von Wissel [156], [157]

Table 2.2: Types of single track vehicle control models. A star (*) indicates the model is for motorcycle control.

as benchmarked and reviewed by Meijaard *et al.* [94], this section therefore focusses on the proposed rider models. The rider's influence on the system can be split into two aspects: a controller; and added system dynamics. The added system dynamics, caused by for example the rider moving relative to the bicycle, could require the vehicle model to be expanded to include these extra dynamics, such as adding a (controlled) pivoted point mass pendulum to the vehicle to simulate upper body lean.

For the modeling of the human controller, authors have followed three roads for the design and development thereof. Firstly there is the classical control approach which has been extensively applied to pilot aircraft modeling. This approach is based on observations and the control is determined using system identification techniques which include rider time delays. At the cross-over frequency (the frequency at which the magnitude of the transfer function is unity) the gain roughly has a 2 dB drop-off per decade. Continuous feedback control systems with human neuromuscular properties (dynamics) are usually included in these models. The second road that authors have traveled down is the optimal control framework, where the rider is assumed to be an optimal controller. The method uses optimal control criteria by weighing control effort against the error in the control task. The third road is a collection of "other" control strategies including fuzzy logic, neural network and very simple "intuitive" controllers. Authors for both the optimal control and "other" control strategies have not limited their research to mimicking a human rider, but have also taken advantage of these control strategies to develop "autopilots". Table 2.2 lists the authors that have applied the different control routes and for which situation, tracking or stabilization, they are used.

All three routes have been reviewed by other authors. These include Guo & Guan [54] and Macadam [86] who reviewed the driver models for general road going vehicles (mostly automobiles). Popov *et al.* [114] reviewed the modeling of the control of single track vehicles and in particular the control of motorcycles, while Sharp [139] reviewed the work on the control of bicycles. Here an updated broad overview of all three routes is given with particular attention paid to the modeling of bicycle control.

Classical control system design

In classical control, feedback of the states is used to create a closed loop controlled system. The systems are usually multiple input multiple output and linear or linearized about a given state. Sometimes nonlinearities like time delays are introduced. McRuer was the first to develop the classical control systems approach for modeling human control. He applied it successfully to pilot aircraft control [88, 89, 91, 92].

Experimental data for a wide variety of single and multiloop situations show that the operator (i.e. pilot, driver or rider) adjusts his/her transfer function, Y_e^c (Fig. 2.2), in each feedback loop such that the open loop function, $Y_e^c Y_e^m$, comprising of the effective vehicle dynamics, Y_e^m , and the operator, in the vicinity of the gain crossover frequency

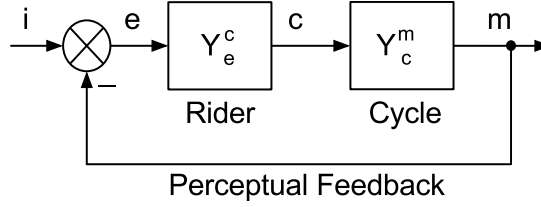


Figure 2.2: Single loop control. Where: i is reference control value; m is actual control value; e is control value error; Y_e^c is rider transfer function; c is rider output control variable; Y_c^m is machine transfer function.

(the frequency at which the gain is unity), ω_c , for that loop has the approximate form:

$$Y_e^c Y_c^m = \frac{\omega_c}{j\omega} e^{-j\omega\tau} \quad (2.1)$$

Where τ is an effective pure time delay that includes rider neuromuscular dynamics as well as any net high frequency vehicle dynamic lags and j is the imaginary unit. The crossover frequency (ω_c) is the product of the rider and vehicle gains. The form of Eq. 2.1 emphasizes that the rider's characteristics are optimized to the specifics of the control situation and the vehicle. However, McRuer also found that the human controller is limited in its physical control capabilities amongst others by the muscle dynamics and neural transport resulting in a delay. He found that a human controller can be described by:

$$Y_e^c = K_p \frac{(T_L j\omega + 1)}{(T_l j\omega + 1)} e^{-j\omega\tau}, \quad (2.2)$$

where T_L is a lead time constant, T_l is a lag time constant, K_p is a static gain, and τ is an effective time delay. This in essence makes the human controller a lag-lead system with time delay and limits the systems that a human operator can control.

Although the classical control method is very promising with respect to determining the performed rider control in individual control loops, it is mathematically less well suited for performing/determining multi-loop control. As bicycles and motorcycles require multi-loop control (stabilization and path following) only a few authors have delved into this method.

Two major classical control, rider projects took place in the early 1970s. The first was a study on the differences in rider control under specific circumstances (effect of drugs, alcohol, etc. on rider control) by Stassen & van Lunteren [140, 141, 151, 152, 153, 154]. The other was a comprehensive theoretical exploration of the manual control of a motorcycle by Weir [160, 161] and experimental validation thereof by Eaton [39]. The major topic of discussion amongst authors is the nature of the applied control: position (angle) control or force (torque) control.

Stassen & van Lunteren assumed position control and carried out system identification experiments on a self developed bicycle simulator. The simulator was a device

that could roll and steer and initially had no visual feedback. With the simulator they experimentally determined the rider control parameters that fit their position (angle) controlled rider model. Unfortunately they only simulated and measured at one fixed forward speed, namely 15 km/h. They measured the simulator's roll angle, steer angle and the rider's lean angle. Stassen & van Lunteren concluded that the human stabilizing control can be described by a PD controller with a time delay for which the input is the frame roll angle and the outputs are the steer angle and upper body lean angle.

The simulator was later extended with visual feedback with which they showed the rider's deviation from a pre-specified path. Further experiments then led Stassen & van Lunteren to conclude that the tracking task does not significantly alter the stabilizing task controller parameter values.

Weir [160, 161], who was aware of the work by Stassen & van Lunteren, found, based on determined transfer functions, that it is unlikely that position control is used by a rider and that torque control is far more likely. The transfer functions for motorcycle rider control actions were theoretically investigated by Weir [160] using a theoretical model of the motorcycle by Sharp [134] and a McRuer style rider model based on transfer functions from literature for the different sensory organ control loops. Weir searched for the best single input to single output transfer functions for rider control in the frequency domain. He found that the best vehicle stabilizing transfer function is that of the roll angle to steer torque due to the relatively high cross over frequency of roughly 1 rad/s (therefore easy to detect) and the accompanying large gain and phase margins. The only other good transfer functions Weir found were roll angle to rider lean angle and yaw rate to rider lean angle. None of these three transfer functions however is suitable for tracking purposes and lateral position (the lateral deviation from the desired position) must be added to the loop for this to be the case. To achieve good stabilization and tracking performance with minimal attention and control workload Weir proposed the rider control model shown in Fig. 2.3. It consists of an inner loop for roll stabilization ($\phi = 0$), a middle loop controlling the heading (ψ) and an outer loop for the lateral position control (y_{lc}). The desired lateral position is expressed in a desired heading angle ψ_c from which the actual heading angle ψ is subtracted, resulting in the heading error ψ_e . This heading error is then used to control the rider upper body lean angle ϕ_R and steering torque T , which are the human outputs.

Also in the early 1970s Roland, Massing & Lynch [122, 123, 124] developed a bicycle (including tires) and rider model to study the effect of design parameters on bicycle stability and control where the end goal was to be able to perform simulations of bicycle maneuvers. They developed a rider model that incorporated a steer and lean torque, delayed PID controller. It was implemented as a simplification for a human lead-lag controller model based on literature [40]. The developed controller was not well documented but it had both tracking and stabilizing control loops [122]. The rider lean torque and steer torque were the outputs for both the stabilizing and tracking controller. The stabilizing controller inputs were the roll: angle, rate, and acceleration. For tracking control, similar to Weir, the vehicle path and heading error information were

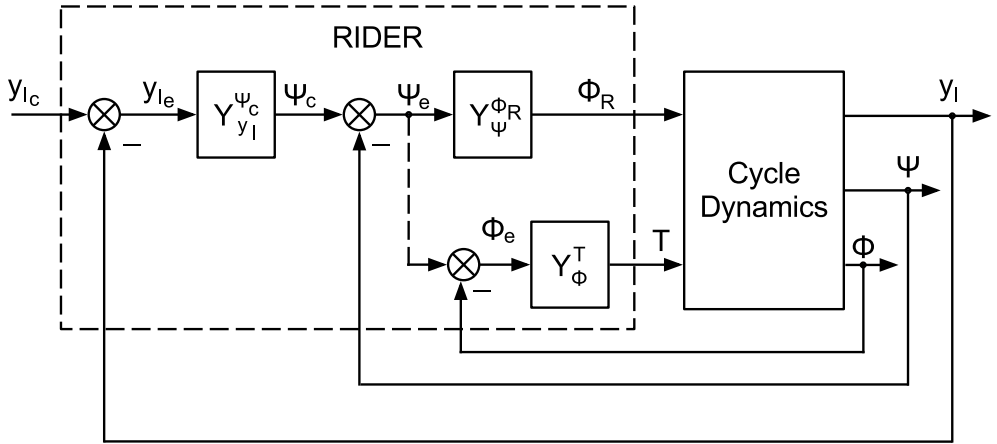


Figure 2.3: Weir's proposed multivariable control loop where: ϕ is roll angle; ψ is heading angle; y_I is lateral position; ϕ_R is upper body lean angle; T is steer torque.

also required. The tracking controller predicted the path based on the current state and comparing this with the desired path and generated an additional roll angle that was added to the desired roll angle. Roland tuned the coefficients of the stabilizing controller by investigating the system's response to driving straight ahead and applying a 20 degree command roll angle (simulating driving straight ahead and going into a constant radius curve). However even for the best controller he had an offset between the desired and obtained roll angle.

To our knowledge Roland never used the rider model that he developed for comparing real maneuvers with simulations, but Rice [118] later used the controller for the simulation of the same maneuver with a motorcycle and riders of different levels of experience. The model however did not compare well with experiments, except for in the transient stage of the maneuver.

Experimental data, certainly for novice riders, collected by Prem & Good [115], suggests that there is a strong coupling between steering and rider upper body leaning inputs. Therefore Prem & Good used Weir's motorcycle and rider models and parameters to analyze the transfer function for roll angle control by rider lean with lean torque to steer torque coupling (see Fig. 2.4). They found that the extra coupling increases the gain of the transfer function, allowing the large rider lean to roll angle error gain values (5.5 deg/deg) found by Weir to be decreased to more realistic values that novice riders can achieve (1.0 deg/deg). They also found that this lean to steer coupling applied in the multiloop situation to have comparable system performance for tracking capabilities. They conclude that the proposed 'unskilled rider' model may have lower stability margins, but requires physically less extreme upper body motions.

Upper body lean control but now for the hands-free situation was investigated by

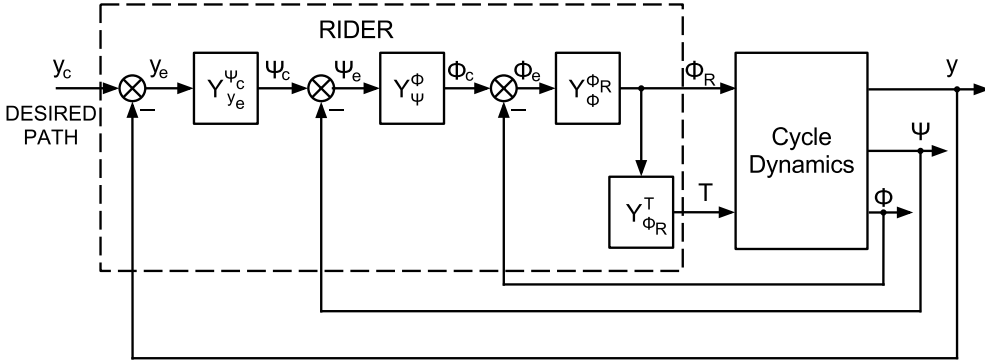


Figure 2.4: Prem & Good's proposed multi variable control loop for a novice rider where: ϕ is roll angle; ψ is heading angle; Y is lateral position; ϕ_R is upper body lean angle; T is steer torque.

Yokomori *et al.* [175]. They were particularly interested in the effect of time delays. Their rider model consisted of a delayed proportional controller with constant gains. By varying the time delays and the forward speeds (5 - 25 km/h) they determined the stable region for the time delay. This time delay stable region was found to increase with increasing speed, and the time delay can even become negative (feed forward!) for speeds above 12 km/h. Yokomori *et al.* did carry out physical experiments to validate their findings but practically all results were within the stable region, and therefore rather inconclusive.

Finally in a recent theoretical study to introduce a task independent handling qualities metric (HQM) to bicycle control, Hess *et al.* [61] directly applied a HQM from aircraft handling studies using the classical control method (shown in Fig. 2.5) to bicycling. They propose that handling qualities of bicycles can be reflected in the maximum magnitude of the transfer function between the inner-loop rate feedback of a variable (U_M) and the command input (C). To remove the effects of control sensitivity they normalize the equation with the magnitude of state feedback gain K_P .

$$HQM = \left| \frac{U_M}{C}(j\omega) \right| \cdot \frac{1}{|K_P|} \quad 1/s \quad (2.3)$$

Hess *et al.* directly import (highly skilled and trained) pilot properties from aircraft handling research into the cycling situation including pilot gains and time delays. In the study different bicycle models were evaluated on handling for a double lane change maneuver but no significant differences were found amongst them. It is unclear if such a direct implementation of the pilot is possible in the cycling situation as there are definitely differences between the tasks of a bicycle rider and those of an aircraft pilot. Certainly turning the handlebar is different from controlling the (joy)stick. However the

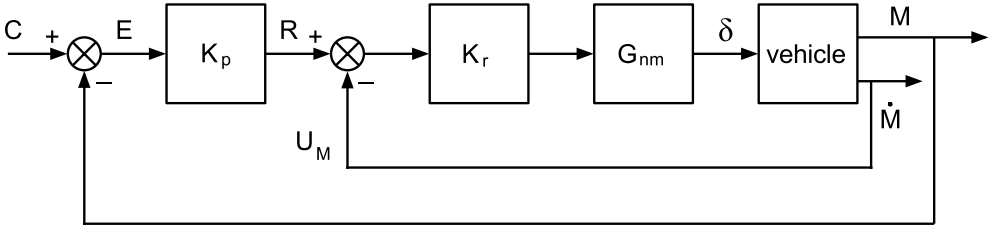


Figure 2.5: Proposed bicycle rider model by Hess et al. [61] for a single-axis tracking task. Where M and \dot{M} are the bicycle output and output rate response for the variable being controlled, and C is the desired value of M . G_{nm} represents the rider neuromuscular dynamics (highly simplified). The gains K_p and K_r are chosen such that a specific bandwidth (K_p) and a specific level of damping at an oscillatory mode (K_r) are achieved.

methodology is encouraging and will hopefully be validated experimentally in the near future.

Optimal control

Optimal control deals with finding a control law for the system such that it optimally fulfills certain criteria. The control problem minimizes a cost function, which is a function of the state and control variables. The optimal control concept is capable of treating multi-variable systems within a single conceptual framework using state-space techniques [14]. The optimal control Linear Quadratic Regulator (LQR) method can be used for multiple input to multiple output (MIMO) systems described in state space form by:

$$\dot{\mathbf{x}}(t) = \mathbf{A}\mathbf{x}(t) + \mathbf{B}\mathbf{u}(t), \quad (2.4)$$

$$\mathbf{y}(t) = \mathbf{C}\mathbf{x}(t). \quad (2.5)$$

where \mathbf{x} is the state vector, \mathbf{u} the input (or control) vector, \mathbf{y} the output vector, \mathbf{A} is the system dynamics matrix, \mathbf{B} is input gain matrix, and \mathbf{C} is the observer matrix. The Linear Quadratic Gaussian (LQG) method can be used for systems described in state space form by:

$$\dot{\mathbf{x}}(t) = \mathbf{A}\mathbf{x}(t) + \mathbf{B}\mathbf{u}(t) + \mathbf{w}(t), \quad (2.6)$$

$$\mathbf{y}(t) = \mathbf{C}\mathbf{x}(t) + \mathbf{v}(t), \quad (2.7)$$

where $\mathbf{w}(t)$ and $\mathbf{v}(t)$ are uncorrelated Gaussian system and observation noise respectively. For both systems the optimal linear feedback gains for \mathbf{B} are calculated by minimizing a cost function (J) which is a function of the state(s) (\mathbf{x}) and the control input(s) (\mathbf{u}), weighted by respectively the matrix \mathbf{Q} and the matrix \mathbf{R} . For an infinite horizon

continuous system the weighting function is described by:

$$J = \int_0^{\infty} (\mathbf{x}^T Q \mathbf{x} + \mathbf{u}^T R \mathbf{u}) dt. \quad (2.8)$$

A drawback to this method can be the consideration required for determining the weighting aspects for the desired input and output signals and the formulation of the cost function, therefore the objective optimal control method can have a subjective nature.

Kleinman, Barron & Levison were the first to fully develop the idea of optimal control for describing human (manual) control back in 1970 [71, 8]. They hypothesize that the human operator works in an optimal manner when carrying out a compensatory control task, but that the actions of the human are bounded by human limitations such as time delay and neuromuscular lag. They derived linear feedback for MIMO human operator models based on the gains calculated from minimizing the cost function (J) and comparing these with actual measured tasks performed by aircraft pilots.

Interestingly the skateboard model by Hubbard [62] shows the similar dynamics to that of the bicycle, with a coupling between the lean and steer and a dynamically unstable speed range. Hubbard [63] applied full state feedback LQR to the stabilizing and tracking control of the skateboard. The human skateboarder is modeled by body lean relative to the skateboard. No human limitations are set and the dynamics of the skateboard itself are neglected. The roll angle of the skateboard is taken as the control input. The analytically derived results were compared to some experiments which show qualitative agreement in the time series. Future plans are to apply system identification techniques in order to determine the feedback gains.

Only a few optimal control investigations for bicycles have been performed. Schwab *et al.* [131] used a similar LQR controller as Hubbard [63] with full state feedback which was implemented in two different situations to investigate the effect of a leaned upper body on the control required to stabilize a bicycle. In the first situation they investigated a rider rigidly attached to the frame of the bicycle and they show that the system can be stabilized easily through steer torque control but that at low speeds the roll feedback gains become unrealistically large. In the second situation the rider is modeled with a leaning upper-body (inverted pendulum). They find that adding a pivoted upper body does not greatly affect the uncontrolled system eigenvalues or eigenmodes. However at low speeds the upper body lean requires large upper body lean feedback gains and similar to the rigid rider case, large roll feedback gains are required for the steer torque. Unlike the rigid rider case they find that at high speeds significant steer and rider lean feedback gains are required for both the upper body lean and steer torque control. Furthermore they find for the situation where the stabilization only takes place by the upper body (hands free situation) that hugely unrealistic feedback gains (all states) are required at low speeds, suggesting that lean is unlikely to be used when steering is possible (hands on situation).

Connors & Hubbard [22] investigated the effect of pedaling on the steering control torque for a recumbent bicycle and modeled the rider's control to balance the bicycle

as LQR steer torque optimal control. They found that for a recumbent bicycle the oscillating legs can drastically increase the roll angle sensitivity and the steer torque required to balance the bicycle. Based on their findings they devise a gear-shifting strategy (to reduce pedal cadence at higher speeds) to reduce the control effort at very high speeds (> 15 m/s).

One of the first to apply LQR optimal control to a motorcycle were Katayama *et al.* [68]. They used optimal control in a tracking with preview problem to investigate the rider control applied during single lane change maneuvers. They modeled the rider as a double pendulum with a lower and upper body connected to the frame and lower body respectively via passive spring-dampers. They use the roll angle and average heading error as the control inputs and the steering torque, upper body lean torque and lower body lean torque (offset center of mass) as control outputs. Oddly they use a car-like optimal control strategy where they take the average heading error as the lateral separation of the desired path and the straight line predicted motorcycle path (not curve!), weighted around a preview point. The lane change maneuver studies indicate that steering torque is the dominant rider control mode, lower body torque assists and that upper body torque is such that the upper body is kept vertical and does not really contribute to the control.

Sharp also showed with LQR tracking with preview optimal control that for motorcycles steer torque is dominant over body lean. Sharp [136, 137] investigated the situation where the desired route is a curve and the control inputs are steer torque and upper body lean torque. The used cost function optimized the tracking errors for different preview lengths and the required control power. It was found that much larger preview distances are required compared to cars; however, extending the preview beyond a certain distance becomes pointless as the gains associated with these preview points reduce to zero. The preview distance however, increases more than proportionally with the speed, meaning that the required preview time increases with increasing speed. A single lane change as prescribed by Rice [118] and an S curve according to Frezza & Beghi [44] were simulated. Qualitative agreement with the lane change experiments performed by Rice [118], Katayama *et al.* [68] and Zellner & Weir [177] were found. Sharp notes that the higher the weighting of the controller power the more the corners are 'cut'. He also notes that there is a strong relationship between the optimal tracking steering control and the motorcycle oscillatory weave mode, giving rise to the idea that if the oscillations of the motorcycle are within the riders control bandwidth, and if the rider is skilled enough, then the rider will perform control at the eigenfrequency to get good response with little control power.

Sharp also theoretically investigated LQR optimal control tracking with preview for bicycles [138, 139]. This was based on the motorcycle research [136, 137] but now implemented on the benchmark bicycle [94] (with slightly adapted bicycle design parameters). For the path following simulations he looked at two different tests: a random road; and a straight section into a circular path (90 degrees) followed by a straight section again. Different weighting factors for tracking errors against control power were

investigated. The feedback gains are clearly speed dependent but again become unrealistically high with reducing speed. Sharp concludes that the necessary preview time, as opposed to the motorcycle case, depends very little on speed. Therefore for bicycles the preview distance is roughly proportional to the speed. Furthermore, he concludes that tight (precise) control requires about 2.5 seconds of preview independent of the forward speed.

Cossalter *et al.* [27, 28] apply optimal control not to model a rider but as a method to solve the problem of the “optimal maneuver” for assessing the intrinsic motorcycle handling and maneuverability properties (for a so-called perfect driver). They point out that the optimal control for a specific maneuver can be vehicle dependent. The optimal maneuver method has handling and maneuverability as part of the cost function, where handling is defined as the “ease to drive” (control effort) and maneuverability as “ability to perform complex maneuvers fast” (performance). First in [27] they apply optimal control to solving the problem of the most efficient trajectory for each specific motorcycle, with its specific parameters, within prescribed boundaries (the road) and between two endpoints. They apply this optimal control to three maneuvers: slalom, lane change, and U-turn. The optimal maneuver is investigated for different motorcycle configurations by carrying out parameter changes to the wheelbase, center of mass position, gyroscopic effect and tyre adhesion. For significant tyre adhesion differences they find that for a U-turn maneuver the trajectory performed during the optimal maneuver also differs significantly. Then in [28] they compare results with experimental data and find good comparison in a racing situation for a set of corners in S configuration. Bertolazzi *et al.* [11] used this optimal maneuver method to investigate how a maneuver changes with increasing upper body lean movement. For a lane change maneuver they show that when upper body lean is used it is possible to increase the performance as it is possible to carry out the maneuver more quickly.

Another form of optimal control is H_∞ control, where the feedback gains (for a multiple input to multiple output system) are chosen such that the peak values in the frequency responses (transfer functions) across each complete frequency range is minimal.

Nishimura *et al.* [67, 107] performed experiments with a motorcycle at 30 km/h to identify the motorcycle dynamics. For both the identified 5th order model and reduced 3rd order model which discarded the small, fast steering mode, they developed an H_∞ optimized steer torque controller that uses the roll angle as input. The simulations performed verified that the models were capable of stabilizing a roll disturbance and that the reduced-order controller exhibits efficient stabilization performance in comparison with the full-order controller.

For a motorcycle model with a leaning rider Mammar *et al.* [87] synthesized a PID steer torque controller with feedforward and feedback capabilities using H_∞ optimal control for the stabilization. Once again the roll angle was used as the input for the steer torque controller. The developed controller is shown to stabilize the motorcycle model, to be able to enter a constant radius corner, and to be robust to parameter

variations for this maneuver.

Finally we mention the mixed H_2/H_∞ controller design for the stabilization of a bicycle robot using gyroscopic precession by Thanh & Parnichkun [147]. They chose to apply the control method to a flywheel to ensure that the bicycle can balance at all speeds (also stationary). The decision to apply an H_2/H_∞ controller was for the good robustness of the optimal controller for systems with uncertainties and not to mimic a rider in any way. However, optimization of such a controller ends up as a complex non-convex problem and for this reason they apply a particle swarm optimization algorithm as it enables fast and structured optimization routes. The control was implemented on a real bicycle and was shown to be stable when the bicycle was stationary and moving slowly in both forward and backward direction.

Other control

A variety of different control methods have been proposed by authors to model riders. These are discussed below.

Intermittent control Doyle [36] used bicycle stabilization observations to develop a stabilizing bicycle rider model with intermittent control (as discussed in section 2.3.1 on page 15). He developed classical style controllers for the dynamic model of the bicycle and applied numerical integration to get the bicycle state solutions in time. He found that the stabilization of the bicycle performed in a similar manner to that observed with real riders can be achieved by steer torque control with continuous feedback of the roll rate and acceleration, in combination with intermittent roll angle feedback. The intermittent feedback takes place in the form of a pulse torque that is triggered when the roll angle exceeds a certain threshold roll angle value, which he finds to be 1.6 degrees in his observations.

Intuitive control An intuitive bicycle controller was developed by Schwab *et al.* [131] for balancing a bicycle using the “steer into the undesired fall” principle. They investigated two situations, the first was a rigidly attached rider and second a rider with a moveable upper body modeled as an inverted pendulum connected to the frame with a passive torsional spring. In both cases they apply a simple steer torque control law: at low speed they apply proportional feedback of the roll rate with the gain increasing with decreasing speed and above the stable speed range proportional feedback of the roll angle with the gain increasing with the speed. For both situations they show through an eigenvalue analysis that the system can have marginal stability for almost the complete forward velocity range. Furthermore they find that the controllers in both situations require far more realistic steer torque feedback gains (K_c and K_v) than for the same models using an LQR optimal controller for determining the feedback gains.

Fuzzy logic For the low speed tracking control of a motorcycle Fujii *et al.* [45] develop a fuzzy PD controller to control the roll angle with respect to some desired roll angle. The gains of the fuzzy controller were determined using a genetic algorithm applied to constant speed, constant roll angle situations for forward speeds ranging from 1 to 15 m/s. To evaluate the controller a 90 degree corner, a lane change maneuver and a set course were evaluated at multiple speeds. Initially the controller was unable to track the desired path at low and high speeds. The genetic algorithm is evaluated using a fitness function and considerable effort had to be invested in developing (altering) the fitness function such that the path tracking capabilities of the fuzzy controller became satisfactory at all speeds. They were able to compare their model simulations with real experimental results and found good agreement with the vehicle states but the applied steer torque only roughly follows the experimental data.

Chen & Dao [19, 20, 21] developed a number of fuzzy logic based steer torque controllers of increasing complexity for a bicycle. First they developed a PID steer torque controller for stabilizing the bicycle where the PID gains are set but the control values are determined via the fuzzy logic controller placed in series. Then they investigated roll angle tracking by introducing a second fuzzy logic controller placed in parallel to the stabilizing fuzzy logic controller. Finally in [21] they optimized the fuzzy logic controllers using a genetic algorithm. They propose a strategy to optimize the fuzzy logic controllers by keeping the rule table fixed but tuning their membership functions and by introducing scaling factors and deforming coefficients. In this way the number of parameters to be trained can be reduced to speed up the learning process. They verify their control schemes with simulations and find good correspondence.

Neural network Cook [23] devised a neural network controller with only two neurons as an example of a simple human bicycle tracking controller. The first neuron is a proportional controller on the heading with a threshold function. It outputs a desired roll angle, which is an input for the second neuron which in turn outputs a steer torque based on PD control. The desired heading is set using way points enabling the bicycle to perform complex tracking tasks. He finds that the controller is relatively robust as (gain)values are not very speed dependent and do not have to be perfectly adjusted to the specific bicycle. The controller works at a range of velocities but it fails at low speed.

Inverse dynamics Controllers with a state observer can be used to predict the future motion of the vehicle based on the current state and inputs. Inverse dynamics is used to determine the forces required to pursue a desired course based on the current state.

Getz [47] developed an inverse dynamics method he calls dynamic inversion which he applies to bicycle control [48, 49]. The controller determines, based on the desired path or roll angle of the bicycle as a function of time, the forces that have to be applied to the steering system as a function of time. Getz illustrates the potential of his controller

in a number of examples such as a straight path at constant speed, a sinusoidal path, a circular path at constant speed and a figure eight trajectory. Each example starts with an offset from the track and all show counter-steering effects. Such an inverse dynamic method is certainly of interest for determining the performed control by a rider based on a traversed path, but it is probably less well suited for determining the control a rider will perform based on a current state and some roughly described desired path.

Forward dynamics Forward dynamics is used to calculate the resulting motion of the vehicle based on the current state and known applied forces. Von Wissel & Nikoukhah [157] applied forward dynamics to investigate the control of a bicycle with a multiple stage obstacle avoiding optimization methodology. They find trajectories for a bicycle in a complex space (a grid with ordinary cells, forbidden cells and end cells). The bicycle has a constant forward speed and a number of discrete steer torque maneuvers can be applied. The selection of the maneuvers is multiple stage. Therefore large tree structure path possibilities evolve. The maneuvers that make the bicycle unstable are discarded first; after this, maneuvers that cause the bicycle to come into forbidden cells are discarded. Finally all but the trajectories that penetrate in the end cells with the lowest cost function are discarded. The method uses a moving window methodology for the path tracking to reduce the computational power required by moving the end cell(s) through the complex space. This speeds up the computing as branches can be deleted along the way and then the simulation can be restarted. They give interesting examples implementing the method and showing how an optimal path changes with the movement of the end cells. In the given example the method is applied at a high (stable) forward speed of 8m/s removing the need for a lateral feedback controller. While it is not clear if the method is directly applicable to a human rider as a rider most likely does not compute all possible paths when determining which route to take, it does give interesting insight into possible route choices and is certainly interesting for automatic vehicles.

A similar approach was used by Cook [23] for determining the stabilizing path of a bicycle. He did this for a forward speed that is lower than the weave speed. At each time step the effect on the trajectory of a handlebar push to the left, right or no push is calculated. The process is repeated at each time step for each path. Each path is evaluated until the bicycle has fallen over and that path ends. This leads too to a large tree of possible paths. The control applied in the example that Cook gives however was unable to stabilize the bicycle over a long distance.

2.3.3 Experimental Validation of Controller Design

Controller models have been validated experimentally by many authors. Authors have generally been interested in validating one of two types of model: rider control models or machine control models. The majority of the authors have been interested in validating the latter in order to make some form of autopilot function possible.

Rider control model validation

While many have developed rider models, only a few authors have gone to the expense of actually validating them. Stassen & van Lunteren [140, 141] were the first to carry out many experiments with riders (on a bicycle simulator), but they never explicitly validated their models. However as they used the experiments to identify the model parameters, they thereby implicitly validated it. Nevertheless, a number of authors including Eaton [38], Roland & Lynch [122], and Koenen *et al.* [73] were critical of the work. In particular the used simulator and the steer angle control models were doubted. In [38] Eaton writes: "While the research represents a pioneering effort in obtaining transfer functions experimentally (with a bicycle simulator), it should be pointed out that van Lunteren's major interest was the performance of the human operator under various conditions (drugs etc.) and not the dynamics of the bicycle. Thus, the accuracy of the simulator dynamics with respect to real bicycles and the validity of the assumption of steering angle control (rather than steering torque) are questionable". Stassen & van Lunteren deemed the simulator sufficient for the intended purpose but the fact that riders had to learn to ride the bicycle simulator is an indication that the control of the simulator was probably not the same as on a real bicycle. Furthermore de Lange [33] (2011) discovered some sign errors in the work of Stassen & van Lunteren and that the complete model of the bicycle with the identified rider model is unstable even after having corrected sign errors in their equations.

Doyle [36] too developed bicycle rider models based on experiments. However, his experiments did take place on real bicycles. He compared the state time series results of a number of control models with measured data, and found that it is insufficient to use an average or filtered angular roll velocity as a feedback signal, the actual roll velocity has to be fed back. Furthermore he found that continuous feedback of the roll angle gives very different simulations from what is seen in real life: instead intermittent torque pulses are required to stabilize the bicycle. The intermittent control is applied when roll angle has grown beyond the threshold of 1.6 degrees.

Doyle also found that "if an attempt is made to control the system by responding to absolute angle without any velocity feed-back then after one or two reversals the velocity reaches such a high value that excessive lean angles are generated before control takes effect". This was also found by de Lange [33], who made a simple desktop computer game style bicycle simulator. The game player had a gamepad to apply steer torque and pedalling force. He based the dynamics of the bicycle on the benchmarked linearized equations of motion from [94] and showed a bicycle moving on a flat surface in the game. He found that it was impossible to stabilize the bicycle except by applying torque pulse inputs when a measure for the roll rate was also indicated on the screen.

The first to do an actual validation of a rider-vehicle model was Eaton [39] who carried out experiments to validate the theoretical Sharp [134] motorcycle model (including tires) and the rider control crossover model by Weir [160]. Eaton investigated the stabilization of the motorcycle roll angle by means of steer torque applied to the

handlebar. Path following tasks and control by body movements were not studied. The rider's body motion was therefore restricted by a rigid brace during the experiments. For low speeds (< 40 mph) significant differences between the motorcycle model and experimental results were found, but at 40 mph they match reasonably well. The identification method Eaton applied, the Wingrove–Edwards method [169], has had many critiques. This method applies no external excitation, all excitations are assumed to be a result of rider remnant. However, the time delay and signal are both small and can vary in size hindering the correct identification of the rider.

While Eaton prevented rider motion relative to the motorcycle, other authors have investigated the influence of rider motion on maneuvers. Interestingly though none have looked at stabilizing, all have looked at maneuvering. Capitani *et al.* [16] found that ignoring rider motions leads to incorrect steer torques and steering angles. Roland, Rice and Katayama *et al.* [122, 123, 124, 118, 68] tried to experimentally validate models of a non-rigid rider. Both Roland, for bicycles, and Rice, for motorcycles, modeled the rider upper-body as an actively controlled pendulum and the lower body as fixed to the machine. Katayama *et al.* [68] in essence extended this to include rider lateral motion on the saddle by modeling the rider as an actively controlled double pendulum. All three had issues.

Roland [122, 123, 124] developed the rider control model that was also used by Rice. The model actively controls the upper body in a closed loop manner in which the rider model feeds steering torque and lean torque inputs to the vehicle dynamics model in response to vehicle roll motion information (for stability) and to vehicle path and heading error information (for guidance). Roland however did not use the algorithm himself, instead he used a very simple guidance control algorithm for a slalom maneuver: the sign of the command roll angle (set at 20 degrees) is opposite to the sign of the current steer angle. This gave very similar qualitative results between model and experiment. However, it is unclear if this was a “lucky shot” that the actual slalom maneuver looks similar, or if this really is a good model for the control carried out by a rider.

In a number of motorcycle rider control observations Rice [118] found significant differences between a novice rider and an expert rider. The expert riders actively use upper body motion as a manner for (feed-forward) control whilst the novice riders only show steer torque and compare well to the model. On the other hand Rice found that during the transient stage of a maneuver both novice and expert riders show similar motion to that of the rider model. This suggests that the maneuver initiating body motion by the expert rider is a result of rider feed-forward control, while during the transient phase the forces are too high for the rider who therefore can contribute little more than in a passive manner. Different rider models should therefore be used for novice and expert riders as they apply different (initiating) maneuver control sequences but during transient stages of a maneuver the motion of the complete system is similar to that of a rider-vehicle model with a controlled upper-body.

The theoretical lane change studies that Katayama *et al.* [68] performed on a double-pendulum rider model were confirmed by his single lane change at 60 km/h experiment:

steering torque is the dominant rider control method; lower body torque (lateral shift on the saddle) assists in the process; upper body lean torque is only such that the upper body is kept vertical and does not really contribute to the control but is used for comfort of the rider. Therefore on those motorcycles where lateral motion of the rider takes place it appears that this motion should be accounted for. Katayama *et al.* however did not test stabilization control (at low, unstable, speeds), nor did they carry out high speed or low speed tracking experiments.

Machine control model validation

In general there are four main methods that authors have used to stabilize and control single track vehicles: steer control; a moving mass; a gyroscope; a combination of the above. An overview of the projects carried out using the different control methods is given in table 2.3.

Steer control Stable control of single track vehicles has been achieved using both steer torque and position (angle) control for both bicycles and motorcycles. However, the vehicle states that were used in the feedback loop and the feedback gains' speed dependency were different for the different approaches.

The first to develop a robotic motorcycle using only steer actuation were Ruijs & Pacejka [126] who used steer torque control based on a Sharp [134] motorcycle model with tires and leaning rider (but they did not include a leaned rider in their hardware). Others that have used steer torque control for robotic single track machines include Saguchi *et al.* [127, 128] who based their bicycle rider robot on a Getz [47] style bicycle model with added tire slip. Michini & Torrez's [96] and Andreo *et al.*'s [3, 18] bicycle robots were based on the benchmark bicycle model. Out of these robots only Saguchi *et al.* investigated tracking control (straight ahead running and constant curve motion) the other three only investigated stabilization control. Ruijs & Pacejka however were able to set the roll angle by a remote link and thereby make the motorcycle able to follow a path.

While at least three of the four used velocity dependent feedback gains (it is unclear if Michini & Torrez calculated feedback gains for multiple speeds or used the same feedback gains for the two speeds that they tested at) each used a different combination of a set of feedback signals and control strategy: Ruijs & Pacejka used pole placement for proportional control on the roll angle, roll rate, and steer rate; Similarly Michini & Torrez also used proportional control but they only used roll angle and roll rate and it is unclear if they used pole-placement in determining the gains or some other method; Andreo *et al.* used linear-parameter-varying (LPV) state feedback control for which they measured the forward speed, roll rate and steer angle and calculate the roll angle through integration; Saguchi *et al.* implemented roll angle tracking by optimal control on the difference between the desired and the actual roll angle, and implemented stabilizing

Control Outputs	Author	Stabilizing Task	Tracking Task	Control Inputs	Successful
Steer Torque	Ruijs & Pacejka [126]* Saguchi <i>et al.</i> [127] [128] Michini & Torrez [96] Andreo <i>et al.</i> [3] [18] luchi <i>et al.</i> [65]	ϕ ϕ ϕ ϕ ϕ		$\delta, \dot{\delta}, \phi, \alpha, \gamma$ ϕ, ϕ ϕ, δ $\delta, \phi, \phi, \beta$	yes yes yes yes yes
Steer Torque & Moving Mass Torque			ϕ		
Steer Torque & Gyroscope Steer Angle	Levandowski <i>et al.</i> [85]* [174]* Miyagishi <i>et al.</i> [97]* Tanaka & Murakami [146] Yamaguchi [170] Lenkeit [83]* Nagai [106]	ϕ ϕ ϕ ϕ ϕ ϕ	y y y, γ, k $\phi, \phi, \ddot{\phi}$ δ or τ_8 y	unclear $\phi, \dot{\phi}, \delta, \gamma$ $\phi, y, \gamma, k, \delta$ $\phi, \phi, \ddot{\phi}$ δ or τ_8 y, δ, ϕ, β	yes yes yes yes Unclear yes
Steer Torque & Angle Position					
Moving Mass Torque	van Zytveld [155]	ϕ		$\phi, \dot{\phi}, \beta, \dot{\beta}$	no
Moving Mass Position	Yamakita <i>et al.</i> [173] [172] [171] [105]	ϕ, β	y	δ, ϕ, β, y	yes
Gyroscope orientation	Thanh & Parnichkun [147]	ϕ		ϕ, φ	yes

Table 2.3: Machine controllers used in experiments. A star (*) indicates the control is for a motorcycle. ϕ is roll angle, δ is steer angle, α is slip angle, γ is yaw angle, y is lateral position, k is the curvature of the path, τ_8 is steer toque. β is the lean angle of a moving mass, and φ is the orientation of the gyroscope.

control, using proportional feedback of the roll angle and rate, steer angle and rate, yaw angle (ω) and slip angle (β), where ω and β are estimated using a Kalman filter.

Despite these major differences all four projects achieved very encouraging results. Ruijs & Pacejka's motorcycle robot was shown theoretically to be stable between 5 m/s and 60 m/s, experimental tests proved that motorcycle is in fact stable from 10 km/h up to at least 110 km/h (2.8–30.6 m/s). The robotic bicycle by Michini & Torrez was shown to stabilize the uncontrolled motion at both an unstable speed ($(\lambda_{weave}) > 0$) and a neutrally stable speed ($(\lambda_{weave}) = 0$) despite the fact that they calculated their feedback gains using bicycle parameter values from Kooijman [81], a totally different bicycle with a much lower mass. With this their LPV controller Andreo *et al.* show their bicycle was able to stabilize at low speeds (from 1.7 down to 1 m/s) and to balance despite an external impulsive roll torque disturbances (for speeds from 2.1 to 1.7 m/s). Saguchi *et al.* demonstrated stable behavior for vertical roll angle target and for 10 degrees roll angle target (steady cornering) at around 2.5 m/s. They also compared experimental results with simulations for straight ahead running with a lateral impulse on the rear frame and found very good agreement.

Three projects have successfully implemented steer angle (position) control: A motorcycle rider robot by Miyagishi *et al.* [97] and two bicycle robots by Tanaka & Murakami [145, 146] and Yamaguchi [170]. However while the motorcycle rider robot by Miyagishi *et al.* was position controlled, the motorcycle itself was torque controlled. The constructed rider robot was designed for carrying out objective handling quality tests and therefore the rider robot was connected via springs and dampers to both sides (left and right) of the handlebar simulating rider passive properties and making the motorcycle itself torque controlled.

Initially Miyagishi split the steering control algorithm into two parts which were constructed in parallel: a PD controller on the roll angle and rate for upright stability was successful. The implemented weighted proportional lateral position controller for tracking conflicted with the stability control. They thus went over to proportionally tracking a target roll angle which is then used as the set point for the posture control. Changing the stabilizing and tracking algorithm to a serially implemented system.

Tanaka & Murakami based the control of their robotic bicycle on the dynamics of a theoretical point mass model of a bicycle (Getz like [47]) with no steering dynamics. They too implemented separate controllers for stabilizing and tracking in series. The stabilizing controller consisted of a PD controller (again roll angle and rate). Two path tracking controllers were implemented: First a lateral velocity controller was tried, based on proportional control with respect to the (set) lateral velocity, which they found to destabilize the posture control as a result of unmodeled dynamics in the system. Secondly they implemented a more robust proportional controller using the desired rate of change of path curvature per path length as the control variable. This tracking controller in combination with the stabilizing controller was found to be stable.

Yamaguchi recently (2011) applied "steer into the lean" control to stabilize a (scaled) bicycle by a biped robot that can pedal and steer. The Biped robot uses PID control of

the roll rate signal from a gyroscope in the robot and uses servos to actuate the joints in the legs and arms. The bicycle is stabilized by the robot but the general heading is remotely controlled by a human. No information is available in the open literature about this bicycling biped robot as yet and thus it is unclear if it is really using steer angle control.

Finally, Lenkeit [83] was the first (and only) to develop a motorcycle robot using steer angle control at low speed and steer torque control at high speed. He had concluded from reviewing Weir's work [161, 162] that to control the motorcycle with only a steer torque actuator (DC motor) that the steer motor had to be configured as a position servo below 30 km/h and a torque servo at higher speeds for which he only required the roll angle to be fed back. The general direction of the motorcycle was controlled by a human via a radio link (tracking not implemented), and switching from position to torque control was done manually at 30 km/h. He reportedly found that good control was achieved below 20 km/h and above 35 km/h whilst between 20 and 35 km/h he describes a lightly damped oscillation being present, but no results were published.

Moving mass control Theoretical results indicate that stabilization and tracking using only lean torque, by an inverted pendulum or laterally moving mass, is far more difficult than through steer control as far larger gains in the feedback are required. Only two projects have attempted to stabilize a bicycle using lean torque control. The first was van Zytveld [155] in the mid 1970s, who applied lean torque control to an inverted pendulum placed on a bicycle powered by a gasoline engine. The project failed to stabilize the bicycle due to the neglected geared inertia of the used electric motor.

The second, larger project which is still ongoing, by Yamakita *et al.* [172, 173, 105, 171, 69], has taken advantage of the modern more controllable electric bicycle as the platform on which they have applied their pendulum control. They are particularly interested in extreme low speed stabilization and the possibility to stably adjust the vehicles vertical orientation, (which is not possible with a gyroscope) and to track a desired vehicle orientation path in time (posture tracking). Therefore they model the bicycle as a double inverted pendulum (roll and lean angle, no steering) to carry out stabilization control at stationary and very low speed (< 2 m/s). While the balance of a bicycle by an inverted pendulum model is interesting, it only works at low speed. The faster the vehicle moves the less it looks like a double pendulum due to its ability to steer.

Yamakita *et al.* independently implemented two separate controllers: a non-linear controller for the stabilization; and a linearized input-output controller for posture tracking. They note that as the two controllers were developed independently and use the same dynamical system they will cause some oscillations and offset to the balance control. Therefore a shift on the lean angle and rate set point for the balance algorithm should be applied. Interestingly though they do not need to perform this offset in either their simulations or experiments as the bike performs well enough without it. They carried out simulations to show that the bicycle is indeed stable and can track an ori-

entation. The experimental machine confirmed this, but they had to use a modified control algorithm by adding an H_∞ controller (in the feedback loop) for robustness as the theoretical controller did not work on the experimental machine. The robustness of the controller was demonstrated by using the same controller in stationary and low speed trials [173, 105]. But as yet no successful stabilization and tracking control has been implemented at a wide range of speeds by moving mass control. In later studies Yamakita *et al.* theoretically implemented trajectory tracking [171] using steer torque control and recently they adapted the moving mass controller and apparatus such that it can also be configured to act as a gyroscope [69].

Control with a gyroscope Single track vehicles with some form of gyroscope control applied have been successfully implemented by a number of authors including [104, 46, 147]. Either the gyroscopic precession or the adjustment of the gyro speed supplies the required torque to keep the bicycle upright. The use of fast spinning gyros is mainly credited by the authors to the extreme level of continuous stability that this method can produce when compared with steer control and moving mass control for stationary and slow moving vehicle. The speed range that the authors generally investigate and apply control to is therefore also generally stationary and low speed (< 1 m/s). Different types of controllers for controlling the required gyroscopic precession have been implemented; based on root locus [46], and H_2/H_∞ control [147]. Active stabilization by the adjustment of the gyro speed has been implemented by Murata [104], who made a robot riding a miniaturized bicycle using a gyroscope inside the robot's torso. The bicycle itself is not controlled, but the robot measures its orientation and calculates its center of gravity and accelerates the gyroscope such that the center of gravity comes over the wheel contact line. The resulting bicycle motion is very un-natural as can be expected from such a stabilized system as the rider has to remain in an upright position at all times to prevent the gyro from reaching its "top" speed and therefore no longer being able to provide the required stabilizing torque. Although both precession and spin rate actively controlled gyroscopes have been shown to work, neither though seems to be an ideal candidate for automatic control though due to the required power.

Strictly speaking the passive implementation of a gyroscope to slowdown the dynamics of the vehicle is not "control" however, it can be used in combination with other forms of control such as steer control. This is the core of the Gyrobike [55] product, where a fast rotating gyroscope inside the bicycle front wheel is used to reduce the level of instability of children's bicycles enabling the child to learn to cycle without the bicycle falling over as quickly as would happen without the gyroscope. By adjusting the gyroscope's rotational speed the level of stability is adjusted. The added value of such a stability enhancement tool is questionable though. The gyroscope changes the dynamics of the bicycle significantly so the user still has to get used to a normal bicycle without a gyroscopic front wheel. Also the duration that the wheel is required (which they claim can be as little as 5 minutes) by the young rider, make it questionable whether it is a financially worthwhile investment.

Multiple control methods Two sets of multiple control methods have been applied successfully. The first is the use of both steer and lean for the stabilization and tracking by Nagai [106] and Iuchi *et al.* [65]. Nagai and Iuchi both applied lean torque (position) control through the use of an inverted pendulum. The second method is the use of steer control in combination with a gyroscope for stabilization and tracking which was implemented by the Berkeley University Blue Team on their Ghost Rider Robot autonomous motorcycle. This motorcycle was designed to participate in the DARPA Grand Challenge 2005, a race across the desert for autonomous vehicles [85, 174], and was far more advanced than the vehicle by Nagai and Iuchi as it had GPS navigation and stereo vision implemented for its autonomous tracking capabilities.

Unlike the Ghost Rider Robot, neither Nagai or Iuchi carried out experiments on the “open road”: Nagai placed the bicycle on a treadmill; Iuchi on rollers, thus the extent to which “tracking” was taking place is debatable. However both did carry out stabilization experiments, whilst Iuchi’s tracking task was simply to keep the bicycle on the rollers, and Nagai performed lane change maneuvers.

To investigate the required control for stabilizing and tracking both Nagai and Iuchi developed simplified linearized equations of motion for a bicycle with a leaned upper body. Nagai used a point mass bicycle (massless front frame and wheels) whilst Iuchi used a very simple double pendulum model. For the control Nagai used the lateral deviation from a preview point (as a function of steering angle) and the roll angle as control variables, Iuchi used the roll angle and roll rate of the bicycle as the reference inputs.

Nagai found good agreement with his models except for the situation in which only leaning for tracking control was used. This difference between the simulation and experiments he contributed to backlash and large time delays in the experimental system. Based on his lane change experiments Nagai concluded the moving mass reduces the time required to carry out a lane change maneuver, however it also increases the size of the steer and roll angle response. Iuchi had to implement completely different control gains on the experimental bicycle compared to the model, in order to stabilize the bicycle, and even then he was not able to keep the bicycle on the rollers for long periods of time. This led him to conclude that the used bicycle model does not consider the physics sufficiently.

The Ghost Rider Robot’s control was, similar to Nagai, based on a simple point mass bicycle model [47] and had to be tested extensively. Due to all the uncertainties between the model and the actual motorcycle they initially used a fuzzy logic controller based on intuition and 125 parameters to stabilize the motorcycle, but this only worked at low speeds (3 – 6 miles per hour). They then changed to a PID controller for which they found the parameter sensitivity to various terrains. This worked better but as it counted heavily on the integrating factor the directional response was slow. To further improve the system they converted the PID controller to a run-time reinforcement learning (neural network) controller based on a stochastic model of the vehicle dynamics. Despite the installed gyroscope, they had trouble controlling vehicle whilst in the

air (jumps).

From the above it appears that it is essential to use a model that describes the motion of the vehicle sufficiently. Even with a relatively simple model (Nagai) good results can be achieved with a very simple controller for both stabilization and tracking. On the other hand when the model is probably not sufficient (Iuchi and the Ghost Rider Robot) far more advanced control models are required and still the results can be mediocre.

2.3.4 Rider Modeling Discussion and Conclusions

Models have found that steering is the dominant control method involved in the stabilizing task for both bicycles and motorcycles and performed observation experiments confirm this. Classical control single output (steer only) motorcycle rider models for the stabilizing task have been shown to compare well with actual rider data. Roll angle to steer torque was found to be the most effective transfer function for stabilizing a motorcycle. But position classic control models have also been developed for a rider on a bicycle simulator, that compare well with experimental data. However no bicycle rider models have been experimentally validated as yet. As both position and force control have been shown to model rider control well it could therefore be interesting to investigate if steering impedance control is even better.

Observation experiments have found that riders appear not to use their upper bodies for stabilization control when they have their hands on the handlebars. LQR optimal control and intuitive control models have also shown that it is highly unlikely that upper body lean will be used for stabilization at low speed as the gains required are too large. Modeling a rider as rigidly attached to the bicycle only able to perform steer actions (based on roll angle information) therefore appears to be a good option for a rider model for stabilizing control.

Classical control multiple output models (steer and lean) have been developed for performing tracking and stabilizing tasks that compare well to actual rider data. The addition of the tracking task does not significantly alter the roll to steer gains for classical control models capable of stabilizing by steering. Stabilization and tracking have successfully been implemented in parallel in machines that use steering and moving mass control. However for machines with only steering control (single output) tracking and stabilization has been successfully implemented in series. An open question is if tracking and stabilization can be implemented in a single controller.

Research into the optimal steering control for tracking with a motorbike shows that good response can be achieved with very little controller effort by applying the control in the vehicle's dominant eigenmode (weave or wobble). Experimental observations performed with a bicycle and rider with hands on the handlebar have found that most steering motion occurs in the pedaling frequency. This could also be due to a similar mechanism as the pedaling motion causes a large cyclic perturbation that has a similar effect as the intrinsic weave or wobble vehicle modes.

The required preview distance for tracking capabilities depends on the vehicle being

used. For bicycles 2.5 seconds is enough, but for motorcycles the preview distance is speed dependent. Optimal control models have also shown that for a bicycle the tracking performance improves with increased preview distance, but that there is a limit after which the extra preview distance does not add to performance anymore as its weighting factor is almost zero. These theoretical results however have not been experimentally validated. The preview time required to safely control a vehicle can be of interest to traffic and road planners as it can have an effect on the design of intersections and tight or blind corners.

Rider upper body motions in general have been shown to only have a small influence on the overall motion. Furthermore it has been shown that upper body motions are most likely to be performed to control the orientation of the rider's head for comfort reasons and not the direct control of the vehicle. However, optimal control models have shown that upper body motion can contribute to maneuver performance, particularly for maneuvers such as a lane change. Motorcycle rider observations have shown that riders perform different control depending on their level of experience. Novice riders apply more roll steer torque than experienced riders to initiate a turn whilst experienced riders can apply large upper body motions as part of their strategy to perform a maneuver more effectively. Therefore for the development of a universal rider model, rider's experience will have to be parameterized. Interestingly though the more difficult the maneuver task that is set, the more alike the experienced and inexperienced rider control actions become. Observations also indicate that for the successful completion of a maneuver the timing of the applied control is more important than the amplitude of the applied control. This fares well with the idea that the applied control can be of an intermittent nature as found for stabilizing control.

2.4 Handling Qualities and Maneuverability

The handling qualities of a vehicle are related to its stability and control characteristics. A vehicle's maneuverability is related to its ability to perform a specific (set of) maneuver(s).

The aircraft industry obviously had most to profit from research on handling qualities. Each airplane has to be controlled precisely in order to be able to land safely, fighter aircraft have to be highly maneuverable to avoid being shot down, yet still have to be controllable for the pilot, and many early aircraft suffered from pilot induced oscillations during flight. Thus it is not surprising that this is also where most of the insight into handling qualities initially was developed. Cooper and Harper [24] were the first to precisely define what they mean by handling qualities of aircraft, namely: 'Those qualities or characteristics of an aircraft that govern the ease and precision with which a pilot is able to perform the tasks required in support of an aircraft role'. Where they defined "task" as 'the actual work assigned to a pilot to be performed in completion of or as representative of a designated flight segment' and "role" as 'the function or

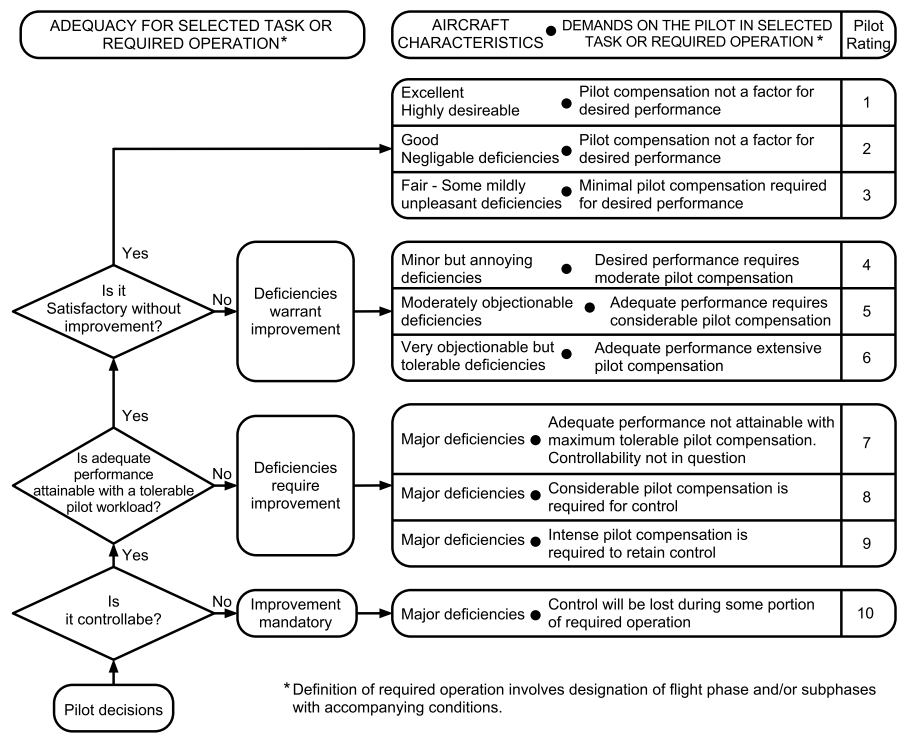


Figure 2.6: *The Cooper-Harper handling qualities rating scale.*

purpose that defines the primary use of an aircraft’.

Cooper and Harper state that both physical and mental workload need to be taken into account when rating a handling quality. They argue that a pilot can perform specific maneuvers just as well in very differently behaving aircraft and that the measurable physical workload can be identical but that the mental workload can be very different. They therefore developed a 10 scale pilot rating system (shown in Figure 2.6) for determining aircraft handling qualities which became the norm for the industry and beyond. This rating system takes the mental workload into account.

Correlations have been found indicating that handling qualities can be linked directly to control effort. McRuer and Jex [90], and Hess [60] found that the pilots perception of the task difficulty and therefore, of vehicle handling qualities are highly correlated to the ‘power’ of the pilots output-rate feedback signal. They therefore only look at the physical workload and use it to define the handling qualities. This changes handling qualities to a control feedback problem. They found that the complete closed loop system wants to act as a first order system (20 dB/decade drop off in a Bode plot) around the cross over frequency and where the desired band width is achieved by the pilot’s control effort.

The most significant difference between aircraft and bicycles and motorcycles, with regard to designing for handling qualities and control strategies, is their ratio of pilot/rider to vehicle mass. The mass of a motorcycle rider is usually around 50% of the total mass while for bicycle the rider can be as much as 90% of the total mass. On the other hand, for a fighter aircraft the pilot mass is typically less than 1% of the maximum take-off weight. The position, orientation and exact mass of a rider on a bicycle or motorcycle have a far greater influence on the open loop dynamics of the system than they do in an aircraft. Furthermore any motions executed by a aircraft pilot that do not disturb the control stick or rudder pedals will have little to no effect on the aircrafts trajectory, whilst for a bicycle or motorcycle the body motions that do not disturb the handlebar directly can still cause a trajectory change of the bike as a result of the lean to steer coupling and relatively large mass of the rider. Examples of how the control strategy influences the trajectory of the vehicle, enabling different riders to complete the same maneuver in different ways were shown by Cossalter [25] for a U-turn maneuver and Rice [118] for a steady turn and for a lane change maneuver. Rice found large differences in control strategy performed by novice and skilled riders. Both Rice and Cossalter concluded that a rider on a motorcycle can successfully carry out a specific maneuver in many different ways. Cossalter however also stresses that the rider's subjective interpretation determines the handling qualities of a vehicle. He points out that this subjective rating depends on the rider's driving style and sensitivity, and on the motorcycles; response to lateral acceleration and yaw rate, sideslip, sensitivity to external disturbances, response to control actions under different circumstances, and the feedback between rider and motorcycle.

Bicycle and motorcycle designers can however only develop the machine part of the complete machine–rider system. They design their machine generally for the following roles:

- accident avoidance maneuvers: safety aspects
- normal riding: the safe use in and amongst traffic whilst obeying the traffic rules
- racing: the completion of a lap around a circuit in the shortest possible time

The first role is more a 'segment' of the 'designated flight plan' for which the designers would want to achieve maximum performance on in all circumstances and this has (logically) received most of the attention. The last two roles generally lead to very different looking vehicles, largely as a result of ergonomic and aerodynamic aspects. The next sections discuss these three roles in order.

2.4.1 Handling Qualities for Accident Avoidance: Safety

Most safety related handling quality work has been done experimentally where the complete system: bicycle and rider, were tested simultaneously. No standard tests were used, making direct quantitative comparisons between experiments impossible. The various tests are shown in Tab.2.4. The 'tasks' that have to be performed for safety are often

categorized under the general terms 'maneuverability' and 'stability'. None of the studies actually defined what they exactly mean by these general terms however the general gist can be extracted from the experiments they carried out.

Bicycles

A number of studies were carried out to investigate the effect of different parameters on the 'stability' and 'maneuverability' of bicycles. Rice, Roland and Massing [121, 122] first investigated the lateral stability and control of 2 types of bicycle that were popular in the late 1960s and early 1970s and then investigated the effect of nine parameter changes on the same instrumented bicycle (load on the rear, the rider and the front, increasing the mass moment of inertia of the front wheel and under-inflating the tires) for 4 experiments (straight line, obstacle avoidance and a narrow and wide slalom). They concluded that the standard bicycle is the best and that load in the rear placed low is good for 'maneuverability' whilst load on the rear placed high is bad for 'maneuverability'.

The effect of different style handlebars (high rise, standard and racing) on the 'maneuverability' of the bicycle was experimentally investigated by Mortimer *et al.* [103]. Riders carried out 7 experiments and rated each bicycle and each task on a 5 point scale. They concluded that 'since the high rise handlebar configuration allowed good maneuvering performance it should be considered an acceptable design. Standard handlebars offer a good compromise between the characteristics of the racing and high rise types, and provided stable, low speed tracking which is important for safe riding on streets in the mix of other traffic.'

Godthelp, Buist and Wouters [51, 52] developed a bicycle which they could change geometric parameters such as the wheelbase, trail, and moments of inertia of front frame and wheels, and carried out 4 experiments in each configuration (see Tab. 2.4). They also carried out these experiments with 4 different style bicycles and motorcycles and conclude that all bicycles have the same high speed stability. For low speed stability and maneuverability they conclude that the rider position is dominant and once again the racing bicycle and the high-rise handlebar bicycle were the worst.

The effect of different riding positions and bicycle styles on a child's ability to control a bicycle safely in traffic was investigated by Arnberg & Tyden [6]. They used the time to complete an experiment as a performance measure in 10 tests to measure the 'stability' and 'maneuverability' of 6 different bicycles when controlled by children for three styles (normal, collapsible and rodeo) of bicycle with two types of handlebar (normal and high rise). They, similarly to [103] concluded that bicycles with extreme handlebars have a poorer maneuverability performance than those with standard handlebars and that the race handlebars make the bicycle least maneuverable whilst high rise handlebars are OK. Also similarly to Roland & Lynch [122], they concluded that the rodeo style bicycles (mass high and to the rear) has the worst maneuverability performance out of the three tested models.

Similar safety experiments with young children were carried out by Wierda, Roos &

Term	Authors	Experiment	Performance Measure
'Maneuverability'	Mortimer, Domas, Dewar [103]	Slalom at 5, 8, 10 and 12 mph and max speed	Crossing boundary and cones, max speed
	Arnberg, Tyden [6]	Block slalom, block pairs, 1 handed curve, 'relay' riding and steady-state circle	Time + interview
'Performance' 'Control'	Godthelp, Buist [51]	Complex slalom	Time
	Wouters [52]		
	Rice, Roland [121]	Slalom	Minimum time
	Roland, Lynch [122]	Slalom	Max speed
	Mortimer, Domas, Dewar [103]	Circle, figure-eight, lane change	Time
High speed 'stability' & maneuverability' Medium/High speed 'stability'	Arnberg, Tyden [6]	10 mph, 90° corner	Minimum radius
		Stationary balance, ride between 2 narrow gates: a) constant speed, b) accelerate from rest	Time + interview
	Godthelp, Buist [51]	Straight + bend with either left, right or both hands on handlebar	Time
	Wouters [52]		
	Mortimer, Domas, Dewar [103]	Straight between two lines	Boundary crossings
Low speed 'stability'	Arnberg, Tyden [6]	Looking backwards over shoulder for a number	Boundary crossing, recalling number
	Godthelp, Buist [51]	Straight between two lines	Relative time between lines
	Wouters [52]		
	Rice, Roland [121]	Hands free straight ahead	Minimum speed
	Roland, Lynch [122]	Straight line hands on	Minimum speed
	Mortimer, Domas, Dewar [103]	Straight between two lines	Boundary crossings
	Arnberg, Tyden [6]	Straight between two lines	Time + interview
	Godthelp, Buist [51]	Straight between two lines	Relative time between lines
	Wouters [52]		

Table 2.4: Bicycle maneuverability and stability experiments and how the performance is rated

Wolf [165, 166] to investigate 'maneuverability'. However, they did not measure the time the rider used to complete the experiments; instead they only recorded the errors made as they view 'safety' completely from the traffic point of view: to safely ride on the roads, the rider should be able to carry out the specified maneuver in a specific section of the road as any deviations could result in contact with another road user. They conclude interestingly enough that there are no major differences in 'maneuverability' between the different bicycle styles for children.

Motorcycles

The 'maneuverability' of a motorcycle and automobile was experimentally compared by Watanabe and Yoshida [158] by carrying out the same evasive maneuver with motorcycles and cars. They found that the motorcycles required significantly longer distances than cars, even though the cars are much wider than a motorcycle. They also found that less skilled riders require 15 to 20% more distance to avoid the obstacle than skilled riders. Furthermore speed has less influence on the performance of skilled riders than unskilled riders who seemed unable to produce large steer-torques at higher speeds. They conclude that for motorcycles riding at speeds above 30 km/h they would consider maneuvering around an object instead of attempting to stop before it as the better evasive maneuver due to the distance to speed relationship that a maneuver has whilst stopping has a distance to speed squared relationship.

Safety discussion

All the experimental ratings listed above are comparative, using relative scales and vehicle/rider combinations. Therefore within a single study vehicles and vehicle properties can be compared, but this is not possible between studies as they are not universal. Also none followed the Cooper-Harper methodology whereby the physical and mental workload had to be measured. Most did not even interview the rider to get an indication of the mental workload level.

However from the above it does appear that most authors refer to 'stability' within the framework of 'safety' as the ability of the bicycle and rider system to remain upright and within a narrow straight path. Stability is measured in terms of deviations from that path or by the minimum speed that the maneuver can be carried out at. The term 'maneuverability' usually refers to the system's ability to change direction, such as in a slalom or lane change. A more 'maneuverable' vehicle can carry out the same maneuver at a higher speed (slalom) or in a shorter time/distance (lane change). The maneuverability of vehicles appears to largely depend on two factors: the mass distribution of the system, in particular the riders location and orientation (moment of inertia) and the style of the handlebar and thus the riders ergonomics.

2.4.2 Handling Qualities for Normal Riding

Normal riding refers to the bulk of a vehicle's usage on open roads: not under extreme circumstances or at the performance limits.

Bicycle research on this role is surprisingly scarce. However, many have hypothesized that a self stable bicycle is preferred over an unstable one as the unstable bicycle requires active rider control to be stabilized [95]. Herfkens [58] carried out bicycle model parameter investigations in the late 1940s. He concluded that to increase the low speed stability of a typical Dutch bicycle the head angle should be increased, the trail decreased, the mass of the front frame decreased and the mass of the front wheel increased.

Jones [66] in a quest to discover what makes a bicycle stable developed a number of what he called "un-rideable bicycles". He reasoned that a bicycle moving slowly is unstable and almost un-rideable i.e. the rider cannot keep the bicycle upright, but a bicycle moving at high speed is stable and also easily rideable, and that the stability is therefore connected to a measure for how rideable the bicycle is. To discover more about the stability of a moving bicycle he made examples that should be unstable and therefore un-rideable. He however found that the destabilizing effect of a counter rotating gyroscope had very little effect on the rider's ability to stabilize the bicycle, while the inherent stability of the bicycle was affected dramatically. On the other hand he reasoned and experimentally found that by adjusting the bicycle's trail he could make a bicycle that was both unstable and un-rideable or uncontrollable for the rider. He attributed this to the trail which has to remain positive and gravitational forces to be overcome to return to the upright straight ahead orientation. Jones' theories on stability were shown to be incomplete by Meijaard *et al.* [94].

The book "Lords of the Chainring" by Patterson [110] has been used by students in a bicycle design class to develop out of the ordinary bicycles with good handling. The book gives design guidelines based on aircraft handling quality analogies. It also discusses that the steering stiffness is an essential design parameter for bicycles. Design guidelines are given including equations such as for the roll control authority which links the roll rate to the hand movement. These equations are only subject to geometrical parameters of the bicycle and not the masses and inertias, making the validity doubtful, however good results are claimed to have been achieved with this method by Patterson & Leone [111].

More has been done for motorcycles. Tony Foale has a whole book on Motorcycle handling and Chassis design [42]. He defines handling as (p.1-1): "By this we mean the ease, style and feel with which the motorcycle does our bidding." Foale continues by saying that this depends on the overall geometry, chassis stiffness, weight and its distribution, tire type and size and that also the rider responses have a major influence on the handling characteristics. In a penultimate chapter he talks about "feel", by which he means the proprioceptive feedback to the rider as a sensor of how far he can get with braking, cornering etc., and points out that this is an important factor in good rider control. In the last chapter he reports on some nice experiments on a BMW R75/5

Test	Handling index	Good handling achieved when
Steady turning	$\text{Roll factor} = \tau / \varphi$ $\text{Acceleration factor} = \frac{\tau}{V^2 / R_c} \cong \frac{\tau}{g \cdot \tan \varphi}$ $\text{Yaw factor} = \frac{\psi}{\delta}$	Low values, small negative steer torque
U-turn	$\text{Koch index} = \frac{\tau_{peak}}{V \cdot \dot{\varphi}_{peak}}$	Low values
Slalom	$\text{Roll transfer function} = \frac{\tau}{\varphi}$	Small phase
Lane Change	$\text{Lane Change Roll index} = \frac{\tau_{p-p}}{\dot{\varphi}_{p-p} \cdot V_{avg}}$	Low values
Obstacle Avoidance	Time lag between τ and $\dot{\varphi}$	Small lag

Table 2.5: *Maneuvers used for rating motorcycle handling, the indexes used to rate them and the corresponding values for good handling according to [25, 32]. Where τ is steer torque, φ roll angle, ψ yaw angle, δ steer angle and v forward speed.*

motorcycle with various head angles and trails. His conclusion is that there is nothing magical about currently used values (27 degrees and 9 cm) almost anything (positive!) is rideable, even given some moderate forward speed with hands-off.

The other research on motorcycles has been largely focussed on developing test maneuvers and then correlating experimental results with simulation results and using simulations for predicting handling.

To rate different maneuvering aspects such as steady state and transient behavior in separate maneuvers five tests have been defined (steady turning, U-turn, slalom, lane change, and obstacle avoidance test) [120, 25]. For each test, handling indexes have been developed, these are described in Tab.2.5. The lane change maneuver has received most attention from researchers.

The ‘Koch index’ [72] was defined to classify the ease with which a turn is entered (transient response) by relating the peak in steer torque to the first opposing peak in roll rate. Later the ‘lane change roll index’ (LC index) [32] was defined to classify the transient lane change maneuver by relating the peak to peak rider input steering torque to the peak to peak roll rate of the motorcycle. Both indexes are normalized by the forward speed. These handling indexes have been found to correspond well with what is perceived as ‘good handling’.

The LC index was shown to be an objective function for comparing motorcycles [32], and in the same study it was shown with an analytic approximation of the LC index that motorcycle ‘maneuverability’ is dominated by front wheel inertia properties. Earlier ‘performance maps’ for a lane change, which are the loci (xy plot) of the steer torque and roll angle (the quotient of which is the roll factor), were investigated by Rice [118]. With these plots he was able to distinguish between successful and unsuccessful maneuvers

Characteristic Value	Nomenclature
Peak steering torque in stationary test	T_{s1}
Peak roll steer torque in stationary test	T_{r1}
Static torque ratio	$\epsilon_1 = (T_{r1}/T_{s1})$
Peak steering torque in actual running test	T_{s2}
Peak roll steer torque in actual running test	T_{r2}
Dynamic torque ratio	$\epsilon_2 = (T_{r2}/T_{s2})$
Resultant dynamic steering torque	$T_2 = \sqrt{(T_{s2})^2 + (T_{r2})^2}$
Rider control torque	$T_{rc} = (\epsilon_2 - \epsilon_1)T_{s2}$

Table 2.6: Characteristic measures used by Kuroiwa et al. [82] to investigate steering effort in a lane change maneuver. They perform two experiments, the first stationary with the motorcycle held upright where the rider applies a $\pm 5^\circ$ sinusoidal steering input. The second experiment is a lane change test.

and different riders.

Lane change maneuvers on motorcycles were simulated and carried out experimentally by Rice and Kunkel [120] and Zellner and Weir [177]. The latter also developed a steady-state turn maneuver and used the roll and yaw factors to compare experiments with simulations with mixed success.

The rider's perceived steering effort in a lane change maneuver has been shown to Correlate with the resultant steer torque and the rate of change of rider control torque (T_2 and T_{rc} see table 2.6) for a lane change experiment by Kuroiwa et al. [82]. Interestingly these measures include the rider applied roll steer torque and was found for a wide range of rider experience.

The influence of the dominant rider mass on the lateral dynamics of mopeds compared to motorcycle dynamics was analytically investigated by Zellner and Weir [178]. They concluded that the moped is more sensitive than the motorcycle for steer torque control yet the required rider lean input is (surprisingly) the same for the motorcycle and much lighter moped.

2.4.3 Handling Qualities for Racing

In racing the main goal is to complete a specified course in the shortest possible time. Here, rider comfort is only deemed of importance if it is a limiting factor for increasing speed and the decreasing lap time. Handling qualities for the racing 'role' are therefore linked to performance factors.

Oddly enough, and despite there being a massive bicycle racing industry, handling quality research within the racing 'role' has only been performed on motorcycles. The only exception is the recent work by Cangle et al. [15] where they model the bicycle (including aerodynamic drag), track and rider, to determine the optimal bicycle for a specific time trial track. On the other hand a plethora of biomechanics, aerodynamics,

physiology, frame and component stiffness and mass, and suspension dynamics research has been carried out over the years with respect to increasing cycling race performance levels [167, 179]. These investigations only focus on optimizing either the riders physical output level, or the material they were using and were never aimed at optimizing speeds for specific corners or the required rider control. Generally, but certainly for road bicycles this is the case, very little has changed over the last 110 years with respect to bicycle geometry other than a sloping upper-tube and the result of adapting material and fabrication techniques. If this is because the design is already near to optimal with respect to handling for racing through the evolution process, or because there is no need for good handling qualities, we do not know. The rest of this section on handling qualities for racing will only focus on motorcycles.

The most active group in the motorcycle racing handling qualities area has been the group of Cossalter at Padua University. For roughly the last 20 years they have been investigating motorcycle dynamics and control. Cossalter [25] has clearly defined what he means when talking about 'Directional stability', 'maneuverability' and 'handling' with respect to racing. They are:

Directional stability: The ease with which a motorcycle naturally tends to maintain its equilibrium and follow a rectilinear path. It depends on the intrinsic vehicle characteristics; inertial properties of the motorcycle, forward speed, geometric properties of the steering head (which collectively determine the aligning effect of the trail), gyroscopic effects and tire properties.

Maneuverability: An intrinsic vehicle performance measure relating its ability to do maneuvers to the time required to do the maneuver. One can therefore quantify a vehicle's 'maneuverability' by finding the best performance (shortest time, shortest distance, etc.) that a the vehicle can do on a specific maneuver and relate that to the performance of other vehicles on the same maneuver.

Handling: Is the ability of the vehicle to do complex maneuvers taking into consideration the driver's limits. It does, however, not include the rider's mental workload. It is evaluated by comparing the control effort required for the different vehicles to perform their specific optimal maneuver, where less effort relates to a better handling vehicle.

To find an objective measure for maneuverability of motorcycles independently of the rider the theoretical 'optimal maneuver method' was developed by Cossalter *et al.* [27, 28]. This optimal control method was discussed earlier in section 2.3.2 on page 26. The required optimal control for a specific maneuver is vehicle dependent; therefore vehicles can be rated by comparing the optimal performance on a specific maneuver. Within the context of the 'optimal maneuver method' when the rider limitations (physical and physiological limits such as the maximum torque the rider is able to apply or maximum steering rate they are able to reach) are included as limitations in the optimal 'maneuver', then the achieved performance quantifies the 'handling'.

Another approach to understanding maneuverability and handling is the concept of the instantaneous screw axis or Mozzi axis about which the vehicle rotates. Cossalter *et al.* [25, 29, 26] link the instantaneous screw axis with the concept of handling by realizing that large movements of the screw axis trace comply with demanding tasks. Using this concept they are able to distinguish different kinds of behavior in transient maneuvers and identify the different phases of a maneuver such as entering and exiting a curve.

Certain parts of a maneuver are more 'complex' than others and this has been linked to the change in kinetic energy associated with the change in orientation of the whole system. To investigate racing rider skill and effort as well as the motorcycles performance, an energy analysis of transient manoeuvres was carried out on data collected under race conditions and analyzed by Cossalter *et al.* [26]. They found that in a U-turn there are 3 locations where there are large changes in kinetic energy and these locations coincide with the counter steer phase (initiating the turn), the point at which maximum rotational energy occurs (after which the throttle is applied again) and at the exit. They therefore predict that the time rate of the rotational kinetic energy can be used to extract phases of the maneuver and the dynamic limit.

Many researchers have investigated handling and maneuverability for racing using multi-body packages in combination with control. Berritta & Mitolo [10] used performance indexes as a measure to investigate how design parameters affected the performance of a U-turn maneuver. Capitani *et al.* [16] modeled a scooter in ADAMS/motorcycle multibody dynamics software and compared with measurements made with a real scooter for a lane change, J-turn, large and small radius 90° turn and a figure eight. The results did not compare well, which they suspected was a result of unmodeled rider motion, as the rider (inadvertently or unconsciously) used movement as part of the scooter maneuver control. Giner *et al.* [50] implemented rider motion as an inverted pendulum in a multi-body model of the motorcycle and rider based on motion capture data of real riders on a stationary motorcycle simulator. The pendulum control was based on the bikes' location in the corner and the equivalent motion capture measurements.

To research the level of detail necessary in a motorcycle model to predict handling Frendo *et al.* [43] investigated the differences with three levels of model detail. They found that a non-linear tire model greatly influences the results. Interestingly the geometric parameter study on handling they carried out, found, trend wise, very little difference between the three different models, indicating that simpler models can be used to predict handling improvements relative to an initial setup.

2.4.4 Handling Qualities Discussion and Conclusions

Bicycle handling quality research has only been interested in safety: accident avoidance. But no standard handling quality tests for bicycles have been developed. There is therefore no way to quantitatively compare the results of different bicycle handling experiments that have been carried out by the different authors.

In the bicycle research performed most authors do not accurately define what they mean by the terms: handling quality, stability or maneuverability, but from the experiments it can be deduced that most mean the same. However authors interested in normal riding generally measure stability as the ability to remain upright, whilst authors working on bicycle safety have an additional requirement that the bicycle continues in the same direction, which is defined as directional stability.

Motorcycle handling quality research has focussed mostly on determining quantifiable measures and repeatable testing procedures based around normal riding and racing situations. This has enabled authors to compare simulations and experiments often performed by different authors and often years apart! Furthermore indices have been developed for the different standard maneuvers with which good and bad handling can be predicted.

For bicycle research it is also essential to develop a standardized set of tests and handling indexes, in a similar manner to those that exist for motorcycles, such that bicycle handling can be compared and quantified both experimentally and in simulations. Another advantage of such a set of handling tests is that a set of handling qualities for normal riding can be determined, such that the designers, who now apply a time consuming trial and error method to developing new bicycle concepts, can determine a-priori what the handling qualities will be.

According to Cooper & Harper, handling qualities (for aircraft) are a factor of the complete rider(pilot)-vehicle system and depend upon both the physical and mental workload of the (pilot)rider. For aircraft, handling and maneuverability can be determined based on frequency and damping of the main dynamic modes. This could also be a method that could be applied to single track vehicles where the (unstable) weave and wobble modes are most likely to be modes of interest.

In single track vehicles, the rider has a large influence on the actual implementation of the maneuver, therefore comparing different riders output can be problematic. Furthermore, large differences have also been noted between the rider control for novice and experienced motorcycle riders. The development of a set of design guidelines based on rider control effort for different rider levels of experience could help manufacturers design bikes that are better suited to a certain group such as novice, intermediate or expert riders.

2.5 Discussion and Conclusions

Much effort has gone into the development of bicycle and motorcycle models. These models have been experimentally validated and can accurately model the dynamics of the vehicle. The Whipple bicycle model is the simplest model that offers the correct bicycle dynamics. On the other hand only a small number of rider control models have been developed of which the majority have been developed to simulate the stabilizing task control. None of the bicycle rider models have been experimentally validated.

There is thus still much to explore on the rider control side of the modeling of bicycles. Important in this discussion is the importance of the upper body. It has been shown for motorcycles that upper body motions only have a small contribution to the overall control of a vehicle, but they are most likely to be important for rider comfort and can be used for achieving better performance during transient maneuvers. However it is unclear if completely dismissing upper body motion on bicycles, where the rider to machine mass is much larger than on a motorcycle and cyclic motions due to pedaling take place, is possible.

There is no coupling at the moment between bicycle human rider control modeling and handling qualities. In fact only a few handling quality indices have been defined for single track vehicles of which all but one have been developed for motorcycles. Furthermore the only handling quality measure for bicycling that has been defined so far has yet to be experimentally validated. While many authors have performed bicycle handling experiments they have all done this according to their own specifications making only qualitative comparisons between different experiments possible. The development of standard performance tests and handling quality measures for bicycling therefore is an exciting area still waiting to be explored.

CHAPTER 3

Bicycle Rider Observations During Normal Cycling

3.1 Introduction

As a result of carrying out rider observations alternative rider models can be developed that could give a new insight into the riders' required control actions, which could in turn help with understanding handling quality aspects. Therefore the objective of these observations is to determine which bicycle rider motions are taking place during normal cycling from the perspective of rider control identification. The literature review in Chapter 2 revealed that authors have modeled the rider on a bicycle in a number of manners including: rigidly; as a (double) inverted pendulum where the lower half is connected to the frame and the upper is able to rotate about some point near the saddle to simulate upper body leaning; or as four moving masses to model the motion of the legs in recumbent cycling. The literature review also revealed that no authors ever verified that any of these models accurately describes the motions of a real bicycle rider. Therefore by actually observing the bicycle rider during normal cycling the importance of modeling certain degrees of freedom can be assessed. By observing the rider control actions at different speeds the importance of modeling specific degrees of freedom at a certain speed can also be evaluated.

Two sets of cycling observations were carried out. The first took place on an instrumented bicycle (see figure 3.1) on which a video camera lens with CCD was placed out in front of the rider and aimed at the rider. This camera was attached to the rear frame and as such any rider lateral motion relative to rear frame could be identified. These observations were used to qualitatively determine which motions are important during normal cycling and indicated that steering is the major control action at all speeds, that rider lean occurs only as a result of pedaling and that at very low speeds lateral motion of the knees occurs.

The second set of observations were motion capture measurements using active markers placed on the rider and bicycle and riding indoor on a large treadmill (see figure 3.3). By applying principal component analysis to reduce the data set and investigating the correlation between principal components and their frequency components it was found that all the lateral upper-body motion is related to pedaling.

3.2 Publication I: Bicycle Rider Observations

Kooijman, J. D. G., Moore, J. K., and Schwab, A. L. (2009). Some observations on human control of a bicycle. In *Proceedings of the ASME 2009 International Design Engineering Technical Conferences & Computers and Information in Engineering Conference*, number DETC2009-86959, DETC2009, Aug 30 – Sep 2, 2009, San Diego, CA.

The aim of the first set of observations was to simultaneously measure the bicycle's motions and observe, from the video, the rider actions during 'normal cycling'. The observations were carried out using a measurement bicycle which consisted of a standard Dutch Batavus city bicycle installed with a camera for collecting video images and a measuring system as shown in figure 3.1.

The measuring system consisted of a robust National Instruments CompactRIO computer that was placed on the rear rack, a geared potentiometer for measuring the steering angle, angular rate sensors for measuring the steer rate, roll rate and yaw rate, a reed relay cadence sensor and a dynamo pressed against the rear tire (an un-powered DC motor) to measure the forward speed. It was decided to use the rather rugged CompactRIO after earlier experiences with a laptop on the back of a bicycle had shown how fragile large electronic devices can be when carrying out mechanical experiments [74]. The CompactRIO, an FPGA controller and realtime computer has no (touch)screen or keyboard and no USB ports, it had an 8 port analogue input, 4 port analogue output, and wireless communication slots installed and ran on a 12V 1500mAh lithium polymer (LiPo) battery. To communicate with the CompactRIO the wireless and Ethernet connections were used.

Two observation experiments were carried out, one on the open road and the other on a large treadmill. The first experiment was carried out on the open road amongst traffic in Delft and included riding local roads, busy main roads, stopping at traffic lights, making a number of corners and riding a roundabout. The riders were instructed to ride as if they were on a normal cycling trip. There were many distractions (a dog even chased down a rider as can be seen in figure 3.2), and uncontrolled influences (wind, traffic) and while both hands were kept on the handlebar most of the time, some sections were ridden using one hand, no hands and one rider even answered his mobile phone whilst riding. Furthermore Delft's unevenly paved roads proved also to be a challenge for the measurement system, in particular for the un-stabilized video observations. All these aspects made it difficult to extract useful data from these experiments.

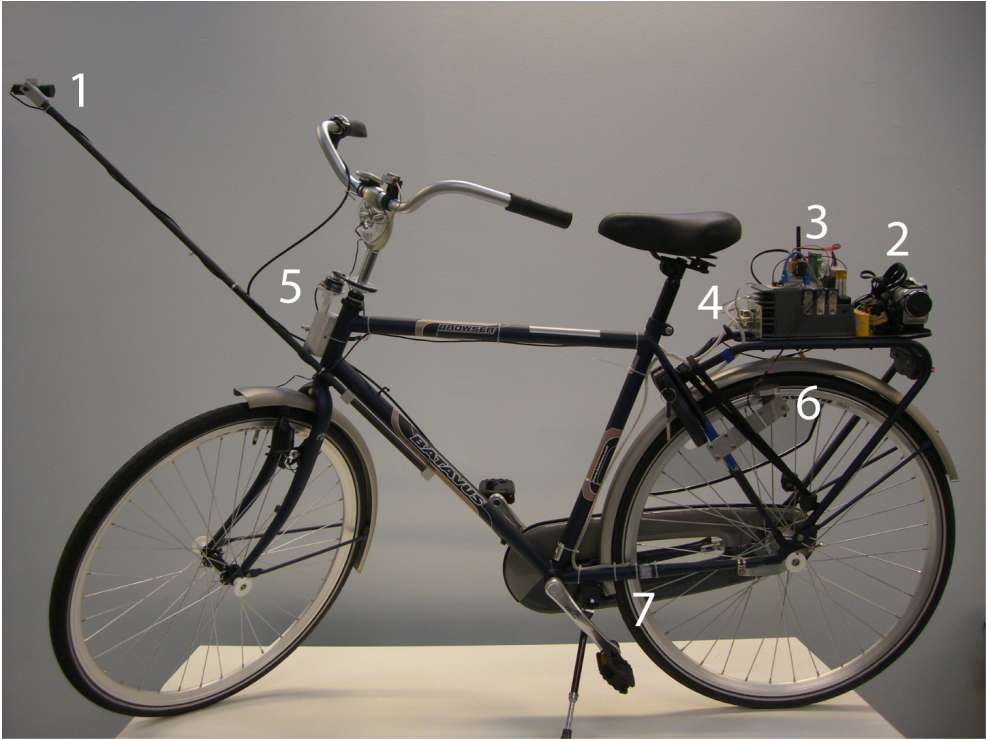


Figure 3.1: The instrumented bicycle with a camera-boom and lens facing the rider (1) at the front and camcorder (2), measurement computer (3), and angular rate sensors (4) for the yaw and lean-rate on the rear rack. A potentiometer and angular rate sensor measure the steer angle and rate (5), motor measures the speed (6) and reed relay the cadence (7).

Despite the above mentioned problems one interesting aspect that is consistently found in the data is that the speed always reduces prior to large steering motions taking place (making a corner). This even occurs when there is no critical parameter at play i.e. the corner is not taken fast enough such that the inside pedal could touch the ground (if it happens to come by the lowest point during the corner) and the tires can provide enough grip to prevent the bicycle from sliding away under the rider in the corner. The initial hypothesis was that the rider reduces the speed to bring the bicycle into the unstable speed range. By doing so the bicycle becomes easier to change direction as it automatically starts to weave. It was hypothesized that this could make it easier to change direction for the rider. However the investigation carried out by Heemskerk *et al.* [57] using the benchmark bicycle model found that the required steering control power (as defined by Sharp [138]) for making a specified corner does not decrease when the speed is reduced below the weave speed, but actually increases and their experimental results confirmed this. They hypothesize therefore that the reason for reducing forward



Figure 3.2: *Dog chasing a rider during the open road experiment*

speed prior to making a corner is psychological. Another hypothesis is that the pedaling motion introduces such a large disturbance or unbalance to the system that the rider stops pedaling to make the control easier. These Hypotheses still have to be tested.

Because of all the disturbances and distractions on the open road a second set of rider observations was carried out under controlled environmental conditions: indoors and on a large 3 m wide, and 5 m long (3 × 5 m) treadmill at the Vrije Universiteit Amsterdam at speeds between 2 and 30 km/h (see figure 5.1 on page 72). This greatly improved the repeatability of the observations. While the dynamics of the bicycle on the treadmill are the same as on the open road (see Chapter 5 and Publication V) the riding sensation is completely different. During normal cycling on the road the world moves relative to the rider, but on the treadmill this is no optic flow and this initially gives a very strange sensation. The fact that the treadmill was located on the 6th floor of the building and directly in front of a large window from which you can see far into the distance (and all the way down to the ground), also did not help the riders feel comfortable, especially when the treadmill was running at the higher speeds. The curtains were therefore shut and the rider was instructed to look at the treadmill belt to generate optic flow. After a couple of minutes of riding on the treadmill the riders became accustomed to the 'new' situation and felt comfortable and could ride normally.

Five experiments were carried out on the treadmill at speeds between 2 and 30 km/h with two very different riders. The riders differed significantly in height, weight, age and background. The riders performed:

- stabilizing while pedaling normally;
- stabilizing without pedaling, where the bicycle was towed by a rope connected at the head tube to prevent the bicycle from rolling backwards on the treadmill. This experiment was done to eliminate the harmonic lateral disturbance caused by the

pedaling motion;

- stabilizing while pedaling normally and recovering from a lateral perturbation. The lateral perturbation was applied by pulling a rope that was laterally attached to the rear frame just underneath the saddle;
- stabilizing while pedaling normally with no hands on the handlebar and;
- stabilizing while pedaling normally with no hands on the handlebar and eyes closed.

The last two experiments could only be done at higher speeds as the riders were unable to ride as slowly without their hands on the handlebar. Furthermore riding with eyes closed turned out to be easy for the rider except that he had no idea about his orientation and thus the experiment had to be terminated very quickly once a small deviation from the straight ahead occurred as he literally rode off the side of the treadmill.

Conclusions of the observations are that despite the significant differences between the two riders they both showed very similar results: From the video analysis the upper body lean appears to be linked to the pedaling motion - when the rider does not pedal no rider upper body motion is detected in the video. At very low speeds rider lateral knee motion suddenly appear in the videos, probably as a form of rider control. This knee motion is most predominantly visible when the rider is pedaling. Based on the measured bicycle states it was found that the steering motion (angle) increases almost exponentially with decreasing speed below the weave speed (unstable speed range). The steering frequency spectra are broad and flat for low speeds, whilst at high speeds there is a single spike in the steering data that corresponds to the pedaling frequency. Interestingly despite the lack of upper-body lean action no open loop eigenfrequencies from the rigid rider model could be detected in any of the experiments.

3.3 Publication II: Rider Motion Identification

Moore, J. K., Kooijman, J. D. G., Schwab, A. L., and Hubbard, M. (2011). Rider motion identification during normal bicycling by means of principal component analysis. *Multibody System Dynamics*, 25 (2) : 225–244.

The first set of observations gave a number of new insights into normal bicycle riding rider control. However, these insights were based only on qualitative observations. In order to be able to make any bold conclusions about the performed rider motions the qualitative observations should be supported by quantitative observations. Therefore a second set of observations was carried out on the treadmill, this time using three similar riders (young adult males with similar height and weight) and two different style bicycles. Optotrak Certus motion capture equipment was used to record the motion of the bicycle and rider enabling the quantitative investigation of the rider motions. Figure 3.3 shows where the markers were placed on the riders and bicycles. The motion capture equipment could measure the position of the markers placed on the rider and

bicycle in space with an accuracy of ± 0.15 mm.



Figure 3.3: *Bicycle and rider instrumented with active markers for motion capture while riding on a large treadmill*

Four experiments were carried out by each rider and on both bicycles. Similar to the qualitative experiments: stabilizing while pedaling normally; stabilizing without pedaling; and no-hands riding was performed. However this time during the no-hands experiment the rider was instructed to place his hands on his hips, to prevent different balancing techniques from being used by the rider at different speeds and amongst the different riders. By placing the hands on the hips the possible range of motions that the arms could perform were greatly reduced.

The fourth experiment was following a line, where the rider was instructed to try to ride with the front wheel on a straight white line drawn along the length of the treadmill belt. With this experiment it was intended to investigate the difference between riding in a general heading with no strong tracking task (the normal cycling experiment) and actively carrying out a tracking task (following a line). However the data was not analyzed in detail as the riders had significant difficulty in carrying out the task. Focussing on the line was difficult for the riders due to the strange optic flow situation

where the treadmill belt was moving but the surroundings were not. For example, one rider who was initially unable to stay on the line for more than a short while even when the belt was moving at a speed slightly above the weave speed (thus in the stable speed range) was able to suddenly change his control actions whilst riding very slowly (at 5 km/h) and ride perfectly along the line. He was able to do this by adjusting his field of vision and completely focussing on the treadmill belt and eliminating the rest of the surroundings. This transition was visible in the measured data, and whilst interesting the collected data obviously could not be used to investigate the difference between tracking a line general straight ahead cycling.

Each of the four experiments was carried out at multiple speeds between 2 and 30 km/h. Each run lasted 1 minute during which the location of each of the 31 markers was recorded at a rate of 100 Hz. In total some 90 runs were performed. Principal Component Analysis was applied to the data in a similar fashion to what was done by Troje [149] in investigating gender walking differences. This data reduction technique splits the recorded motion into its principal components. The 10 principal components with the largest variance were then analyzed in a self-developed graphical user interface (GUI) running in Matlab shown in figure 3.4.

The components were examined and the movements that were seen were described. A single component can display a number of motions. For example, components displaying leg movement usually also display movement of the upper body. The components were then grouped according to frequency correlation to make classes. With these classes motions were described. The motions and classes are depicted in figure 3.5. As an example we discuss the pedaling motion of the feet. Due to the phase shift amongst the components, the pedaling motion was found to consist of at least two components: in the first the feet move vertically up and down; whilst in the second they move horizontally forwards and backwards. As the two motions are obviously coupled their components have similar frequency content, and are highly correlated. This technique was thus used to indicate which components form a single class. When the components are viewed simultaneously the complete circular foot motion is reconstructed. However also rider lean, spine bend and rider twist motions were found to be present in the components that make up the pedaling class.

Interestingly the 3 different riders all show similar components, motions and classes at the same speed, but the motions switch components for different speeds. In all cases the upper body motions are all linked to pedaling. Furthermore the steering motion predominantly takes place in the pedaling frequency, while the steering motion in classes without upper body motion look like random white noise. This leads to the conclusion that steering is performed in the pedaling frequency.

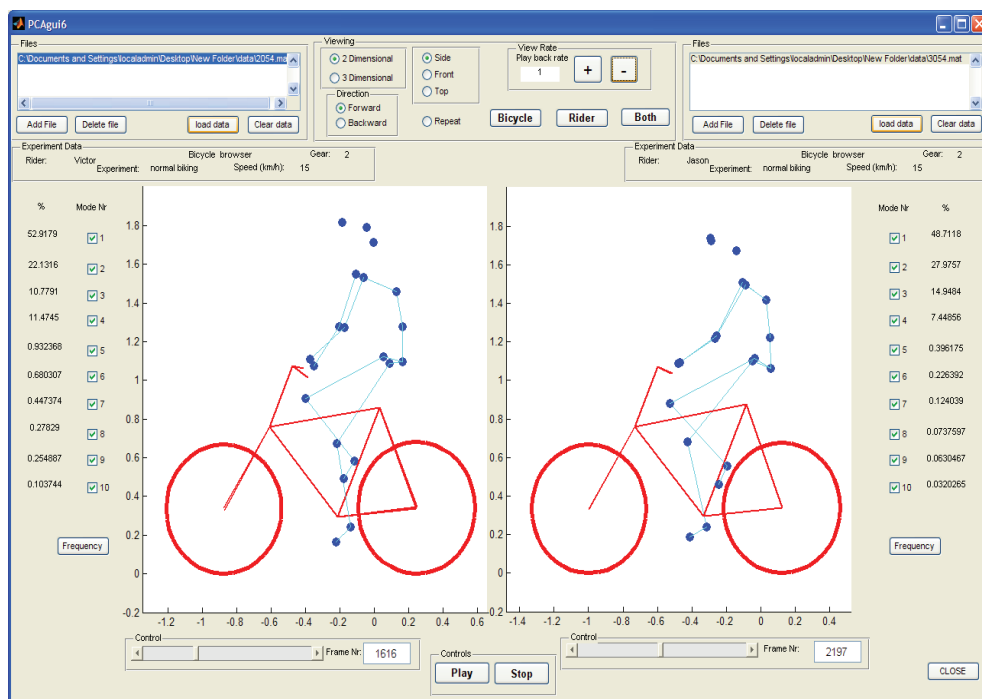


Figure 3.4: Screen shot of the Matlab graphical user interface used to visualize principal components and compare between different components and runs

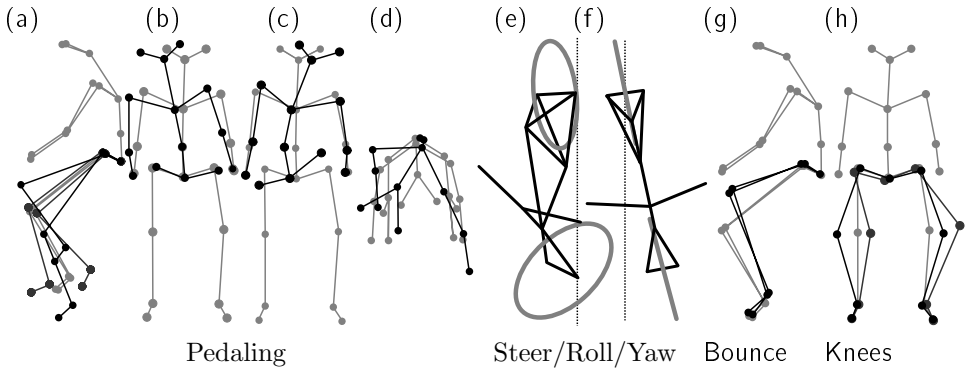


Figure 3.5: Diagrams of the common motions grouped as classes. Pedaling class: (a) horizontal and vertical components of pedaling, (b) rider lean, (c) spine bend, (d) top view of rider twist. Steer/Roll/Yaw class: (e) top view of bicycle steer and roll, (f) bicycle yaw. Bounce class: (g) knee bounce. Knees class: (h) two lateral knee motions. All but pedaling (a) are exaggerated in size for clarity.

3.4 Conclusions

No significant upper-body leaning control motions were detected during the observations carried out with the instrumented bicycle with video camera. The experiments also indicate that the human rider predominantly uses steering actions to stabilize the bicycle. Upper-body lean motions were seen during the normal bicycling experiments but they appear to be linked to the pedaling motion. These observations were confirmed in the second set observations where motion capture technology was used to record the exact motion of the rider and bicycle. After applying the principal component analysis data reduction technique to the recorded data, three dominant upper body motions were found for normal bicycling: upper-body lean, spine bend and twist, all of which appear to be linked to the pedaling motion. Therefore it is hypothesized that lateral control is mainly accomplished by steering as upper-body motion was only observed at the pedaling frequency. If upper-body motions are used for control then this control is carried out at the pedaling frequency.

Considering variations of rider motion with respect to speed, it was observed in both experiments that there is large amplitude steering motion at low speeds but this decreases in magnitude as speed increases. This is generally true for all motions and shows that the bicycle-rider system becomes more stable at higher speeds with few detectable control actions.

Contrary to intuition also at very low speed there is no upper-body lean motion. However lateral knee motions are observed which are probably more effective at augmenting steering control for lateral balance than upper body motions. However when the

riders are not pedaling not all riders display significant lateral knee motion. Furthermore it is not clear if the lateral knee motion that is detected is due to active control of the legs by the rider or if it is due to passive rider motions as a result of the dynamics of the bicycle.

The bicycle model with rigid rider predicts that the weave mode is stable above about 16 km/h. Intuitively it can be expected that the major eigenfrequency of the system, the oscillatory weave frequency, can be detected in the frequency spectrum of the measured closed loop bicycle motions, but it is not the case. No evidence was found of a distinct weave frequency in the steer angle time histories of any run. For neither experiments in the unstable speed region or the stable speed range. In fact, the only distinct frequency that sometimes appeared was the pedaling frequency.

CHAPTER 4

Stability and Control of Bicycles with Passive Rider Models

4.1 Introduction

The experimental observations in Chapter 3 indicate that the rider, certainly when not pedaling, could be modeled as rigidly fixed to the rear frame as no upper body lean motion was noted during the experiments other than that connected directly to the pedaling motion. It is thus interesting to model the real bicycle rider system as a Whipple bicycle model, where the bicycle is extended with a hands-free rider rigidly attached to the bicycle rear frame, and compare this with the observations. Therefore a method for modeling the bicycle and rider was developed which is discussed in section 4.2.

The Whipple bicycle model with corresponding parameters for the used bicycle and modeled hands-free rigid rider was implemented in the analysis of the observations of Chapter 3. However, as discussed in Chapter 3, in none of the experiments, and at none of the speeds carried out, did the open loop dynamics predicted by the the Whipple bicycle model with a hands-free rigidly attached rider, resemble that of the measured motions during the experiments. The rigidly attached rider in hands free situation therefore appears not to describe the actual motion. By analyzing the full rider motions that had been recorded in the motion capture experiments, two distinctly different rider postures were detected. This led to the development of two passive rider models. In these models a mechanisms is introduced such that the hands of the rider are connected to the handlebar, but no extra degrees of freedom are introduced to the model. These models are discussed in section 4.3.

4.2 Publication III: Physical Properties of a Bicycle and Rider

Moore, J. K., Kooijman, J. D. G., Hubbard, M., and Schwab, A. L. (2009). A method for estimating physical properties of a combined bicycle and rider. In *Proceedings of the ASME 2009 International Design Engineering Technical Conferences & Computers and Information in Engineering Conference*, number DETC2009-86947, DETC2009, Aug 30 – Sep 2, 2009, San Diego, CA.

To predict bicycling motions a model of the complete system, bicycle and rider, is required. In earlier work [81] it was shown that the Whipple bicycle model can accurately predict the dynamics of a normal bicycle at low and medium speeds. Therefore an expansion of the Whipple bicycle model to include the rider is a logical next step. In observation experiments performed in Chapter 3 it was found that the rider upper body motions that are seen are linked to the pedaling motion. When the rider does not pedal, no rider upper body motions are seen. Therefore modeling the rider as rigidly attached to the rear frame seems to be a logical first approximation for the complete bicycle rider system. Thus a method is required to determine the physical properties of the complete bicycle and rider system. Döhring [35], was the first to do so. He measured the center of mass and moments of inertia of a motorcycle with rider using a large measuring table as shown in figure 4.1. As such equipment was not available for us to use, another method was developed to determine the physical parameters of the combined bicycle and rider. The bicycle and rider are modeled separately and then added.

To model a certain bicycle with the Whipple bicycle model, all 25 parameters required for the model must be measured on the physical machine. The wheelbase, steer axis tilt, trail and wheel radii are relatively easy to measure. Determining the mass of the four different components is slightly less trivial as wheels and bearings consist of components that belong to two different parts. For example the wheel of a bicycle consists of a tire (and inner-tube), rim, spokes, hub, axle, axle nuts, and bearings. The axle and axle nuts do not rotate, and should therefore be counted as part of the front frame assembly mass. The bearings have an outer ring that rotates with the wheel, an inner ring that does not rotate, and ball bearings that rotate at some other speed. For ease of measurement and because the mass of the axle, axle nuts and bearings is relatively small they are all accounted for as the mass of the wheel. The location of the center of mass of the front and rear frame was found by hanging the frames in different orientations in the clamp of a torsional pendulum. The torsional pendulum consisted of a long vertically hung, slender steel rod that was fixed at the upper end as shown in figure 4.2. The clamp was able to rotate about the horizontal axis such that the center of mass of the frame could be located directly below and along the axis of the long slender rod. By taking a digital photograph of the setup with the frame in each orientation and extending the plumb line (long slender rod) in the photographs and then digitally superimposing the photographs in such a manner that the bicycle is always in the same orientation and location, the three extended plum-lines then pinpoint the location of the center of



Figure 4.1: Test setup used by Döhning [35] to measure the moments of inertia of a motorcycle and rider. This photograph is a scan of the original which can be found in his thesis in the ETH Zurich repository.

mass. To determine the moments of inertia of the frames and wheels the clamp was then blocked from rotating about the horizontal axis and a small amount of torsion was applied to the shaft. The moments of inertia were then determined from the oscillation time of the shaft, the orientation under which the component was hung and the mass of the component.

A method that is both easy and practical was developed for determining the rigid rider properties. The rider is split into 10 segments each modeled by a simple geometric shape: the head and neck are represented by a sphere; the torso as a cuboid and; two upper and lower arms and upper and lower legs, for which each limb is represented by a cylinder. The rider model is shown in Figure 4.3. The mass of the rider is split amongst the different segments based on cadaver studies from literature [34]. Therefore only the rider's total mass and 14 easily attained anthropometric rider measurements are required. However to be able to determine the rider's center of mass location and moments of inertia the rider's specific orientation on the bicycle is required thus 10 extra bicycle measurements are required such that the rider's segments can be placed in the correct locations and orientation.

This method for determining the combined bicycle and rider physical properties was successfully applied to two bicycles (Batavus Browser and Batavus Stratos) and four different riders on both bicycles.

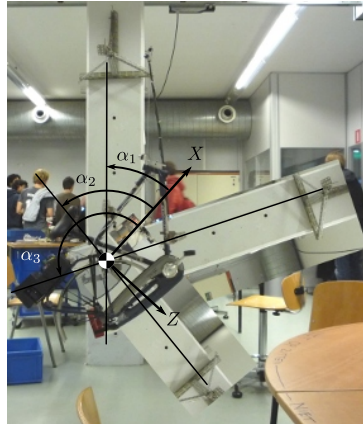


Figure 4.2: Superimposed photographs of the bicycle frame hanging in three orientations from the torsional pendulum showing the center of mass location and orientation angles.

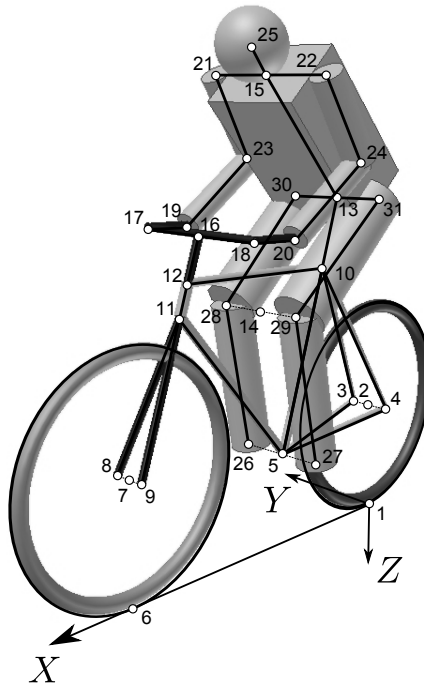


Figure 4.3: The rider modeled using simple geometric shapes. The grid points are found through the easily measurable lengths from rider and bicycle measurements and are used to place the rider at the correct location and in the correct orientation relative to the bicycle

4.3 Publication IV: Dynamics of Bicycles with Passive Rider Models

Schwab, A. L., Meijaard, J. P. and Kooijman, J. D. G. (2012). Lateral dynamics of a bicycle with passive rider model: stability and controllability. *Vehicle System Dynamics*, 50 (8) : 1209—1224.

The experiments performed in chapter 3 and in particular the motion capture analysis experiments section 3.3 gave two very clear insights into bicycle rider control motions. First of all it was found that all rider upper-body (lean) motions seem to be connected to the pedaling motion and secondly it was found that there are two distinctly different rider postures observed on different style bicycles. During the motion capture experiment of section 3.3 two different style bicycles, shown in Figure 4.4, were used to investigate if the very differently experienced “handling” of these two bicycles influences the performed rider control and motions. From the experiments it was observed that not only do the riders have different postures on the two different bicycles but their performed motions are also very different.

On the first bicycle, the Batavus Stratos ((a) in Figure 4.4), a leaned forward upper body is observed which is kept in place by (partly) leaning on the handlebar with the stretched arms. When the handlebar is turned the upper-body pivots about a point near the pelvis. Therefore the arms do not change shape (unlike the flexed arms seen on the Browser), but only their orientation changes slightly. On the second bicycle, the Batavus Browser ((b) in Figure 4.4), an upright body posture with flexed arms was observed. The rider’s arms move with the handlebar and flex at the elbows but the rider’s upper-body does not rotate with the handlebar.

Two sets of contradicting results were found in the observation experiments: firstly the Whipple bicycle model with a hands-free rigidly attached rider to the bicycle as modeled in the manner described in the previous section predicts open-loop motions that were not measured in the observation experiments, and; secondly the riders noted that the “handling” (subjectively) for the two bicycles was different, whilst very little difference in the open loop dynamics is predicted for the two bicycles by the Whipple bicycle model. The model gives relatively similar eigenvalues and modes for both bicycles, suggesting that the motions should be similar and thus that it could be expected that the “handling” should also be experienced in a similar manner. Yet the riders, even when they are not pedaling, and thus not showing any form of upper-body motion, still experience very different “handling” of the two bicycles.

These contradictions lead to investigating the effect of adding a passive upper-body rider model to the bicycle without adding any degrees of freedom to the Whipple bicycle model. Such a passive upper-body rider model simply consists of a mechanism linking the lower body (which is fixed to the bicycle rear frame) to the handlebar (at the hands). Two different models were developed to model the two distinctly different rider postures. These are shown in Figure 4.5. The eigenvalue plots that are found for the two rider postures for different speeds look very different to each other. While the leaned forward

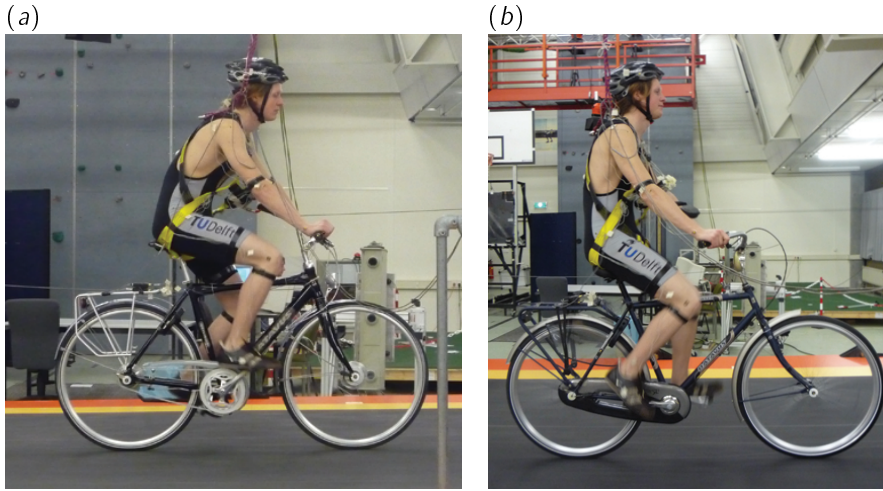


Figure 4.4: The same rider on the two different style bicycles showing the different distinct rider postures. (a) The Batavus Stratos hybrid bicycle with body leaned forward and stretched arms. (b) The Batavus Browser city bicycle with an upright body and flexed arms.

straight armed posture's eigenvalue plot remains relatively similar to that of the rigid hands-free rider Whipple bicycle model, that of the upright, flexed arms posture does not. The upright, flexed arms posture is found to have an unstable capsize mode at every forward speed investigated whilst the weave mode is stable at every speed.

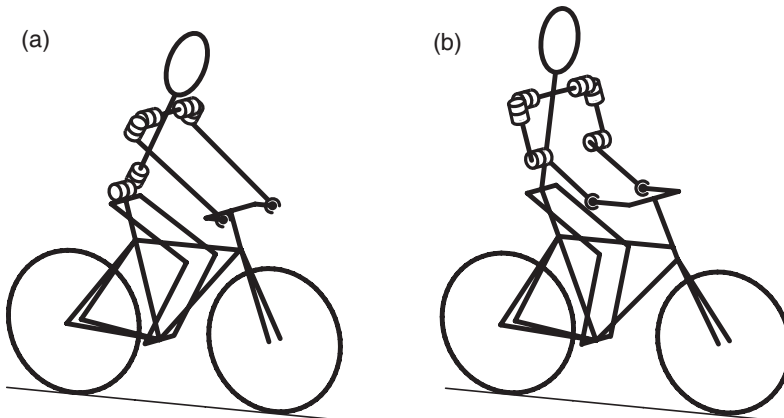


Figure 4.5: Two distinct bicycle models which include a passive rider: (a) rider with forward leaned body and stretched arms and (b) ride with upright body and flexed arms.

Interestingly when a rider becomes anxious or aware of a possible upcoming “challenge” such as when riding on an icy road or when riding along a narrow plank, the rider often “freezes” up, stiffening the arms and shoulders. The rider thereby changes from a flexed arms model to a rigid - straight arms (but the arms may still be bent) model, thus improving the open loop lateral stability. Whether the rider does this (unconsciously) for this reason remains to be seen.

With an always present unstable mode in the upright flexed arms posture model, the question arises how easily such a bicycle can be controlled. Therefore the controllability of the models and their modal controllability was investigated where either steer torque or upper-body lean torque were considered as the control input. To do this the models had to be expanded such that upper body lean was a degree of freedom in the models. Therefore the models were expanded to include the upper-body lean degree of freedom by adding a hinge between the rear frame and the torso located at the saddle with the hinge axis along longitudinal axis of the bicycle. This introduces two extra eigenvalues and modes to the system one of which is unstable at all forward speeds and corresponds to the uncontrolled inverted pendulum like mode of the upper-body.

For both passive rider models four uncontrollable speeds are found for steer torque control and two are found for upper body lean torque control. Of these six speeds only two uncontrollable speeds relate to unstable modes and are therefore of interest. However, the speed at which the upper body lean torque control has an unstable mode is practically zero for both models, making this irrelevant in practical terms. Therefore one practical, uncontrollable mode remains which is that of the steer torque control on the upper body lean mode, however this mode can easily be stabilized by adding a passive spring and damper between the upper body (torso) and lower body or frame. In a real human rider such a spring and damper will automatically be present due to the presence of muscles and fatty tissue. Both rider models can in essence therefore stabilize all modes at all speeds by either steer torque control or upper body lean torque control. Furthermore for both bicycle-rider models the unstable modes have very good steer torque modal controllability but are marginally controllable by lateral upper body motions. This result supports the experimental observations as it indicates that most control actions for lateral balance on a bicycle are performed by steer control only and not by lateral upper body motions.

4.4 Conclusions

A simple and easy to perform method for determining the physical parameters of a combined bicycle and rider has been developed.

Two different rider postures for controlling a bicycle have been observed. The first posture leans forward with stretched arms and hands on the handlebar, the second has a more upright posture with flexed arms and hands on the handlebar. Both rider postures have been modeled as passive upper body mechanisms on the bicycle, such that they do

not add any degrees of freedom to the Whipple bicycle model. The posture can have a large effect on the open loop dynamics when compared to a hands-free rigidly attached rider. For the leaned forward stretched arms posture there is little change. However the upright posture with flexed arms, hands on the handlebar, drastically changes the open loop dynamics as all self-stability is lost.

The unstable modes of both bicycle–rider combinations have very good modal controllability for steer torque control but are marginally controllable by lateral upper body motions. This indicates that most control actions for lateral balance on a bicycle are performed by steer control only and not by lateral upper body motions.

CHAPTER 5

Experimental Validation of Bicycle Dynamics

5.1 Introduction

This chapter investigates some robustness aspects of the Whipple bicycle model. First its applicability to model an ordinary bicycle design for the case that the tire–road contact is altered is considered by investigating the lateral dynamics of a bicycle on a treadmill. Secondly the applicability of the Whipple bicycle model to extreme designs is investigated through the design of the Two Mass Skate bicycle. This bicycle has no gyroscopic effects, negative trail, very small wheels and a very different weight distribution when compared with normal bicycles.

The three-degree-of-freedom Whipple bicycle model [164] is the most commonly used model to describe the lateral motion of a bicycle in literature. The model was benchmarked and reviewed by Meijaard *et al.* [94] in 2007 and describes the lateral dynamics of a bicycle through steer and roll motion and forward speed as the sole degrees of freedom. The Whipple model is a gross simplification of the real cycling system as it simplifies the bicycling system to just four rigid bodies: the front and rear wheels, front frame and rear frame (including a rigidly attached rider). These four rigid bodies are interconnected via three revolute joints: front wheel connects to the front frame; rear wheel to the rear frame; front frame to the rear frame. The model does not take frame flexibilities into account, nor is there any form of play present and it models the tires as rigid non slipping knife edged wheels. The model therefore excludes all tire dynamics and instead models the wheels as infinitely stiff, perfectly rolling point contact with the ground. Yet despite these assumptions for an ordinary uncontrolled bicycle it describes the motion well at low and moderate speeds for an ordinary bicycle as was found in an earlier experimental study where the goal was to experimentally validate the model [74, 81].

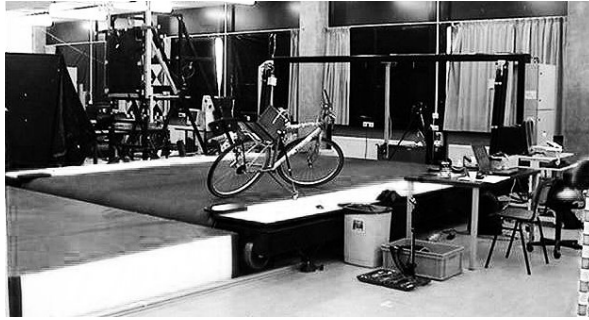


Figure 5.1: Large treadmill, 3×5 m, max calibrated speed 35 km/h, courtesy of the faculty of Human Movement Sciences, Vrije Universiteit Amsterdam.

Performing experiments on a treadmill is of interest to many authors due to the ease with which repeatable measurements can be performed on them, therefore this chapter first experimentally investigates the dynamics of a bicycle on a treadmill. A bicycle running on a treadmill could in theory be modeled in the same way as one running roughly straight ahead on the open road, and thus the Whipple model should describe the motion of a bicycle on a treadmill. However there are two significant differences that can be expected. First there is the lateral stiffness of the treadmill belt, which should be high enough, and secondly there is the constant treadmill velocity, which runs at a constant speed and fixed orientation, whilst the bicycle does not remain in the same orientation. The experimental investigation therefore compares the lateral dynamics of the measurement bicycle that was previously used to validate the Whipple bicycle model on flat level ground [81] and compare its motion on the treadmill with that of the corresponding Whipple model.

The second experiment investigates the applicability of the Whipple bicycle model to an extreme out-of-the-ordinary bicycle design: the experimental Two Mass Skate (TMS) bicycle. This experimental TMS bicycle de-bunks some of the myths associated with bicycle self stability but has non standard dimensions as can be seen in Figure 5.2.

Some of the TMS bicycle's strange attributes include: a small moment of inertia about the steering axis; a small amount of negative trail; very little friction in the head bearing; small diameter, knife edged wheels and counter rotating wheels to eliminate the gyroscopic effect. It has small, sharp, aluminium wheels and is used on a compliant rubber sports hall floor. This attribute in particular differs significantly from the modeled point contact in the Whipple model. But can the Whipple bicycle model despite these differences still be used to predict the motion accurately? With these small numbers, friction could become a far more important parameter at this scale and other non-linearities could also have a significant effect on the overall stability. The Whipple bicycle model predicts stable motion but it assumes ideal situations with no play, friction, or other non-linearities and only for a small lateral perturbation. In real the experimental



Figure 5.2: Self-stable experimental TMS bicycle rolling and balancing (photo by Sam Rentmeester/FMAX).

bicycle might actually just fall over, that is the test for the experimental TMS bicycle, how far can the real bicycle differ from the theoretical and still show the same general lateral dynamics.

5.2 Publication V: Lateral Dynamics of a Bicycle on a Treadmill

Kooijman, J. D. G. and Schwab A. L. (2009). Experimental validation of the lateral dynamics of a bicycle on a treadmill. In *Proceedings of the ASME 2009 International Design Engineering Technical Conferences & Computers and Information in Engineering Conference*, DETC2009-86965, DETC2009, Aug 30 – Sep 2, 2009, San Diego, CA.

Analyzing the data of the rider observations on the open road it became clear that a more controlled environment was required to be able to carry out repeatable experiments. Riders rode over bumps, had to deal with traffic, gusts of wind, were chased by dogs and did not carry out exactly the same maneuvers, making comparisons very difficult. Therefore other options, to eliminate these uncontrolled circumstances, were proposed such as riding on an athletics track (flat, no traffic), in an indoor sports hall (flat, no traffic or weather conditions) and on a treadmill (flat, no traffic or weather conditions, but no heading changes possible).

A second challenge that was foreseen for future experiments was that a method was required to be able to apply an external force to excite the bicycling system for system

identification purposes. Roland & Massing [123] who had worked on a similar project in the 1970's had shown that a rocket attached to the bicycle was not ideal for applying a lateral force as it only caused a large yawing motion and not an oscillating steering and rolling motion. Other options such as riding with large weights on either side of the rear rack and dropping one of the two were also considered, but a number of technical obstacles were also expected with such a system and the large mass change would also change the dynamic response of the bicycle. An unexplored route was to keep the bicycle stationary by riding on a treadmill. Applying a lateral force to the bicycle then becomes a trivial case. However the problem with most treadmills is that they are generally made for running, and are thus relatively narrow (< 1 m wide) and short (< 2 m long) and have a relatively low top speed (< 25 km/h). However at the Human Movement Sciences department of the Vrije Universiteit Amsterdam a treadmill that does not have these characteristics is available.

The treadmill, shown in Figure 5.1, is 3 m wide, and 5 m long allowing enough room for a bicycle to maneuver on easily and perform experiments on. The treadmill is calibrated to run at a constant velocity in steps of 0.1 km/h between 2 km/h and 35 km/h and has a top speed of 40km/h. The treadmill can also be inclined in steps of 0.5° which is useful when carrying out experiments so that the rider has to apply some force to remain on the treadmill - otherwise due to the lack of air-resistance the rider can easily apply too much force to the pedals accelerating the bicycle forward and causing the bicycle to be ridden off the front of the treadmill.

An initial test with a normal city bicycle on the treadmill indicated that riding on the treadmill was not the same as riding on the open road. Obviously the fact that the surroundings were not moving relative to the rider and the rider had no optic flow meant that the rider had to adjust to the new situation. But the riders also noted that the handling of the bicycle felt as if the rear tire was under-deflated. As this was not the case the question arose: is the dynamics of a bicycle on a treadmill the same as on the open road? The tire-treadmill belt contact could be different from normal road contact as the thin treadmill belt could comply laterally, or there could be a large amount of slip between the tire and the belt. A third cause for the difference in riding experience could be that the belt has a constant velocity. The bicycle moving at a constant speed does not have a constant velocity, as slight direction changes occur. When the bicycle no longer moves parallel to the direction of the belt it is accelerated in the direction of the belt rotation. However when the corners are small this effect should be small and have little effect on the motion of the bicycle.

Therefore it was decided to experimentally investigate the lateral dynamics of the bicycle on the treadmill. To do this the measurement bicycle that had previously been developed to experimentally validate the Whipple bicycle model was (re)used [74, 81]. This bicycle, shown in Figure 5.3 is equipped with a potentiometer for the steer angle and rate gyros for the roll and yaw rate. A reed relay and a 10 magnet ring placed in the rear wheel is used to measure the wheel rotation. The sensors are powered by a 5V battery pack and the signals are fed to a USB National Instruments DAQ 6009 data



Figure 5.3: *Instrumented bicycle from [81], with all the measurement equipment installed. Sensors are present for measuring the roll rate, yaw rate, steering angle, and rear wheel rotation. Data are collected via a USB connected data acquisition unit on the laptop computer, mounted on the rear rack.*

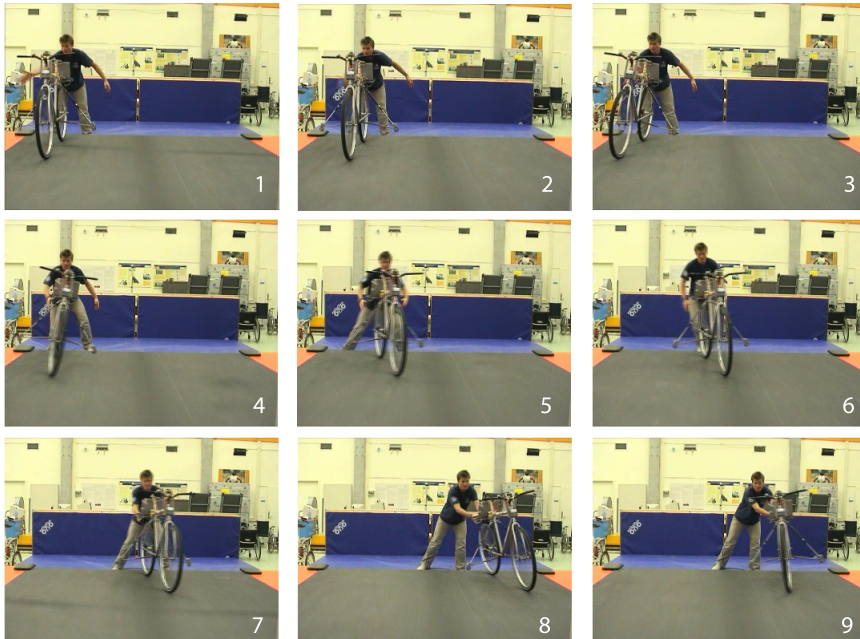


Figure 5.4: *Lateral perturbation experiment carried out with the measurement bicycle at 16 km/h (stable speed range). Bicycle is perturbed in 2, it recovers and moves freely 3–6, is caught in 7, and returned to the starting point in 8 and 9.*

acquisition device connected to a laptop that is placed on the rear rack.

To validate the Whipple bicycle model for the lateral dynamics of a bicycle all 25 parameters of the measurement bicycle had been determined. With the measurement bicycle experiments had been carried out in a sports hall at multiple speeds to investigate if the dynamics of the Whipple bicycle model were the same as those of the measurement bicycle. During each of these experiments the bicycle was brought up to speed released and perturbed (if required) to laterally excite the bicycle. From the measured signals for each run the oscillation period and decay were extracted using a best fit function and the speed of the bicycle was also determined. The frequency and decay for each speed measured during the different runs were compared to the weave mode eigenvalue of the model at the different speeds. The results compared well.

By repeating the experiments on the treadmill with the measurement bicycle, and once again comparing the found frequency and decay of the weave oscillation with those of the Whipple bicycle model, if they compare well then the motion of the bicycle on the treadmill can be said to be equivalent to that on flat level ground. In Figure 5.4 some screen shots of one of the experiments with the measurement bicycle on the treadmill are shown.

5.2.1 Conclusions

The experimental results show good agreement with the Whipple bicycle model for the motion of an uncontrolled bicycle. The transition from stable to unstable speeds is also well predicted. This shows that the tire-belt compliance and tire-belt slip, and the small changes in bicycle heading relative to the belt velocity are not important for the lateral dynamics of the bicycle on a treadmill.

Therefore it is concluded that riding a bicycle on a treadmill with constant belt velocity is dynamically equivalent to riding a bicycle on flat level ground around the straight ahead direction with constant speed.

However despite the actual motion of the bicycle on the treadmill being the same to that of on the open road for riding roughly straight ahead, riding a bicycle on a treadmill is not experienced by the human rider in the same manner as on the open road due to the missing optic flow.

5.3 Publication VI: Self-Stable Bicycle without Gyro or Trail

Kooijman, J. D. G., Meijaard, J. P., Papadopoulos, J. M., Ruina, A., and Schwab, A. L. (2011). A bicycle can be self-stable without gyroscopic or caster effects. *Science*, 332 (6027) : 339–342.

The core of this chapter is the experimental proof that a bicycle can be self stable without gyroscopic or trail effects.

Even before the safety bicycle had been developed the ability of a moving bicycle to balance itself, without any outside intervention was already known [59]. Generally people have, and still do, attribute this self-stability to gyroscopic and trail effects. This is probably at least in part due to a number of published works, two of these are well known and very respected publications. The first is the fourth book on gyroscopes by Felix Klein (of the Klein bottle), Arnold Sommerfeld (who was nominated for the Nobel prize 81 times) and Fritz Noether (the brother of Emmy Noether) [70] who investigated bicycle stability using the Whipple bicycle model and concluded that gyroscopic effect is essential. The second publication, the paper by David Jones [66], has been widely accepted, and even published twice in *Physics Today*. Jones carried out many experiments to develop an un-rideable-bicycle and insists that ‘trail’, the distance that the front wheel trails behind the steer axis, is necessary for bicycle stability. He reasoned that the front wheel of a shopping cart castor trails behind its support bearing and so must a bicycle front wheel.

Jim Papadopoulos, working with Andy Ruina and Scott Hand at Cornell University in 1985 worked on modeling the lateral dynamics of a bicycle [56] as they suspected that these explanations for bicycle self stability were missing at least part of the picture. They first developed a model, along the lines of Whipple and Carvallo [164, 17] (the first to develop a model for the lateral dynamics of a bicycle around 1899), for the lateral dynamics of a bicycle and compared this to the models found in literature. However they, frustratingly, found very little agreement with their model to that of others. Even more frustrating was that they also found very little agreement amongst the different models in literature.

In 2003 the modeling work re-received attention when Arend Schwab working with SPACAR software, and Jaap Meijaard who was modeling motorcycles in AutoSim at the time, compared their results with that of the “pencil and paper” derived model by Hand and Papadopoulos [56], and this time all three agreed. This result was the start of what would turn into a major project to experimentally validate [81] and benchmark the model [94]. In the process all the bicycle models from the literature were also reviewed [94].

Despite the uncertainty about the correctness of the model at the time due to the inconsistencies with literature, Papadopoulos continued to search for the essence of bicycle self stability in the mid 1980s. The model predicted self stability for common bicycle designs as experienced in real life. But for common bicycle designs the complexity of the full 25-parameter Whipple bicycle model (see [94]) makes it hard to probe for theoretical insights as the differential equation matrix entries are a combination of all 25 parameters. Therefore they looked at simpler and simpler dynamical models [56], until they found a minimal two-mass-skate (TMS) bicycle that theory predicted, should be self-stable [109]. This theoretical bicycle has no gyroscopic effect and no trail, yet predicts self stability.

Once the bicycle model’s correctness had been established in 2003, the essence of bicycle self balance re-became a fundamental question to investigate. It began with

delivering physical proof that such a TMS bicycle would indeed be self stable. The experimental proof is the core of this chapter.

Once the self stability of the TMS bicycle had been shown, the theoretical analysis was investigated further [76]. In this theoretical analysis it was shown that neither caster trail nor gyroscopic effect are necessary nor sufficient for a bicycle to self balance. Examples were shown in [76] for cases and included a bicycle with gyroscopic wheels and positive trail that is not stable at any speed. No simple real physical explanation equivalent to the mathematical statement that all eigenvalues must have negative real parts could be found. Even the automatic turning toward a fall although necessary, is not sufficient to guarantee self-stability. However within the domain of the linearized equations of motion, two “simple” necessary conditions were found: To hold a self-stable bicycle in a right steady turn requires a left torque on the handlebar. And secondly: At least one factor coupling lean to steer must be present. These coupling terms arise from combinations of trail, spin momentum, steer axis tilt, and center of mass locations and products of inertia of the front and rear assemblies.

The project concluded with a literature review on the explanation for bicycle self stability [95]. The complete work was published in Science Magazine, April 15th 2011 [75].

The remainder of this chapter describes the development of the experimental two-mass-skate bicycle based on the theoretical result initially developed by Papadopoulos [109]. It begins though with a short review of the linearized equations of motion of a bicycle model, the so called Whipple bicycle model, and then a simplified version of the general Whipple bicycle, the theoretical two-mass-skate (TMS) bicycle, is considered. This theoretical TMS bicycle is the core that the experimental TMS bicycle is built on. There are various complications in reducing the point-mass concepts to a manufacturable and experimentally working design (section 5.3.2), and then still more problems when building the machine (section 5.3.3). The experiments are then described (section 5.3.5). However, anyone attempting to reproduce the experiments should be aware of various experimental subtleties (section 5.3.6).

5.3.1 Review of the Whipple Bicycle Model

The so-called Whipple bicycle model [164], benchmarked and reviewed in Meijaard *et al.* [94], consists of four rigid bodies connected by three hinges (see Figure 5.5). The contacts between the knife-edged wheels and the flat level surface are modeled by holonomic constraints in the vertical direction, and by non-holonomic constraints in the longitudinal and lateral directions. It assumes no-hands operation with either no rider or with a rigid hands-free rider. The resulting non-holonomic mechanical model has three velocity degrees of freedom: forward speed v , lean rate $\dot{\phi}$, and steering rate $\dot{\delta}$.

The full derivation of the following brief review of the linearized equations of motion for small perturbations of the upright steady forward motion of a bicycle are given in Meijaard *et al.* [94].

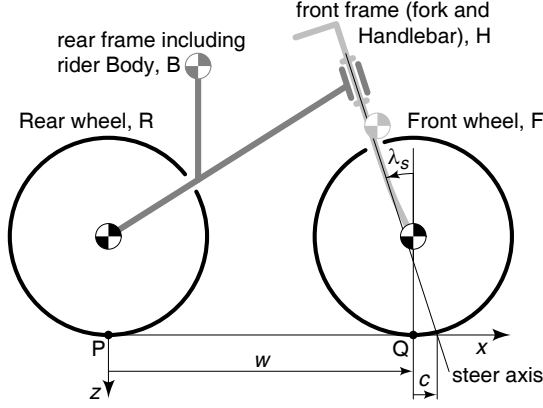


Figure 5.5: The Whipple bicycle model is described with 25 geometry and mass parameters. There are two frames B (rear frame plus rider Body) and H (fork plus Handlebar) connecting two wheels R (Rear) and F (Front). Each has geometric and mass parameters. The steer axis tilt λ_s , and trail c , are positive, as shown, on conventional bicycles.

The linearized dynamics of the lateral and the forward motion are decoupled in the upright straight ahead configuration and therefore in these linearized equations, the forward speed is constant. The equations of motion for the lateral dynamics are expressed in terms of the rear frame rightward roll angle, ϕ , and the rightward steering angle, δ , both measured relative to the upright straight ahead configuration $[\phi, \delta] = [0, 0]$. At forward speed v the linearized lateral dynamics equations are

$$\mathbf{M}\ddot{\mathbf{q}} + v\mathbf{C}_1\dot{\mathbf{q}} + [g\mathbf{K}_0 + v^2\mathbf{K}_2]\mathbf{q} = \mathbf{f}, \quad (5.1)$$

where the time-varying variables are $\mathbf{q} = [\phi, \delta]^T$ and the generalized torques $\mathbf{f} = [T_\phi, T_\delta]^T$. For the uncontrolled case these generalized torques are zero. The subscripts for the \mathbf{C} and \mathbf{K} matrices are chosen to match the exponents of the v multipliers.

The constant entries in matrices \mathbf{M} , \mathbf{C}_1 , \mathbf{K}_0 and \mathbf{K}_2 have the following structure,

$$\mathbf{M} = \begin{bmatrix} M_{\phi\phi} & M_{\phi\delta} \\ M_{\delta\phi} & M_{\delta\delta} \end{bmatrix}, \quad \mathbf{C}_1 = \begin{bmatrix} 0 & C_{1\phi\delta} \\ C_{1\delta\phi} & C_{1\delta\delta} \end{bmatrix}, \quad (5.2)$$

$$\mathbf{K}_0 = \begin{bmatrix} K_{0\phi\phi} & K_{0\phi\delta} \\ K_{0\delta\phi} & K_{0\delta\delta} \end{bmatrix}, \quad \mathbf{K}_2 = \begin{bmatrix} 0 & K_{2\phi\delta} \\ 0 & K_{2\delta\delta} \end{bmatrix}.$$

Each of the matrix entries is defined in terms of the 25 design parameters (see Meijaard *et al.* [94]).

Briefly, \mathbf{M} is a symmetric positive-definite mass matrix which gives the kinetic energy of the bicycle system at zero forward speed by $\dot{\mathbf{q}}^T \mathbf{M} \dot{\mathbf{q}}/2$. The damping-like (there is no real damping) matrix $\mathbf{C} = v\mathbf{C}_1$ is linear in the forward speed v and captures gyroscopic

torques due to steer and lean rate, inertial reaction from the rear frame yaw rate (due to trail), and inertial reaction from yaw acceleration proportional to steer rate. The stiffness matrix \mathbf{K} is the sum of two parts: a velocity-independent symmetric part $g\mathbf{K}_0$ proportional to the gravitational acceleration, which can be used to calculate changes in potential energy with $\mathbf{q}^T [g\mathbf{K}_0]\mathbf{q}/2$; and a part $v^2\mathbf{K}_2$ which is quadratic in the forward speed and is due to gyroscopic and centrifugal effects.

With these coefficient matrices and the assumption of exponential motions $\mathbf{q} = \mathbf{q}_0 \exp(\lambda_i t)$, the characteristic equation,

$$\det (\mathbf{M}\lambda^2 + v\mathbf{C}_1\lambda + g\mathbf{K}_0 + v^2\mathbf{K}_2) = 0, \quad (5.3)$$

can be formed and the eigenvalues (roots of the polynomial), λ_i , can be calculated. A bicycle is self-stable when, at speed v all the real parts of the (generally) complex eigenvalues are less than zero (negative), thus when the motion \mathbf{q} is a damped exponential for each λ_i .

This characteristic equation from 5.3 is a fourth order polynomial in λ ,

$$A\lambda^4 + B\lambda^3 + C\lambda^2 + D\lambda + E = 0, \quad (5.4)$$

and the coefficients of this polynomial are themselves polynomials in the forward speed v :

$$\begin{aligned} A &= A_0 \\ B &= B_1 v \\ C &= C_0 + C_2 v^2 \\ D &= D_1 v + D_3 v^3 \\ E &= E_0 + E_2 v^2. \end{aligned} \quad (5.5)$$

The individual coefficients for v (e.g., A_0, B_1, \dots) are lengthy expressions in the 25 bicycle parameters. The Routh [125] stability criteria now state that for all eigenvalues λ satisfying the quartic characteristic equation (5.4) to have a negative real part, all polynomial coefficients A, B, C, D, E and the Routh determinant $X = BCD - ADD - EBB$ must have the same sign. This last determinant is a sixth order polynomial in v of the form,

$$X = X_2 v^2 + X_4 v^4 + X_6 v^6, \quad (5.6)$$

where the coefficients (X_2, X_4 and X_6) are even longer expressions in terms of the 25 bicycle parameters.

The first coefficient $A = A_0 = \det(\mathbf{M}) > 0$ because the mass matrix is positive-definite (except for special singular mass distributions). Thus for stability B, C, D, E , and X are required to be positive. For a conventional bicycle design, B_1, C_2, D_3, E_0 are positive and C_0, D_1, E_2 are negative. Therefore the following simple statement is a general summary of the above:

Because the dependence of these coefficients on the 25 bicycle parameters is complicated there is no simple way to describe what bicycles are stable and at what speeds.

However, for some simple designs such as the theoretical two-mass-skate (TMS) bicycle, described briefly below and discussed in depth in [76], some general results have been found [76].

Theoretical two-mass-skate (TMS) bicycle

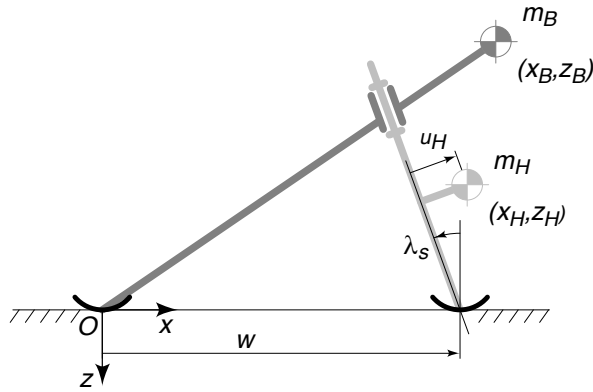


Figure 5.6: *Theoretical two-mass-skate (TMS) bicycle. The wheels are replaced with skates.*

To determine the essence of bicycle self stability a theoretical investigation was done into finding the most simple, self stable, bicycle possible [109, 76]. This bicycle was called the theoretical two-mass-skate (TMS) bicycle and it was developed with as many parameters set to zero as possible, to simplify equations 5.5 and 5.6 as far as possible, yet such that it still shows self stability. The theoretical TMS bicycle has zero trail and massless wheels. Therefore the dynamics of the bicycle is equivalent to that of a bicycle with ice skates instead of wheels, see Figure 5.6. Furthermore the rear and the front frame are made of simple point masses (therefore there are no moments of inertia terms). Thus the theoretical TMS bicycle only has eight non-zero parameters. These are shown in Figure 5.6 and Table 5.1.

The eigenvalues for this theoretical TMS bicycle are shown in Figure 5.7. Self stability occurs at speeds for which the real parts of all the eigenvalues are less than zero. For the theoretical TMS bicycle all the eigenvalues are less than zero (negative) for the shaded region, for the forward speed range of $2.8 \text{ m/s} < v < \infty$ (Figure 5.7). The full analysis of the theoretical TMS bicycle is given in [76].

Based on this theoretical TMS bicycle an experimental TMS bicycle was designed and this is discussed in the following sections.

Parameter	Symbol	Value
Wheel base	w	1 m
Steer axis tilt	λ_s	5°
Rear frame assembly B mass	m_B	10 kg
Rear frame assembly B center of mass	(x_B, z_B)	(1.2, -0.4) m
Front fork and handlebar assembly H mass	m_H	1 kg
Front fork and handlebar assembly H center of mass	(x_H, z_H)	(1.02, -0.2) m

Table 5.1: Parameters and values for a theoretical two-mass-skate (TMS) bicycle. Only non-zero values are mentioned. The values given are for the ideal target-design of the experiments described in Chapters 5.3.2–5.3.6.

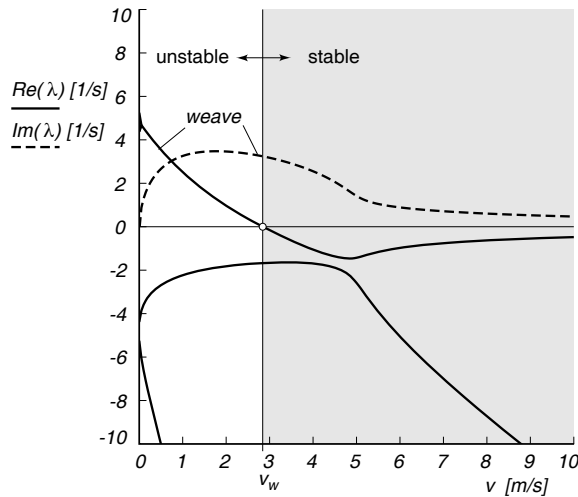


Figure 5.7: Eigenvalues for a theoretical two-mass-skate bicycle from Figure 5.6 and Table 5.1 in a forward speed range of $0 \leq v \leq 10$ m/s. Note that the real parts of all eigenvalues are negative for $v > 2.8$ m/s.

5.3.2 From Theoretical Two-Mass-Skate (TMS) Bicycle to Experimental TMS Bicycle

For the construction of an experimental two-mass-skate bicycle certain “physical” aspects have to be taken into account.

Firstly the theoretical TMS shown in Figure 5.6 will tip over forward in real life as the center of gravity is not between the two contact points. An extra point mass, if added exactly at either contact point, will have no effect on the lateral balance equations. Therefore adding a mass at rear the contact for the experimental machine is essential for preventing the bicycle from tipping over forward.

The theoretical two-mass-skate bicycle has zero trail. While trail is positive on common bicycles, it can be made slightly negative on the TMS bicycle without destroying its stability. However, to maintain self-stability the steer axis tilt then needs to be increased. One can further increase the stability by adding some mass moment of inertia to the front frame where one principal axis is aligned along the steer axis.

Thirdly, because the final physical design cannot be made of infinitesimal point masses (the machine will have mass moments of inertia properties), and the mass at the rear ground contact can never be located exactly at the rear contact point (it will always be slightly above), the parameters of the experimental bicycle have to be chosen carefully in order to preserve stability. Therefore all of the experimental bicycle parameters had to be fine-tuned in order to get a stable forward speed range which starts at a low enough speed and has enough margin in the negative real part of the eigenvalues (not too close to zero) to be robust.

An iterative design process was applied to go from the infinitesimal point-mass concept (theoretical TMS bicycle) as described in the previous section to a final physical design (experimental TMS bicycle). This process consisted of:

- Draw a constructible bicycle in a computer aided design (CAD) package (Solid-Works).
- Export the mass, the location of the center of mass and the mass moments of inertia of each of the four rigid bodies of the bicycle model from this CAD model into the bicycle lateral dynamics model implemented in the Matlab program JBIke6 [37].
- Investigate how the CAD model might be adjusted such that the dynamic model has not only a stable forward speed range which starts at a low enough speed but also has enough margin in the negative real part of the eigenvalues (not too close to zero) to be robust.
- Return to step 1.

Mark1 : Full Scale TMS Bicycle

Andrew Dressel at Cornell University had tried to make a down-scaled version (shorter wheelbase) of the theoretical TMS bicycle in the fall of 2006. The bicycle was based around adapting an at the time very popular model mini foldable scooter. The bicycle however had failed to show stability. It was presumed that the front frame of the scooter was too light, its inertia not large enough to overcome the static friction in the steering assembly (head bearing). Therefore it was decided to make a full scale version, which incorporated larger masses, able to overcome the steering static friction.

The initial design for the experimental TMS bicycle was directed at reproducing the theoretical TMS as closely as possible (see the JBIke6 model screen-dump in Figure 5.8). It had a wheelbase of 1.01 m, with the front and rear frame consisting of as little material as possible - just two straight steel tubes - as shown in Figure 5.9. The front and rear

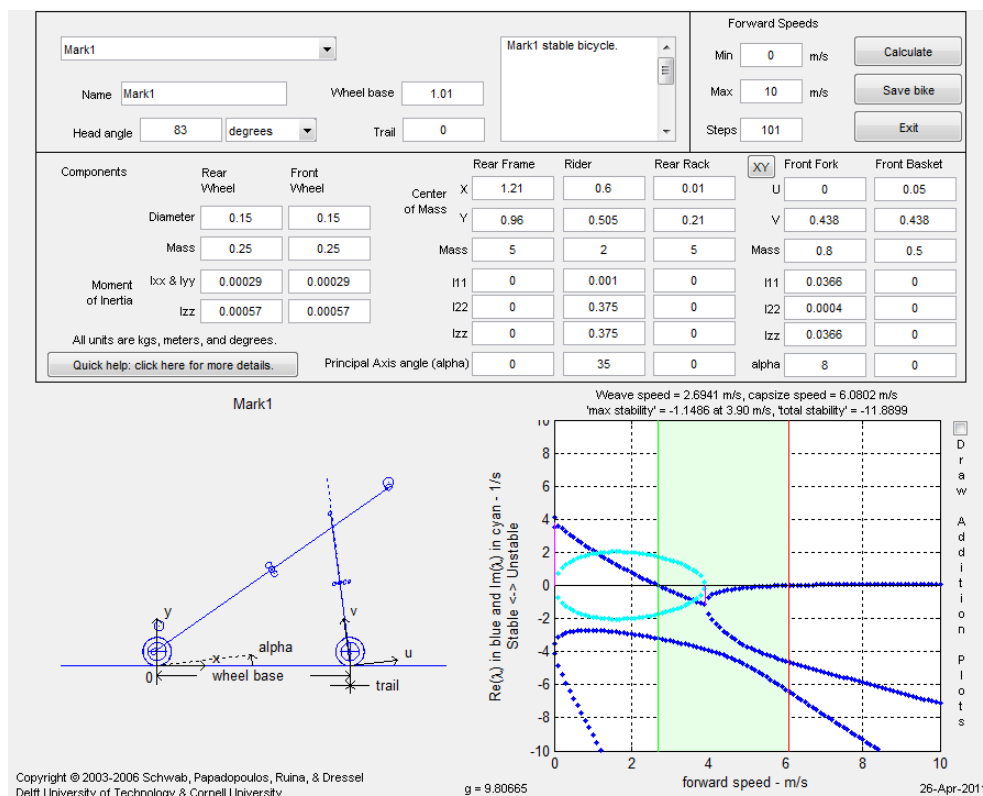


Figure 5.8: A screen-dump of the Mark1 Full Scale TMS bicycle modeled in the Matlab program Jbike6 [37]. In the upper part the model parameters are input. In the lower half of the diagram: To the left a diagram of the model bicycle mass and moments of inertia. To the right the eigenvalues for the bicycle for forward speeds ranging from 0–10 m/s. The light blue displays the imaginary part of the eigenvalue, the dark blue indicates the real part. The green band indicates the region where the bicycle is self stable, as all the real parts of the eigenvalues are smaller than 0.

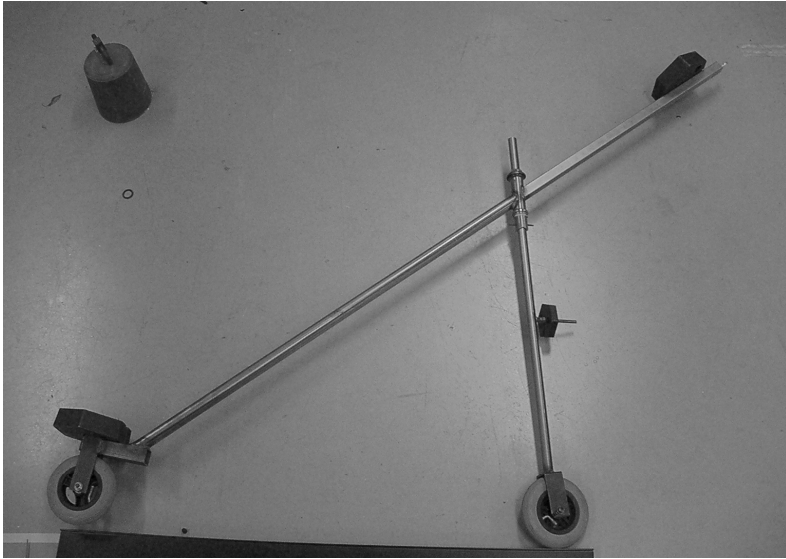


Figure 5.9: *The Mark1 Full Scale TMS bicycle with a wheel base of 1.01 m, two 5 kg mass weights on the rear frame and 0.5 kg mass on the front frame and installed with $6 \times 1\frac{1}{4}$ pneumatic tires.*

frame (tubes) were connected via a standard bicycle 1" head bearing. The 'point' masses consisted of 5 kg blocks of steel placed at the front and rear of the rear-frame (to prevent the bicycle from tipping forward), and 0.5 kg block was placed on the front frame in front of the steering axis. This smaller size mass (5 kg instead of 10 kg) was placed higher (0.96 m instead of 0.4 m) to ensure that the machine was still "manageable" in the experiments as even in this state the total mass of the bicycle was roughly 15 kg. Using two 10 kg masses would have made the complete machine have a mass > 25 kg.

Small 6 inch wheels with solid rubber tires were initially installed on the machine. Small wheels were used to eliminate most of the gyroscopic effect. As the mass of the small wheels (± 300 g) is far less than that of larger normal sized wheels (± 1800 g). Therefore small wheels also have small amounts of inertia compared to normal sized wheels (due to the r^2 relationship). Furthermore since the bicycle does not have to go fast to become stable (2.8 m/s), ω remains small and therefore the gyroscopic effect is also very small for small wheels (and presumed ignorable).

The solid rubber wheels were replaced, first by $6 \times 1\frac{1}{4}$ pneumatic tires, and then later on by solid aluminium near knife edge wheels (3 mm crown radius) as a measure to reduce the scrubbing torque which was deemed preventing the natural dynamics of the bicycle from occurring during experiments. However even after all these major adjustments and countless mass position and head tension/play alterations and experiments the bicycle

still failed to show self balance. Therefore the design was abandoned due to the following issues:

- Friction in the head bearing.
- Scrubbing torque created at the wheel road contact patch.
- Front frame flexure. Parasitic oscillations could be seen in frame fork, causing the front wheel to “hop” after even the smallest excitation.
- The bicycle was too large and heavy to manage easily during experiments.

Mark 2: Experimental TMS bicycle

With the knowledge gained with Mark1, a second iterative design process was performed, where extra attention was given to the design issues of Mark1. The model was based around a shorter wheelbase, stiffer frame and smaller point masses. This time the bicycle was also developed to have negative trail and counter rotating wheels were implemented to completely eliminate the remaining gyroscopic effect. The Mark2 bicycle is shown in Figure 5.11 and a production drawing is shown in Figure 5.10. This bicycle, when it was built, was found to be stable. The remainder of this chapter gives a detailed account of the final design of this experimental TMS bicycle the experiments performed with it and general observations.

5.3.3 Experimental Two-Mass-Skate (TMS) Bicycle Construction

Based on the theory described above, the design pursued has mass extending forward and above the front wheel contact. For ease of operation the model was given a smaller wheel-base than a conventional bicycle, 0.75 m. To make non-gyroscopic wheels we added counter-rotating wheels [66, 7]. The final total mass is 8.837 kg. A photograph of the experimental TMS bicycle is shown in Figure 5.11 together with the nomenclature of the different frame parts. Table 5.2 gives an overview of the mass distribution of the bicycle.

The ‘point’ masses from the theoretical TMS bicycle model were made, for the experimental machine, of 50 mm diameter lead rods. One 1.45 kg cylinder of lead was placed 35 mm in front of and parallel to the steer axis with its center of mass 387.5 mm above the ground. Two lead cylinders, each of mass 1 kg, were each attached 100 mm above the ground to each side of the rear frame at the same longitudinal position as the rear contact point. Two 1 kg lead cylinders were connected to the carbon upper frame tube via a bracket and threaded rod 1.15 m in front and 0.90 m above the rear wheel contact point. The threaded rod allows for the compensation of miss-alignments during the assembly of the bicycle: by adjusting the mass positions to get the net center of mass in the bicycle mid-plane.

A parameter study of the location of the 2-kg mass on the front of the rear frame indicated that the fore-aft position is less critical than the vertical position of the mass.

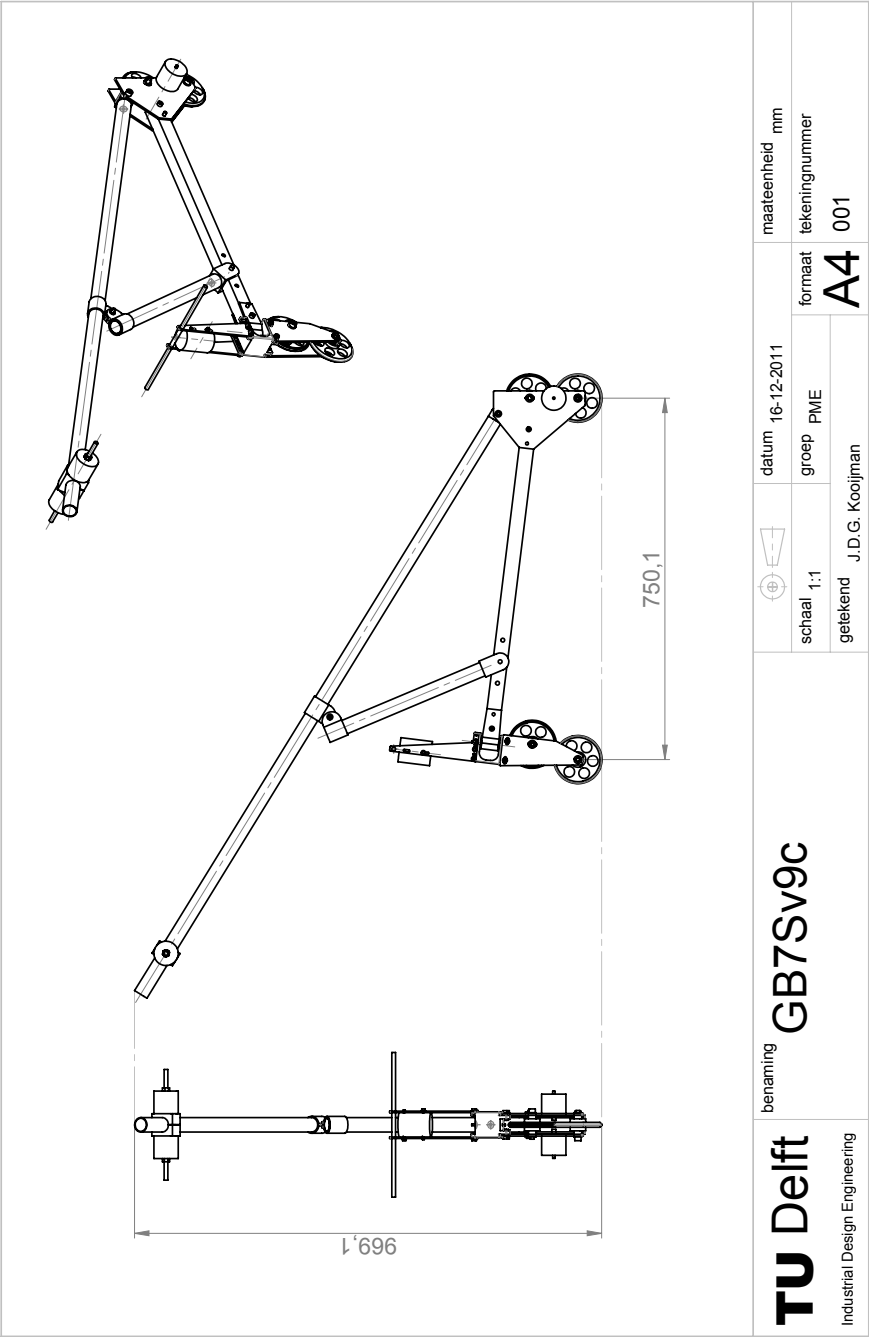


Figure 5.10: Production drawing of the complete experimental TMS bicycle.

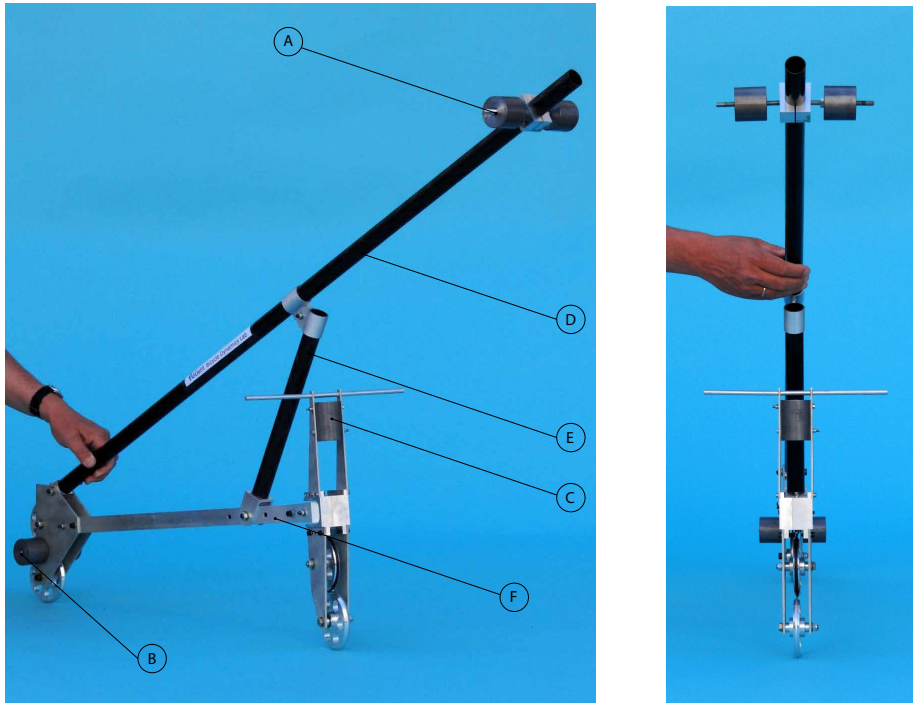


Figure 5.11: left) Overview of the experimental two-mass-skate bicycle, with (A) 2 kg rear frame forward point mass, (B) 2 kg point mass at the rear contact point, (C) Point mass front frame, (D) Rear frame upper tube, (E) Rear frame support tube (F) Lower rear frame member. **right)** Front view of the experimental two-mass-skate bicycle.

Therefore a 1400 mm long upper frame tube, originating at the rear wheels is used as frame member allowing for the shallowest orientation of the beam (see Figure 5.11). On the one hand, the dynamic calculations show that stability depends on the rear frame having low inertia, on the other hand the lead cylinders require a sturdy support to ensure that no large parasitic vibrations occur. For this reason a 30 mm diameter, 1.5 mm thick carbon fiber composite tube was used for the frame material (for both the upper tube and the support tube). To further increase the ability to adjust the location of the rear frame front mass (in case the machine did not work as expected) two extra holes were drilled in the lower rear frame member (a square cross section - $30 \times 30 \times 1.5$ mm aluminum tubing), one to each side of the calculated position such that the lower end of the carbon fiber composite support tube could be placed over each of the three holes, thereby enabling the forward end of the upper frame tube to be raised or lowered by 5 cm.

The carbon tubes are connected to the aluminum lower frame by aluminum insert-brackets. The bracket-half of the insert-bracket is bolted to the the aluminum frame

Part	Mass [g]
Wheels	
Rotating	174
Counter rotating	167
Total	341
Rear frame	
Point mass at front	2197
Point mass at rear contact point	2013
Supporting construction	1874
Wheels	341
Total	6425
Front frame	
Point mass	1453
Supporting construction	618
Wheels	341
Total	2412
Total bicycle	8837

Table 5.2: *Mass distribution of the experimental TMS bicycle.*

by a single 8 mm bolt, whilst the insert half is glued (two-component epoxy) to the inside of the carbon tube. A jig was used to align the brackets and carbon tubes during the gluing process ensuring frame symmetry. The brackets used to connect the upper shaft with the support shaft were produced using the wire electric discharging machining (EDM) method.

A crucial part of the construction of the bicycle is the ‘head bearing’ required for steering. This ‘head bearing’ enables relative rotations between the front frame and rear frame. Its construction details are shown Figure 5.12. Both minimal play and minimal friction in this joint is required. Two small, 4 mm inner diameter, open single row deep groove ball bearings (D) were aligned by boring a hole straight through the aluminum head material (A) such that a bearing could be inserted from the top and bottom of the hole. To prevent the bearings from displacing axially, a cylinder (E), of which the outer surface was glued to the bored head, was placed between the two bearings (D). For a play-free connection between the front frame and rear frame a dowel (C) with thread on both ends was used as the axle through the bearings (D). Furthermore the two holes in the front frame head-bracket (B) were bored in one motion to ensure alignment. The gap between either side of the front frame head-bracket and the bearings was filled with a single spacer custom made to size (F). The dowel (C) was then clamped in place by nuts (H) tightened at both ends.

Using small bearings (D) ensures that the arm about which the friction occurs is only roughly 4 mm, therefore minimal steering torque is required to overcome the bearing friction. As the bicycle is intended to be used only on a smooth level surface, and without a rider, the axial loads on the small bearings remain within the bearing specifications.

To achieve zero gyroscopic effect, without being restricted to ice skating rinks, the bicycle was designed with two extra wheels that counter-rotate, one relative to the front wheel and the other relative to the rear wheel [66, 7]. The addition of counter-rotating wheels eliminates the net gyroscopic effect. In the dynamics model, the mass properties of the set of rotating and counter-rotating wheels contribute to the masses and moments of inertia of the front and rear frame.

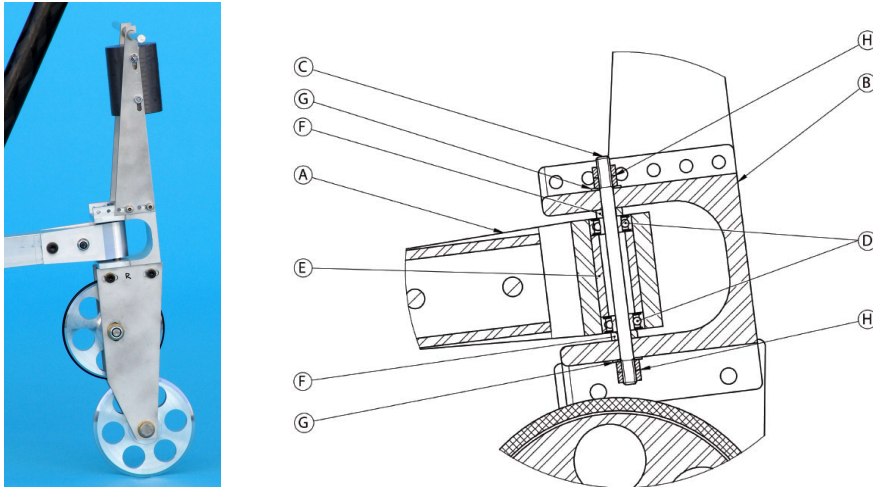


Figure 5.12: *left*) Side view of the front assembly of the experimental TMS bicycle. *right*) Front frame and steering head cross-section. (A) Rear frame head bracket, (B) Front frame head bracket, (C) Dowel with threaded ends, (D) Bearings, (E) Glued bearing spacer, (F) Spacer, (G) Washer, (H) Nuts.

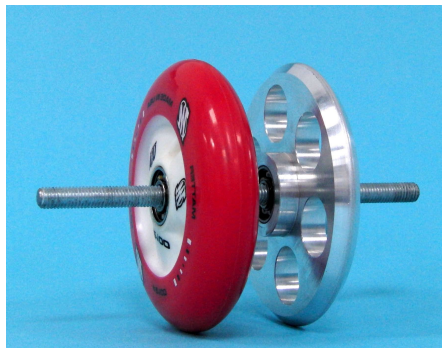


Figure 5.13: Two different types of 100 mm diameter wheels used, *left*: a polyurethane “inline skate” wheel, which didn't work, and *right*: the sharp aluminum wheel, with a crown radius of 2 mm, that was used in the experiments presented.

Another important design parameter is the mass moment of inertia of the front frame about the steering axis. For self-stability this should not be too large. Therefore the counter rotating wheels had to be placed approximately in line with the steering axis. However to counteract the offset of the front frame head bracket the counter rotating wheel was placed slightly more aft as can be seen in Figure 5.12.

A major concern was the wheel-to-ground contact. In the dynamics model, point contact is assumed. For conventional-size bicycle wheels with high-pressure pneumatic tires this has been shown to be reasonably accurate [81]. However, this model has small wheels. Initially 100 mm diameter polyurethane wheels (sold for use on inline skates) were used, see Figure 5.13 and section 5.3.6. However, with these polyurethane wheels rolling on a rubber gym floor, the experimental TMS bicycle showed no self stability. We conjecture that the large contact patch introduced a too large scrubbing torque, thereby destroying the steering dynamics. Next aluminum (7075-T6) wheels of 100 mm diameter were tried, with holes drilled through to reduce the mass, see Figure 5.13. These wheels have a 2 mm crown radius shape. With these sharp hard wheels on a rubber gym floor the experimental machine did show self-stability. A defect of this design, which was never improved upon, is the low coefficient of friction between aluminum and the rubber floor. The experiments were thus limited to small lean angles. At larger lean angles the wheels would slip laterally causing a low-side fall.

To keep the counter-rotating wheel rotating at the same speed as the ground-contact wheel, a groove was turned into the wheel tread of the counter-rotating-wheel and a rubber O-ring was placed in this groove, thereby making the total outer diameter of the counter-rotating-wheel 100 mm once more. This rubber O-ring increased the coefficient of friction between the counter-rotating and rotating wheel.

Slotted holes in the two fork plates (both front and rear) allow the counter-rotating wheels to be displaced. By tightening the axle bolt the counter rotating wheel can be fixed in place with some pressure between the two wheels, thereby preventing slip between the wheels.

5.3.4 Verification of the Produced Experimental TMS Bicycle

When the experimental TMS bicycle was produced all 143 parts (counting each bearing as single a part) were weighed individually and/or in subassemblies. Parts/subassemblies weighing less than 10 g were weighed to an accuracy of 0.01 g, those up to 2 kg with an accuracy of 1 g and for the assemblies up to 5 kg with an accuracy of 2 g. Table 5.3 specifies all the parts, their material and their masses. Note that the table is organized according to part type, while many parts were weighed as a set of a specific sub-assembly such that they could be compared with the independently developed SolidWorks CAD model. This reduces the precision for the nuts and bolts to 1 g instead of 0.01 g. The total mass predicted by the CAD model differed from the measured 8837 g by less than one gram.

Table 5.3: Part mass specified. Note that the part masses together do not add up to the sub totals indicated in table 5.2 , due to rounding off.

Part	Material	Nr of Units	Mass/Unit [g]	Total Mass [g]
Wheels				
Alu wheel	Aluminium 7075 T6	2	149	298
Alu counter wheel	Aluminium 7075 T6	2	137	274
Alu wheel cylinder	Aluminium 7075 T6	4	-	15
O-ring 90 x 4	rubber	2	5	10
Deep groove ball bearing, single row, unsealed	(SKF 608) d8,D22,B7	8	-	85
Front Frame				
Head	Aluminium 7075 T6	1	206	206
Handlebar	Aluminium 6082 T6	1	41	41
Handlebar fork plate	Aluminium 6082 T6	2	-	70
Front lead	Lead	1	1453	1453
Front fork plate	Aluminium 6082 T6	2	85	170
Front wheel spacer	Aluminium 7075 T6	4	-	12
Head bracket spacer	Aluminium 7075 T6	2	0.01	0.02
Dowel	CrNiMo Steel	1	7	7
Rear Frame				
Rear frame upper tube 1400x30x1.5	Carbon	1	316	316
Rear frame support tube 350x30x1.5	Carbon	1	79	79
Rear frame	Aluminium 6060	1	565	565
Rear bottom bracket	Aluminium 7075 T6	1	94	94
Rear plate	Aluminium 6082 T6	2	-	329
Lead rear half	Lead	2	997	1994
Wheel spacer	Aluminium 7075 T6	4	1	4
Middle bracket rear	Aluminium 7075 T6	1	40	40
Middle bracket front	Aluminium 7075 T6	1	46	46
Front bottom bracket	Aluminium 7075 T6	1	90	90
Head bracket	Aluminium 7075 T6	1	92	92
Head bracket cylinder	Aluminium 7075 T6	1	5.13	5.13
Deep groove ball bearings, single row, unsealed	(SKF 624) d4,D13,B5	2	-	5,38
Clamp	Aluminium 7075 T6	1	124	124
8mm threaded rod	Galvanized steel	2	31	62
Lead front half	Lead	2	972	1944
Bolts and Nuts & Rings				
DIN912-M8x50-8.8	Bolt (ISO 4762)	4	24	96
ISO4014- M8x55-A2-70	Bolt (DIN 931)	2	27	54
DIN125-B8,4- 140HV-St-Zn	Ring (ISO 7090)	12	-	20
Continued on next page				

Table 5.3 – continued from previous page

Part	Material	Nr of Units	Mass/Unit [g]	Total Mass [g]
DIN985-M8-8-Zn	Nylon locknut	6	5	30
JVK3D-M8-elekt.verz	3xh-M8 nut	2	25	50
DIN934-M8-8-ZnZ	Nut (ISO 4032)	2	5	10
DIN912-M4x10-A2-70	Bolt (ISO 4762)	4	-	7
DIN912-M4x65-8.8	Bolt (ISO 4762)	2	6	12
DIN125-A4,3-A2-140HV	Ring (ISO 7089)	10	-	2
DIN985-M4-8-Zn	Nylon locknut	2	1	2
DIN934-M4-A2-70	Nut (ISO 4032)	4	-	5
DIN912-M5x16-8.8	Bolt (ISO 4762)	4	-	14
DIN125-B5,3-A2	Bolt (ISO 7090)	8	-	3
DIN912-M5x35-8.8	Bolt (ISO 4762)	1	6	6
ISO1207-M5x55-4.8Zn	Bolt (DIN 84)	2	-	15
DIN985-M5-8-Zn	Nylon locknut	2	1	2
DIN912-M6x50-8.8	Bolt (ISO 4762)	4	13	52
DIN912-M6x25-8.8	Bolt (ISO 4762)	1	7	7
DIN125-B6,4-140HV-St-Zn	Ring (ISO7090)	10	1	10
DIN985-M6-8-Zn	Nylon locknut	5	2	10
TOTAL				8837.53

Measure of gyroscopic cancelation

How well have the gyroscopic effects been canceled by the counter rotating wheel? A rough measure of the size of the gyroscopic effect of the wheels is described by the non-dimensional coefficient (C_{ang}) of the spin angular momentum of a wheel divided by the mass of the bicycle, its forward speed and a characteristic length (height of the center of mass):

$$C_{ang} = \frac{\text{spin angular momentum of a wheel}}{(\text{mass of bicycle}) \cdot (\text{speed of bicycle}) \cdot (\text{height of bicycle})}$$

$$= \frac{J\omega_{wheel}}{m_{bicycle}vh} = \frac{Jv/r_{wheel}}{m_{bicycle}vh} = \frac{J}{m_{bicycle}hr_{wheel}}.$$

For a normal riderless bicycle $C_{ang} \approx 0.02$ and for the experimental TMS bicycle, before adding the counter-rotating wheels, $C_{ang} \approx 0.0008$. The counter-rotating wheels further reduce 90 % of even that effect. Why not 100 %? Because the counter rotating wheels have an aluminum groove cut out and an O-ring placed in the groove that is 6 g lighter. This makes the counter-rotating wheel only have 90 % of the rotary inertia of the rolling wheel. Thus the small light wheel has about 5 % the gyroscopic contribution of a normal bicycle wheel and 90 % of that is canceled. In total our bicycle thus has about 0.5 % (one part in 200) the gyroscopic effect of a normal bicycle. At 99.5 % gyro-free, the

author feels comfortable saying 'no-gyro'. Furthermore this value could have been easily reduced to zero or less, had the author thought through beforehand that rubber O-rings have a lower density than aluminium.

Experimental TMS parameter measurements

The developed SolidWorks CAD model was used to calculate the moments of inertia and locations of centers of mass. The geometry parameters such as wheelbase, steer axis tilt and location of the point masses were measured with standard mechanical hardware. A special procedure was used to measure the small negative trail.

To measure the trail the bicycle is placed in the upright position with a piece of paper placed underneath the front wheel and stuck to the ground with tape. The rear frame of the bicycle is clamped to prevent it from moving. The handlebar is then turned either way a number of times such that the wheel marks the paper. The bicycle is removed from the clamp and the mark on the paper is examined. The mark follows an arc, a line is drawn tangentially to either end of the mark. The point where the two lines cross indicates the point about which the wheel rotates. Next the arc traversed by the middle of the contact 'point' is drawn on the paper. The distance from the center point to the arc is approximately the trail. When the trail was measured in this manner it turned out to be -4 mm, that is, the contact point is 4 mm ahead of the intersection of the steer axis with the ground, or 4 mm negative trail.

The parameters of the experimental TMS bicycle are shown in Table 5.4. With these parameters a striking similarity between the eigenvalues of the theoretical TMS bicycle, Figure 5.7, and the final design of the experimental TMS bicycle, Figure 5.14, has been achieved.

5.3.5 Experimental Procedure and Results

When the experimental TMS bicycle had been refined to show self-stability, at least some times, and could even be perturbed laterally without falling over, the question rose how close the motion was to that predicted by the dynamic (Whipple) model. However, during the design stage it had explicitly been decided that no effort would be applied to making and integrating a measurement system for the bicycle, and all the effort was to be focussed on developing a bicycle that would show self stability. Therefore a measuring system had to be developed that could be added to the bicycle but did not interfere with the working or destroy its stable speed range. The required measurable variables were the rear frame lean and yaw angles and rates and the speed of the rear wheel. With these measured variables the model simulations can be compared with actual experiments with the experimental TMS bicycle.

Parameter	Symbol	Value for experimental TMS bicycle
Wheel base	w	0.750 m
Trail	c	-0.004 m
Steer axis tilt ($90^\circ - \text{head angle}$)	λ_s	7°
Gravity constant	g	$(90^\circ - 83^\circ)$ 9.81 N/kg
Forward speed	v	various m/s
Rear wheel R		
Radius	r_R	0.050 m
Mass	m_R	0 kg
Effective spin inertia	I_{Ryy}	$1.8 \cdot 10^{-5} \text{ kgm}^2$
Rear Body and frame assembly B		
Position center of mass (x_B, z_B)		$(0.5044, -0.4279) \text{ m}$
Mass	m_B	6.425 kg
Mass moments of inertia	$\begin{bmatrix} I_{Bxx} & 0 & I_{Bxz} \\ 0 & I_{Byy} & 0 \\ I_{Bxz} & 0 & I_{Bzz} \end{bmatrix}$	$\begin{bmatrix} 0.875295 & 0 & 1.18665 \\ 0 & 2.59262 & 0 \\ 1.18665 & 0 & 1.73573 \end{bmatrix} \text{ kgm}^2$
Front Handlebar and fork assembly H		
Position center of mass (x_H, z_H)		$(0.7338, -0.3022) \text{ m}$
Mass	m_H	2.412 kg
Mass moments of inertia	$\begin{bmatrix} I_{Hxx} & 0 & I_{Hxz} \\ 0 & I_{Hyx} & 0 \\ I_{Hxz} & 0 & I_{Hzz} \end{bmatrix}$	$\begin{bmatrix} 0.038384 & 0 & -0.00055657 \\ 0 & 0.038071 & 0 \\ -0.00055657 & 0 & 0.00143206 \end{bmatrix} \text{ kgm}^2$
Front wheel F		
Radius	r_F	0.050 m
Mass	m_F	0 kg
Effective spin inertia	I_{Fyy}	$1.8 \cdot 10^{-5} \text{ kgm}^2$

Table 5.4: Parameters of the experimental two-mass-skate (TMS) bicycle (shown in Figure 5.11).

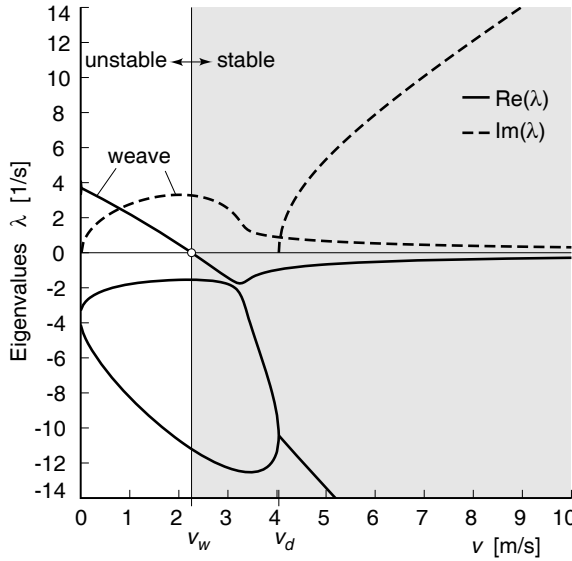


Figure 5.14: Eigenvalues for the experimental two-mass-skate (TMS) bicycle from Figure 5.11 and Table 5.4 in a forward speed range of $0 \leq v \leq 10$ m/s. Note that the real parts of all eigenvalues are negative for $v > 2.3$ m/s.

Measuring equipment

Not wanting the measuring system to substantially change the mass distribution we opted to use a Philips Pi-Node wireless transmitting inertial sensor measuring 3-D orientation, rate of turn and acceleration. Since added mass near the rear-wheel contact point has little effect on the lateral dynamics, the wireless transmitting inertial sensor was mounted just above the rear wheel for measuring the bicycle lean and yaw angles and rates (see Figure 5.15). The forward speed was measured post-facto by using a high speed video camera and counting the number of frames for a fixed number of rear-wheel rotations.

Here are some more details about the measured quantities:

Forward Speed: Half of the aluminum rear wheel was covered with black tape. A Casio Exilim EX-F1 digital photo camera was placed facing nearly perpendicular to the direction of the bicycle and used to video the motion of the bicycle with a frame rate of 300 frames per second. The launch speed of the bicycle was calculated by counting the number of frames (n_{frames}) required for the wheel to make three complete rotations by:

$$v = \frac{3 \cdot \pi \cdot 0.1}{\left(\frac{n_{frames}}{300}\right)} \text{ m/s} \quad (5.7)$$

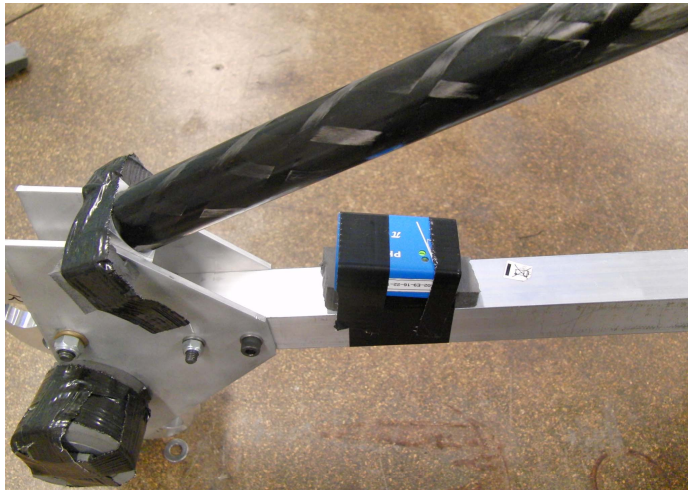


Figure 5.15: *The Philips Pi-Node Inertial Sensor located near the rear wheels and taped to padding, which in turn is taped to the lower rear frame member.*

Lean and Yaw: A Philips Pi-Node, a wireless transmitting inertial sensor that uses 3-D accelerometers and 3-D magnetometers to provide drift free orientation data and 3 gyroscopes to track fast changes in orientation, was used. The sensor has a wireless transmitting range of 100 m. The Pi-Node upper acceleration limit is 2 *g*. The small amplitude, but high frequency vibrations due to the road unevenness can cause this limit to be reached, which degrades the signal. The sensor was thus taped to padding that in turn was taped on the rear frame near the rear wheel (see figure 5.15). This padding attenuated the transmission of high-frequency small amplitude vibrations to the sensor.

Experimental procedure

Each experiment was carried out in a gym with a rubber-like floor by two experimenters. The first experimenter worked with the bicycle, the second operated the measurement laptop computer to start and stop the data recording and operated the high-speed video camera. An experimental run starts when the collection of data on the laptop computer has started and the high speed camera is running.

The handlebar of the bicycle is initially held in the straight ahead position whilst the bicycle is brought up to speed by pushing it along in a straight line. The experimenter releases the bicycle when the bicycle feels stable (as depicted in Figure 5.2). The experimenter then continues running alongside the bicycle until the lateral motions of the bicycle have mostly died out and the bicycle moves in a straight line. This is the start of the measurement. Next the bicycle is perturbed laterally by striking it (applying

an impulse) on the upper (carbon fiber) frame tube, instantly giving the rear frame a lean rate. The experimenter now follows the bicycle and catches it just before it either collides with another object (gym wall) or falls over due to the reduced speed. The bicycle is then returned to the initial location in preparation for the start of the next run.

Experimental Results

The experimental results of the measured motion are compared with the Whipple model as described by [94]. To do this first the matrix coefficients for the linearized equations of motion (see coefficients in equation 5.2) are determined with the parameter values from Table 5.4 resulting in

$$\begin{aligned} \mathbf{M} &= \begin{bmatrix} 2.310172 & 0.006029 \\ 0.006029 & 0.002974 \end{bmatrix}, & \mathbf{C}_1 &= \begin{bmatrix} 0 & 4.093917 \\ 0 & 0.027376 \end{bmatrix}, \\ \mathbf{K}_0 &= \begin{bmatrix} -3.477968 & -0.033536 \\ -0.033536 & -0.004099 \end{bmatrix}, & \mathbf{K}_2 &= \begin{bmatrix} 0 & 4.602036 \\ 0 & 0.044374 \end{bmatrix}. \end{aligned} \quad (5.8)$$

The theoretical transient response of the rear frame lean angle ϕ and the steer angle δ can then be calculated from the linearized equations of motion (5.1).

The yaw angle of the rear frame, ψ , is a so-called ignorable coordinate and does not show up in the equations of motion, (see [94]). The yaw angle can be calculated from the kinematic equation,

$$\dot{\psi} = \frac{v}{w} \cos(\lambda_s) \delta + \frac{c}{w} \cos(\lambda_s) \dot{\delta}, \quad (5.9)$$

which, with substitution of the bicycle parameters from Table 5.4, is

$$\dot{\psi} = 1.3234 v \delta - 0.0052936 \dot{\delta}. \quad (5.10)$$

For the initial conditions we take the upright configuration, $\phi_0 = 0$, straight ahead, $\delta_0 = 0$. We assume that the initial steer rate is zero, $\dot{\delta}_0 = 0$. The initial lean rate, $\dot{\phi}_0$, is now the only remaining parameter. This initial condition is determined from a best fit of the measured lean rate to the simulated one.

Figure 5.16 shows how the experiment (run 19) was carried out. Figures 5.17 and 5.18 show the measured and simulated states for the same experiment. Just prior to $t = -1$ the bicycle is released by the experimenter. The freely coasting bicycle is perturbed at $t = 0$ whilst it is moving at 3.6 m/s. At $t = 3$ the speed of the bicycle has reduced to 2.4 m/s. Shortly after the shown 5 seconds the bicycle is caught by the experimenter and returned to the start. To fit the simulation to the measured data an initial 0.45 rad/s ($t = 0$) lean rate, $\dot{\phi}$, was imposed in the simulation and the initial speed of 3.6 m/s was used. Obviously as the bicycle reduces speed the simulation deviates from the actual experiment.

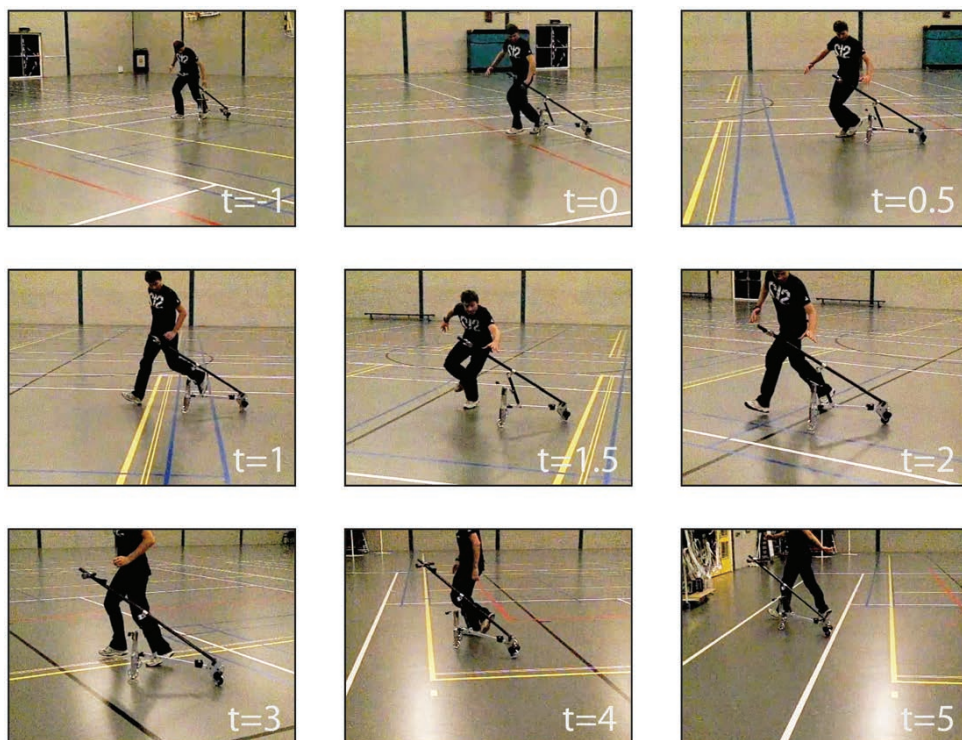


Figure 5.16: Still shots taken with the high speed camera of the experiment. At $t=0$ (top middle picture) the bicycle is given an impulse to the left (hit by the hand of the experimenter). The bicycle changes direction faster than the experimenter can and thus it looks like the experimenter wants to grab hold of the bicycle at $t=1.5$ (center picture).

Figure 5.18 shows that the bicycle's initial upright orientation was nearly vertical, even though the lean rate, shown in Figure 5.17, was not quite zero prior to the application of the impulse. The data shows that the direction of the bicycle was also not quite along the length of the sports hall (yaw angle equals zero when moving along the length of sports hall (from north to south)). This can also be seen in the recorded movie data.

During the first 3.5 seconds after the perturbation the simulation and experimental results in both lean and yaw angle and rate are very similar. After 1 second the lean and lean rate measurement results start to deviate a little from that of the simulation but the experimental measurements closely follow the trend of the simulation. After 3.5 seconds the yaw angle and yaw rate drastically deviate from that of the simulation. This coincides with roughly the moment the bicycle begins to become unstable due to the loss in speed as after 3 seconds $v = 2.4$ m/s, and according to the dynamics model (see figure 5.14) the bicycle is only stable for $v > 2.3$ m/s.

Directly after the perturbation there is a distinct difference between the experimental and simulation results in the yaw motion. The simulation indicates that (as expected) the externally applied lateral force to the left (positive steer angle is to the right) causes the bicycle to turn directly to the left. However in the experimental results we see that the bicycle initially turns to the right (as seen in both the yaw and yaw rate data). Initially the sensor readings were doubted. However, in some of the movies that we had made, the camera was positioned behind the bicycle on a skateboard that followed the bicycle from behind. These movies showed that when the bicycle is struck to the left (at a high point on the frame) it starts to lean to the left, as expected. Simultaneously, however, the front wheel slips to the right causing the recording of a sudden yaw to the right. However the bicycle generally quickly recovers from this slip (requires roughly 0.3 s).

5.3.6 The Experiment, General Observations and Experiences

Physical experiments are performed in the real world, in non-ideal situations. Therefore it was envisioned that some sort of damping would be required in the wheels to compensate for the vertical unevenness of the floor. The first version of the final experimental machine had 100 mm diameter polyurethane inline-skate wheels (Figure 5.13). However the bicycle fitted with these wheels seemed to have 'locked steering' similar to what was seen earlier with the Mark1 bicycle. Again this was presumably because of the high friction in the contact patch.

The aluminum knife-edged wheels were installed to reduce the large scrubbing torque. However, with the aluminum wheels we found performance differences that were floor dependent. The very hard wooden sports hall floors had the drawback that the surface was not continuous. The transition from one plank to the next destabilized the bicycle, occasionally tipping the bicycle or causing it to shift. The slightly softer, continuous, linoleum floor did not have the drawback of the transitions, but the coefficient of friction between the aluminum wheel and linoleum floor was so small that the smallest lateral

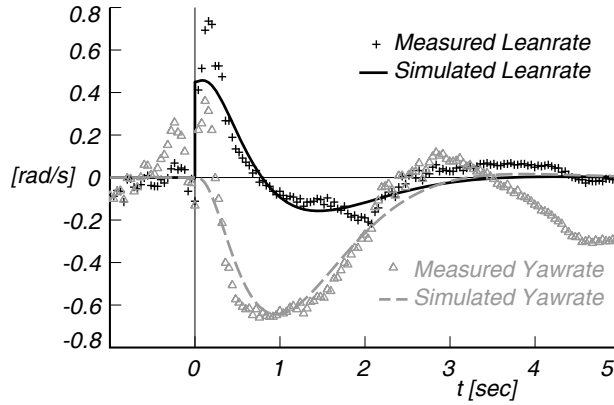


Figure 5.17: Transient motion after a disturbance for the physical TMS bicycle. Measured and predicted lean and yaw rates are shown.

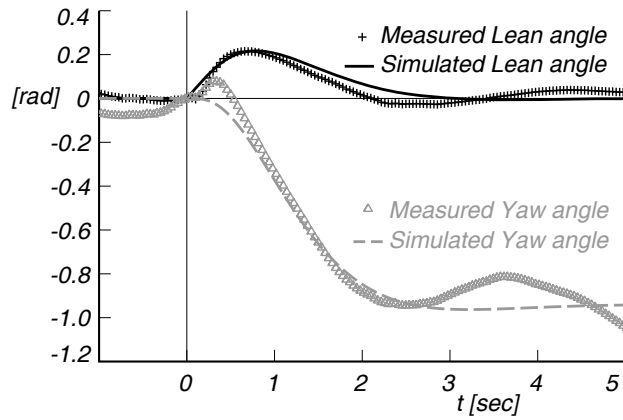


Figure 5.18: Transient motion after a disturbance for the physical TMS bicycle. Measured and predicted lean and yaw angles are shown.



Figure 5.19: snapshot of the TU Delft sports hall nr. 2 floor directly after the wheel of the experimental TMS bicycle has been lifted up off the ground. The 2 cm wheel indent is clearly visible (5–7 cm) below the ruler.

perturbation caused the front wheel to slip away, making the bicycle fall over. The Delft University of Technology's sports center has two large sports halls with a rubber floor. The coefficient of friction between the rubber floors and the aluminum wheels is significantly larger than between the harder wooden and linoleum floors and the wheels. However sports hall number 1 has a relatively thick and soft rubber floor which significantly deforms under the bicycle wheels. The damping of this floor was so large that the bicycle reduced speed too fast to get a chance to see self-stability. The floor of sports hall number 2 was made of a thinner layer of rubber, which showed far less damping, allowing the experiments to be carried out successfully.

The rapid reduction in speed can be attributed to the significant rolling resistance that the wheels experience on the soft rubber floor. The contact between the wheels and the ground could hardly be called “point” contact. On the rubbery surface the wheels left an indent in the floor that was roughly 20 mm long. This contact length (S) is shown in Figure 5.19. For a rolling wheel the hysteresis in the rubber causes the net resultant reactive force (N) acting on the wheel to be shifted forward with respect to the center of the wheel, thus resulting in a net moment acting in the opposite direction to the motion of the wheel as shown in figure 5.20.

For a wheel the resulting rolling resistance coefficient (C_r) can be calculated as

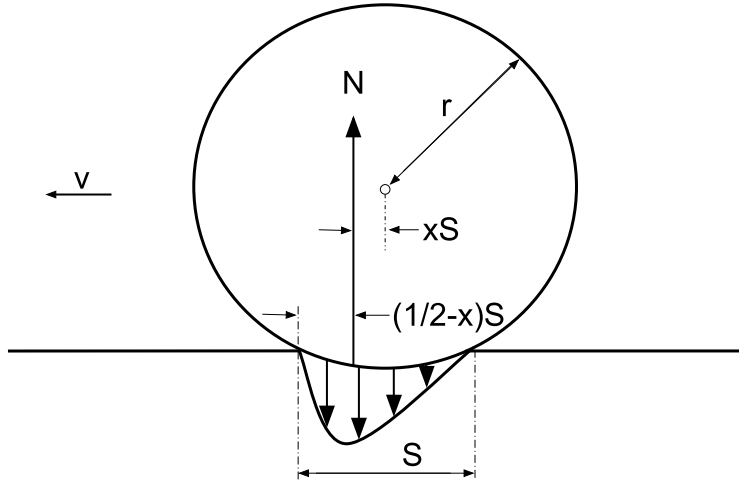


Figure 5.20: A wheel rolling forward deforms the rubber floor of the sports hall. The pressure pattern due to the hysteresis of the rubber causes a resultant vertical force that acts in front of the middle of the contact length (S), resulting in a resistive torque.

follows:

$$\begin{aligned}
 M &= x \cdot S \cdot N & : M \text{ can also be estimated as} \\
 M &= r \cdot F_R & \text{where } F_R \text{ is the rolling resistance} \\
 F_R &= C_r \cdot N & \text{therefore,} \\
 r \cdot C_r \cdot N &= x \cdot S \cdot N \\
 C_r &= x \cdot \frac{S}{r}.
 \end{aligned}$$

If the pressure distribution remains constant (x is constant) then the rolling resistance coefficient C_r depends on the ratio of the contact length (S) with the wheel radius (r). Thus the rolling resistance coefficient in this case, can be expected to be roughly an order larger than for a normal bicycle.

A method to determine the rolling resistance coefficient of the wheels on the sports hall floor uses the average deceleration during the measurements with the recorded video material. The speed is determined for the bicycle just prior to the perturbation (when it is already rolling freely) and then the speed is measured again a number of seconds later near the end of the experiment. The deceleration is calculated from the speed difference and time between the two measurements, with the result being $C_r = 0.035$. This value is about 10 times larger than that for conventional bicycle tires on hard pavement [167].

Interestingly the trail of the TMS bicycle can in theory be varied between -9 mm and $+20$ mm and still remain stable. The weave speed will however be very different at these values. For -9 mm the weave speed will drop to 1.7 m/s whilst at $+20$ mm

it will have increased to 9.5 m/s. In summary, the wheel contact was surely far from point contact and the results are sensitive to the contact conditions. That the physical model, when it worked, corresponded well in behavior to the theoretical model could in fact be partly fortuitous.

Lateral symmetry turned out also to be a delicate issue. Because of damage and misalignments that occurred during falls, and because of padding added to prevent damaging the gym floor in the event of a fall, the bicycle was not perfectly symmetrical. We found that any small lateral symmetry offset had a large effect on the resulting stable path. A slight imbalance led to a circular path. Adjustment of the lateral position of the rear frame front masses (recall the threaded rod holding the rear frame front masses) could restore the symmetry and change the stable path back to a straight one.

Another issue that the bicycle has is a high frequency steering oscillation that appears when the bicycle is brought up to speed. Whilst small and undetectable in photographs, this steering motion can clearly be seen in high speed videos of the experiments [148]. This small amplitude oscillation has a frequency of roughly 20 Hertz. When the bicycle was not self stable (locked steering, polyurethane wheels, etc.) the high frequency steering oscillation was not present.

It was not directly clear what the cause of this oscillation was so we carried out a number of tests to determine its origin. We noticed that the oscillations occur on all the floors we experimented on, and the phenomenon always started at roughly walking speed. From the high speed videos that we made we determined that the oscillations have roughly the same frequency on all surfaces, about 20 Hz. The amplitude is also roughly similar (we did not measure it) on all surfaces we tested on and always settles into a limit cycle. This suggested that the cause of the oscillations could be front wheel shimmy. Shimmy is an oscillatory, combined lateral-yaw motion [108, 12]. It is normally caused by the frame and wheel structural dynamics and the dynamic tire behavior (or in this case most likely the dynamic ground behavior). To investigate whether it was indeed shimmy we started by investigating the effect of adjusting the play about the head bearing by adjusting the nuts (H) on the dowel (C) in Figure 5.12. When the tension was decreased (play occurs in the head), no significant change was noted in the situation. However when the tension was increased and (any play remaining was removed) a small amount of pretension was placed on the head bearing, not only did the self stability of the bicycle disappear, but so did the high frequency steering oscillation indicating that it is indeed a shimmy phenomenon.

To be certain that the phenomenon really was shimmy we investigated further. Firstly we tried pressing down hard on the frame whilst pushing it along. This did not change the situation, the vibrations continued. Next we investigated the effect of the interaction between the rotating and counter-rotating wheel. First we firmly pressed the counter rotating wheel against the rotating wheel. This was done to be absolutely sure that the wheels were not slipping relative to one and other, this also made no difference to the vibration, but did cause the bicycle to decelerate drastically. Next to be sure that any angle offset between the rotating and counter-rotating wheels causing gyroscopic

steering torque was not the cause, the counter-rotating wheel was lifted slightly such that it no longer made contact with the rotating wheel so that the counter-rotating wheel no longer rotated, leaving just the ordinary situation with one rotating wheel. This made no difference to the shimmy either. As this adaption was not performed in the sports hall it is unclear if it had an effect on the stability of the bicycle. Completely removing the counter-rotating wheel altogether did not significantly improve the situation either. The final modification (with respect to the standard situation where both wheels were installed and the machine had straight ahead, upright, stability) that was tried was to drastically adjust the front frame's mass and inertia. We did this by removing the front frame point mass (C in Figure 5.11). This drastically changed the steering characteristics of the bicycle, which no longer showed any steering tendency and of course no self-stability, but it also completely removed the steering vibration. Thus we conclude that this high frequency oscillation is indeed shimmy and which is in this case of little influence on the global dynamics of the bicycle.

5.3.7 Conclusions

The Whipple bicycle model, with its gross simplifications of the real bicycling system is a very robust model capable of accurately predicting the general lateral motion of a bicycle. It is capable of accurately predicting the uncontrolled bicycle lateral behavior even when the actual bicycle significantly stretches some of the modeled assumptions. The experimental TMS bicycle, with its small aluminium wheels, can certainly no longer be said to make pure rolling point contact with the soft rubber sports hall floor. The front wheel was also found to slip laterally slightly after the bicycle was perturbed laterally and due to the large contact length and resulting deformation of the floor the bicycle suffers from roughly ten times as much rolling resistance as a normal bicycle tire does on a hard dry surface. Yet the experimental TMS bicycle still displays very similar dynamics to that of the theoretical TMS bicycle model demonstrating the robustness of the Whipple bicycle model.

The TMS bicycle works due to its small parameter values, in particular with respect to the front frame and wheel. The roll to steer coupling is very small for the theoretical TMS bicycle due to the massless steering assembly and small point mass placed close to the nearly vertical steering axis. Therefore the experimental TMS bicycle must have the same characteristics and in order for the experimental TMS bicycle to show lateral dynamics the steering frictions as a result of the tire scrub and the friction in the head bearing must be kept to a minimum. For this reason the implementation of industry standard one inch (or larger) diameter bicycle head bearings, and a rubber wheel/tire are insufficient for the correct working of the TMS bicycle. The required light and delicate front assembly has another disadvantage as the physical construction is susceptible to misalignments that can easily occur when the bicycle falls over, which also prevents the correct working of the bicycle.

The experimental TMS bicycle very clearly displays a high frequency oscillation of

the steering assembly when rolling forward which has been determined to be shimmy and predominantly caused by play in the head bearing. The shimmy however only slightly influences the general lateral dynamics of the experimental TMS bicycle. Thus even though the Whipple bicycle model does not model shimmy it is capable of accurately predicting the general lateral motion.

5.4 General Conclusions

The results of the treadmill measurements compare very well to those of the Whipple bicycle model. Therefore riding a bicycle on a treadmill with constant belt velocity is dynamically equivalent to riding a bicycle on flat level ground around the straight ahead direction with constant speed. However riding a bicycle on a treadmill is not experienced by the human rider in the same manner as on the open road due to the missing optic flow.

The Whipple bicycle model is a robust model that can be used for predicting the lateral dynamics of a bicycle. It can be used to predict bicycle lateral motions even when some of the model assumptions are not really met such as the idealized point contact between wheel and ground and the play and frictionless joints. It was shown with the experimental TMS (Two-Mass-Skate) bicycle, which has small wheels and a light steering system that the general motion of the bicycle can be predicted accurately despite the play in the head bearing causing shimmy to take place, the relatively large wheel to ground contact length resulting in significant rolling resistance and initial slip of the front wheel when the bicycle is laterally perturbed.

CHAPTER 6

Conclusions and Recommendations for Further Research

6.1 Conclusions

No generally accepted and experimentally validated bicycle rider models exist that describe bicycle rider control. While many authors have observed rider control qualitatively, only few have quantitatively observed the performed rider control. This lack of actual observation data has led to a wide set of unsubstantiated assumptions amongst authors about possible control methods. These assumptions include upper body lean control, and many forms of parameter optimization control (control effort, trajectory deviation, time, distance) (Chapter 2).

A number of performance criteria measures have been proposed for motorcycles, but only one quantitative metric has been proposed for bicycles. This task independent performance criterion for bicycle handling is based on the research carried out for pilot-aircraft control modeling and has yet to be validated for the bicycle-rider situation. All the other handling quality work that has been performed for bicycles has been qualitative and experimental in nature. Due to the different settings and experiments performed by the different authors the results are not directly comparable amongst each other (Chapter 2).

The treadmill and open-road observation experiments performed in our work with the instrumented bicycle and motion capture equipment (Chapter 3) show that:

- A rider performs steering actions to stabilize the bicycle and the amplitude of the steering motion is inversely proportional to the speed.
- With the rider's hands on the handlebar all of the bicycle rider's upper body motion is linked to the pedaling motion. When the rider does not pedal, no upper body motion takes place.

- At very low forward speed, where the bicycle and rider system is highly unstable, a second control action is observed. The knees are seen to move laterally, both in phase and out of phase.
- On two different style bicycles, two different riding postures have been observed and the riders perform different motions when stabilizing the bicycle in these two different postures. Posture 1: The rider has stretched arms and leans forward to reach the handlebar. The arms can rotate about the shoulders and the upper-body can rotate about the pelvis. The complete upper-body rotates when the rider steers in this posture. Posture 2: An upright rider upper-body posture where the arms are bent at the elbows seen on typical city bicycles. In this posture the performed rider motion consists of only moving the arms which can rotate at the shoulders and elbows.

A first step in modeling actual rider motions has been performed by introducing a passive rider model to the Whipple bicycle model. The inclusion of rider pelvis- and shoulder-rotational degrees of freedom (posture 1) does not significantly alter the open loop stability but the upright posture with shoulder- and elbow- rotational degrees of freedom (posture 2) does significantly alter the open loop stability. For both postures however, the system is controllable at all forward moving speeds (Chapter 4).

At present bicycle handling cannot be predicted as there are no generally accepted and experimentally validated bicycle rider models. However, it is suspected, but not yet proven, that the ease with which a bicycle can be ridden is correlated with the self-stability of the uncontrolled bicycle, or at least to not too much self-instability. There has been near universal acceptance that either the spin angular momentum (gyroscopic effect) or trail of the front wheel or both are necessary for self-stability. However, in this thesis (Chapter 5) it is shown that neither is necessary and that a bicycle can be built without gyros and with no trail that is self stable. It is not denied that gyroscopic effect and trail can contribute to self-stability, however other parameters are also important, especially the front-assembly mass distribution. Of the necessary conditions for self-stability one has been found which can be physically interpreted: a self-stable bicycle must steer into the fall.

6.2 Recommendations for Future Work

The work presented in this thesis has given new insight into the control actions that a rider performs on a bicycle but has certainly not come to the definitive answer on how a rider controls a bicycle. Questions that have arisen as a result of this work include:

- *system identification*

To identify the performed rider control during different situations system identification techniques can be applied to the bicycle-rider system. This is similar to the well developed field of aircraft pilot control identification and can be performed in a similar manner to Weir [160] (theoretically) and Eaton [39] (experimentally)

who performed system identification for motorcycle rider control and the work by de Lange [33] who applied it to riding a bicycle on a narrow treadmill. Unlike in the field of aircraft simulation there are no bicycle simulators. However as the dangers involved are far lower in cycling, system identification could be performed on a real bicycle. To perturb the bicycle either the steering could be actuated (for example by using a steer by wire system so that the rider does not feel the perturbation directly on the handlebar) or the frame could be tilted (for example by moving a large mass on the rear rack). System identification of the bicycle rider control can be performed to investigate a number of aspects including:

- Investigating the difference in the control performed when the rider is rigidly attached (braced) to the bicycle and when the rider is free to move (normal situation).
 - Identifying the feed forward tracking control that is performed by the rider during normal riding situations.
 - Determining the linearity of rider control. Is the control linear in the time and/or linear in amplitude?
 - Determining in what way the control performed by a particular group of cyclists (elderly, young children, etc.) differs from that of modal riders.
 - Determining whether a rider performs different control (optimizations) under different circumstances, such as during normal riding and racing circumstances.
 - Identifying how riders adapt and optimize their control when learning to ride a bicycle or as they adjust to a new bicycle.
 - Determining the effect of adding stability enhancing devices on rider control.
- *Intermittent control*

Whilst most authors have modeled rider control as a continuous controller it could be beneficial to investigate intermittent control for normal bicycling where the rider follows a path (road/treadmill). In intermittent control, control actions are only performed from time to time such as when some parameter goes beyond some pre-determined value. The measured bicycle steering angle in both the treadmill experiments and the open road experiment (Chapter 3) show that at low speeds there is wide bandwidth of low frequency steering motion taking place. This wide band is uncharacteristic for a simple continuous control system and suggests that discrete control is being performed by the rider. Doyle [36] previously investigated intermittent control both theoretically and experimentally and found good agreement, making this route very promising.

- *optimal control*

It is generally accepted that humans are (sub)optimal controllers. However it is unclear what a bicycle rider is optimizing. Using experimental data from stabilizing and tracking experiments and inversely applying it to the optimal control procedure could give insight into the rider optimizing behavior.

- *low speed rider control*

Many of the cycling accidents occur at very low speeds. In the observation experiments it was seen that the knees are moved laterally at very low speeds. Adding two degrees of freedom to the passive rider models (Chapter 4) to enable the legs to rotate (about the plane through the hip and foot) could give insight into the cause for this seen rider motion, and give insight into low speed rider control.

- *rider posture*

The rider posture has a significant effect on the open loop dynamics. It is unclear how the posture is linked to control effort, and the handling quality and should be investigated both experimentally and theoretically. Particular interest for practical experiments are the widely available in height adjustable handlebar. Handling tests can then be performed using the same bicycle but with the handlebar in two different positions: up and towards the rider; or down and further forward, and thereby substantially change the rider posture. Initial qualitative tests have indicated that the rider perceives very different handling in the two situations.

- *handling control metrics*

This area is still largely unexplored. No standard handling maneuvers have been defined for bicycles and no validated task independent handling control metrics are available; therefore there is still a great deal of research to be done in this field.

- *bicycle design scope*

Even without a complete handling metric using the assumption that bicycle self stability or at least not to large instability is essential for good handling, bicycle configurations specifically aimed at improving certain situations can be explored. Examples include configurations that enhance low speed stability which could be beneficial for elderly riders, and rear wheel steer bicycle configurations that could enable sleeker, more aerodynamic bicycles for high speed commuting purposes.

- [1] Abbink, D. and Mulder, M. (2010). *Advances in Haptics*, volume 109, chapter Neuromuscular Analysis as a Guideline in designing Shared Control, pages 499 – 516. InTech.
- [2] Abbink, D., Mulder, M., Van der Helm, F., Mulder, M., and Boer, E. (2011). Measuring neuromuscular control dynamics during car following with continuous haptic feedback. *Systems, Man, and Cybernetics, Part B: Cybernetics, IEEE Transactions on*, 41(5):1239 – 1249.
- [3] Andreo, D., Cerone, V., Dzung, D., and Regruto, D. (2009). Experimental results on l_{pv} stabilization of a riderless bicycle. In *American Control Conference, 2009. ACC '09*, pages 3124 – 3129.
- [4] Aoki, A. (1979). Experimental study on motorcycle steering performance. Technical Report 790265, SAE.
- [5] Aoki, A., Nishimi, T., Okayama, T., and Katayama, T. (1999). Effectiveness of the basic model for motorcycle dynamics. *Japan Society of Mechanical Engineers*, (98-1925):110 – 116.
- [6] Arnberg, P. W. and Tyden, T. (1974). Stability and maneuverability performance of different types of bicycles. Technical Report 45 A, National Swedish Road and Traffic Research Institute.
- [7] Åström, K. J., Klein, R. E., and Lennartsson, A. (2005). Bicycle dynamics and control; adapted bicycles for education and research. *IEEE Control Systems Magazine*, 25(4):26 – 47.

- [8] Baron, S., Kleinman, D. L., and Levison, W. H. (1970). An optimal control model of human response part II: Prediction of human performance in a complex task. *Automatica*, 6(3):371 – 383.
- [9] Bellati, A., Cossalter, V., and Garbin, S. (2003). Mechanisms of steering control of motorcycles. In *9th International Conference "High-Tech Cars and Engines"*, Modena, Italy.
- [10] Berritta, R. and Mitolo, L. (2002). Evaluation of motorcycle performance in U turn test using multibody code LMS DADS. In *"High-Tech Cars and Engines", Components, Materials, Technologies and Innovative Systems, May 30 – 31*.
- [11] Bertolazzi, E., Biral, F., DaLio, M., and DallaFontana, M. (2006). Motion planning algorithms based on optimal control for motorcycle-rider system. In *The 31st FISITA World Automotive Congress (FISITA 2006)*, number F2006V209.
- [12] Besselink, I. (2000). *Shimmy of Aircraft Main Landing Gears*. PhD thesis, Delft University of Technology.
- [13] Bocciolone, M., Cheli, F., Leo, E., and Pezzola, M. (2007). Experimental identification of kinematic coupled effects between driver – motorcycle. In *IMAC - XXV: A Conference & Exposition on Structural Dynamics*, number ISBN: 0912053968, February 19 – 22, Orlando FL.
- [14] Bryson, A. and Ho, Y. (1975). *Applied optimal control*. Wiley New York.
- [15] Cangle, P., Passfield, L., Carter, H., and Bailey, M. (2010). Modelling mechanical enhancements in competitive cycling. In *Proceedings, Bicycle and Motorcycle Dynamics 2010 Symposium on the Dynamics and Control of Single Track Vehicles*, 20 - 22 October 2010, Delft, The Netherlands.
- [16] Capitani, R., Masi, G., Meneghin, A., and Rosti, D. (2006). Handling analysis of a two-wheeled vehicle using MSC.ADAMS/motorcycle. *Vehicle System Dynamics*, 44, Supplement:698 – 707.
- [17] Carvallo, E. (1899). *Théorie du mouvement du monocycle et de la bicyclette*. Gauthier-Villars, Paris, France. (Submitted in 1897 for the Prix Fourneyron, awarded shared second place in 1898.).
- [18] Cerone, V., Andreo, D., Larsson, M., and Regruto, D. (2010). Stabilization of a riderless bicycle, a linear-parameter-varying approach. *IEEE Control Systems Magazine*, 30(5):23 – 32.
- [19] Chen, C. K. and Dao, T. S. (2005). Dynamics and path-tracking control of an unmanned bicycle. In *Proceedings of IDETC/CIE 2005*, number DETC2005-84107. ASME.

- [20] Chen, C. K. and Dao, T. S. (2006). Fuzzy control for equilibrium and roll-angle tracking of an unmanned bicycle. *Multibody System Dynamics*, 15(4):325 – 350.
- [21] Chen, C. K. and Dao, T. S. (2007). Genetic fuzzy control for path-tracking of an autonomous robotic bicycle. *Journal of System Design and Dynamics*, 1(3):536 – 547.
- [22] Connors, B. and Hubbard, M. (2008). Modelling and stability analysis of a recumbent bicycle with oscillating leg masses. In Estivalet, M. and Brisson, P., editors, *The Engineering of Sport 7*, volume 1, pages 677 – 685. ISEA, Springer Paris.
- [23] Cook, M. (2004). It takes two neurons to ride a bicycle. In *Proceedings of the 18th Annual Conference on Neural Information Processing Systems*.
- [24] Cooper, G. E. and Harper, R. P. (1969). The use of pilot rating in the evaluation of aircraft handling qualities. Technical Report NASA TN D-5153, National Aeronautics and Space Administration (NASA).
- [25] Cossalter, V. (2002). *Motorcycle Dynamics*. Number ISBN 0972051406. Race Dynamics, Greendale, WI., first edition.
- [26] Cossalter, V., Bellati, A., Doria, A., and Peretto, M. (2008). Analysis of racing motorcycle performance with additional considerations for the Mozzi axis. *Vehicle System Dynamics*, 46, Supplement:815 – 826.
- [27] Cossalter, V., DaLio, M., Biral, F., and Fabbri, L. (1998). Evaluation of motorcycle maneuverability with the optimal maneuver method. Technical Report 983022, SAE.
- [28] Cossalter, V., DaLio, M., Lot, R., and Fabbri, L. (1999). A general method for the evaluation of vehicle manoeuvrability with special emphasis on motorcycles. *Vehicle System Dynamics*, 31:113 – 135.
- [29] Cossalter, V. and Doria, A. (2004). Analysis of motorcycle slalom manoeuvres using the Mozzi axis concept. *Vehicle System Dynamics*, 42(3):175 – 194.
- [30] Cossalter, V., Doria, A., Fabris, D., and Maso, M. (2006). Measurement and identification of the vibration characteristics of motorcycle rider. In *Proceedings of ISMA 2006*, pages 1793 – 1806.
- [31] Cossalter, V., Lot, R., Massaro, M., and Sartori, R. (2011). Development and validation of an advanced motorcycle riding simulator. *Proceedings of the Institution of Mechanical Engineers, Part D: Journal of Automobile Engineering*, 225:705 – 720.
- [32] Cossalter, V. and Sadauckas, J. (2006). Elaboration and quantitative assessment of manoeuvrability for motorcycle lane change. *Vehicle System Dynamics*, 44(12):903 – 920.

- [33] de Lange, P. (2011). Rider control identification in bicycling. Master's thesis, Delft University of Technology.
- [34] Dempster, W. T. (1955). Space requirements of the seated operator, geometrical, kinematic and mechanical aspects of the body with special reference to the limbs. Technical Report WADC 55-159, Wright-Patterson AFB, Ohio.
- [35] Döhning, E. (1953). *Über die Stabilität und die Lenkkräfte von Einspurfahrzeugen*. PhD thesis, Braunschweig.
- [36] Doyle, A. J. R. (1988). The essential human contribution to bicycle riding. *Training, Human Decision Making and Control*, pages 351 – 370.
- [37] Dressel, A. E. (2006). The benchmarked linearized equations of motion for an idealized bicycle (implemented in software and distributed via the internet). Master's thesis, Cornell University.
- [38] Eaton, D. (1973). An experimental study of the motorcycle roll stabilization task. Technical Report N75 19145, Highway Safety Research Institute, University of Michigan, Ann Arbor.
- [39] Eaton, D. (1973). *Man-Machine Dynamics in the Stabilization of Single-Track Vehicles*. PhD thesis, University of Michigan.
- [40] Elkind, J. (1956). Characteristics of simple manual control systems. Technical Report 111, MIT, Lincoln laboratory Technical Report.
- [41] Evertse, M. (2010). Rider analysis using a fully instrumented motorcycle. Master's thesis, Delft University of Technology.
- [42] Foale, T. (2006). *Motorcycle Handling and Chassis Design*. Number ISBN 8493328634. Mediaprint, second edition.
- [43] Frendo, F., Sisi, A., Guiggiani, M., and Di Piazza, S. (2006). Analysis of motorcycle models for the evaluation of the handling performances. *Vehicle System Dynamics*, 44, Supplement:181 – 191.
- [44] Frezza, R. and Beghi, A. (2003). *New Trends in Nonlinear Dynamics and Control*, chapter Simulating a motorcycle driver, pages 175 – 186. Berlin Heidelberg: Springer-Verlag.
- [45] Fujii, S., Panfilov, S. A., and Ulyanov, S. V. (2004). A model for motorcycle rider operation based on genetic algorithms. *Yamaha Motor Technical Review*, (38):132–139. Journal Code: L3777A.
- [46] Gallaspy, J. M. and Hung, J. Y. (1999). Gyroscopic stabilization of a stationary unmanned bicycle. Auburn University.

- [47] Getz, N. H. (1995). *Dynamic Inversion of Nonlinear Maps with Applications to Nonlinear Control and Robotics*. PhD thesis, University of California at Berkeley.
- [48] Getz, N. H. (1995). Internal equilibrium control of a bicycle. In *Proceedings of the 34th Conference on Decision & Control*, pages 4285 – 4287, December 1995, New Orleans, LA.
- [49] Getz, N. H. and Marsden, J. E. (1995). Control for an autonomous bicycle. In *IEEE International Conference on Robotics and Automation*.
- [50] Giner, D. M., Brenna, C., Symeonidis, I., and Kavadarlic, G. (2008). Mymosa towards the simulation of realistic motorcycle manoeuvres by coupling multibody and control techniques. In *Proceedings of IMECE2008 2008 ASME International Mechanical Engineering Congress and Exposition*, number IMECE2008-67297, November 2 – 6, 2008, Boston, Massachusetts.
- [51] Godthelp, J. and Buist, M. (1975). Stability and manoeuvrability characteristics of single track vehicles. Technical Report IZF 1975 C-2, TNO - IZF.
- [52] Godthelp, J. and Wouters, P. (1978). Koers houden door fietsers en bromfietsers. *Verkeerskunde*, (11):537 – 543.
- [53] Goetz, T. and von Drais von Sauerbronn, K. F. C. L. (1820). Draisinen. *Journal für Literatur, Kunst, Luxus und Mode*, pages 365 – 377.
- [54] Guo, K. and Guan, H. (1993). Modelling of driver/vehicle directional control system. *Vehicle System Dynamics*, 22(3-4):141 – 184.
- [55] Gyrobike (2012). <http://www.thegyrobike.com/>.
- [56] Hand, R. S. (1988). Comparisons and stability analysis of linearized equations of motion for a basic bicycle model. Master's thesis, Cornell University.
- [57] Heemskerk, R., Janssen, R., Bots, R., and Hutschemaekers, J. (2010). Waarom remmen voor de bocht? Bachelor's thesis, Delft University of Technology.
- [58] Herfkens, B. D. (1949). De stabiliteit van het rijwiel. Technical Report S-98-247-50-10-'49, Instituut voor Rijwielontwikkeling.
- [59] Herlihy, D. V. (2004). *Bicycle: The History*. New Haven and London: Yale University Press, 2004. ISBN: 0300120478, 9780300120479.
- [60] Hess, R. (1977). Prediction of pilot opinion ratings using an optimal pilot model. *Human Factors: The Journal of the Human Factors and Ergonomics Society*, 19(5):459 – 475.

- [61] Hess, R. A., Moore, J. K., and Hubbard, M. (2012). Modeling the manually controlled bicycle. *IEEE Transactions on Systems, Man and Cybernetics, Part A: Systems and Humans*, 42(3):545 – 557.
- [62] Hubbard, M. (1979). Lateral dynamics and stability of the skateboard. *Journal of Applied Mechanics*, 46:931 – 936.
- [63] Hubbard, M. (1980). Human control of the skateboard. *Journal of Biomechanics*, 13(9):745 – 754.
- [64] Imaizumi, H., Fujioka, T., and Omae, M. (1996). Rider model by use of multibody dynamics analysis. *Japanese SAE*, 17:75 – 77.
- [65] Iuchi, K., Niki, H., and Murakami, T. (2005). Attitude control of bicycle motion by steering angle and variable COG control. In *IECON 2005*, pages 2065 – 2070.
- [66] Jones, D. E. H. (1970). The stability of the bicycle. *Physics Today*, 23(4):34 – 40. (reprinted in September 2006).
- [67] Kamata, Y. and Nishimura, H. (2003). System identification and attitude control of motorcycle by computer-aided dynamics analysis. *JSAE Review*, 24(20034526):411 – 416.
- [68] Katayama, T., Aoki, A., and Nishimi, T. (1988). Control behaviour of motorcycle riders. *Vehicle System Dynamics*, 17:211 – 229.
- [69] Keo, L., Yoshino, K., Kawaguchi, M., and Yamakita, M. (2011). Experimental results for stabilizing of a bicycle with a flywheel balancer. In *2011 IEEE International Conference on Robotics and Automation*, pages 6150 – 6155, Shanghai International Conference Center, May 9 – 13, 2011, Shanghai, China.
- [70] Klein, F. and Sommerfeld, A. (1910). *Über die Theorie des Kreisels*. Teubner, Leipzig. Ch IX §8, Stabilität des Fahrrads, by F. Noether, pages 863 – 884.
- [71] Kleinman, D. L., Baron, S., and Levison, W. H. (1970). An optimal control model of human response part I: Theory and validation. *Automatica*, 6(3):357 – 369.
- [72] Koch, J. (1978). *Experimentelle und Analytische Untersuchungen des Motorrad-Fahrer Systems*. PhD thesis, Berlin.
- [73] Koenen, C., Pacejka, H., Timan, D., and Zwaan, J. (1977). Beweging van motorrijwielen verstoord door wegdek onregelmatigheden. Technical Report 104, Rijkswaterstaat, Dienst Verkeerskunde.
- [74] Kooijman, J. D. G. (2006). Experimental validation of a model for the motion of an uncontrolled bicycle. Master's thesis, Delft University of Technology.

- [75] Kooijman, J. D. G., Meijaard, J. P., Papadopoulos, J. M., Ruina, A., and Schwab, A. L. (2011). A bicycle can be self-stable without gyroscopic or caster effects. *Science*, 332(6027):339 – 342.
- [76] Kooijman, J. D. G., Meijaard, J. P., Papadopoulos, J. M., Ruina, A., and Schwab, A. L. (2011). A bicycle can be self-stable without gyroscopic or caster effects. *Science*, 332(6027):339 – 342. Supporting Online Material Text Section 1–11.
- [77] Kooijman, J. D. G., Moore, J. K., and Schwab, A. L. (2008). Some observations on human control of a bicycle. In Zobory, I., editor, *11th mini Conference on Vehicle System Dynamics, Identification and Anomalies (VSDIA2008)*, Budapest, Hungary, pages 65 – 72. Budapest University of Technology and Economics.
- [78] Kooijman, J. D. G., Moore, J. K., and Schwab, A. L. (2009). Some observations on human control of a bicycle. In *Proceedings of the ASME 2009 International Design Engineering Technical Conferences & Computers and Information in Engineering Conference*, number DETC2009-86959, DETC2009, Aug 30 – Sep 2, 2009, San Diego, CA.
- [79] Kooijman, J. D. G. and Schwab, A. L. (2009). Experimental validation of the lateral dynamics of a bicycle on a treadmill. In *Proceedings of the ASME 2009 International Design Engineering Technical Conferences & Computers and Information in Engineering Conference*, number DETC2009-86965, DETC2009, Aug 30 – Sep 2, 2009, San Diego, CA.
- [80] Kooijman, J. D. G. and Schwab, A. L. (2011). A review on handling aspects in bicycle and motorcycle control. In *Proceedings of the ASME 2011 International Design Engineering Technical Conferences & Computers and Information in Engineering Conference*, DETC2011-47963, August 28 – 31, 2011, Washington, DC, USA.
- [81] Kooijman, J. D. G., Schwab, A. L., and Meijaard, J. P. (2008). Experimental validation of a model of an uncontrolled bicycle. *Multibody System Dynamics*, 19:115 – 132.
- [82] Kuroiwa, O., Baba, M., and Nakata, N. (1995). Study of motorcycle handling characteristics and rider feeling during lane change. Technical Report 950200, SAE.
- [83] Lenkeit, J. F. (1995). A servo rider for the automatic and remote path control of a motorcycle. Technical Report 950199, SAE.
- [84] Lessing, H.-E. (2003). *Automobilität; Karl Drais und die unglaublichen Anfänge*. Leipzig: Maxime.
- [85] Levandowski, A., Schultz, A., Smart, C., Krasnov, A., Song, D., Lee, H., Chau, H., Majusiak, B., and Wang, F. (2005). Autonomous motorcycle platform and navigation blue team darpa grand challenge 2005. Technical report, DARPA.

- [86] Macadam, C. C. (2003). Understanding and modeling the human driver. *Vehicle System Dynamics*, 40(1-3):101 – 134.
- [87] Mammar, S., Espié, S., and Honvo, C. (2005). Motorcycle modelling and roll motion stabilization by rider leaning and steering torque. In *Proceedings of the 2005 IEEE Conference on Control Applications*, pages 1421 – 1426, August 28 – 31, Toronto, Canada. IEEE.
- [88] McRuer, D. T., Graham, D., and Krendel, E. S. (1967). Manual control of single-loop systems: Part I. *Journal of the Franklin Institute*, 283(1):1 – 29.
- [89] McRuer, D. T., Graham, D., and Krendel, E. S. (1967). Manual control of single-loop systems: Part II. *Journal of the Franklin Institute*, 283(2):145 – 168.
- [90] McRuer, D. T. and Jex, H. R. (1967). A review of quasi-linear pilot models. *Human Factors in Electronics, IEEE Transactions on*, HFE-8(3):231 – 249.
- [91] McRuer, D. T. and Krendel, E. S. (1959). The human operator as a servo system element: Part I. *Journal of the Franklin Institute*, 267(5):381 – 403.
- [92] McRuer, D. T. and Krendel, E. S. (1959). The human operator as a servo system element: Part II. *Journal of the Franklin Institute*, 267(6):511 – 536.
- [93] Means, J. (1896). Wheeling and flying. *The Aeronautical Annual 1896*, 2:23 – 25.
- [94] Meijaard, J. P., Papadopoulos, J. M., Ruina, A., and Schwab, A. L. (2007). Linearized dynamics equations for the balance and steer of a bicycle: a benchmark and review. *Proceedings of the Royal Society A*, 463:1955 – 1982.
- [95] Meijaard, J. P., Papadopoulos, J. M., Ruina, A., and Schwab, A. L. (2011). History of thoughts about bicycle self-stability. *eCommons@Cornell*.
- [96] Michini, B. and Torrez, S. (2006). Autonomous stability control of a moving bicycle. Massachusetts Institute of Technology course 16.622 report.
- [97] Miyagishi, S., Kageyama, I., Takama, K., Baba, M., and Uchiyama, H. (2003). Study on construction of a rider robot for two-wheeled vehicle. *JSAE Review*, 24(20034256):321 – 326.
- [98] Moore, J. K., Hubbard, M., Schwab, A., Kooijman, J., and Peterson, D. L. (2010). Statistics of bicycle rider motion. *Procedia Engineering*, 2(2):2937 – 2942. The Engineering of Sport 8 - Engineering Emotion.
- [99] Moore, J. K., Hubbard, M., Schwab, A. L., and Kooijman, J. D. G. (2010). Accurate measurement of bicycle parameters. In *Proceedings, Bicycle and Motorcycle Dynamics 2010 Symposium on the Dynamics and Control of Single Track Vehicles*, 20 – 22 October 2010, Delft, The Netherlands.

- [100] Moore, J. K., Kooijman, J. D. G., Hubbard, M., and Schwab, A. L. (2009). A method for estimating physical properties of a combined bicycle and rider. In *Proceedings of the ASME 2009 International Design Engineering Technical Conferences & Computers and Information in Engineering Conference*, number DETC2009-86947, DETC2009, Aug 30 – Sep 2, 2009, San Diego, CA.
- [101] Moore, J. K., Kooijman, J. D. G., and Schwab, A. L. (2009). Rider motion identification during normal bicycling by means of principal component analysis. In K. Arczewski, J. Fraczek and M. Wojtyra, editor, *MULTIBODY DYNAMICS 2009, ECCOMAS Thematic Conference*, 29 June – 2 July 2009, Warsaw, Poland.
- [102] Moore, J. K., Kooijman, J. D. G., Schwab, A. L., and Hubbard, M. (2011). Rider motion identification during normal bicycling by means of principal component analysis. *Multibody System Dynamics*, 25(2):225 – 244.
- [103] Mortimer, R. G., Domas, P. A., and Dewar, R. E. (1973). The relationship of bicycle maneuverability to handlebar configuration. Technical Report UM-HSRI-HF-TM-73-5, Highway Safety Research Institute, Univeristy of Michigan, Huron Parkway & Baxter Road, Ann Arbor, Michigan 48105.
- [104] Murataboy (2006). http://www.murata.com/corporate/boy_girl/boy/index.html.
- [105] Murayama, A. and Yamakita, M. (2007). Development of autonomous bike robot with balancer. In *SICE Annual Conference*, pages 1048 – 1052, Sept. 17 – 20, 2007, Kagawa University, Japan.
- [106] Nagai, N. (1983). Analysis of rider and single-track-vehicle system; its application to computer-controlled bicycles. *Automatica*, 19(6):737 – 740.
- [107] Nishimura, H., Zhu, S., Kamata, Y., Iwamatsu, S., and Tajima, H. (2006). Control of a motorcycle and its multibody dynamics analysis. In *FISITA 2006*.
- [108] Pacejka, H. B. (2002). *Tyre and Vehicle Dynamics*. Butterworths, London.
- [109] Papadopoulos, J. M. (1987). Bicycle steering dynamics and self-stability: a summary report on work in progress. Cornell Bicycle Research Project.
- [110] Patterson, W. B. (2004). *Lords of the Chainring*. Santa Maria.
- [111] Patterson, W. B. and Leone, G. L. (2010). The application of handling qualities to bicycle design. In *Proceedings, Bicycle and Motorcycle Dynamics 2010 Symposium on the Dynamics and Control of Single Track Vehicles*, 20 – 22 October 2010, Delft, The Netherlands.
- [112] Pierini, M., Baldanzini, N., Brenna, C., Symeonidis, I., Schuller, E., and Peldschus, S. (2008). Development of a virtual rider. In *Procedings of the International Conference on Noise & Vibration Engineering*, pages 2219 – 2228, Leuven, September 2008.

- [113] Plöchl, M. and Edelmann, J. (2007). Driver models in automobile dynamics application. *Vehicle System Dynamics*, 45(7-8):699 – 741.
- [114] Popov, A. A., Rowell, S., and Meijaard, J. P. (2010). A review on motorcycle and rider modelling for steering control. *Vehicle System Dynamics*, 48:775 – 792.
- [115] Prem, H. and Good, M. C. (1984). Motorcycle rider skills assessment. Technical Report CR 34, University of Melbourne, Parkville, Victoria, Australia, 3052.
- [116] Rankine, W. J. M. (1869). On the dynamical principles of the motion of velocipedes. *The Engineer*, 28:79,129,153,175 and 29:2 (1870).
- [117] Rice, R. S. (1975). Accident avoidance capabilities of motorcycles. In *Proceedings International Motorcycle Safety Conference, December 16-17 1975*, pages 121–134. U.S. Department of Transportation, National Highway Traffic Safety Administration, Washington D.C.
- [118] Rice, R. S. (1978). Rider skill influences on motorcycle maneuvering. In *Motorcycle Dynamics and Rider Control*, number 780312 in SP-428, Feb 27 – Mar 03, SAE Congress Detroit, Michigan.
- [119] Rice, R. S., Davis, J. A., and Kunkel, D. T. (1975). Accident-avoidance capabilities of motorcycles. Technical Report ZN- 5571-V-1 and ZN- 5571-V-2, Calspan Corporation, Calspan Corporation 4455 Genesee Street Buffalo, New York 14221. V-1 = Report, V-2 = Appendices.
- [120] Rice, R. S. and Kunkel, D. (1976). Accident avoidance capabilities of motorcycles - lane change maneuver simulation and full-scale tests. Technical Report ZN-5899-V-1, Calspan Corporation.
- [121] Rice, R. S. and Roland, R. D. (1970). An evaluation of the performance and handling qualities of bicycles. Technical Report VJ-2888-K, Cornell Aeronautical Laboratory, Inc. Buffalo, NY.
- [122] Roland, R. and Lynch, J. (1972). Bicycle dynamics, tire characteristics and rider modeling. Technical Report YA-3063-K-2, Cornell Aeronautical Laboratory, Inc. Buffalo, NY.
- [123] Roland, R. and Massing, D. E. (1971). A digital computer simulation of bicycle dynamics. Technical Report YA-3063-K-1, Cornell Aeronautical Laboratory, Inc. Buffalo, NY.
- [124] Roland, R. D. (1973). Computer simulation of bicycle dynamics. In *Mechanics and Sport*, pages 35 – 83. The winter annual meeting of the American society of mechanical engineers, Detroit MI, November 11 – 15 1973, ASME.

- [125] Routh, E. J. (1873). Stability of a dynamical system with two independent motions. *Proceedings of the London Mathematical Society*, 1(1):97 – 99.
- [126] Ruijs, P. and Pacejka, H. (1986). Recent research in lateral dynamics of motorcycles. In *Proceedings of 9th IAVSD Symposium on The Dynamics Of Vehicles on roads and on tracks, Sweden June 24-28 1985*, volume supplement to Vehicle System Dynamics, Volume 15, pages 467 – 480.
- [127] Saguchi, T., Takahashi, M., and Yoshida, K. (2006). Stable running control of autonomous bicycle robot. In *Dynamics and Design Conference 2006*. In Japanese.
- [128] Saguchi, T., Yoshida, K., and Takahashi, M. (2007). Stable running control of autonomous bicycle robot. *Transactions of the Japan Society of Mechanical Engineers. C*, 73(731):2036 – 2041.
- [129] Schwab, A. L. and Kooijman, J. D. G. (2010). Controllability of a bicycle. In *5th Asian Conference on Multibody Dynamics*, August 23 – 26, 2010, Kyoto, Japan.
- [130] Schwab, A. L. and Kooijman, J. D. G. (2010). Lateral dynamics of a bicycle with passive rider model. In *The 1st Joint International Conference on Multibody System Dynamics, IMSD2010*, May 25 – 27, 2010, Lappeenranta, Finland.
- [131] Schwab, A. L., Kooijman, J. D. G., and Meijaard, J. P. (2008). Some recent developments in bicycle dynamics and control. In Belyaev, A. K. and Indeitsev, D. A., editors, *Fourth European Conference on Structural Control (4ECSC)*, pages 695 – 702. Institute of Problems in Mechanical Engineering, Russian Academy of Sciences.
- [132] Schwab, A. L., Meijaard, J. P., and Kooijman, J. D. G. (2012). Lateral dynamics of a bicycle with a passive rider model: stability and controllability. *Vehicle System Dynamics*, 50(8):1209 – 1224.
- [133] Seffen, K. A. (1999). Bicycle-rider dynamics: Equations of motion and controllability. Technical Report CUED/C-EDC/TR79, Cambridge Engineering Design Centre.
- [134] Sharp, R. S. (1971). The stability and control of motorcycles. *Journal of Mechanical Engineering Science*, 13(5):316 – 329.
- [135] Sharp, R. S. (1978). A review of motorcycle steering behavior and straight line stability characteristics. In *Motorcycle Dynamics and Rider Control*, number 780303 in SP-428, Feb 27 – Mar 03, SAE Congress Detroit, Michigan.
- [136] Sharp, R. S. (2006). Optimal linear time-invariant preview steering control for motorcycles. *Vehicle System Dynamics*, 44(Supplement):329 – 340.
- [137] Sharp, R. S. (2007). Motorcycle steering control by road preview. *ASME Journal of Dynamic Systems, Measurement, and Control*, 129:373 – 381.

- [138] Sharp, R. S. (2007). Optimal stabilization and path-following controls for a bicycle. *Proc. IMechE Part C: J. Mechanical Engineering Science*, 221:415 – 428.
- [139] Sharp, R. S. (2008). On the stability and control of the bicycle. *Applied Mechanics Reviews*, 61(6):060803.
- [140] Stassen, H. G. and van Lunteren, A. (1967). Het stabilisatie proces van een fietser op een rechte weg. Technical Report 36, Technische Hogeschool Delft.
- [141] Stassen, H. G. and van Lunteren, A. (1973). Progress report January 1970 until January 1973 of the man-machine systems group. Technical Report 55, Technische Hogeschool Delft.
- [142] Stevens, D. (2009). The stability and handling characteristics of bicycles. Bachelor's thesis, University of New South Wales.
- [143] Tak, T. O., Won, J. S., and Baek, G. Y. (2010). Design sensitivity analysis of bicycle stability and experimental validation. In *Proceedings, Bicycle and Motorcycle Dynamics 2010 Symposium on the Dynamics and Control of Single Track Vehicles*, 20 – 22 October 2010, Delft, The Netherlands.
- [144] Talaia, P., Moreno, D., Hajzman, M., and Hyncik, L. (2008). A 3D model of a human for powered two-wheeler vehicles. In *Proceedings of the International Conference on Noise & Vibration Engineering*, pages 2229 – 2238, Leuven, September 2008.
- [145] Tanaka, Y. and Murakami, T. (2004). Self sustaining bicycle robot with steering controller. In *The 8th IEEE International Workshop on Advanced Motion Control, 2004. AMC '04*, pages 193 – 197.
- [146] Tanaka, Y. and Murakami, T. (2009). A study on straight-line tracking and posture control in electric bicycle. *IEEE Transactions on Industrial Electronics*, 56(1):159 – 168.
- [147] Thanh, B. T. and Parnichkun, M. (2008). Balancing control of bicyrobo by particle swarm optimization-based structure-specified mixed H2/Hinfinity control. *International Journal of Advanced Robotic Systems*, 5(4):187 – 195.
- [148] TMS (2011). <http://youtu.be/wfrrK2chOZk> The high frequency oscillations are clear from about $t = 28s$.
- [149] Troje, N. F. (2002). Decomposing biological motion: A framework for analysis and synthesis of human gait patterns. *Journal of Vision*, 2:371 – 387.
- [150] Ulrich, D. A., Burghardt, A. R., Lloyd, M., Tiernan, C., and Hornyak, J. E. (2011). Physical activity benefits of learning to ride a two-wheel bicycle for children with down syndrome: A randomized trial. *Physical Therapy*, 91(10):1463 – 1477.

- [151] van Lunteren, A. and Stassen, H. G. (1970). Annual report 1969 of the man machine system group. Technical Report WTHD21, Technische Hogeschool Delft.
- [152] van Lunteren, A. and Stassen, H. G. (1970). On the variance of the bicycle rider's behavior. In *Proceedings of the 6th Annual Conference on Manual Control*, pages 701 – 722, 7 – 9 April, Wright Patterson AFB, Ohio.
- [153] van Lunteren, A. and Stassen, H. G. (1973). Parameter estimation in linear models of the human operator in a closed loop with application of deterministic test signals. In *Proceedings of the 9th Annual Conference on Manual Control*, pages 503 – 520, May 23 – 25, Massachusetts Institute of Technology, Cambridge, MA.
- [154] van Lunteren, A., Stassen, H. G., and Schlemper, M. S. H. (1970). On the influence of drugs on the behavior of a bicycle rider. In *proceedings of the 6th annual conference on manual control*, pages 419 – 437, 7 – 9 april, Wright Patterson AFB, Ohio.
- [155] van Zytveld, P. J. (1975). A method for the automatic stabilization of an unmanned bicycle. Master's thesis, Stanford University.
- [156] von Wissel, D. (1996). *DAE Control of Dynamical Systems: Example of a Riderless Bicycle*. PhD thesis, École des Mines de Paris.
- [157] von Wissel, D. and Nikoukhah, R. (1995). Maneuver-based obstacle-avoiding trajectory optimization: Example of a riderless bicycle. *Mechanics of Structures and Machines*, 23(2):223 – 255.
- [158] Watanabe, Y. and Yoshida, K. (1973). Motorcycle handling performance for obstacle avoidance. In *Second International Congress on Automotive Safety*, number 73033. Dept. of Transportation. July 16 – 18, San Fransisco.
- [159] Weingarten, N. C. (2005). History of in-flight simulation at General Dynamics. *Journal of Aircraft*, 42(2):290 – 298.
- [160] Weir, D. H. (1972). *Motorcycle Handling Dynamics and Rider Control and the Effect of Design Configuration on Response and Performance*. PhD thesis, University of California at Los Angeles.
- [161] Weir, D. H. (1973). A manual control view of motorcycle handling. In *Second International Congress on Automotive Safety*, number 73018. Dept. of Transportation. July 16 – 18, San Fransisco.
- [162] Weir, D. H. and Zellner, J. W. (1978). Lateral-directional motorcycle dynamics and rider control. In *Motorcycle Dynamics and Rider Control*, number 780304 in SP-428, Feb 27 – Mar 03, SAE Congress Detroit, Michigan.

- [163] Wesemann, P. and Weijer, W. (2011). Verkeersveiligheidsverkenning 2020. Technical Report R-2011-1, SWOV.
- [164] Whipple, F. J. W. (1899). The stability of the motion of a bicycle. *Quarterly Journal of Pure and Applied Mathematics*, 30:312 – 348.
- [165] Wierda, M. and Roos, E. (1988). *Gangbare kinderfietsen op comfort, manoeuvreerbaarheid en remweg vergeleken*. Haren: Verkeerskundig Studiecentrum, Rijksuniversiteit Groningen.
- [166] Wierda, M. and Wolf, J. (1989). *Drie typen kinderfietsen op manoeuvreerbaarheid en remweg vergeleken*. Haren: Verkeerskundig Studiecentrum, Rijksuniversiteit Groningen.
- [167] Wilson, D. G. (2004). *Bicycling Science*. Number ISBN-13: 9780262731546. The MIT Press, 3rd edition.
- [168] Wilson-Jones, R. A. (1951). Steering and stability of single-track vehicles. *Proceedings Automobile Division Institution of Mechanical Engineers*, pages 191 – 213.
- [169] Wingrove, R. C. and Edwards, F. G. (1968). Measurement of pilot describing functions from flight test data with an example from Gemini X. In *4th Annual NASA - University Conference on Manual Control*, March 1968, University of Michigan.
- [170] Yamaguchi, M. (2011). <http://ai2001.ifdef.jp/>.
- [171] Yamakita, M. and Lyche, K. (2008). Trajectory control for an autonomous bicycle with balancer. In *IEEE / ASME International Conference on Advanced Intelligent Mechatronics, AIM 2008*, number 4601741, pages 676 – 681.
- [172] Yamakita, M. and Utano, A. (2005). Automatic control of bicycles with a balancer. In *Proceedings of the 2005 IEEE/ASME International Conference on Advanced Intelligent Mechatronics*, pages 1245 – 1250, 24 – 28 July, 2005, Monterey, California.
- [173] Yamakita, M., Utano, A., and Sekiguchi, K. (2006). Experimental study of automatic control of bicycle with balancer. In *Proceedings of the 2006 IEEE/RSJ International Conference on Intelligent Robots and Systems*, pages 5606 – 5611, October 9 – 15, 2006, Beijing, China.
- [174] Yi, J., Song, D., Levandowski, A., and Jayasuriya, S. (2006). Trajectory tracking and balance stabilization control of autonomous motorcycles. In *ICRA 2006*, pages 2583 – 2589. ISBN 0-7803-9505-0.
- [175] Yokomori, M., Oya, T., and Katayama, A. (2000). Rider control behavior to maintain stable upright position at low speed. *JSAE Review*, 21(20004023):61–65.

- [176] Yokomori, M., Yamaguchi, S., Oya, T., and Katayama, A. (1999). The riders motion for control of stability of motorcycle and rider system on low speed. Technical Report 1999-01-3278, SAE. JSAE Report Number: 9938033.
- [177] Zellner, J. W. and Weir, D. H. (1978). Development of handling test procedures for motorcycles. In *Motorcycle Dynamics and Rider Control*, number 780313 in SP-428, Feb 27 – Mar 03, SAE Congress Detroit, Michigan.
- [178] Zellner, J. W. and Weir, D. H. (1979). Moped directional dynamics and handling qualities. Technical Report 790260, SAE.
- [179] Zinn, L. (1998). *Mountain Bike Performance Handbook*. Number ISBN-13: 9780933201958. MBI.

Kooijman, J. D. G., Moore, J. K., and Schwab, A. L. (2009). Some observations on human control of a bicycle. In *Proceedings of the ASME 2009 International Design Engineering Technical Conferences & Computers and Information in Engineering Conference*, number DETC2009-86959, DETC2009, Aug 30 – Sep 2, 2009, San Diego, CA.

DETC2009-86959

SOME OBSERVATIONS ON HUMAN CONTROL OF A BICYCLE

J.D.G. Kooijman
A.L. Schwab*

Laboratory for Engineering Mechanics
Faculty of 3mE
Delft University of Technology
Mekelweg 2, NL 2628CD Delft
The Netherlands
Email: jodikooijman@gmail.com
a.l.schwab@tudelft.nl

Jason K. Moore

Sports Biomechanics Laboratory
Department of Mechanical and Aeronautical Engineering
University of California,
One Shields Avenue
Davis, California 95616
Email: jkmoor@ucdavis.edu

ABSTRACT

The purpose of this study is to identify human control actions in normal bicycling. The task under study is the stabilization of the mostly unstable lateral motion of the bicycle-rider system. This is done by visual observation of the rider and measuring the vehicle motions. The observations show that very little upper-body lean occurs and that stabilization is done by steering control actions only. However, at very low forward speed a second control is introduced to the system: knee movement. Moreover, all control actions are performed at the pedaling frequency, whilst the amplitude of the steering motion increases rapidly with decreasing forward speed.

INTRODUCTION

Riding a bicycle is an acquired skill. At very low speed the bicycle is highly unstable. However, at moderate speed the bicycle is easy to stabilize. These observations are confirmed by a stability analysis on a simple dynamical model of an uncontrolled bicycle [1] and some experiments [2] and [3]. Although there is little established knowledge on how we stabilize a bicycle, two basic features are known: some uncontrolled bicycles can balance themselves given some initial speed, and one can balance a forward moving bicycle by turning the front wheel in

the direction of the undesired lean. But when observing a rider on a bicycle, not only the handlebars are moving but also the upper body and other extremities. These rider body motions are even more profound when riding a motorcycle [4].

The purpose of this study is to identify the major human control actions in normal bicycling where we focus on the stabilizing task only, but not tracking. The identification is done by visual observation of the rider and measurement of the vehicle motions on an instrumented bicycle, see Fig. 1. In order to observe the human control actions a number of experiments were carried out. First a typical town ride was made to investigate what sort of actions take place during normal riding. After this, experiments were carried out in a controlled environment, on a large treadmill (3×5 m), at various speeds. The same bicycle was used during all the experiments. The bicycle was ridden by two averagely skilled riders. Three riding cases were considered: normal bicycling, towing and normal bicycling with lateral perturbations. These experiments were carried out to identify the effect of upper body motion and the effect of the pedaling motion on the control. The rider was told to simply stabilize the bicycle and to generally ride in the longitudinal direction of the treadmill; no tracking task was set. Recorded data were the rigid body motions of the bicycle rear frame and the front assembly. The rider motion relative to the rear frame was recorded via video.

*Address all correspondence to this author.



Figure 1. THE INSTRUMENTED BICYCLE WITH CAMERA BOOM AND VIDEO CAMERA LENS (1). ON THE REAR RACK THE MEASUREMENT COMPUTER (2), VIDEO CAMCORDER (3) AND BATTERY PACKS (4) ARE POSITIONED. MEASURED SIGNALS ARE THE STEER ANGLE AND STEER-RATE (5), REAR FRAME LEAN- AND YAW-RATE (6) AND FORWARD SPEED (7).

INSTRUMENTED BICYCLE

A standard Dutch bicycle, a 2008 model Batavus Browser was chosen for the experiments and is shown in Fig. 1. This is a bicycle of conventional design, fitted with a 3-speed SRAM rear hub and coaster brakes. Some of the peripheral components were removed in order to be able to install measurement equipment and sensors (see Tab. 1).

The bicycle was equipped with a 1/3" CCD color bullet-camera with 2.9mm (wide angle) lens. The camera was located at the front and directed towards the rider and rotated 90 degrees clockwise to get portrait aspect ratio. The video signal was recorded, via the AV-in port, on DV tape of a Sony Handycam located on the rear rack of the bicycle. The bullet camera was placed horizontally, approximately 65 cm in front of the handle-bars and 1.2 m above the ground and held in place by a carbon-fiber boom connected to the down-tube of the rear frame, see Fig. 1.

A National Instruments' CompactRIO (type CRIO-9014) computer was used for data collection. The CompactRIO was installed on the rear rack of the bicycle. It was fitted with a 32-channel, 16 bit analogue input module and a 4-channel, 16 bit analogue output module as well as a CRIO WLAN-MH1000 wireless modem by S.E.A. Datentechnik GmbH for a wireless connection with a "ground station" router, to which a laptop was connected. The measurement system is able to run autonomously once a measurement sequence is initiated. The CompactRIO was powered by a 11.1V, 1500mAh Lithium Polymer battery which



Figure 2. SCREEN-SHOT OF VIDEO MADE WITH THE BULLET CAMERA CONNECTED TO THE BICYCLE FRAME, FACING REARWARDS, SHOWING THE RIDER POSITION DURING NORMAL CYCLING.

was also placed on the bicycle's rear rack.

The recorded signals were the lean, yaw and steer rates, the steer angle, the rear wheel speed and the pedaling cadence frequency. The angular rates were measured using 3 Silicon Sensing CRS03, single axis angular rate sensors with a rate range of ± 100 deg/s. The steer angle was measured using a potentiometer placed on the rear-frame against the front of the head tube and connected via a belt and pulley pair. The angular rate sensors and the angular potentiometer were powered by a 4.8V, 2100mAh Nickel Cadmium battery. The forward speed was measured by measuring the output voltage of a Maxon motor that was driven by the rear wheel. The cadence frequency was measured by a reed-relay placed on the rear frame, and a magnet placed on the left crank-arm.

TOWN RIDE EXPERIMENT

As a first step in human rider control observations a short, 15 minute, ride around town was carried out. This experiment took place under normal riding conditions (dry weather, daylight, etc.), on roads that the rider was familiar with. The course covered included a round-a-bout, dedicated cycling paths, speed-bumps, pavement, normal tarmac roads, tight bends in a residential area and the rider had to stop at a number of traffic lights. There were no special precautions taken and the experiment was carried out amongst other traffic. From the recorded video material and measured data two observations were made:

1. The video material showed that there was very little upper body lean relative to the rear-frame, carried out during the whole ride. The relative upper body lean that was noted appeared to be as a result of pedaling. Only in the last few seconds prior to a sharp corner was an upper body lean angle observed - indicating that the lean was carried out because of a sudden heading change.
2. The recorded data, part of which is shown in Fig. 3, clearly shows that only very small steering actions (± 3 deg) are

Table 1. USED SENSORS

Measurement	Sensor Type	Manufacturer	Type	Specification
Steer-rate Yaw-rate Lean-rate	MEMS Angular Rate	Silicon Sensing	CRS03	Full range output ± 100 deg/s
Steer angle	Potentiometer	Sakae	FPC40A	1 turn, conductive plastic, Servo mount
Forward speed	DC-motor	Maxon	2326-940-12-216-200	Graphite brush motor with a 5cm diameter disk on the shaft
Cadence	Reed relay and magnet	-	-	Kitchen magnet

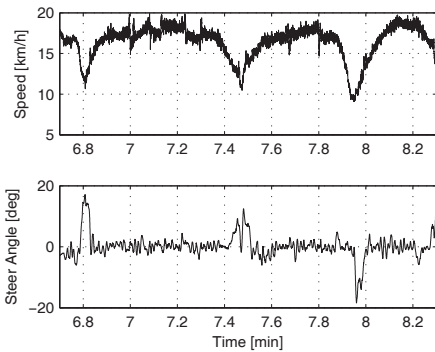


Figure 3. DATA COLLECTED DURING A RIDE AROUND TOWN. UPPER GRAPH SHOWS THE SPEED THE BICYCLE WAS TRAVELING AT, THE LOWER THE STEERING ANGLE.

carried out during most of the the experiment. Only when the forward speed has dropped, prior to making a corner, are large steer angles (± 15 deg) seen.

TREADMILL EXPERIMENTS

Riding a bicycle on the open road amongst normal traffic subjects the bicycle-rider system to many external disturbances such as side wind, traffic and road unevenness. To eliminate these disturbances a more controlled environment was selected to carry out further studies on human rider control for stabilizing tasks. The experiments were carried out on a large (3×5 m) treadmill, shown in Fig. 4. The dynamics of a bicycle on a treadmill were shown to be the same as for on flat level ground by [3].

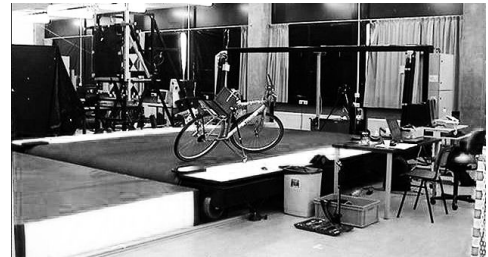


Figure 4. LARGE TREADMILL, 3×5 M, MAX SPEED 35 KM/H, COURTESY OF THE FACULTY OF HUMAN MOVEMENT SCIENCES, VU UNIVERSITY AMSTERDAM.

Table 2. RIDER CHARACTERISTICS

Rider	Weight [kg]	Height [cm]	Age
1	102	187	53
2	72	183	26

The experiments were carried out by two, male, average ability, riders of different age and build on the same bicycle. The saddle height was adjusted for each rider to ensure proper seating for bicycling. The rider characteristics are given in Tab. 2. For both riders very similar results were found. The data and figures given in this paper were collected with rider 1.

The uncontrolled dynamics of the bicycle rider combination can be described by the linearized model of the bicycle [1]. This model consists of four rigid bodies, viz. the rear frame with rigid rider connected, the front handlebar and fork assembly, and the two wheels. These are connected by ideal hinges and the wheels have idealized pure-rolling contact with level ground (no tire models). Reference [5] describes the method used to determine the properties for the instrumented bicycle and rider. The

Table 3. BICYCLE PARAMETER VALUES

parameter	symbol	value for bicycle & rider
wheel base	w	1.12 m
trail	c	0.055 m
steer axis tilt ($\pi/2 - \text{head angle}$)	λ	0.375 rad
gravity	g	9.81 N kg^{-1}
forward speed	v	various m s^{-1}
Rear wheel R		
radius	r_R	0.342 m
mass	m_R	3.12 kg
mass moments of inertia	(I_{Rxx}, I_{Ryy})	$(0.078, 0.156) \text{ kg m}^2$
rear Body and frame B		
position centre of mass	(x_B, z_B)	$(0.30, -1.08) \text{ m}$
mass	m_B	116 kg
mass moments of inertia	$\begin{bmatrix} I_{Bxx} & 0 & I_{Bxz} \\ 0 & I_{Byy} & 0 \\ I_{Bxz} & 0 & I_{Bzz} \end{bmatrix}$	$\begin{bmatrix} 16.784 & 0 & -3.616 \\ 0 & I_{Byy} & 0 \\ -3.616 & 0 & 0.035 \end{bmatrix} \text{ kg m}^2$
front Handlebar and fork assembly H		
position centre of mass	(x_H, z_H)	$(0.88, -0.78) \text{ m}$
mass	m_H	4.35 kg
mass moments of inertia	$\begin{bmatrix} I_{Hxx} & 0 & I_{Hxz} \\ 0 & I_{Hyy} & 0 \\ I_{Hxz} & 0 & I_{Hzz} \end{bmatrix}$	$\begin{bmatrix} 0.345 & 0 & -0.044 \\ 0 & I_{Hyy} & 0 \\ -0.044 & 0 & 0.065 \end{bmatrix} \text{ kg m}^2$
Front wheel F		
radius	r_F	0.342 m
mass	m_F	2.02 kg
mass moments of inertia	(I_{Fxx}, I_{Fyy})	$(0.081, 0.162) \text{ kg m}^2$

parameters for the instrumented bicycle with rigid rider are given in Tab. 3 and, the linearized stability is depicted in Fig. 5. At low speed the important motion is the unstable oscillatory weave motion. This weave motion becomes stable around 18 km/h, the so-called weave speed. At higher speeds the non-oscillatory capsize motion becomes unstable but since this instability is so mild it is very easy to control. Summarizing: the instrumented bicycle rider combination is in need of human stabilizing control below 18 km/h and is stable above this speed.

For safety reasons the riders were fitted with a harness that was connected to the ceiling via a long climbing rope. This ensured that should the rider fall over no contact with the moving part of the treadmill would be made. Also a retractable dog leash

was connected between the front of the harness and the treadmill kill switch. This ensured that the treadmill would immediately come to a halt, should the bicycle go too far back, reducing the chance that the bicycle could go off the end of the treadmill.

Three types of riding experiments were carried out: normal bicycling, towing and bicycling with lateral perturbations. The normal bicycling experiment was carried out to investigate what type of control actions a rider carries out to stabilize a bicycle. The towing experiment was carried out to remove the dominant pedaling motion, seen during the town-ride experiment, from the system. The bicycling with lateral perturbations was performed to investigate how the human rider recovers from an unstable situation which was simulated by applying a lateral impulse to

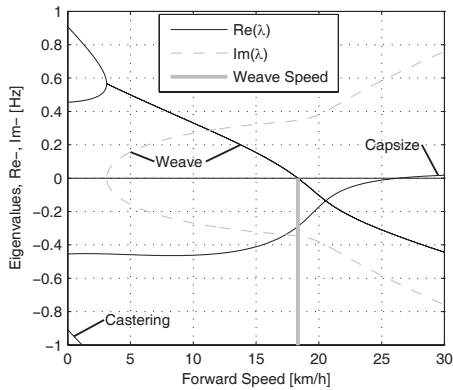


Figure 5. EIGENVALUES FOR THE LINEARIZED STABILITY ANALYSIS OF AN UNCONTROLLED BICYCLE-RIDER COMBINATION FOR THE STEADY UPRIGHT MOTION IN THE FORWARD SPEED RANGE OF 0-30 KM/H. SOLID LINES ARE REAL PARTS, DOTTED LINES ARE IMAGINARY PARTS. THE BICYCLE IS PRACTICALLY STABLE FROM THE WEAWE SPEED, 18 KM/H AND ABOVE.

the rear frame.

Each experiment was carried out at 6 different speeds: 30, 25, 20, 15, 10 and 5 km/h. In total 36 experiments were performed. During the normal bicycling and bicycling with lateral perturbations experiments the rider pedaled normally and used first gear during the 5 and 10 km/h runs. Second gear was used in the 15 and 20 km/h runs and third gear was used during the 25 and 30 km/h runs. The cadence varied between 24 rpm at 5 km/h and 80 rpm at 30 km/h. During the towing series of experiments the bicycle and rider were towed by a rope connected to the bicycle rear frame at the lower end of the head tube. The rider kept the pedals in the horizontal position during these experiments. The crank arm side that was placed forward was left to rider preference. During the lateral perturbations experiment the bicycle was perturbed by applying a lateral impulse to the rear frame. The impulse was applied by a manually actuated rope tied to the seat tube. The rider could not see the rope being actuated to ensure that the rider was unprepared, however, they knew the direction of the perturbation.

The riders were instructed to stay on the treadmill and to generally ride in the longitudinal direction of the treadmill but not to concentrate on their position on the treadmill in order to prevent the rider from performing a tracking task. Data was collected for 1 minute during each experiment with a 100Hz sample rate. Video footage can be found at the website [6].

Normal Bicycling; Pedaling

Visual inspection of the video footage showed very little lean action during the experiment other than that resulting directly from the pedaling motion. During the low speed run at 5 km/h, the rider's upper body was almost stationary, i.e. it could be considered to be rigidly attached to the rear-frame. However at this speed the rider's knees showed significant lateral motion. This lateral knee motion can be seen in the video image in Fig. 6. A third observation was that the rider turned the handlebars more at lower speeds than at higher speeds.



Figure 6. SCREEN-SHOT OF NORMAL PEDALING AT LOW SPEED (5 KM/H) SHOWING LARGE LATERAL (LEFT) KNEE MOTION AND (RIGHT) STEERING ACTION. THE GREY VERTICAL LINE INDICATES THE MIDPLANE OF THE BICYCLE. NOTE THAT THERE IS ALMOST NO UPPER BODY LEAN PRESENT.

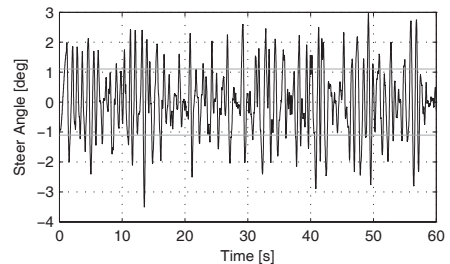


Figure 7. STEER ANGLE TIME HISTORY PLOT FOR 20 KM/H DURING NORMAL BICYCLING. THE STANDARD DEVIATION OF THE STEER ANGLE IS SHOWN IN GREY.

This third observation is confirmed by the measured steer angle data. Figures 7 and 8 show the time history of the steer angle for the experiments carried out at 20 and 5 km/h respectively.

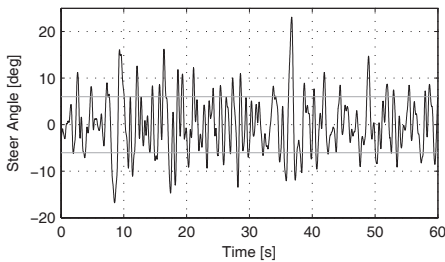


Figure 8. STEER ANGLE TIME HISTORY PLOT FOR 5 KM/H DURING NORMAL BICYCLING. THE STANDARD DEVIATION OF THE STEER ANGLE IS SHOWN IN GREY.

The standard deviation of the steer angle during the sixty seconds of measurement is also shown in the figures. At speeds above 20 km/h the average steer angle remains approximately constant. However the average magnitude of the steer angle grows by more than 500% when the speed is decreased from 20 km/h to 5 km/h. This increase in steer angle magnitude for the decreasing speeds is illustrated in Fig. 9.

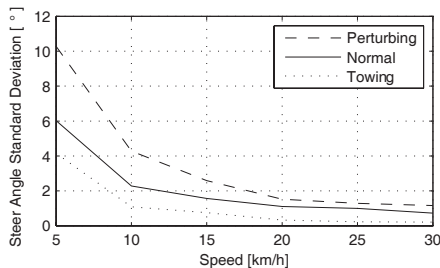


Figure 9. THE STANDARD DEVIATION OF THE STEER ANGLE FOR THE SIX DIFFERENT SPEEDS FOR THE THREE DIFFERENT EXPERIMENTS.

The frequency content of the steering signal for the different forward speeds is shown in Fig. 10. The grey vertically dashed line indicates the rigid rider/bicycle weave frequency. Figure 10 clearly shows that at none of the speeds the rigid rider/bicycle weave frequency is a frequency in which the bicycle/rider system operates.

The black vertical dashed line in each of the plots in Fig. 10 indicates the measured pedaling frequency. The figure clearly

shows that during normal pedaling most of steering action takes place at, or around, the pedaling frequency, irrespective of the speed that the bicycle is moving. The pedaling frequency is especially dominant in the steering signal at the highest speeds where practically all of the steering takes place in the pedaling frequency.

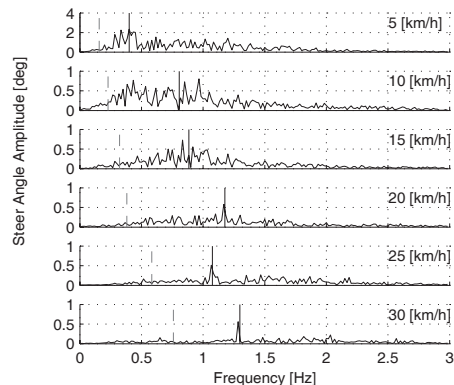


Figure 10. STEER ANGLE AMPLITUDE PLOT FOR THE SIX DIFFERENT SPEEDS FOR NORMAL PEDALING EXPERIMENT. SOLID VERTICAL LINE INDICATES THE PEDALING FREQUENCY. DASHED VERTICAL GREY LINE INDICATES THE BICYCLE & RIGID RIDER WEAVE EIGENFREQUENCY.

Figure 11 shows that if the steering signal is assumed to consist of just one frequency - namely the frequency with the largest amplitude, how this maximum amplitude reduces with increasing speed. This assumption becomes more valid with increasing speed as indicated by Fig. 10. The plot in Fig. 11 has a similar shape to the standard deviation plot in Fig. 9.

Towing; No Pedaling

Visual inspection of the video footage revealed, similar to the normal bicycling experiment, that no upper body leaning at any of the measured speeds and that larger steer angles occurred at the slower speeds. However, unlike the normal bicycling experiment, no knee motion could be detected from the video footage at any of the speeds, other than small remnant motion as a result of slight steering deviations from straight ahead.

The recorded steer angle data also indicated that larger steer angles were made at decreasing speeds. Figure 9 shows how the

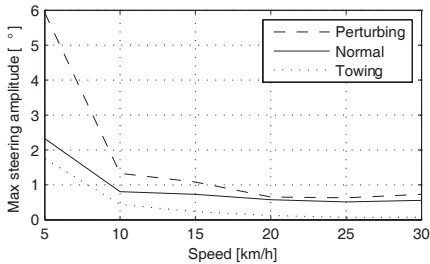


Figure 11. MAXIMUM STEERING AMPLITUDE IF THE STEERING SIGNAL CONSISTED OF A SINGLE FREQUENCY FOR THE THREE DIFFERENT EXPERIMENTS AT THE SIX DIFFERENT SPEEDS.

standard deviation of the steer angle reduces rapidly with increasing speed up to 20 km/h and from then on remains approximately constant. The figure also shows that the average steering amplitude at all speeds is lower than that for pedaling. The standard deviation is less than a degree for all speeds above 10 km/h indicating that the average steer angle at the higher speeds is almost straight ahead!

The steer angle frequency spectrum for each of the speeds is shown in Fig. 12. It was expected that the rigid rider/bicycle weave frequency would be a dominant frequency in the frequency spectrum. However there appears to be no connection with the open loop weave frequency even in the unstable speed range. In fact the frequency spectrum shows a wide range of frequencies of similar amplitude at all the speeds and none of the speeds show a single dominant frequency. Therefore the assumption that the steering action whilst towing can be characterized by a single steering frequency, as it could for the normal bicycling experiment, does not hold for any of the speeds.

Perturbing; Pedaling

The video footage showed that, as a result of the lateral perturbation, the bicycle was pulled laterally away from under the rider causing the bicycle to lean over and in turn cause a short transient lean motion of the rider's upper body. The upper body appears to only lag behind the lower body and bicycle during this destabilizing part of the perturbation maneuver. During the subsequent recovery of the bicycle to the upright, straight ahead position, no body lean could be noted other than that as a result of the normal pedaling.

A second phenomenon observable on the video footage, as shown in Fig. 13, is that at all speeds there is lateral knee motion during the short transient recovery process of the bicycle to the upright position. The lateral knee motion was very large during the 5 km/h measurement and much smaller at the higher speeds,

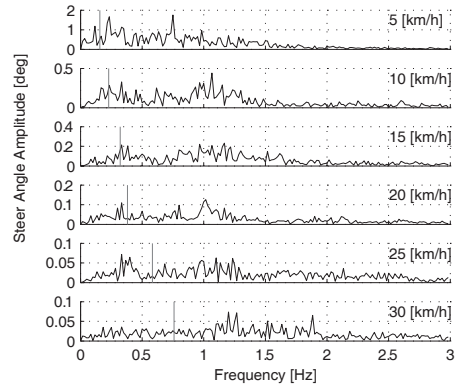


Figure 12. STEER ANGLE AMPLITUDE PLOT FOR THE SIX DIFFERENT SPEEDS FOR THE TOWING EXPERIMENT. VERTICAL LINE INDICATES THE BICYCLE & RIGID RIDER EIGENFREQUENCY.



Figure 13. SCREEN-SHOT DIRECTLY AFTER A PERTURBATION (LATERAL FORCE APPLIED FROM THE RIDER'S RIGHT BY A ROPE AT THE SADDLE TUBE) AT 5 km/h. VERTICAL GREY LINE INDICATES THE BICYCLE MIDPLANE. NOTE THE LATERAL RIGHT KNEE MOTION AND STEERING ACTION AND THE SMALL UPPER BODY LEAN ACTION.

but even at 30 km/h it is visible.

From the video footage it can be concluded that the angle that the handlebars are turned during and after a perturbation decreased with increasing speed as can also be seen in the measured steer angle data as shown in Fig. 9.

Figure 14 shows the frequency spectrum of the measured steer angle. Once again, for the higher speeds, the steer control action is carried out at the pedaling frequency. At the lower speeds (5 - 10 km/h) a wider frequency range is again present but the steering motion appears around the pedaling frequency. It is therefore again reasonable to assume that the steering motion is a

function of a single frequency as for the normal bicycling experiment. Figure 11 shows the steering amplitude for the frequency with the maximum amplitude. Again the values for the highest speeds are similar to those of the standard deviation of the steer angle.

The frequency spectrum shows no significant steering motion taking place at the rigid rider/bicycle weave eigenfrequency for any of the speeds.

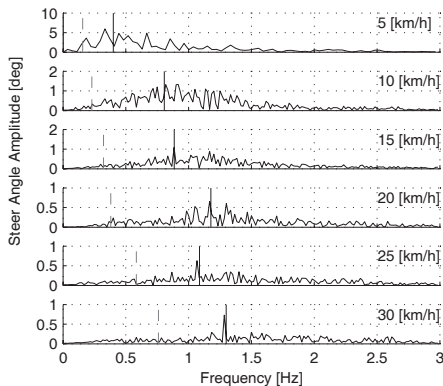


Figure 14. STEER ANGLE AMPLITUDE PLOT FOR THE SIX DIFFERENT SPEEDS FOR PERTURBATION EXPERIMENT. SOLID VERTICAL LINE INDICATES THE PEDALING FREQUENCY. DASHED VERTICAL GREY LINE INDICATES THE BICYCLE & RIGID RIDER EIGENFREQUENCY.

CONCLUDING REMARKS

The observations show that human stabilizing control of the lateral motions of a bicycle during normal bicycling does not show any significant upper body lean, and that most of the stabilizing control actions are done with steering control. Only at very low forward speed is a second control added to the system: knee movement. Moreover, this lateral knee motion only occurs during pedaling. All steering actions are mainly performed at the pedaling frequency whilst the amplitude of the steering motion increases rapidly with decreasing forward speed.

FUTURE WORK

Future work is directed at measuring the motion of a person riding a bicycle on a treadmill by means of a human motion

capture system with active markers. This will allow for the identification of the motions of the individual body parts of the rider relative to bicycle and thus identify rider control in a quantitative manner.

ACKNOWLEDGMENT

We would like to thank Knoek van Soest from the Faculty of Human Movement Sciences of the VU University Amsterdam for usage of their treadmill.

REFERENCES

- [1] Meijaard, J. P., Papadopoulos, J. M., Ruina, A., and Schwab, A. L., 2007. "Linearized dynamics equations for the balance and steer of a bicycle: a benchmark and review". *Proceedings of the Royal Society A*, **463**, p. 19551982.
- [2] Kooijman, J. D. G., Schwab, A. L., and Meijaard, J. P., 2008. "Experimental validation of a model of an uncontrolled bicycle". *Multibody System Dynamics*, **19**, pp. 115–132.
- [3] Kooijman, J. D. G., and Schwab, A. L., 2009. "Experimental validation of the lateral dynamics of a bicycle on a treadmill". In ASME 2009 International Design Engineering Technical Conferences & Computers and Information in Engineering Conference on Multibody Systems, Nonlinear Dynamics, and Control, IDETC/CIE 2009, August 30–September 2, 2009, San Diego, CA, USA.
- [4] Cossalter, V., 2002. *Motorcycle Dynamics*. No. ISBN 0-9720514-0-6. Race Dynamics, Greendale, WI.
- [5] Moore, J. K., Kooijman, J. D. G., Hubbard, M., and Schwab, A. L., 2009. "A method for estimating the physical properties of a combined bicycle and rider". In ASME 2009 International Design Engineering Technical Conferences & Computers and Information in Engineering Conference on Multibody Systems, Nonlinear Dynamics, and Control, IDETC/CIE 2009, August 30–September 2, 2009, San Diego, CA, USA.
- [6] <http://bicycle.tudelft.nl/schwab/Bicycle/index.htm>.

Moore, J. K., Kooijman, J. D. G., Schwab, A. L., and Hubbard, M. (2011). Rider motion identification during normal bicycling by means of principal component analysis. *Multibody System Dynamics*, 25 (2) : 225–244. Reprinted with kind permission of Springer Science and Business Media.

Rider motion identification during normal bicycling by means of principal component analysis

Jason K. Moore · J.D.G. Kooijman · A.L. Schwab ·
Mont Hubbard

Received: 18 December 2009 / Accepted: 9 September 2010 / Published online: 9 October 2010
© The Author(s) 2010. This article is published with open access at Springerlink.com

Abstract Recent observations of a bicyclist riding through town and on a treadmill show that the rider uses the upper body very little when performing normal maneuvers and that the bicyclist may, in fact, primarily use steering input for control. The observations also revealed that other motions such as lateral movement of the knees were used in low speed stabilization. In order to validate the hypothesis that there is little upper body motion during casual cycling, an in-depth motion capture analysis was performed on the bicycle and rider system.

We used motion capture technology to record the motion of three similar young adult male riders riding two different city bicycles on a treadmill. Each rider rode each bicycle while performing stability trials at speeds ranging from 2 km/h to 30 km/h: stabilizing while pedaling normally, stabilizing without pedaling, line tracking while pedaling, and stabilizing with no-hands. These tasks were chosen with the intent of examining differences in the kinematics at various speeds, the effects of pedaling on the system, upper body control motions and the differences in tracking and stabilization.

Principal component analysis was used to transform the data into a manageable set organized by the variance associated with the principal components. In this paper, these principal components were used to characterize various distinct kinematic motions that occur during

J.K. Moore (✉) · M. Hubbard
Mechanical and Aerospace Engineering, University of California, Davis, One Shields Avenue, Davis,
CA 95616-5294, USA
e-mail: jkmoor@ucdavis.edu

M. Hubbard
e-mail: mhubbard@ucdavis.edu

J.D.G. Kooijman · A.L. Schwab
Laboratory for Engineering Mechanics, Delft University of Technology, Mekelweg 2, 2628 CD Delft,
The Netherlands

J.D.G. Kooijman
e-mail: jodikooijman@gmail.com

A.L. Schwab
e-mail: a.l.schwab@tudelft.nl

stabilization with and without pedaling. These motions were grouped on the basis of correlation and conclusions were drawn about which motions are candidates for stabilization-related control actions.

Keywords Bicycle · Principal component analysis · Motion capture · Human control

1 Introduction

Much progress has been made in understanding the rigid body dynamics of an uncontrolled bicycle [1, 2] and various control schemes have been explored for tracking purposes [3–5], but little is understood about how a bicyclist stabilizes a bicycle during normal riding. A bicycle and rider system is unique among vehicles in that the rider is 80 to 90% of the total mass of the system, the system is laterally unstable, and the rider is flexibly coupled to the bicycle in such a way that many body motions can be used as control inputs. Previous research into realistic bicycle control has focused on both steering and rider lean as control inputs, but there has been no experimental verification of which motions a rider actually uses for control. Recent observations of a bicyclist riding through town and on a treadmill [6] show that the rider moves the upper body very little when performing normal maneuvers and that the bicyclist may, in fact, primarily use steering input for control. This corresponds well with the fact that control by leaning requires high gains compared to the gains required for steering when employing an optimal control strategy on a model [3–5]. The observations also revealed that the rider may use other control inputs such as drastic knee movements at low speeds. These conclusions were drawn by visually reviewing video data, so a more rigorous objective method of characterizing the dominant movements of the bicyclist while stabilizing a bicycle was needed. In order to validate the hypothesis that there is little upper body motion during normal cycling, motion capture techniques were used on the bicycle and rider system with the intent to employ principal component analysis to identify the major motion patterns.

Principal component analysis has successfully been used with data collected from motion capture techniques to identify the dominant modes of motion of a person walking on a treadmill [7] and to characterize different types of walking. We use similar methods for steady, normal bicycle riding on a treadmill. Cyclic motions, such as pedaling, are easily identified and separated from the other less cyclic control actions. Identifying the patterns of movement gives insight into which body movements are primarily used and are candidates for control inputs. This will be valuable for our overall research goals that include the design of a realistic biomechanical-based control system of a bicycle rider, among other things.

2 Experiments

To test our hypotheses, three riders performed a set of stability tasks in a controlled environment while the motion of the bicycle and rider were collected with a motion capture system. The tasks were performed on a 3×5 meter treadmill Fig. 1 capable of belt speeds up to 35 km/h. The treadmill was chosen because the envelope of space was suitable for the motion capture system and it eliminated any disturbances such as wind, rough ground, and obstacles. We chose three male riders of similar age [31, 23, 26 years], build [height (1.76, 1.84, 1.83 m) and mass (72, 74, 72 kg)]. We also used two different Dutch bicycles: a 2008 Batavus Browser with a 3 speed hub and a 2008 Batavus Stratos Deluxe with

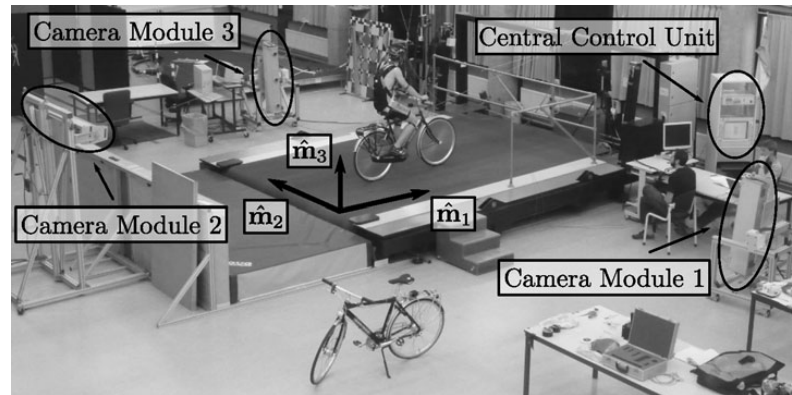


Fig. 1 The 3 × 5 m treadmill at the Vrije Universiteit Amsterdam

a 7 speed hub. The Browser is described by the manufacturer as “stable” and the Stratos Deluxe as “nervous.”

We made use of the Optotrak Certus Motion Capture System [8] to record the motion of the bicycle and rider during the stability tasks. The system is based on active infrared emitting markers that are placed on the moving bodies and connected to a central control unit. Each marker emits a sequential infrared signal and the infrared pulses are captured by camera modules each containing three cameras. The accuracy of the three dimensional measurements is ± 0.15 mm [8]. The system has no hardware-based noise reduction. Wiring harnesses were built for both the rider and the bicycles to facilitate easy bicycle and rider exchange Fig. 2.

The marker coordinates were measured with respect to an inertial frame, \mathbf{M} , where the plane normal to $\hat{\mathbf{m}}_3$ is coplanar with the treadmill surface and $\hat{\mathbf{m}}_3$ is directed upward. We collected the three dimensional locations of 31 markers, 11 of which were located on the bicycle and 20 mapped the rider Fig. 3.

The markers were placed on the bicycle so that we could easily extract the rigid body motion (i.e., body orientations and locations) of the bicycle frame and fork. Four markers were attached to the fork and seven markers were attached to the rear frame. A marker was attached on the right and left sides of the center of each wheel, the seat stays, the ends of the handlebars, and the head tube. A single marker was also attached to the back of the seat post.

We recorded the locations of 20 points on the rider Fig. 3: left and right sides of the helmet near the temple, back of the helmet, shoulders (greater tuberosity of the humerus), elbows (lateral epicondyle of the humerus), wrists (pisiform of the carpus), between the shoulder blades on the spine (T6 of the thoracic vertebrae), the tail bone (coccyx), midpoint on the spine between the coccyx and shoulder blades (L1 on the lumbar vertebrae), hips (greater trochanter of the femur), knees (lateral epicondyle of the femur), ankles (lateral malleolus of the fibula) and feet (proximal metatarsal joint). The body markers were not necessarily placed such that a complete rigid body model could easily be fit to the data. This was done to save setup and processing time because we only wanted a stick figure representation of the rider that allowed us to visually observe the dominant motions of the rider.

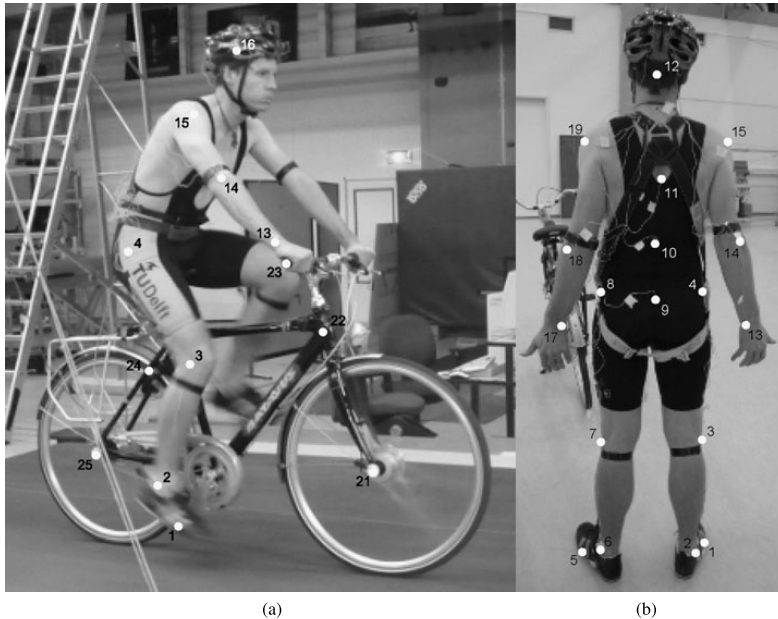
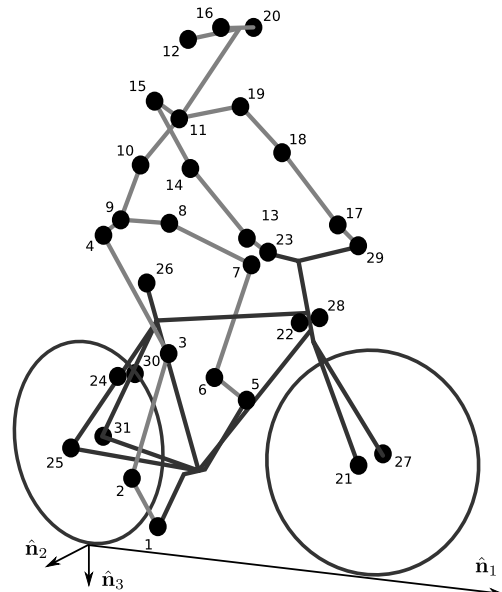


Fig. 2 (a) Rider 1 and the Batavus Stratos Deluxe with marker positions. (b) Body marker positions visible from the rear

The stability tasks were designed such that the rider would ride at a constant speed within the range of 2 to 30 km/h. The bicyclists were told to maintain an upright straight-ahead course on the treadmill and to look into the distance, with exception of the line tracking task. The bicyclists were instructed to bicycle comfortably at the designated speed and data recording was started at random. In all cases, the subject rode at the set speed until comfortable, then data was taken for 60 seconds at a 100 hertz sampling rate. Each task was performed on both bicycles with each rider. The following list describes the various tasks:

- Normal pedaling** The subject was instructed to simply stabilize the bicycle while pedaling and keep the heading in approximately the forward direction. The speed started at 5 km/h and increased in 5 km/h increments up to 30 km/h. The speeds were then decreased in the same fashion to 5 km/h. From then on the speed was decreased in 1 km/h increments until the subject was not able to stabilize the bicycle any longer. Therefore, there were two sets of data for each speed and each bicycle except speeds below 5 km/h. Several additional runs were also performed with the rider pedaling using a different gear, and thus a different cadence.
- Without pedaling** This was the same as the normal pedaling task except that a string was attached to the head tube of the bicycle such that the bicycle was fixed

Fig. 3 Schematic of the marker positions. The rider and bicycle are colored light gray and dark gray, respectively



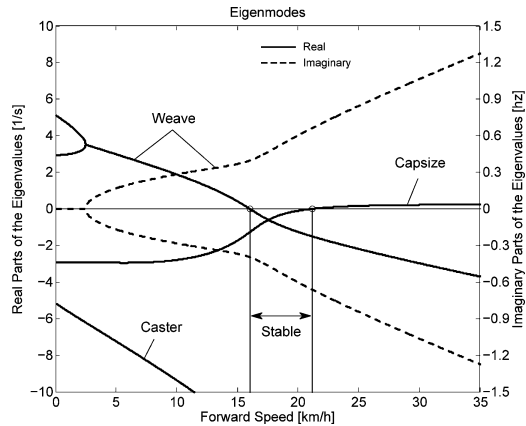
	longitudinally relative to the treadmill and no pedaling was required. The rider kept the feet in the same position throughout the task.
No-hands	The riders stabilized the bicycle without using steering for control. They were instructed to keep their hands on their hips while bicycling. The rider started at 30 km/h and decreased in 5 km/h increments through 20 km/h and thereafter the speeds were decreased in 1 or 2 km/h increments until the rider was not able to comfortably stabilize the bicycle.
Line tracking	This was the same as normal pedaling except that the rider was instructed to track a line on the treadmill surface with the front wheel. A smaller subset of speeds was performed.

These tasks were designed with the intent to answer several questions:

1. What upper body motions are used while bicycling?
2. How does the system motion change with respect to changes in forward speed?
3. How does pedaling influence the control actions?
4. Can the open loop rigid body dynamics be detected in the controlled state?
5. What does the rider do differently to control the bicycle when riding no-hands?
6. Do different bicyclists perform similar motions while performing the same task?
7. Is there a difference in motion when stabilizing and trying to track a line?

Since there is no room to address all of these questions in this paper, we focus on a single rider on the Browser bicycle and two of the tasks: normal pedaling and without pedaling. We were able to draw some conclusions on questions 1 through 4 with this smaller data set.

Fig. 4 Eigenvalues of the Browser bicycle with the third rider rigidly attached as a function of speed. Note that the initially unstable weave motion becomes stable above 16 km/h, the weave speed



3 Open loop rigid body dynamics

One question we have is whether or not the eigenfrequencies of the weave motion for the uncontrolled system can be detected in the results from the stabilization tasks. In order to predict the uncontrolled (open loop) eigenvalues of the rigid rider system, the basic geometry, mass, center of gravity locations, and moments of inertia of the bicycle were measured. Also, the riders were measured and weighed such that the body segment geometry, mass, center of gravity locations, and moments of inertia could be estimated. The physical parameter estimation methods are described in [9]. This data was used to calculate eigenvalues and eigenvectors of the uncontrolled open loop system Fig. 4.

4 Data processing

4.1 Missing markers

The Optotrak Certus Motion Capture System [8] is based on the cameras' ability to detect the infrared light from the sensors so there are occasional gaps in the coordinate data due to the markers going out of view. We attempted to minimize this by careful marker and camera placement but were not able to totally eliminate the error. Any missing markers on the bicycle were reconstructed using the assumption that the bicycle is a rigid body. We had more than three markers on both the frame and fork, so if one marker location was not detected we used the relative location of the remaining markers to reconstruct the missing marker. The gaps in the data of the markers on the human were repaired by fitting a cubic spline through the data. The spline estimated the marker coordinates during the gaps. We only used the splined data if the gaps were less than 10 time steps, or 0.1 sec; otherwise the trials were discarded.

4.2 Relative motion

We were interested in the analysis of three different marker combinations: the bicycle alone, the rider relative to the bicycle and the bicycle and rider together. The motion of the bicycle

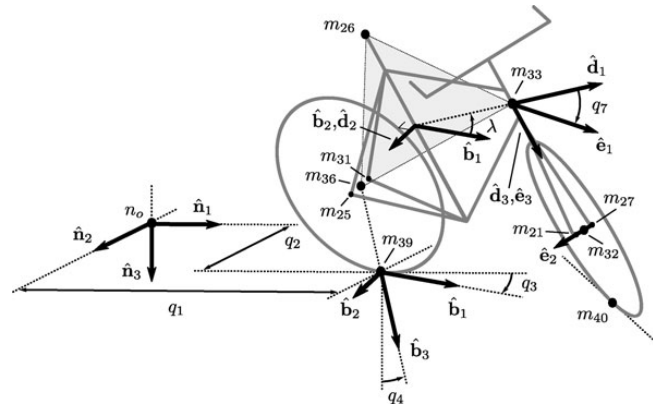


Fig. 5 Diagram of the bicycle's inertial frame **N**, rear frame **B**, front frame **E** and configuration variables

and the bicycle-rider were calculated with reference to the **N** inertial frame¹ and the motion of the rider was calculated with respect to the rear frame of the bicycle **B** Fig. 5. These three marker combinations allowed us to differentiate more easily between rider specific and bicycle specific motions. Furthermore, six of the variables that describe the configuration of the bicycle in time were calculated to give insight into the rigid body dynamics. The configuration variables q_1 and q_2 locate the contact point of the rear wheel of the bicycle. The **B** frame captures the yaw (q_3) and roll (q_4) motions of the bicycle frame, the **D** frame is an intermediate frame that differs from **B** only by the bike's headtube angle (λ), and the **E** frame captures the steering angle (q_7) of the bicycle fork relative to the bicycle frame. The pitch of the bicycle frame (q_6) is assumed to be zero. Details of these calculations are shown in [Appendix](#).

4.3 Principal component analysis

We used Principal Component Analysis, PCA, [10] to extract and characterize the dominant motions of the system. Calculating the principal components effectively transforms the space of the data to a space that maximizes the variance of the data. The typical advantage of PCA is that the dimension of the system can be reduced and still retain enough information to adequately describe the system. We are primarily interested in the way that PCA is able to extract linear components and rank them in order of variance from the mean position. If we assume that the components with the largest kinematic variance are motions that are the dominant motions used for control and propulsion (which in general is not necessarily true for dynamical systems) the comparison of these components for different riding conditions can give insight into what motions may be important for developing a biomechanical control model of the bicyclist.

¹The **N** frame is used instead of the **M** frame to comply with the vehicle coordinate standards used in [1]. See [Appendix](#) for the derivation.

The repaired data from the motion capture measurements contained the x , y , and z coordinates of each marker 1 through l at each time step $j = 1, 2, \dots, n$. Each marker has three coordinates so there are a total of $m = 3l$ coordinates $i = 1, 2, \dots, m$. The coordinates at each time step can be collected in vector \mathbf{p}_j .

$$\mathbf{p}_j^T = [x_{1j} \quad \cdots \quad x_{lj} \quad y_{1j} \quad \cdots \quad y_{lj} \quad z_{1j} \quad \cdots \quad z_{lj}] = [p_{1j} \quad p_{2j} \quad \cdots \quad p_{mj}]$$

We can organize these coordinate vectors into a matrix, \mathbf{P} , where the rows, i , map a single coordinate of a marker through n time steps.

$$\mathbf{P} = \begin{bmatrix} | & | & & | & | \\ \mathbf{p}_1 & \mathbf{p}_2 & \cdots & \mathbf{p}_j & \cdots & \mathbf{p}_n \\ | & | & & | & | \end{bmatrix}$$

The principal components were calculated for the three marker combinations as described earlier where $n = 60 \times 100 = 6000$ time steps. The number of rows of \mathbf{P} were ($m = 3 \times 31 = 93$), ($m = 3 \times 11 = 33$) and ($m = 3 \times 20 = 60$) for the bicycle-rider, the bicycle alone and the rider alone, respectively.

One method of determining the principal components is to calculate the eigenvectors of the covariance matrix of the mean-subtracted data. We begin by calculating the mean \mathbf{u} (1) of the rows of \mathbf{P} and subtracting it from each column of \mathbf{P} to form the mean-subtracted data matrix $\tilde{\mathbf{P}}$, (2).

$$\mathbf{u} = \frac{1}{n} \sum_{j=1}^n \mathbf{p}_j \quad (1)$$

A vector of ones

$$\mathbf{h}^T = [h_1 \quad h_2 \quad \cdots \quad h_j \quad \cdots \quad h_n] \quad \text{where } h_j = 1 \text{ for all } j$$

allows us to subtract \mathbf{u} from each column of \mathbf{P} ,

$$\tilde{\mathbf{P}} = \mathbf{P} - \mathbf{u}\mathbf{h}^T \quad (2)$$

The covariance matrix \mathbf{C} of $\tilde{\mathbf{P}}$ can then be calculated with (3).

$$\mathbf{C} = \frac{1}{n-1} \tilde{\mathbf{P}}\tilde{\mathbf{P}}^T \quad (3)$$

Calculating the eigenvectors \mathbf{v}_i and eigenvalues λ_i of the covariance matrix effectively transforms the space to one where the variances are maximized and the covariances are zero. The eigenvectors are the principal components of the data set and the corresponding eigenvalues represent the variance of each principal component. The eigenvectors are ordered by decreasing eigenvalue where \mathbf{v}_1 is the eigenvector corresponding to the largest eigenvalue. The eigenvalues and eigenvectors are calculated by finding the independent solutions to (4).

$$\mathbf{C}\mathbf{v}_i = \lambda_i\mathbf{v}_i \quad (4)$$

Each time step can now be represented as a linear combination of the principal components.

$$\mathbf{p}_j = \mathbf{u} + a_{1j}\mathbf{v}_1 + a_{2j}\mathbf{v}_2 + \cdots + a_{mj}\mathbf{v}_m \quad (5)$$

The coefficients a_{ij} can be solved at each time step j by reformulating (5) and solving the system of linear equations.

$$\mathbf{P} - \mathbf{u}\mathbf{h}^T = \begin{bmatrix} | & | & & | \\ \mathbf{v}_1 & \mathbf{v}_2 & \cdots & \mathbf{v}_m \\ | & | & & | \end{bmatrix} \begin{bmatrix} a_{11} & \cdots & a_{1n} \\ \vdots & \ddots & \vdots \\ a_{m1} & \cdots & a_{mn} \end{bmatrix} = \mathbf{V}\mathbf{A} \quad (6)$$

and

$$\mathbf{A} = \mathbf{V}^{-1}(\mathbf{P} - \mathbf{u}\mathbf{h}^T). \quad (7)$$

With the principal components \mathbf{v}_i being constant, the behavior in time is described by the coefficients a_{ij} where the discretization in time is indexed by j . The order of the system can be reduced by eliminating principal components that have little variance. We arbitrarily decided to examine the first $k = 10$ principal components knowing that the first five would be based around the larger motions such as pedaling and that the remaining five may reveal some of the motions associated with control. The variance of each component, $\text{var}(\mathbf{a}_i) = \lambda_i$, is summed to determine the cumulative percentage of variance of the principal components, g_k .

$$g_k = 100 \frac{\sum_{i=1}^k \lambda_i}{\sum_{i=1}^m \lambda_i} \quad \text{where } 1 \leq k \leq m \quad (8)$$

Highly correlated data will show that even when $k \ll m$, g_k is close to 100%. Using 10 components g_{10} covers 100% (standard deviation, $\sigma = 10^{-14}\%$) of the variation in the data for the bicycle, rider and bicycle-rider. The matrix \mathbf{A} can then be reduced to a $k \times n$ matrix and eigenvectors greater than \mathbf{v}_k can be eliminated.

4.4 Data visualization

We developed a Graphical User Interface, GUI, in MATLAB that easily allows different trials to be compared with one another Fig. 6. The program loads in two different trials along with information on each trial. A graphical representation of the rider and bicycle are displayed in two adjacent screens and can be viewed from multiple perspectives. The animations of the runs can be played at different speeds, rewound and fast forwarded. The principal components are shown beside the corresponding animation display and combinations can be turned on and off for identification and comparison. Frequency and amplitude information for the temporal coefficients a_{ij} can also be displayed for comparison.

5 Results

5.1 Motion identification

The reduced set of data provides two important pieces of information for the identification of motion: the principal components \mathbf{v}_i and the corresponding coefficients a_{ij} . The principal components represent linear trajectories of the markers and the coefficients show how the markers follow the trajectories with time. We began processing the data by reviewing each principal component of each trial in the GUI and noting what type of motion we saw Table 1. These descriptions were subjective because we grouped marker movement based on

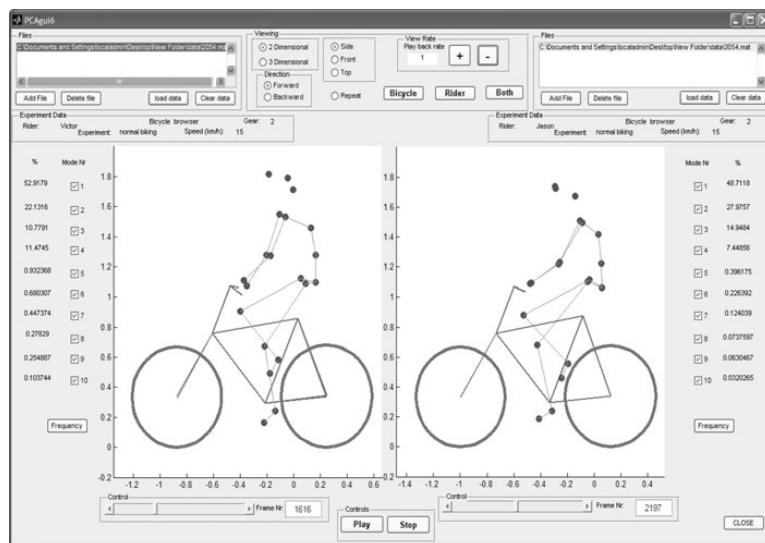


Fig. 6 Screen shot of the MATLAB graphical user interface (GUI) used to visualize principal components and compare between different components and trials

Table 1 Example raw trial description for the bicycle and rider during normal pedaling at 10 km/h

<i>i</i>	% Variance	Motion description	Frequency description
1	45.50	primarily longitudinal motion, some lateral	max amp = 0.6 m, most freq below 0.5 Hz, tiny spike at 1.6 Hz
2	29.39	primarily lateral motion, some longitudinal, small feet motion	max amp = 0.35 m, little spike at 0.8 Hz, most freq below 0.5 Hz
3	15.41	vertical pedaling, slight spine bend, hip/head/shoulder sway out of phase with pedaling	max amp = 0.27 m, large dominant spike at 0.8 Hz
4	8.27	horizontal pedaling, head/shoulder sway	large dominant spike at 0.8 Hz with 0.19 m amp
5	0.82	yaw, knees stay still	max amp = 0.04 m at 0.33 Hz, most freq below 1 Hz
6	0.27	erratic left-hand movement	max amp = 0.018 m, most freq below 2 Hz
7	0.21	steer, left-hand movement, slight roll	most freq below 2 Hz, spike at 0.33 Hz and 1.58 Hz
8	0.07	knee and head bounce	dominant spike at 1.58 Hz
9	0.04	lateral knee movement, head jiggle	spikes at 1.58 Hz and 2.37 Hz, most freq below 2.5 Hz
10	0.02	head and knee jiggle	spikes at 1.58 Hz and 3.17 Hz, most freq below 3.5 Hz

Fig. 7 Coefficients a_{ij} versus time of the first five principal components for normal pedaling at 10 km/h

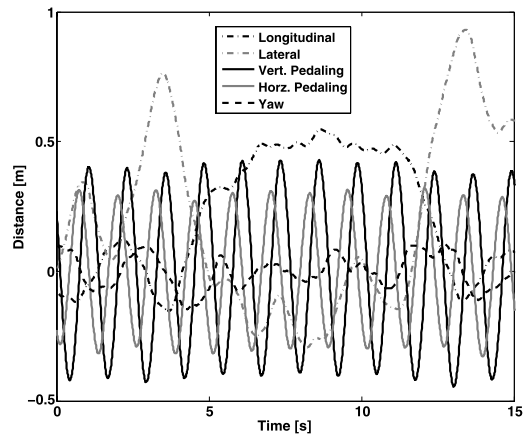
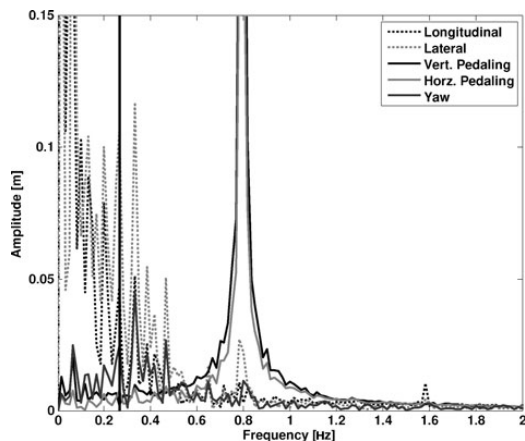


Fig. 8 The frequency content of the first five principal components for normal pedaling at 10 km/h. The vertical black line represents the open loop weave frequency (0.28 Hz) determined from Fig. 4 at this forward speed. The pedaling frequency is about 0.8 Hz at this speed; see Fig. 11



our preconceived understanding of rider and bicycle motion. Some of the components displayed motions that were not physically possible such as the upper leg stretching in length during the knee bounce. This is possible when examining a single component but when superimposed over the rest of the components the unrealistic motions are not present. Furthermore, for each component we examined amplitude and frequency content of the associated coefficients a_{ij} as shown in Figs. 7 and 8 and noted the shape of the frequency spectrum and the frequencies at any distinct spikes.

Several conclusions can be drawn from examining the coefficient data. First, some of the components are linked by the frequencies of the coefficients and describe an identifiable motion. The most obvious of these is that the vertical and horizontal pedaling components make up the circular pedaling motion. Both vary periodically and have a dominant frequency which is defined by the cadence. In the example trial, Table 1, the upper body motions are also linked to the pedaling. Components 8 and 9 both correspond to a frequency that is

twice the pedaling frequency, which may be due to the forces created during each pedal stroke. Component 6 seems to be the result of a bad marker signal. Components 5 and 7 are interesting because they display motions of the bicycle that are not dominated by the pedaling frequency and may be candidate control motions. The percentage variance of each component gives an idea of the relative amplitude of the components. The descriptions of each trial were used to compile a list of motions that contribute to the principal components. These motions, illustrated in Fig. 9, are:

Drift The bicycle and rider drift longitudinally and laterally on the surface of the treadmill. The motions are typically defined by two components that are not necessarily orthogonal or aligned with the inertial coordinate system. The motion is random and at low frequencies.

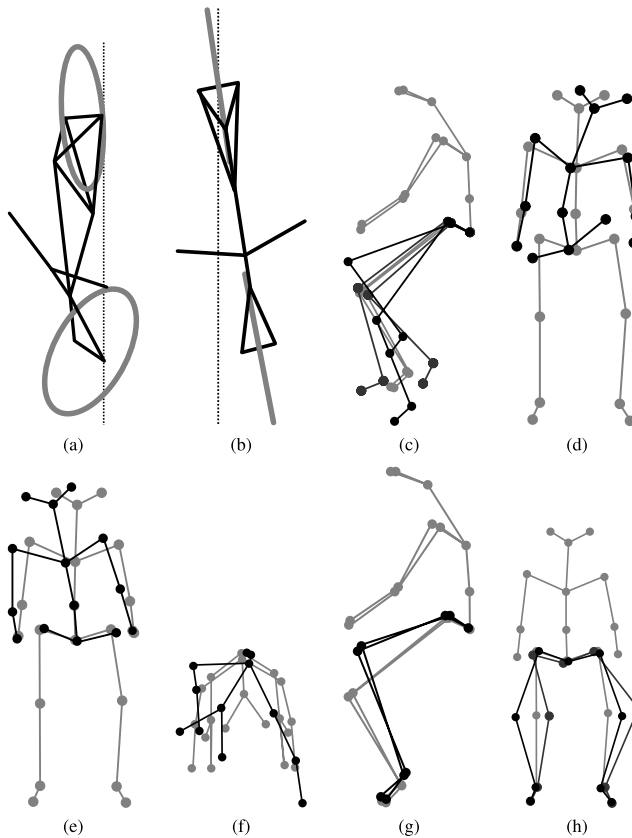


Fig. 9 Diagrams of the common motions. (a) Top view of bicycle steer and roll, (b) bicycle yaw, (c) horizontal and vertical components of pedaling, (d) spine bend, (e) rider lean, (f) top view of rider twist, (g) knee bounce and (h) two lateral knee motions. All but pedaling (c) are exaggerated for clarity

Steer	Rotation of the front assembly with respect to the rear frame. The steering may appear linked to one of the pedaling components at the pedaling frequency or may be in one or more components sometimes combined with roll and/or yaw at more random frequencies, Fig. 9(a).
Roll	The bicycle and the rider roll with respect to the ground plane. Roll is typically linked with steer and/or yaw and often at the pedaling frequency, Fig. 9(a).
Yaw	The heading angle of the bicycle and rider change together with respect to the ground plane. This is typically linked with steer, roll, and/or the drift, Fig. 9(b).
Pedaling	This motion is defined by two or more components, typically a vertical and horizontal motion of the feet, that show the feet rotating around the crank axle at a distinct frequency and the legs following suit, Fig. 9(c).
Bend	The spine bent laterally and was always connected with the vertical pedaling component, Fig. 9(d).
Lean	The upper body, shoulders and head lean laterally with respect to the rear frame and was always linked with the horizontal pedaling component, Fig. 9(e).
Twist	The shoulders rotate about the torso axis. This was linked to components that contained steering motions, both random and at the pedaling frequency, Fig. 9(f).
Bounce	The knee markers bounce up and down, the back straightens and the head nods at twice the pedaling frequency, Fig. 9(g).
Knees	The knees move laterally relative to the bicycle frame in both opposing directions and the same direction at random low frequencies, Fig. 9(h).
Head	Head twists and random head motions showed up often. These seemed to be due to the rider looking around randomly.

5.2 Motion characterization

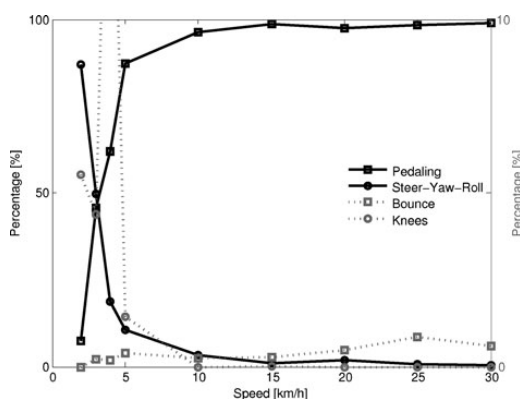
To identify how bicycling changes with speed it would be ideal to investigate how the amplitude of each component varies with speed. However, the analysis does not return the same set of components for each run so such a comparison is typically not possible. Therefore, components were grouped into classes, where each class shows a specific physically relevant motion. The same total motion of the class can be described by one set of components in one trial and another, probably different, set of components in another trial. How the amplitudes of these classes vary among experiments can be used as a measure for how the rider and bicycle motion varies among trials.

To objectively identify which coefficients show the same type of motion and could therefore form a class, the frequency content of each of the time coefficients in a single trial was correlated to that of each of the other components in that trial. Next, a minimum correlation value was set to determine which coefficients were correlated to each other. When the minimum was set at 0.9 only the coefficients making up the pedaling motion could be considered correlated. On the other hand, when a minimum level of 0.7 was used practically every coefficient was correlated to each other. The only exception was the coefficient that displayed the bounce. Its maximum correlation with another coefficient was no higher than 0.4 for any of the tested speeds. The 0.8 level gave a number of distinct classes of components, and thus this level was used to identify which coefficients were connected. Finally, the correlated coefficients were viewed simultaneously in the GUI enabling the determination of the motion class.

The correlated coefficients were used to form six different classes of motions, Table 2, each made up of combinations of the previously described motions in Fig. 9.

Table 2 The six primary motion classes

Class name	Class description
Drift	Drift
Pedaling	Pedaling 9(c), Bend 9(d), Lean 9(e), Twist 9(f)
Steer-Yaw-Roll	Steer and Roll 9(a), Yaw 9(b)
Bounce	Bounce 9(g)
Knees	Knees 9(h)
Other	Head and components that showed noise of some sort

Fig. 10 The relative percent variance of the four classes: Pedaling, Steer-Yaw-Roll, Bounce and Knees, at the different speeds when the Drift and Other classes were removed from the results for normal pedaling. The solid lines are scaled to 100% (left axis), the dotted lines are scaled to 10% (right axis)

In most cases, the correlated coefficients described a single class. However, sometimes, this was not the case and the coefficients were used to describe more than one class. An example is that at low speed the components containing the drift motions also contained large steer, yaw, and roll motions. Therefore, the motions were placed in both the Drift and the Steer-Yaw-Roll classes.

Since the rider was not instructed to hold a specific location on the treadmill the Drift class, which was usually the class with the largest amplitude, was not used in further analysis of the motion and neither was the 'Other' class. For each of the remaining classes, the percentages of variance of the remaining components were recalculated without the components placed in the Drift and the Other classes.

We also calculated various configuration variables from the bicycle marker locations (see [Appendix](#)) independent of the PCA perspective for more specific motion characterizations. This allowed us to investigate the bicycle's configuration variable time histories and frequency content explicitly.

5.3 Characterization of motions during normal pedaling

Figure 10 shows how the relative percent variance of the four classes: Pedaling, Steer-Yaw-Roll, Bounce and Knees varies with speed for Rider 3 on the Batavus Browser bicycle. The percentage is the average of two runs at speeds 5 km/h and above. From the

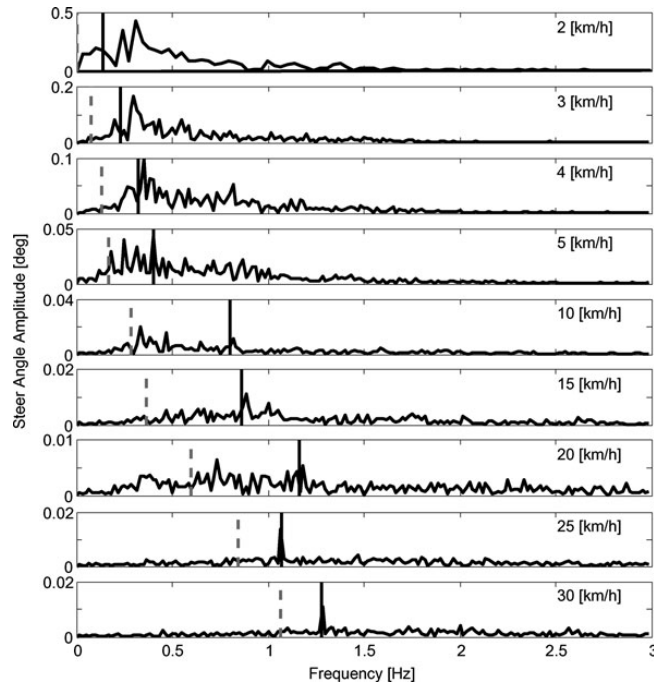
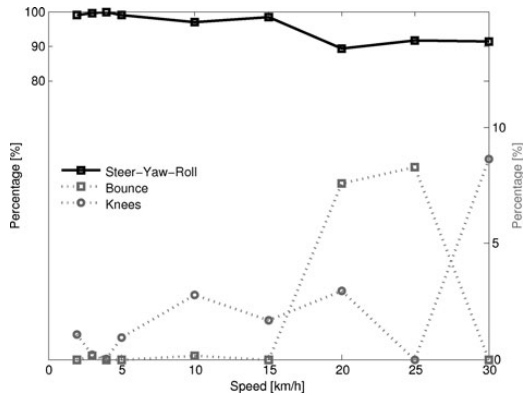


Fig. 11 Steer angle amplitude plot for the nine different speeds for normal pedaling experiment. *Solid vertical line* indicates the pedaling frequency. *Dashed vertical gray line* indicates the bicycle-rigid rider open loop weave eigenfrequency from Fig. 4

graph, it is clear that at 10 km/h and higher speeds practically all the motion that is taking place is the pedaling motion class. Below 10 km/h, the Steer-Yaw-Roll class becomes increasingly active and the relative percentage of the motion taking place in the pedaling class drops. Also, at speeds below 10 km/h, the lateral knee motion (Knees) class percentage increases with decreasing speed. The increase is not as significant as that of the Steer-Yaw-Roll class (increase to roughly 5% at 2 km/h), but it is certainly visible. The spike at 4 km/h can be attributed to the fact that the classes may contain higher variance motions because the classification method is based on principal components that are not necessarily consistent between runs. The Bounce roughly remains constant at all speeds.

The steer angle amplitude-frequency plot for each of the speeds calculated from the bicycle rigid body motions is given in Fig. 11. It clearly shows that the steering actions take place at or around the pedaling frequency for high and low speeds, respectively. It also shows that the amplitude of the steering angle increases by 5000% when the speed decreases from 30 km/h to 2 km/h. Figure 11 also shows the open loop, rigid rider, weave eigenfrequency for each speed obtained from Fig. 4. Apparently the open loop eigenfrequency is not a frequency at which the bicycle-rider operates.

Fig. 12 The percent variance of each of the three classes: Steer-Yaw-Roll, Bounce and Knees, at the different speeds when the Drift and Other classes were removed from the results for trials without pedaling. The solid lines are scaled to 100% (left axis), the dotted lines are scaled to 15% (right axis)



5.4 Characterization of motions without pedaling

During normal pedaling, all motions, including the control tasks, are dominated by the pedaling motions. Therefore we also looked at the motions of bicycle-rider system without the influence of pedaling. Figure 12 shows how the percent variance of Steer-Yaw-Roll, Bounce and Knees varies with speed for Rider 3 on the Batavus Browser bicycle without pedaling. Since the bicycle is towed and the riders feet remain in the same, constant, position relative to bicycle, there is no pedaling class present in analysis. Furthermore, no bend, lean or twist motions with high variance were detected during the experiments. It is clear that at all speeds most motion takes place in the Steer-Yaw-Roll class. Also interesting is that, unlike in the normal pedaling situation, the Knee motion percentage does not increase at low speeds. This may mean that the lateral knee motion is connected to pedaling in some way. Like for the pedaling case, the Bounce and Knee classes may contain different principal components and a statistical approach to evaluate the percent variance of the classes would provide clearer results. Also note that as the bicycle becomes self stable above 16 km/h the total variance is tiny and thus any sort of random knee motion can be a relatively large motion.

Figure 13 shows the bicycle rigid body steer angle frequency-amplitude plot for different speeds. Compared to normal pedaling, the amplitudes are about half the size at the low speeds and one tenth the size at high speeds, indicating that smaller steering angles were made. The frequency content now also shows a much wider, flatter spectrum compared to normal pedaling. At 10 and 15 km/h, the frequency with the largest amplitude is near the open loop weave eigenfrequency. However, at the other speeds, this is not the case, once again indicating that the rigid body open loop weave eigenfrequency is not the frequency at which the bicycle is controlled.

6 Conclusions

The view provided by principal component analysis into bicycle-rider interaction, biomechanics and control has led us to several conclusions. During normal bicycling there are

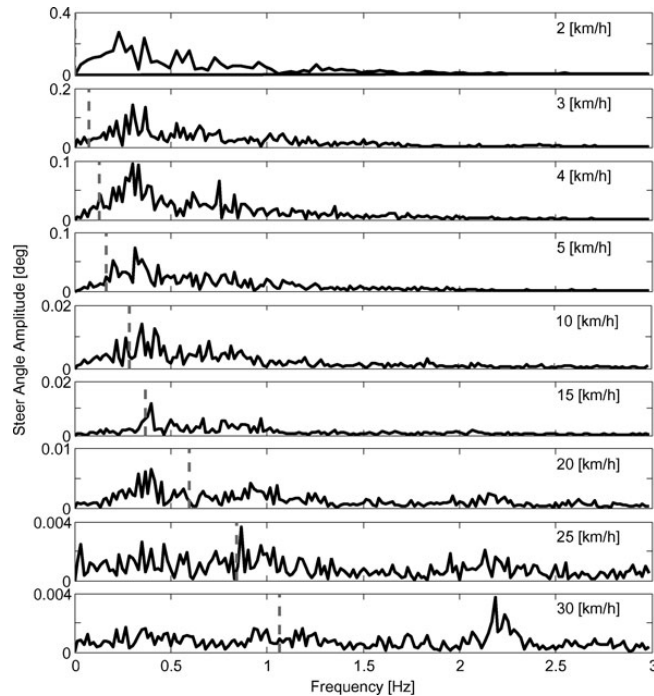


Fig. 13 Steer angle amplitude plot for the nine different speeds for the tasks without pedaling. *Dashed vertical grey line* indicates the bicycle-rigid rider open loop weave eigenfrequency obtained from Fig. 4

several dominant upper body motions: lean, bend, twist and bounce, all of which seem to be linked to the pedaling motion. This is important for understanding which inputs are related to fundamental balance control and which are reactions to pedaling. We hypothesize that lateral control is mainly accomplished by steering since only upper body motion was observed at the pedaling frequency. If upper body motions are used for control then this control is carried out at the pedaling frequency. Considering variations of motion with respect to speed, we observed that there is a great deal of steering at low speeds but this decreases in magnitude as speed increases. This is generally true for all motions and shows that the bicycle-rider system becomes more stable at higher speeds with few detectable control actions. At low speeds additional lateral knee motions are observed which are probably more effective at augmenting steering control for lateral balance than upper body motions.

The bicycle model predicts that the weave mode is stable above about 16 km/h. Intuition might possibly lead one to believe, if the weave mode is already stable, that the weave frequency might be relatively undisturbed by rider control actions and therefore present in the closed loop dynamics. However, we found no evidence of a distinct weave frequency in the steer angle time histories of any run. In fact, the only distinct frequency that sometimes appeared was the pedaling frequency.

Principal component analysis provided a unique view into the control actions of a rider on a bicycle, but limitations in data reduction and motion grouping leave room for more objective statistical views into the motion of the bicycle-rider system.

Acknowledgements We would like to thank Knoek van Soest and Richard Casius of the Faculty of Human Movement Sciences at the Vrije Universiteit, Amsterdam, for their cooperation and use of their equipment for the experiments and for Richard's expertise and help in operating the motion capture system and data processing. Also, we thank Victor Ahlm for a tireless day of bicycling and the Dutch bicycle manufacturer, Batavus, for supplying the bicycles.

Open Access This article is distributed under the terms of the Creative Commons Attribution Noncommercial License which permits any noncommercial use, distribution, and reproduction in any medium, provided the original author(s) and source are credited.

Appendix: Inertial frames and configuration variables

The transformation from marker coordinates to rigid body inertial frames and configuration variables shown in Fig. 5 is described here. A reference frame, \mathbf{N} , with origin n_o corresponding with the benchmark bicycle [1] is defined with respect to the Optotrak reference frame, \mathbf{M} , (9).

$$\mathbf{N} = \begin{bmatrix} \hat{\mathbf{n}}_1 \\ \hat{\mathbf{n}}_2 \\ \hat{\mathbf{n}}_3 \end{bmatrix} = \begin{bmatrix} 1 & 0 & 0 \\ 0 & -1 & 0 \\ 0 & 0 & -1 \end{bmatrix} \begin{bmatrix} \hat{\mathbf{m}}_1 \\ \hat{\mathbf{m}}_2 \\ \hat{\mathbf{m}}_3 \end{bmatrix} \quad (9)$$

Thirty-one marker locations were recorded and the vector to each is defined as \mathbf{r}^{m_k/n_o} where $k = 1, 2, \dots, l$ for the original markers and $k = l + 1, \dots$ for any additional virtual markers. To calculate the reference frame attached to the rear bicycle we formed a frame center plane from the seat post marker, m_{26} , and two new additional virtual markers at the center of the rear wheel, m_{36} , and the center of the head tube, m_{33} . For example, the center of the rear wheel was calculated by (10) where m_{25} and m_{31} are the left and right rear wheel markers.

$$\mathbf{r}^{m_{36}/n_o} = (\mathbf{r}^{m_{25}/n_o} + \mathbf{r}^{m_{31}/n_o})/2 \quad (10)$$

The normal vector to the plane through the rear wheel center, seat post, and the head tube center is

$$\hat{\mathbf{b}}_2 = \frac{\mathbf{r}^{m_{36}/m_{26}} \times \mathbf{r}^{m_{33}/m_{26}}}{|\mathbf{r}^{m_{36}/m_{26}} \times \mathbf{r}^{m_{33}/m_{26}}|} \quad (11)$$

The heading vector of the rear frame is then $\hat{\mathbf{b}}_1 = \hat{\mathbf{b}}_2 \times \hat{\mathbf{n}}_3$ and $\hat{\mathbf{b}}_3 = \hat{\mathbf{b}}_1 \times \hat{\mathbf{b}}_2$ follows. These unit vectors define a reference frame that leans and yaws with the rear frame. We assumed that the rear frame pitch is negligible. The marker locations of the rider can now be expressed relative to the bicycle's inertial frame with reference to a point on the bicycle frame m_{36} . Equation (12) shows that the vector from any marker on the rider relative to m_{36} can be expressed in the bicycle reference frame, \mathbf{B} , rather than the inertial frame, \mathbf{N} . This formulation was used in the PCA of the rider-only markers to look specifically at rider motion relative to the bicycle. The subscripts, \mathbf{N} and \mathbf{B} , in (12) signify which reference frame the position vectors are expressed in.

$$\mathbf{r}_{\mathbf{B}}^{m_k/m_{36}} = (\mathbf{r}_{\mathbf{N}}^{m_k/m_{36}} \cdot \hat{\mathbf{b}}_1) \hat{\mathbf{b}}_1 + (\mathbf{r}_{\mathbf{N}}^{m_k/m_{36}} \cdot \hat{\mathbf{b}}_2) \hat{\mathbf{b}}_2 + (\mathbf{r}_{\mathbf{N}}^{m_k/m_{36}} \cdot \hat{\mathbf{b}}_3) \hat{\mathbf{b}}_3 \quad (12)$$

A reference frame \mathbf{D} that is aligned with the steering axis of the rear frame can be formulated by rotation about the $\hat{\mathbf{b}}_2$ axis through the steer axis angle λ , which is measured for each bicycle [9].

$$\mathbf{D} = \begin{bmatrix} \hat{\mathbf{d}}_1 \\ \hat{\mathbf{d}}_2 \\ \hat{\mathbf{d}}_3 \end{bmatrix} = \begin{bmatrix} \cos \lambda & 0 & -\sin \lambda \\ 0 & 1 & 0 \\ \sin \lambda & 0 & \cos \lambda \end{bmatrix} \begin{bmatrix} \hat{\mathbf{b}}_1 \\ \hat{\mathbf{b}}_2 \\ \hat{\mathbf{b}}_3 \end{bmatrix} \quad (13)$$

The handlebar/fork inertial frame \mathbf{E} is then calculated by defining $\hat{\mathbf{e}}_2$ to be aligned with the front wheel axle (14).

$$\hat{\mathbf{e}}_2 = \frac{\mathbf{r}^{m_{21}/n_o} - \mathbf{r}^{m_{27}/n_o}}{|\mathbf{r}^{m_{21}/n_o} - \mathbf{r}^{m_{27}/n_o}|} \quad (14)$$

The handlebar/fork frame rotates around $\hat{\mathbf{d}}_3 = \hat{\mathbf{e}}_3$ and then $\hat{\mathbf{e}}_1 = \hat{\mathbf{e}}_3 \times \hat{\mathbf{e}}_2$. Equation (15) gives the instantaneous rear wheel radius which is used to formulate the vector to the rear wheel contact point (16).

$$r_R = -\frac{\mathbf{r}^{m_{36}/n_o} \cdot \hat{\mathbf{n}}_3}{\hat{\mathbf{b}}_3 \cdot \hat{\mathbf{n}}_3} \quad (15)$$

$$\mathbf{r}^{m_{39}/n_o} = \mathbf{r}^{m_{36}/n_o} + r_R \hat{\mathbf{b}}_3 \quad (16)$$

This now allows us to calculate six of the eight configuration variables of the bicycle as a function of time (q_5 and q_8 are the rear and front wheel rotations, respectively).

$$\text{Distance to the ground contact point: } q_1 = \mathbf{r}^{m_{39}/n_o} \cdot \hat{\mathbf{n}}_1, \quad (17)$$

$$\text{Distance to the ground contact point: } q_2 = \mathbf{r}^{m_{39}/n_o} \cdot \hat{\mathbf{n}}_2, \quad (18)$$

$$\text{Yaw angle: } q_3 = \arccos(\hat{\mathbf{b}}_1 \cdot \hat{\mathbf{n}}_1), \quad (19)$$

$$\text{Roll angle: } q_4 = \arccos(\hat{\mathbf{b}}_3 \cdot \hat{\mathbf{n}}_3), \quad (20)$$

$$\text{Pitch angle: } q_6 = 0, \quad (21)$$

$$\text{Steer angle: } q_7 = \arccos(\hat{\mathbf{d}}_1 \cdot \hat{\mathbf{e}}_1), \quad (22)$$

References

1. Meijaard, J.P., Papadopoulos, J.M., Ruina, A., Schwab, A.L.: Linearized dynamics equations for the balance and steer of a bicycle: a benchmark and review. *Proc. R. Soc., A Math. Phys. Eng. Sci.* **463**(2084), 1955–1982 (2007)
2. Kooijman, J.D.G., Schwab, A.L., Meijaard, J.P.: Experimental validation of a model of an uncontrolled bicycle. *Multibody Syst. Dyn.* **19**, 115–132 (2008)
3. Peterson, D.L., Hubbard, M.: Yaw rate and velocity tracking control of a hands-free bicycle. In: *International Mechanical Engineering Congress and Exposition*, Boston, Oct. 2008. ASME, New York (2008)

4. Schwab, A.L., Kooijman, J.D.G., Meijaard, J.P.: Some recent developments in bicycle dynamics and control. In: Belyaev, A.K., Indeitsev, D.A. (eds.) Fourth European Conference on Structural Control (4ECSC), pp. 695–702. Institute of Problems in Mechanical Engineering, Russian Academy of Sciences, Moscow (2008)
5. Sharp, R.S.: On the stability and control of the bicycle. *Appl. Mech. Rev.* **61**(6), 1–24 (2008)
6. Kooijman, J.D.G., Schwab, A.L., Moore, J.K.: Some observations on human control of a bicycle. In: Proceedings of the ASME 2009 International Design and Engineering Technical Conferences & Computers and Information in Engineering Conference, 2009
7. Troje, N.F.: Decomposing biological motion: a framework for analysis and synthesis of human gait patterns. *J. Vis.* **2**(5), 371–387 (2002)
8. Northern Digital Incorporated. Optotrak Certus Motion Capture System (2009)
9. Moore, J.K., Kooijman, J.D.G., Hubbard, M., Schwab, A.L.: A method for estimating physical properties of a combined bicycle and rider. In: Proceedings of the ASME 2009 International Design Engineering Technical Conferences & Computers and Information in Engineering Conference, IDETC/CIE 2009, San Diego, CA, USA, August–September 2009. ASME, New York (2009)
10. Jolliffe, I.T.: Principal Component Analysis. Springer Series in Statistics, 2nd edn. Springer, New York (2002)

Moore, J. K., Kooijman, J. D. G., Hubbard, M., and Schwab, A. L. (2009). A method for estimating physical properties of a combined bicycle and rider. In *Proceedings of the ASME 2009 International Design Engineering Technical Conferences & Computers and Information in Engineering Conference*, number DETC2009-86947, DETC2009, Aug 30 – Sep 2, 2009, San Diego, CA.

Proceedings of the ASME 2009 International Design Engineering Technical Conferences &
Computers and Information in Engineering Conference
IDETC/CIE 2009
August 30-September 2, 2009, San Diego, USA

DETC2009-86947

A METHOD FOR ESTIMATING PHYSICAL PROPERTIES OF A COMBINED BICYCLE AND RIDER

Jason K. Moore*

Mont Hubbard

Sports Biomechanics Laboratory
Department of Mechanical and Aeronautical Engineering
University of California
One Shields Avenue
Davis, California 95616
Email: jkmoor@ucdavis.edu
mhubbard@ucdavis.edu

J. D. G. Kooijman

A. L. Schwab

Laboratory for Engineering Mechanics
Faculty of 3mE
Delft University of Technology
Mekelweg 2, 2628CD Delft
The Netherlands
Email: jodikooijman@gmail.com
a.l.schwab@tudelft.nl

ABSTRACT

A method is presented to estimate and measure the geometry, mass, centers of mass and the moments of inertia of a typical bicycle and rider. The results are presented in a format for ease of use with the benchmark bicycle model [1]. Example numerical data is also presented for a typical male rider and city bicycle.

INTRODUCTION

Meijaard et al. [1] recently provided not only a complete review of the bicycle literature but also a concise summary of the equations of motion of the Whipple model [2] as well as benchmark calculations for comparison with other authors' numerical results. Kooijman [3] presented an experimental verification of the weave eigenvalue of Whipple [2] vs. speed. More recently Sharp [4] has reviewed the stability and control of the bicycle by applying optimal control schemes to the model. Building on published bicycle research [1–4], a recent investigation into handling qualities of a bicycle [5] has begun by examining rider control during normal bicycling. As [1–4] make clear, all theoretical or computational models of bicycle dynamics depend crucially on a sound and accurate knowledge of the inertial and geometric parameters of the vehicle and rider.

A non-minimum set of 25 physical parameters is needed to compute solutions to the equations of motion. The present paper outlines a method to estimate these from experiment. They are calculated from the geometry, mass, center of mass locations, and moments of inertia of both the bicycle and rider. We use the methods described in [3] for experimentally measuring the properties of the bicycle. By combining that method with one that estimates the rider's physical properties based on representing the rider as a collection of geometrical shapes we can obtain an estimate of the parameters for the combined bicycle and rider. As an example, the methods are used to calculate the necessary inputs to the benchmark model for a Dutch city bicycle and a male rider that were used in the experiments in [5]. The Netherlands boasts one of the highest percentages of bicycle trips of any country and the bicycle we chose is commonly used for travel.

BICYCLE MEASUREMENTS

The geometry, mass, centers of mass, and moments of inertia of a 2008 Batavus Browser city bicycle were measured using the experimental methods described in [3]. Estimates of these properties can be determined with a detailed CAD model but we chose to measure the quantities for accuracy and time considerations. The bicycle was assumed to be made up of four rigid bod-

*Address all correspondence to this author.

ies: the rear frame (Bf), the front wheel (F), the rear wheel (R) and the handlebar/fork assembly (H).

Geometry

Fifteen geometrical measurements (Fig. 1) of the bicycle were taken using a ruler (± 0.002 m) and an angle gage (± 0.5 deg). Only five of the measurements, w , c , λ^1 , r_R and r_F , are required for the benchmark model (Tab. 12). The rest of the measurements are used to estimate the seated position of the rider described in the *HUMAN PARAMETER ESTIMATION* section. We use the same global coordinate system as the benchmark model. The origin is at the rear wheel contact point with the X -axis pointing forward along the ground, the Z -axis downward and the Y -axis to the right (Fig. 1). All of the dimensions were taken as if they were projections into the XZ -plane except for the hub widths². Note that in the model the top tube is assumed to be horizontal and the measurements were taken from the intersections of tube centerlines. The wheel radii were measured by rolling the bicycle forward with the rider seated on the bicycle for nine revolutions of the wheel. The distance traversed along the ground was measured with a ruler, divided by nine and converted to wheel radii using the relationship between radius and circumference, $r = \frac{c}{2\pi}$. The head tube angle λ_{ht} and the seat tube angle λ_{st} were measured using an electronic angle gage while the bicycle was fixed in the upright position. The trail c was measured by aligning a straightedge along the centerline of the steering axis and measuring the distance along the ground between the front wheel contact point and the end of the straight edge. The values from the measurements of the Batavus Browser are shown in Tab. 1.

Mass

The bicycle was then disassembled into four parts representing four rigid bodies (rear wheel, front wheel, rear frame, and the handlebar/fork assembly) to facilitate the measurement of the properties of each individual body. The parts' masses (Tab. 2) were measured using a large tabletop scale with an accuracy of ± 0.02 kg.

Center of Mass Locations

The rear frame and handlebar/fork assembly centers of mass were estimated by hanging the parts from a torsional pendulum at three different orientations through the assumed XZ -plane of symmetry (Fig. 2). They were photographed at each orientation and the photos were then pasted into a drafting software package, scaled and rotated such that the part was in the normal upright orientation. The angles, α_i , from the ground plane (XY -plane) to the pendulum axis were estimated with a ± 1 degree accuracy.

¹ $\lambda = 90^\circ - \lambda_{ht}$

²Not shown in the figure.

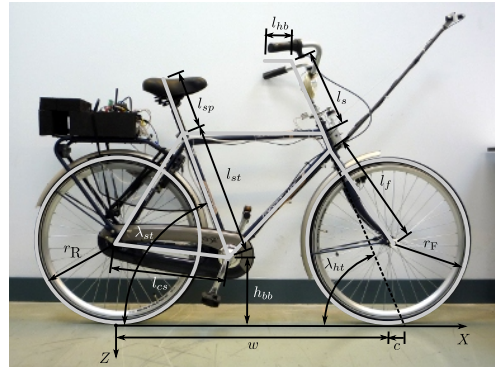


Figure 1. GEOMETRICAL DIMENSIONS OF THE BATAVUS BROWSER BICYCLE SHOWN WITH DATA ACQUISITION EQUIPMENT.

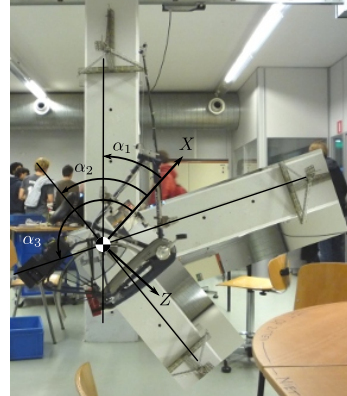


Figure 2. SUPERIMPOSED PHOTOGRAPHS OF THE BICYCLE FRAME HANGING IN THREE ORIENTATIONS FROM THE TORSIONAL PENDULUM SHOWING THE CENTER OF MASS LOCATION AND ORIENTATION ANGLES.

The centers of mass were located where the pendulum axes intersected each other. The location relative to the benchmark coordinate system was recorded with a ± 0.02 m accuracy (Tab. 3). The centers of mass of the wheels were assumed to be at their geometric centers as dictated by the benchmark model.

Table 1. BATAVUS BROWSER BICYCLE DIMENSIONS (ACCURACY OF ± 0.002 M AND ± 0.5 DEG).

Description	Symbol	Value	Units
bottom bracket height	h_{bb}	0.295	m
chain stay length	l_{cs}	0.460	m
fork length	l_f	0.455	m
front hub width	w_{fh}	0.100	m
front wheel radius	r_F	0.342	m
handlebar length	l_{hb}	0.190	m
head tube angle	λ_{ht}	68.5	deg
rear hub width	w_{rh}	0.130	m
rear wheel radius	r_R	0.342	m
seat post length	l_{sp}	0.240	m
seat tube angle	λ_{st}	68.5	deg
seat tube length	l_{st}	0.530	m
stem length	l_s	0.250	m
trail	c	0.055	m
wheel base	w	1.120	m

Table 2. BATAVUS BROWSER BICYCLE MASSES (ACCURACY OF ± 0.02 KG).

Description	Symbol	Value	Units
front wheel mass	m_F	2.02	kg
handlebar/fork mass	m_H	4.35	kg
rear frame mass	m_{Bf}	14.05	kg
rear wheel mass	m_R	3.12	kg

Moments of Inertia

Three measurements were made to estimate the globally referenced moments and products of inertia (I_{xx} , I_{xz} and I_{zz}) of the rear frame and handlebar/fork assembly. The same torsional pendulum used in [3] was used to measure the averaged period \bar{T}_i of oscillation of the rear frame and handlebar/fork assembly at three different orientation angles α_i , where $i = 1, 2, 3$, as shown in Fig. 2. The parts were perturbed lightly, less than 1 degree, and allowed to oscillate about the pendulum axis through at least ten periods. The time of oscillation was recorded via a stop-

Table 3. POSITION OF THE CENTERS OF MASS OF THE REAR FRAME AND HANDLEBAR/FORK ASSEMBLY (ACCURACY OF ± 0.02 M).

Description	Symbol	Value	Units
handlebar/fork	(x_H, z_H)	(0.88, -0.78)	(m, m)
rear frame	(x_{Bf}, z_{Bf})	(0.25, -0.62)	(m, m)

Table 4. REAR FRAME AND HANDLEBAR/FORK MEASURED MOMENTS OF INERTIA.

Rear frame			
i	\bar{T}_i (s)	α_i (deg)	J_i (kg m ²)
1	3.60 ± 0.06	41 ± 1	1.65 ± 0.05
2	3.40 ± 0.06	81 ± 1	1.47 ± 0.05
3	2.50 ± 0.06	150 ± 1	0.79 ± 0.04
Handlebar/fork assembly			
i	\bar{T}_i (s)	α_i (deg)	J_i (kg m ²)
1	1.50 ± 0.06	37 ± 1	0.29 ± 0.02
2	0.70 ± 0.03	105 ± 1	0.06 ± 0.01
3	1.20 ± 0.06	139 ± 1	0.18 ± 0.02

watch (± 1 s). This was done three times for each frame and the recorded times were averaged. The coefficient of elasticity k for the torsional pendulum had previously been measured in [3] and found to be $k = 5.01 \pm 0.01 \frac{\text{Nm}}{\text{rad}}$. Three moments of inertia J_i about the pendulum axes were calculated with

$$J_i = \frac{k\bar{T}_i^2}{4\pi^2} \quad (1)$$

and the numerical values are shown in Tab. 4.

The moments and products of inertia of the rear frame and handlebar/fork assembly with reference to the benchmark coordinate system were calculated by formulating the relationship between inertial frames

$$\mathbf{J}_i = \mathbf{R}_i^T \mathbf{I} \mathbf{R}_i \quad (2)$$

where \mathbf{J}_i is the inertia tensor about the pendulum axes, \mathbf{I} is the inertia tensor in the global reference frame and \mathbf{R} is the rotation

Table 5. REAR FRAME AND HANDLEBAR/FORK INERTIA TENSORS.

Symbol	Value	Units
\mathbf{I}_{Bf}	$\begin{bmatrix} 1.12 & -0.44 \\ -0.44 & 1.34 \end{bmatrix} \pm \begin{bmatrix} 0.06 & 0.04 \\ 0.04 & 0.06 \end{bmatrix}$	kg m^2
\mathbf{I}_H	$\begin{bmatrix} 0.35 & -0.04 \\ -0.04 & 0.06 \end{bmatrix} \pm \begin{bmatrix} 0.03 & 0.02 \\ 0.02 & 0.01 \end{bmatrix}$	kg m^2

matrix relating the two frames. The global inertia tensor is defined as

$$\mathbf{I} = \begin{bmatrix} I_{xx} & -I_{xz} \\ -I_{xz} & I_{zz} \end{bmatrix}. \quad (3)$$

The inertia tensor can be reduced to a 2×2 matrix because the I_{yy} component is not needed in the linear formulation of the benchmark bicycle³ and the bicycle is assumed to be symmetric about the XZ -plane. The simple rotation matrix about the Y -axis can similarly be reduced to a 2×2 matrix where $s_{\alpha i}$ and $c_{\alpha i}$ are defined as $\sin \alpha_i$ and $\cos \alpha_i$, respectively.

$$\mathbf{R} = \begin{bmatrix} c_{\alpha i} & s_{\alpha i} \\ -s_{\alpha i} & c_{\alpha i} \end{bmatrix} \quad (4)$$

The first entry of \mathbf{J}_i in Eq. 2 is the moment of inertia about the pendulum axis and is written explicitly as

$$J_i = c_{\alpha i}^2 I_{xx} + 2s_{\alpha i} c_{\alpha i} I_{xz} + s_{\alpha i}^2 I_{zz}. \quad (5)$$

Calculating all three J_i allows one to form

$$\begin{bmatrix} J_1 \\ J_2 \\ J_3 \end{bmatrix} = \begin{bmatrix} c_{\alpha 1}^2 & 2s_{\alpha 1} c_{\alpha 1} & s_{\alpha 1}^2 \\ c_{\alpha 2}^2 & 2s_{\alpha 2} c_{\alpha 2} & s_{\alpha 2}^2 \\ c_{\alpha 3}^2 & 2s_{\alpha 3} c_{\alpha 3} & s_{\alpha 3}^2 \end{bmatrix} \begin{bmatrix} I_{xx} \\ I_{xz} \\ I_{zz} \end{bmatrix} \quad (6)$$

and the unknown global inertia tensor can be solved for. The numerical results are given in Tab. 5.

Finding the inertia tensors of the wheels is less complex because the wheels are symmetric about three orthogonal planes so there are no products of inertia. The $I_{xx} = I_{zz}$ moments of inertia

³The pitch of the rear frame and handlebar/fork assembly are quadratic functions of the lean and steer [6], so the pitch becomes zero in the linear model.



Figure 3. FRONT BICYCLE WHEEL MOUNTED IN A COMPOUND PENDULUM FROM [3].

Table 6. WHEEL MEASURED INERTIA COMPONENTS.

Front wheel	
$\bar{T}(\text{s})$	$I \text{ (kg m}^2\text{)}$
0.78 ± 0.06	$I_{Fxx} = 0.08 \pm 0.01$
1.37 ± 0.06	$I_{Fyy} = 0.16 \pm 0.03$
Rear wheel	
$\bar{T}(\text{s})$	$I \text{ (kg m}^2\text{)}$
0.79 ± 0.06	$I_{Rxx} = 0.08 \pm 0.01$
1.51 ± 0.06	$I_{Ryy} = 0.16 \pm 0.04$

were calculated by measuring the averaged period of oscillation about an axis in the XZ -plane using the torsional pendulum setup and Eq. 1. The I_{yy} moment of inertia was calculated with a compound pendulum as described in [3] and shown in Fig. 3 using

$$I_{yy} = \left(\frac{\bar{T}}{2\pi} \right)^2 mgl - ml^2 \quad (7)$$

where $l = 0.303 \pm 0.002 \text{ m}$ is the pendulum length, m is the mass of the wheel, \bar{T} is the averaged period and g is the local acceleration due to gravity. Table 6 gives the calculated values.

HUMAN PARAMETER ESTIMATION

The measurement of the physical properties of a human is more difficult than for a bicycle because the human body parts are not as easily described as rigid bodies with defined joints and inflexible geometry. Döhring [7] measured the moments of inertia and centers of mass of a combined rider and motor-scooter with a large measurement table, but this is not always practical. The validity of the present method could be determined if such data existed for a bicycle and rider.

Many methods exist for estimating the geometry, centers of mass and moments of inertia of a human including cadaver measurements [8–10], photogrammetry, ray scanning techniques [11, 12], water displacement [13], and mathematical geometrical estimation of the body segments [14]. We estimated the physical properties of the rider in a seated position using a simple mathematical geometrical estimation similar in idea to [14] in combination with mass data from [8].

Several measurements of the human rider were needed to calculate the physical properties. The mass of the rider was measured along with fourteen anthropomorphic measurements of the body (Tab. 7 and Tab. 8). These measurements in combination with the geometrical bicycle measurements taken in the previous section (Tab. 1) are used to define a model of the rider made up of simple geometrical shapes (Fig. 4). The legs and arms are represented by cylinders, the torso by a cuboid and the head by a sphere. The feet are positioned at the center of the pedaling axis to maintain symmetry about the XZ -plane.

All but one of the anthropomorphic measurements were taken when the rider was standing casually on flat ground. The lower leg length l_{ll} is the distance from the floor to the knee joint. The upper leg length l_{ul} is the distance from the knee joint to the hip joint. The length from hip to hip l_{hh} and shoulder to shoulder l_{ss} are the distances between the two hip joints and two shoulder joints, respectively. The torso length l_{to} is the distance between hip joints and shoulder joints. The upper arm length l_{ua} is the distance between the shoulder and elbow joints. The lower arm length l_{la} is the distance from the elbow joint to the center of the hand when the arm is outstretched. The circumferences are taken at the cross section of maximum circumference (e.g. around the bicep, around the brow, over the nipples for the chest). The forward lean angle λ_{fl} is the approximate angle made between the floor (XY -plane) and the line connecting the center of the rider's head and the top of the seat while the rider is seated normally on the bicycle. This was estimated by taking a side profile photograph of the rider on the bicycle and scribing a line from the head to the top of the seat. The measurements were made as accurately as possible with basic tools but no special attention is given further to the accuracy of the calculations due to the fact that modeling the human as basic geometric shapes already introduces a large error. The values are reported to the same decimal places as the previous section for consistency.

The masses of each segment (Tab. 8) were defined as a pro-

Table 7. RIDER ANTHROPOMORPHIC MEASUREMENTS.

Description	Symbol	Value	Units
chest circumference	c_{ch}	0.94	m
forward lean angle	λ_{fl}	82.9	deg
head circumference	c_h	0.58	m
hip joint to hip joint	l_{hh}	0.26	m
lower arm circumference	c_{la}	0.23	m
lower arm length	l_{la}	0.33	m
lower leg circumference	c_c	0.38	m
lower leg length	l_{ll}	0.46	m
shoulder to shoulder	l_{ss}	0.44	m
torso length	l_{to}	0.48	m
upper arm circumference	c_{ua}	0.30	m
upper arm length	l_{ua}	0.28	m
upper leg circumference	c_{ul}	0.50	m
upper leg length	l_{ul}	0.46	m

Table 8. BODY MASS AND SEGMENT MASSES.

Segment	Symbol	Equation	Value	Unit
mass of rider body	m_{Br}	N/A	72.0	kg
head	m_h	$0.068m_{Br}$	4.90	kg
lower arm	m_{la}	$0.022m_{Br}$	1.58	kg
lower leg	m_{ll}	$0.061m_{Br}$	4.39	kg
torso	m_{to}	$0.510m_{Br}$	36.72	kg
upper arm	m_{ua}	$0.028m_{Br}$	2.02	kg
upper leg	m_{ul}	$0.100m_{Br}$	7.20	kg

portion of the total mass of the rider m_{Br} using data from cadaver studies by [8].

The geometrical and anthropomorphic measurements were converted into a set of 31 grid points in three dimensional space that mapped the skeleton of the rider and bicycle (Fig. 4). The position vectors to these grid points are listed in Tab. 10. Several intermediate variables used in the grid point equations are listed in Tab. 11 where f_o is the fork offset and the rest arise from the multiple solutions to the location of the elbow and knee joints and have to be solved for using numeric methods. The correct

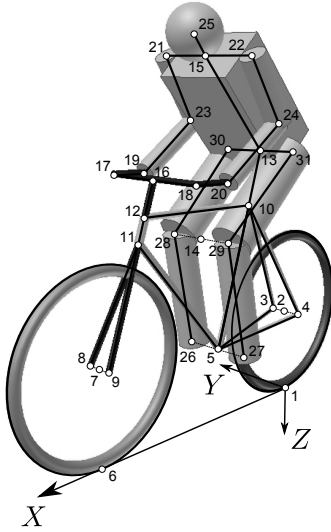


Figure 4. LOCATIONS OF GRID POINTS AND SIMPLE GEOMETRIC SHAPES. SEE ALSO TAB. 10.

solutions are the ones that force the arms and legs to bend in a natural fashion. The grid points mark the center of the sphere and the end points of the cylinders and cuboid. The segments are aligned along lines connecting the appropriate grid points. The segments are assumed to have uniform density so the centers of mass are taken to be at the geometrical centers. The midpoint formula is used to calculate the local centers of mass for each segment in the global reference frame. The total body center of mass can be found from the standard formula

$$\mathbf{r}_{Br} = \frac{\sum m_i \mathbf{r}_i}{m_{Br}} = [0.291 \quad 0 \quad -1.109] \text{ m} \quad (8)$$

where \mathbf{r}_i is the position vector to the centroid of each segment and m_i is the mass of each segment. The local moments of inertia of each segment are determined using the ideal definitions of inertia for each segment type (Tab. 9). The width of the cuboid representing the torso l_y is defined by the shoulder width and upper arm circumference.

$$l_y = l_{ss} - \frac{c_{ua}}{\pi} \quad (9)$$

The cuboid thickness was estimated using the chest circumfer-

Table 9. SEGMENT INTERIA TENSORS. HERE THE x , y AND z AXES ARE LOCAL.

Segment	Moment of Inertia
cuboid	$\frac{1}{12}m \begin{bmatrix} l_y^2 + l_z^2 & 0 & 0 \\ 0 & l_x^2 + l_z^2 & 0 \\ 0 & 0 & l_x^2 + l_y^2 \end{bmatrix}$
cylinder	$I_x, I_y = \frac{1}{12}m \left(\frac{3c^2}{4\pi^2} + l^2 \right), I_z = \frac{mc^2}{8\pi^2}$
sphere	$I_x, I_y, I_z = \frac{mc^2}{10\pi^2}$

ence measurement and assuming that the cross section of the chest is similar to a stadium shape.

$$l_x = \frac{c_{ch} - 2l_y}{\pi - 2} \quad (10)$$

The local $\hat{\mathbf{z}}_i$ unit vector for the segments was defined along the line connecting the associated grid points from the lower numbered grid point to the higher numbered grid point. The local unit vector in the y direction was set equal to the global $\hat{\mathbf{Y}}$ unit vector with the $\hat{\mathbf{x}}_i$ unit vector following from the right hand rule. The rotation matrix needed to rotate each of the moments of inertia to the global reference frame can be calculated by dotting the global unit vectors $\hat{\mathbf{X}}, \hat{\mathbf{Y}}, \hat{\mathbf{Z}}$ with the local unit vectors $\hat{\mathbf{x}}_i, \hat{\mathbf{y}}_i, \hat{\mathbf{z}}_i$ for each segment.

$$\mathbf{R}_i = \begin{bmatrix} \hat{\mathbf{X}} \cdot \hat{\mathbf{x}}_i & \hat{\mathbf{X}} \cdot \hat{\mathbf{y}}_i & \hat{\mathbf{X}} \cdot \hat{\mathbf{z}}_i \\ \hat{\mathbf{Y}} \cdot \hat{\mathbf{x}}_i & \hat{\mathbf{Y}} \cdot \hat{\mathbf{y}}_i & \hat{\mathbf{Y}} \cdot \hat{\mathbf{z}}_i \\ \hat{\mathbf{Z}} \cdot \hat{\mathbf{x}}_i & \hat{\mathbf{Z}} \cdot \hat{\mathbf{y}}_i & \hat{\mathbf{Z}} \cdot \hat{\mathbf{z}}_i \end{bmatrix} \quad (11)$$

The local inertia matrices are then rotated to the global reference frame with

$$\mathbf{I}_i = \mathbf{R}_i \mathbf{J}_i \mathbf{R}_i^T. \quad (12)$$

The local moments of inertia can then be translated to the center of mass of the entire body using the parallel axis theorem

$$\mathbf{I}_i^* = \mathbf{I}_i + m_i \begin{bmatrix} d_y^2 + d_z^2 & -d_x d_y & -d_x d_z \\ -d_x d_y & d_x^2 + d_z^2 & -d_y d_z \\ -d_x d_z & -d_y d_z & d_x^2 + d_y^2 \end{bmatrix} \quad (13)$$

where d_x , d_y and d_z are the distances along the the X , Y and Z axes, respectively, from the local center of mass to the global

center of mass. Finally, the local translated and rotated moments of inertia are summed to give the total moment of inertia of the rider by

$$\mathbf{I}_{Br} = \sum \mathbf{I}_i^* = \begin{bmatrix} 8.00 & 0 & -1.93 \\ 0 & 8.07 & 0 \\ -1.93 & 0 & 2.36 \end{bmatrix} \text{ kg m}^2. \quad (14)$$

COMBINED REAR FRAME AND RIDER

The mass, center of mass and moment of inertia is calculated similarly to what was previously described. The total mass is

$$m_B = m_{Bf} + m_{Br}. \quad (15)$$

The center of mass position is

$$\mathbf{r}_B = \frac{m_{Bf}\mathbf{r}_{Bf} + m_{Br}\mathbf{r}_{Br}}{m_B}. \quad (16)$$

The two moments of inertia are translated to the center of mass location using the parallel axis theorem (Eq. 13) and the components summed to find the final moments of inertia.

RESULTS

The final results are presented in the form used by the benchmark model (Tab. 12). These can be used to populate the canonical form

$$\mathbf{M}\ddot{\mathbf{q}} + \mathbf{v}\mathbf{C}_1\dot{\mathbf{q}} + [\mathbf{g}\mathbf{K}_0 + \mathbf{v}^2\mathbf{K}_2]\mathbf{q} = 0 \quad (17)$$

of the linear benchmark equations of motion presented in [1]. The coefficient matrices for the example rider and bicycle follow in Eqs. 18-21 along with the standard eigenvalue plot for the Whipple model (Fig. 5).

$$\mathbf{M} = \begin{bmatrix} 106.87 & 1.41 \\ 1.41 & 0.22 \end{bmatrix} \quad (18)$$

$$\mathbf{C}_1 = \begin{bmatrix} 0 & 27.06 \\ -0.57 & 0.97 \end{bmatrix} \quad (19)$$

$$\mathbf{K}_0 = \begin{bmatrix} -93.73 & -1.58 \\ -1.58 & -0.58 \end{bmatrix} \quad (20)$$

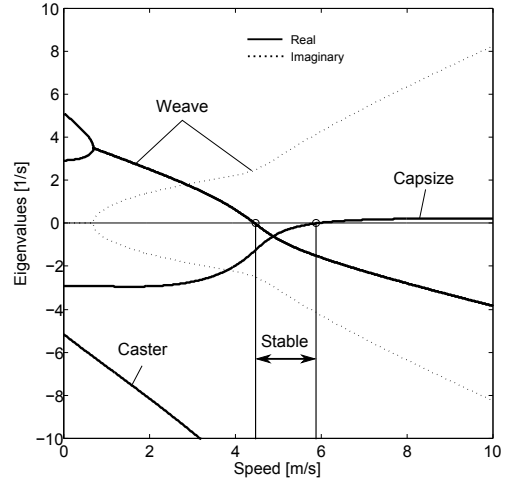


Figure 5. EIGENVALUES OF THE EXAMPLE BICYCLE AND RIDER AS A FUNCTION OF SPEED.

$$\mathbf{K}_2 = \begin{bmatrix} 0 & 78.72 \\ 0 & 1.48 \end{bmatrix} \quad (21)$$

CONCLUSIONS

A simple new and different method of estimating the physical properties of a combined bicycle and rider for use with the linearized benchmark bicycle was presented. The methods described allow one to obtain reasonable estimations of the parameters used to predict the dynamic modes of the benchmark model with minimal experimental equipment and effort. This is unlike the more general methods described in the references because it is specific for a bicycle and rider. The accuracy of the bicycle moment of inertia measurements can be improved by measuring time more accurately with a rate gyro and simple DAQ system and measuring the pendulum angles more accurately with a precision level. The estimations of the human's properties can be improved but not without more time consuming measurement and modeling techniques as described in some of the references.

NOMENCLATURE

α pendulum orientation angle
 λ geometric angle

c circumference except for the definition of trail that matches the benchmark model from [1] and the abbreviation for \cos
 c_α $\cos \alpha$
 d distance
 f_o fork offset
 g local acceleration due to gravity
 h height
 k pendulum torsional stiffness
 l length
 m mass
 r radius
 s, t, u, v intermediate variables, v is also used for forward speed
 s_α $\sin \alpha$
 w width except for the definition of wheelbase that matches the benchmark model
 x center of mass x coordinate for the benchmark bicycle
 z center of mass z coordinate for the benchmark bicycle
 I global inertia component
 J inertia component
 T period
 \mathbf{q} state vector
 \mathbf{r} position vector defined relative to the benchmark reference frame $[r_x \ r_y \ r_z]$ or to a local reference frame $[r_x \ r_y \ r_z]$
 xyz local axes
 \mathbf{R} rotation matrix
 \mathbf{I} globally referenced inertia matrix
 \mathbf{J} inertia matrix
 $\mathbf{M}, \mathbf{C}_1, \mathbf{K}_0, \mathbf{K}_2$ benchmark canonical matrices
 \mathbf{XYZ} global axes

REFERENCES

- [1] Meijaard, J. P., Papadopoulos, J. M., Ruina, A., and Schwab, A. L., 2007. "Linearized dynamics equations for the balance and steer of a bicycle: A benchmark and review". *Royal Society of London Proceedings Series A*, **463**, August, pp. 1955–1982.
- [2] Whipple, F. J. W., 1899. "The stability of the motion of a bicycle". *Quarterly Journal of Pure and Applied Mathematics*, **30**, pp. 312–348.
- [3] Kooijman, J. D. G., 2006. "Experimental validation of a model for the motion of an uncontrolled bicycle". MSc thesis, Delft University of Technology.
- [4] Sharp, R. S., 2008. "On the stability and control of the bicycle". *Applied Mechanics Reviews*, **61**(6), November, p. 24.
- [5] Kooijman, J. D. G., and Schwab, A. L., 2008. "Some observations on human control of a bicycle". In 11th mini Conference on Vehicle System Dynamics, Identification and Anomalies (VSDIA2008), Budapest, Hungary, I. Zobory, ed., Budapest University of Technology and Economics, p. 8.
- [6] Petersen, D. L., and Hubbard, M., 2007. "Analysis of the holonomic constraint in the Whipple bicycle model". In *The Engineering of Sport: 7*, M. Estivalet and P. Brisson, eds., Springer.
- [7] Döhring, E., 1953. "Über die stabilität und die lenkkräfte von einspurfahrzeugen". PhD thesis, Technical University Braunschweig, Germany.
- [8] Dempster, W. T., 1955. Space requirements of the seated operator, geometrical, kinematic and mechanical aspects of the body with special reference to the limbs. Technical Report WADC 55-159, Wright-Patterson AFB, Ohio.
- [9] Clauser, C. E., McConville, J. T., and Young, J. W., 1969. Weight, volume and center of mass of segments of the human body. Tech. Rep. AMRL TR 69-70, Wright-Patterson Air Force Base, Ohio. NTIS No. AD-710 622.
- [10] Chandler, R. F., Clauser, C. E., McConville, J. T., Reynolds, H. M., and Young, J. W., 1975. Investigation of inertial properties of the human body. Tech. Rep. AMRL TR 74-137, Wright-Patterson Air Force Base, Ohio. NTIS No. AD-A016 485.
- [11] Zatsiorsky, V., and Seluyanov, V., 1983. "The mass and inertia characteristics of the main segments of the human body". In *Biomechanics VIII-B*, H. Matsui and K. Kobayashi, eds., Human Kinetic, pp. 1152–1159.
- [12] Zatsiorsky, V., Seluyanov, V., and Chugunova, L., 1990. "In vivo body segment inertial parameters determination using a gamma-scanner method". In *Biomechanics of Human Movement: Applications in Rehabilitation, Sports and Ergonomics*, N. Berme and A. Cappozzo, eds., Bertec, pp. 186–202.
- [13] Park, S. J., Kim, C., and Park, S. C., 1999. "Anthropometric and biomechanical characteristics on body segments of Koreans". *Applied Human Sciences*, **18**(3), May, pp. 91–9.
- [14] Yeadon, M. R., 1990. "The simulation of aerial movement-II. A mathematical inertia model of the human body". *Journal of Biomechanics*, **23**, pp. 67–74.

Table 10. SKELETON GRID POINTS WITH RESPECT TO THE GLOBAL FRAME. SEE FIG. 4

Description	Equation	Value (m)
rear contact point	$\mathbf{r}_1 = [0 \ 0 \ 0]$	[0 0 0]
rear wheel center	$\mathbf{r}_2 = [0 \ 0 \ -r_R]$	[0 0 -0.342]
right rear hub center	$\mathbf{r}_3 = \mathbf{r}_2 + [0 \ \frac{w_{rh}}{2} \ 0]$	[0 0.065 -0.342]
left rear hub center	$\mathbf{r}_4 = \mathbf{r}_2 + [0 \ -\frac{w_{rh}}{2} \ 0]$	[0 -0.065 -0.342]
bottom bracket center	$\mathbf{r}_5 = [\sqrt{l_{cs}^2 - (r_R - h_{bb})^2} \ 0 \ -h_{bb}]$	[0.458 0 -0.295]
front wheel contact point	$\mathbf{r}_6 = [w \ 0 \ 0]$	[1.120 0 0]
front wheel center	$\mathbf{r}_7 = \mathbf{r}_6 + [0 \ 0 \ -r_F]$	[1.120 0 -0.342]
right front hub center	$\mathbf{r}_8 = \mathbf{r}_7 + [0 \ \frac{w_{fh}}{2} \ 0]$	[1.120 0.050 -0.342]
left front hub center	$\mathbf{r}_9 = \mathbf{r}_7 + [0 \ -\frac{w_{fh}}{2} \ 0]$	[1.120 -0.050 -0.342]
left front hub center	$\mathbf{r}_{10} = \mathbf{r}_5 + [-l_{st} \cos \lambda_{st} \ 0 \ -l_{st} \sin \lambda_{st}]$	[0.263 0 -0.788]
top of seat tube	$\mathbf{r}_{11} = \mathbf{r}_7 + [-f_o \sin \lambda_{ht} - \cos \lambda_{ht} \sqrt{l_f^2 - f_o^2} \ 0 \ f_o \cos \lambda_{ht} - \sin \lambda_{ht} \sqrt{l_f^2 - f_o^2}]$	[0.887 0 -0.733]
top of head tube	$\mathbf{r}_{12} = [r_{X11} - \frac{r_{Z11} - r_{Z10}}{\tan \lambda_{ht}} \ 0 \ r_{Z10}]$	[0.865 0 -0.788]
top of seat	$\mathbf{r}_{13} = \mathbf{r}_{10} + [-l_{sp} \cos \lambda_{st} \ 0 \ -l_{sp} \sin \lambda_{st}]$	[0.175 0 -1.011]
center of knees	$\mathbf{r}_{14} = \mathbf{r}_5 + [s \ 0 \ -t]$	[0.551 0 -0.746]
shoulder midpoint	$\mathbf{r}_{15} = \mathbf{r}_{13} + [l_{so} \cos \lambda_{fl} \ 0 \ -l_{so} \sin \lambda_{fl}]$	[0.235 0 -1.488]
top of stem	$\mathbf{r}_{16} = \mathbf{r}_{12} + [-l_s \cos \lambda_{ht} \ 0 \ -l_s \sin \lambda_{ht}]$	[0.773 0 -1.021]
right handlebar	$\mathbf{r}_{17} = \mathbf{r}_{16} + [0 \ \frac{l_h}{2} \ 0]$	[0.773 0.220 -1.021]
left handlebar	$\mathbf{r}_{18} = \mathbf{r}_{16} + [0 \ -\frac{l_h}{2} \ 0]$	[0.773 -0.220 -1.021]
right hand	$\mathbf{r}_{19} = \mathbf{r}_{17} + [-l_{hb} \ 0 \ 0]$	[0.583 0.220 -1.021]
left hand	$\mathbf{r}_{20} = \mathbf{r}_{18} + [-l_{hb} \ 0 \ 0]$	[0.583 -0.220 -1.021]
right shoulder	$\mathbf{r}_{21} = \mathbf{r}_{15} + [0 \ \frac{l_s}{2} \ 0]$	[0.235 0.220 -1.488]
left shoulder	$\mathbf{r}_{22} = \mathbf{r}_{15} + [0 \ -\frac{l_s}{2} \ 0]$	[0.235 -0.220 -1.488]
right elbow	$\mathbf{r}_{23} = \mathbf{r}_{19} + [-u \ \frac{l_{se}}{2} \ -v]$	[0.321 0.220 -1.222]
left elbow	$\mathbf{r}_{24} = \mathbf{r}_{23} + [0 \ -l_{ss} \ 0]$	[0.321 -0.220 -1.222]
center of head	$\mathbf{r}_{25} = \mathbf{r}_{15} + [\frac{c_h}{2\pi} \cos \lambda_{fl} \ 0 \ -\frac{c_h}{2\pi} \sin \lambda_{fl}]$	[0.246 0 -1.579]
right foot	$\mathbf{r}_{26} = \mathbf{r}_5 + [0 \ \frac{l_{fb}}{2} \ 0]$	[0.458 0.130 -0.295]
left foot	$\mathbf{r}_{27} = \mathbf{r}_5 + [0 \ -\frac{l_{fb}}{2} \ 0]$	[0.458 -0.130 -0.295]
right knee	$\mathbf{r}_{28} = \mathbf{r}_{14} + [0 \ \frac{l_{kb}}{2} \ 0]$	[0.551 0.130 -0.746]
left knee	$\mathbf{r}_{29} = \mathbf{r}_{14} + [0 \ -\frac{l_{kb}}{2} \ 0]$	[0.551 -0.130 -0.746]
right hip	$\mathbf{r}_{30} = \mathbf{r}_{13} + [0 \ \frac{l_{hb}}{2} \ 0]$	[0.175 0.130 -1.011]
left hip	$\mathbf{r}_{31} = \mathbf{r}_{13} + [0 \ -\frac{l_{hb}}{2} \ 0]$	[0.175 -0.130 -1.011]

Table 11. GRID POINT INTERMEDIATE VARIABLES.

Symbol	Equation
f_o	$r_F \cos \lambda_{ht} - c \sin \lambda_{ht}$
s	$0 = l_{ul}^2 - l_{ll}^2 - (r_{Z13} - r_{Z5})^2 - (r_{X5} - r_{X13})^2 - 2(r_{Z13} - r_{Z5})\sqrt{(l_{ll}^2 - s^2)} - 2s(r_{X5} - r_{X13})$
t	$\sqrt{l_{ll}^2 - s^2}$
u	$0 = l_{la}^2 - l_{ua}^2 + (r_{Z21} - r_{Z19})^2 + (r_{X19} - r_{X21})^2 + 2(r_{Z21} - r_{Z19})\sqrt{(l_{la}^2 - u^2)} - 2u(r_{X19} - r_{X21})$
v	$\sqrt{l_{la}^2 - u^2}$

Table 12. COMBINED BICYCLE AND RIDER PARAMETER VALUES.

Parameter	Symbol	Value
wheel base	w	1.120 m
trail	c	0.055 m
steer axis tilt ($\pi/2 - \lambda_{ht}$)	λ	0.38 rad
gravity	g	9.81 N kg ⁻¹
forward speed	v	various m s ⁻¹
Rear wheel R		
radius	r_R	0.342 m
mass	m_R	3.12 kg
mass moments of inertia	(I_{Rxx}, I_{Ryy})	(0.08, 0.16) kg m ²
rear Body and frame B		
position center of mass	(x_B, z_B)	(0.28, -1.03) m
mass	m_B	86 kg
mass moments of inertia	$\begin{bmatrix} I_{Bxx} & 0 & I_{Bxz} \\ 0 & I_{Byy} & 0 \\ I_{Bxz} & 0 & I_{Bzz} \end{bmatrix}$	$\begin{bmatrix} 11.89 & 0 & -2.13 \\ 0 & I_{Byy} & 0 \\ -2.13 & 0 & 3.73 \end{bmatrix}$ kg m ²
front Handlebar and fork assembly H		
position center of mass	(x_H, z_H)	(0.88, -0.78) m
mass	m_H	4.35 kg
mass moments of inertia	$\begin{bmatrix} I_{Hxx} & 0 & I_{Hxz} \\ 0 & I_{Hyy} & 0 \\ I_{Hxz} & 0 & I_{Hzz} \end{bmatrix}$	$\begin{bmatrix} 0.35 & 0 & -0.04 \\ 0 & I_{Hyy} & 0 \\ -0.04 & 0 & 0.07 \end{bmatrix}$ kg m ²
Front wheel F		
radius	r_F	0.342 m
mass	m_F	2.02 kg
mass moments of inertia	(I_{Fxx}, I_{Fyy})	(0.08, 0.16) kg m ²

Schwab, A. L., Meijaard, J. P. and Kooijman, J. D. G. (2012). Lateral dynamics of a bicycle with passive rider model: stability and controllability. *Vehicle System Dynamics*, 50 (8) : 1209—1224. Reprinted with kind permission of Taylor & Francis Group.

Lateral dynamics of a bicycle with a passive rider model: stability and controllability

A.L. Schwab^{a*}, J.P. Meijaard^b and J.D.G. Kooijman^a

^a*Laboratory for Engineering Mechanics, Delft University of Technology, Mekelweg 2, NL 2628 CD Delft, The Netherlands;* ^b*Mechanical Automation and Mechatronics, Faculty of Engineering Technology, University of Twente, Enschede, The Netherlands*

(Received 18 May 2011; final version received 23 July 2011)

This paper addresses the influence of a passive rider on the lateral dynamics of a bicycle model and the controllability of the bicycle by steer or upper body sideway lean control. In the uncontrolled model proposed by Whipple in 1899, the rider is assumed to be rigidly connected to the rear frame of the bicycle and there are no hands on the handlebar. Contrarily, in normal bicycling the arms of a rider are connected to the handlebar and both steering and upper body rotations can be used for control. From observations, two distinct rider postures can be identified. In the first posture, the upper body leans forward with the arms stretched to the handlebar and the upper body twists while steering. In the second rider posture, the upper body is upright and stays fixed with respect to the rear frame and the arms, hinged at the shoulders and the elbows, exert the control force on the handlebar. Models can be made where neither posture adds any degrees of freedom to the original bicycle model. For both postures, the open loop, or uncontrolled, dynamics of the bicycle–rider system is investigated and compared with the dynamics of the rigid-rider model by examining the eigenvalues and eigenmotions in the forward speed range 0–10 m/s. The addition of the passive rider can dramatically change the eigenvalues and their structure. The controllability of the bicycles with passive rider models is investigated with either steer torque or upper body lean torque as a control input. Although some forward speeds exist for which the bicycle is uncontrollable, these are either considered stable modes or are at very low speeds. From a practical point of view, the bicycle is fully controllable either by steer torque or by upper body lean, where steer torque control seems much easier than upper body lean.

Keywords: bicycle dynamics; non-holonomic systems; multibody dynamics; human control; modal controllability

1. Introduction

The bicycle is an intriguing machine as it is laterally unstable at low speeds and stable, or easy to stabilise, at high speeds. During the last decade a revival in the research on dynamics and control of bicycles has taken place [1–3]. Most studies use the so-called Whipple model [4] of a bicycle. In this model, a hands-free rigid rider is fixed to the rear frame. However, from experience it is known that some form of control is required to stabilise the bicycle and follow a path. This control is either applied by steering or by performing some set of upper body

*Corresponding author. Email: a.l.schwab@tudelft.nl

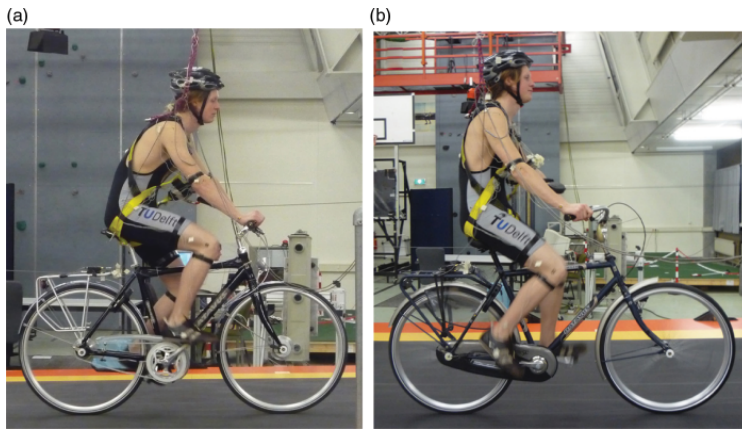


Figure 1. Bicycling on a treadmill, two distinct postures: (a) Rider A on the hybrid bicycle with body leaned forward and stretched arms and (b) Rider A on the city bicycle with an upright body and flexed arms.

motions. The precise control used by the rider is currently under study [5,6]. Here, we focus on two subjects: (i) the contribution of passive body motions to the uncontrolled dynamics of a bicycle, and (ii) the controllability of these extended models with either steering or upper body lean as a control input.

From observations [5,6], two distinct rider postures can be identified. In the first posture, the upper body leans forward with stretched arms on the handlebar, see Figure 1(a). For steering, the upper body needs to twist. In the second rider posture, the upper body stays upright and fixed with respect to the rear frame and the arms, hinging at the shoulders and the elbows, are connected to the handlebar, see Figure 1(b). For both postures, models can be made with the same number of degrees of freedom as the original Whipple bicycle model. In other words, both rider models just add a mechanism to the original system without any additional degrees of freedom. In order to describe the control by applying a lean torque from the lower body to the upper body, both posture models are extended with an extra degree of freedom to describe the upper body lean.

Only a few people have investigated the controllability of a bicycle. Nagai [7] used a simple bicycle model in which only the rear frame and rider have mass, the trail is zero and the steer angle and upper body sideways lean angle are kinematic control inputs. He finds one non-zero forward speed and one condition on the mass distribution which result in uncontrollability for the system. Seffen *et al.* [8] investigate controllability for a bicycle model similar to the model derived by Sharp [9] with steer torque as the control input. They introduce an index, based on [10], which should indicate the difficulty of riding. The index is based on the ratio of the largest and smallest singular values of the controllability matrix. Neither work addresses whether the uncontrollable mode is stable or unstable, although Seffen *et al.* [8] mention stabilisability. It could well be that the uncontrollable or nearly uncontrollable mode is a stable mode of the system that is inessential for the desired output and therefore of no concern to the rider. This paper tries to resolve that problem by determining the forward speed at which the bicycle is uncontrollable and then identifying whether this corresponds to a stable or unstable mode. This approach results in discrete speeds for which the system is uncontrollable. To investigate the controllability by a continuous measure, the concept of modal controllability, as introduced by Hamdan and Nayfeh [11], is applied.

The paper is organised as follows. First the original bicycle model is presented. Next the extension of this model with a twisting upper body or flexed arms is presented and the stability of the lateral motions is compared with that of a rigid rider model in a forward speed range 0–10 m/s. Then the models are extended with a degree of freedom for the upper body sideway lean and the controllability is investigated for the two cases in which either the steer torque or the upper body lean torque is a control input. The paper ends with some conclusions. The appendix summarises the data for the bicycle models.

2. Bicycle model

The basic bicycle model used is the so-called Whipple model [4], which recently has been benchmarked [2]. The model, see Figure 2, consists of four rigid bodies connected by revolute joints. The contact between the knife-edged wheels and the flat level surface is modelled by holonomic constraints in the normal direction, prescribing the wheels to touch the surface, and by non-holonomic constraints in the longitudinal and lateral directions, prescribing zero longitudinal and lateral slips. In this original model, it is assumed that the rider is rigidly attached to the rear frame and has no hands on the handlebar. The resulting non-holonomic mechanical model has three velocity degrees of freedom: forward speed v , lean rate $\dot{\phi}$ and steering rate $\dot{\delta}$.

For the stability analysis of the lateral motions, we consider the linearised equations of motion for small perturbations about the upright steady forward motion. These linearised equations of motion are fully described in [2]. They are expressed in terms of small changes in the lateral degrees of freedom (the rear frame roll angle, ϕ , and the steering angle, δ) from the upright straight-ahead configuration $(\phi, \delta) = (0, 0)$, at a forward speed v , and have the form

$$\mathbf{M}\ddot{\mathbf{q}} + v\mathbf{C}_1\dot{\mathbf{q}} + [g\mathbf{K}_0 + v^2\mathbf{K}_2]\mathbf{q} = \mathbf{f}, \quad (1)$$

where the time-varying variables are $\mathbf{q} = [\phi, \delta]^T$ and the lean and steering torques are $\mathbf{f} = [T_\phi, T_\delta]^T$. The coefficients in this equation are: a constant symmetric mass matrix, \mathbf{M} , a damping-like (there is no real damping) matrix, $v\mathbf{C}_1$, which is linear in the forward speed v , and a stiffness matrix which is the sum of a constant symmetric part, $g\mathbf{K}_0$, and a part, $v^2\mathbf{K}_2$, which is quadratic in the forward speed. The forces on the right-hand side, \mathbf{f} , are the applied forces which are energetically dual to the degrees of freedom \mathbf{q} . In the upright straight-ahead

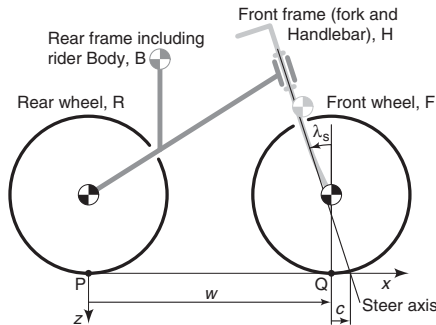


Figure 2. The bicycle model: four rigid bodies (rear wheel R, rear frame B, front handlebar assembly H and front wheel F) connected by three revolute joints (rear hub, steering axis and front hub), together with the coordinate system.

configuration, the linearised equation of motion for the forward motion is decoupled from the linearised equations of motion of the lateral motions and simply reads $\dot{v} = 0$.

Besides the equations of motion, kinematic differential equations for the configuration variables that are not degrees of freedom have to be added to complete the description. For the forward motion, the equations for the rotation angles of the wheels are $\dot{\theta}_R = -v/r_R$, $\dot{\theta}_F = -v/r_F$, where θ_R and θ_F are the rotation angles of the rear and front wheel and r_R and r_F are the corresponding wheel radii. For the lateral motion, the equations for the yaw (heading) angle, ψ , and the lateral displacement of the rear wheel contact point, y_P , are $\dot{\psi} = (v\delta + c\dot{\delta}) \cos \lambda_s/w$ and $\dot{y}_P = v\psi$. For the case of the bicycle, these equations can be considered as a system in series with the system defined by the equations of motion (1) with \mathbf{q} and $\dot{\mathbf{q}}$ as inputs and the configuration variables as outputs. The stability and controllability of the two systems can therefore be studied separately.

The entries in the constant coefficient matrices \mathbf{M} , \mathbf{C}_1 , \mathbf{K}_0 and \mathbf{K}_2 can be calculated from a non-minimal set of 25 bicycle parameters as described in [2]. A procedure for measuring these parameters for a real bicycle is described in [12], whereas measured values for the bicycles used in this study are listed in Table A2 of the appendix. Then, with the coefficient matrices the characteristic equation,

$$\det(\mathbf{M}\lambda^2 + v\mathbf{C}_1\lambda + g\mathbf{K}_0 + v^2\mathbf{K}_2) = 0, \quad (2)$$

can be formed and the eigenvalues, λ , can be calculated. In principle, there are up to four eigenmodes, where oscillatory eigenmodes come in pairs. Two are significant and are traditionally called the *capsize* mode and the *weave* mode, see Figure 3(a). The capsize mode corresponds to a real eigenvalue with an eigenvector dominated by lean: when unstable, the bicycle follows a spiralling path with increasing curvature until it falls. The weave mode is an oscillatory motion in which the bicycle sways about the heading direction. The third remaining eigenmode is the overall stable *castering* mode, like in a trailing caster wheel, which corresponds to a large negative real eigenvalue with an eigenvector dominated by steering. The eigenvalues corresponding to the kinematic differential equations are all zero and correspond to changes in the rotation angles of the wheels, a constant yaw angle and a linearly increasing lateral displacement.

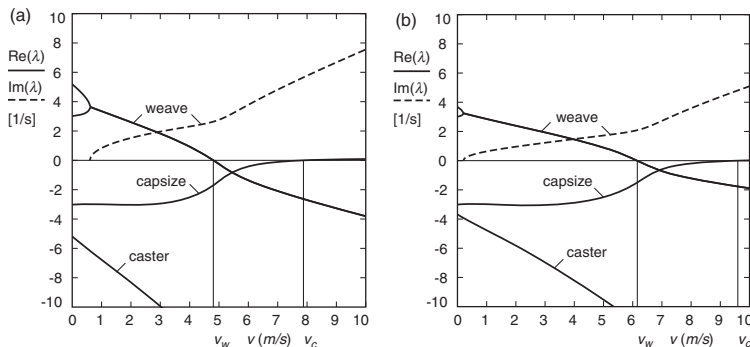


Figure 3. Eigenvalues for the lateral motions of a bicycle-rider combination in a forward speed range of $0 \text{ m/s} < v < 10 \text{ m/s}$, (a) with a completely rigid rider and hands-free and (b) with a rider with stretched arms, hands on the handlebar and a yawing upper body according to the model from Figure 4(a). Note that the bicycle is passively self-stable between the weave speed v_w and the capsize speed v_c .

At near-zero speeds, typically $0 \text{ m/s} < v < 0.5 \text{ m/s}$, there are two pairs of real eigenvalues. Each pair consists of a positive and a negative eigenvalue and corresponds to an inverted-pendulum-like falling of the bicycle. The positive root in each pair corresponds to falling, whereas the negative root corresponds to a righting motion. For $v = 0$, these two are related by a time reversal of the motion. When speed is increased, two real eigenvalues coalesce and then split to form a complex conjugate pair; this is where the oscillatory weave motion emerges. At first, this motion is unstable, but at $v = v_w \approx 4.8 \text{ m/s}$, the weave speed, these eigenvalues cross the imaginary axis at a Hopf bifurcation and this mode becomes stable. At a higher speed, the capsize eigenvalue crosses the origin at a pitchfork bifurcation at $v = v_c \approx 7.9 \text{ m/s}$, the capsize speed, and the bicycle becomes mildly unstable. The speed range for which the uncontrolled bicycle shows asymptotically stable behaviour, with all eigenvalues having negative real parts, is $v_w < v < v_c$.

3. Passive rider models

The original Whipple model is extended with a passive rider without adding any degrees of freedom. From observations of riding on a large treadmill ($3 \times 5 \text{ m}^2$) [5,6], two distinct postures emerged which are both modelled. In the first posture model the upper body is leaned forward and the arms are stretched and connected to the handlebar whereas the upper body is allowed to twist, see Figure 4(a). The second posture model has a rigid upper body connected to the rear frame and hinged arms at the shoulder and elbow connected to the handlebar, see Figure 4(b). Neither model adds any degree of freedom to the original Whipple model. This means that the number and structure of the linearised equations of motion (1) stay the same and only the entries in the matrices change.

For the modelling of the geometry and mass properties of the rider, the method as described by Moore *et al.* [13] is used. Here the human rider is divided into a number of simple geometric objects, namely cylinders, blocks and a sphere of constant density (see Figure A1(a) in the appendix). Then with the proper dimensions and the estimates of the masses of the individual body parts and the necessary skeleton points describing the posture, the mechanical model can be made. For Rider A used in this study, these anthropomorphic data can be found in Table A3 of the appendix, whereas the procedure for calculating the necessary skeleton points is presented in Table A4 of the appendix.

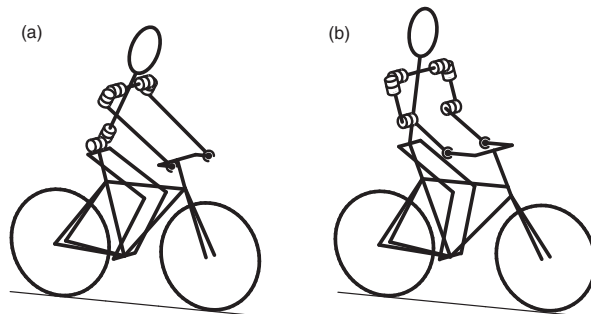


Figure 4. Two distinct bicycle models which include a passive rider: (a) rider with forward leaned body and stretched arms and (b) rider with upright body and flexed arms.

The geometric and mass properties of the two bicycles used in this study were obtained by the procedure described in [12] and the results are presented in Tables A1 and A2 of the appendix.

The complete model of the bicycle with a passive rider was analysed with the multibody dynamics software package SPACAR [14]. This package can handle systems of rigid and flexible bodies connected by various joints in both open and closed kinematic loops, where parts may have rolling contact [15,16]. The package generates numerically, and solves, full non-linear dynamics equations using minimal coordinates (constraints are eliminated). It can also be used to find the numeric coefficients for the linearised equations of motion based on a semi-analytic linearisation of the non-linear equations. This technique has been used here to generate the constant coefficient matrices \mathbf{M} , \mathbf{C}_1 , \mathbf{K}_0 and \mathbf{K}_2 from the linearised equations of motion (1), which serve as a basis for generating the eigenvalues of the lateral motions in the desired forward speed range.

3.1. Forward leaned passive rider

In the model for leaned forward posture, the arms are stretched and the upper and lower arms are modelled as one rigid body each, connected by universal joints to the torso and by ball joints to the handlebar (see Figure 4(a)). The torso is allowed to twist and pitch. Note that in a first-order approximation, the pitching motion is zero, which follows directly from symmetry arguments. The legs are rigidly attached to the rear frame. The linearised equations of motion are derived as described above and the eigenvalues and eigenmotions of the lateral motions are calculated in a forward speed range 0–10 m/s. These eigenvalues are shown in Figure 3(b). For comparison, the eigenvalues of a Whipple-like rigid rider model are shown in Figure 3(a). In the rigid rider model we assume the same forward leaned posture but now with no hands on the handlebar and the complete rider rigidly attached to the rear frame.

Compared with the rigid rider solutions, there are some small changes in the eigenvalues, but the overall structure is the same. Most noticeable are that the stable speed range goes up and that the frequency of the weave motion goes down. These changes can be explained from two major contributing factors. The first is that the attached passive mechanism of arms and twisting upper body adds a mass moment of inertia to the steering assembly. This increases the diagonal mass term $M_{\delta\delta}$ of the mass matrix for the steering degree of freedom from 0.28 to 0.72 kg m². The off-diagonal terms increase slightly (10%). The added mass increases the weave speed and decreases the weave frequencies over the considered speed range. The second factor is the added stiffness to the steering assembly due to the compressive forces exerted by the hands on the handlebar. This affects several entries in the matrices of the linearised equations; the most noticeable are the changes in the symmetric static stiffness matrix $g\mathbf{K}_0$. The diagonal term for the steering stiffness, $gK_{0\delta\delta}$, decreases from -6.9 to -9.7 N m/rad and the off-diagonal terms decrease by 10%. The effects on the eigenvalues are an increased weave and capsize speed and an overall decrease of weave frequencies, whereas the structure of the eigenvalues with respect to the forward speed remains about the same. It should also be noted that the more the direction of the stretched arms is parallel to the steer axis, the less the change in the dynamics compared with the rigid rider model is.

3.2. Upright passive rider

In the upright posture, the torso and the legs are rigidly connected to the rear frame. The upper arms are connected to the torso by universal joints and the lower arms are connected to the upper arms by single hinges at the elbows and by ball joints at the handlebar (see Figure 4(b)).

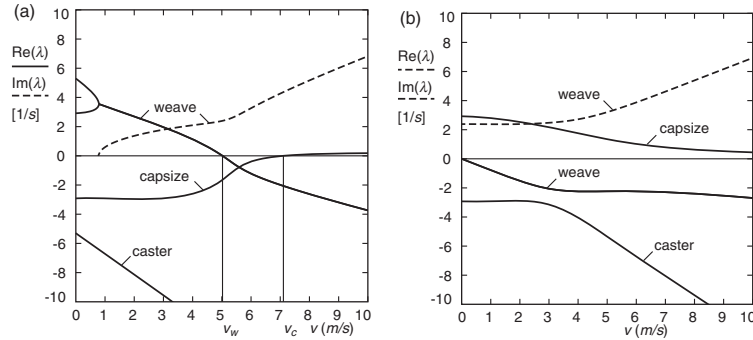


Figure 5. Eigenvalues for the lateral motions of a bicycle–rider combination (a) with a fully rigid rider and hands-free and (b) with a rider with rigid upper body and flexed arms and hands on the handlebar according to the model from Figure 4(b).

The linearised equations of motion are derived as described above and the eigenvalues of the lateral motions are computed. These eigenvalues are shown in Figure 5(b). For comparison, the eigenvalues of a Whipple-like rigid rider model are shown in Figure 5(a). In the rigid rider model, we assume the same upright posture, but now with no hands on the handlebar and the complete rider rigidly attached to the rear frame.

Compared with the rigid rider solutions, there are dramatic changes in the eigenvalues and their structure. The stable forward speed range has disappeared completely, because the weave speed has decreased to zero and the capsize motion is always unstable. Note that the weave motion is now always stable but gets washed out by the unstable capsize. This dramatic change can be explained as follows. By adding the hinged arms to the handlebar, a stable pendulum-type of oscillator has been added to the steer assembly. Although this oscillator stabilises the initially unstable weave motion, it kills the self-stability of the bicycle; the steer-into-the-fall mechanism is made ineffective. The added pendulum mass is most noticeable in the diagonal mass matrix entry related to steering, $M_{\delta\delta}$, which increases from 0.25 to 0.46 kg m². More dramatic is the change in the constant symmetric stiffness matrix $g\mathbf{K}_0$, where the stiffness related to steering, $gK_{0\delta\delta}$, increases from a negative value, -6.6 N m/rad, to a positive value, 2.3 N m/rad, which partly explains the dramatic change in the eigenvalue structure.

4. Controllability

The controllability of the bicycles with passive rider models is investigated where either steer torque or upper body lean torque are considered as a control input. Therefore, both posture models will be extended with an extra degree of freedom to describe the upper body lean. The extended models for both postures are shown in Figure 6. The upper body lean angle θ is made possible by a hinge between the rear frame and the torso located at the saddle, position number 13 in Figure A1(b) of the appendix, with the hinge axis along the lengthwise x -direction.

The structure of the linearised equations of motion remains identical to that of Equation (1), but the number of equations increases from two to three. The three degrees of freedom for the lateral motion are now the rear frame roll angle, ϕ , the steer angle, δ , and the upper body lean angle, θ . The equations are linearised in the upright straight ahead configuration $(\phi, \delta, \theta) = (0, 0, 0)$ at a forward speed v and have the form of Equation (1) where the time-varying variables are now $\mathbf{q} = [\phi, \delta, \theta]^T$ and the lean and steering torques are $\mathbf{f} = [T_\phi, T_\delta, T_\theta]^T$.

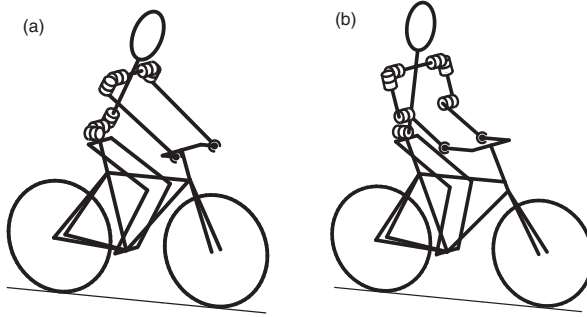


Figure 6. Two distinct bicycle models which include a leaned and steering rider: (a) rider with forward leaned body and stretched arms and (b) rider with upright body and flexed arms.

T_ϕ is an externally applied torque, and T_δ and T_θ are usually provided by a combination of internal torques in one or more of the joints of the arms and between the upper and lower body.

To investigate the controllability of the bicycle–rider system we rewrite these linearised equations of motion into a set of first-order differential equations, the so-called state–space equations, as

$$\dot{\mathbf{x}} = \mathbf{A}\mathbf{x} + \mathbf{B}\mathbf{u}, \quad (3)$$

with the state vector $\mathbf{x} = [\phi, \delta, \theta, \dot{\phi}, \dot{\delta}, \dot{\theta}]^T$ and the control input vector $\mathbf{u} = [T_\delta, T_\theta]^T$. The applied rear frame torque T_ϕ is not considered as a possible control input. Since we wish to address the control inputs separately, we split the input vector \mathbf{u} and the associated matrix \mathbf{B} into, respectively, two scalars and two associate vectors,

$$\dot{\mathbf{x}} = \mathbf{A}\mathbf{x} + \mathbf{b}_\delta T_\delta + \mathbf{b}_\theta T_\theta. \quad (4)$$

For the bicycle–rider system, the coefficient matrix, \mathbf{A} , and the control input vectors, \mathbf{b}_δ and \mathbf{b}_θ , are given by

$$\mathbf{A} = \begin{bmatrix} \mathbf{0} & \mathbf{I} \\ -\mathbf{M}^{-1}(g\mathbf{K}_0 + v^2\mathbf{K}_2) & -\mathbf{M}^{-1}(v\mathbf{C}_1) \end{bmatrix}, \quad (5)$$

$$\mathbf{b}_\delta = \begin{bmatrix} \mathbf{0} \\ \mathbf{M}^{-1} \begin{bmatrix} 0 \\ 1 \\ 0 \end{bmatrix} \end{bmatrix}, \quad \mathbf{b}_\theta = \begin{bmatrix} \mathbf{0} \\ \mathbf{M}^{-1} \begin{bmatrix} 0 \\ 0 \\ 1 \end{bmatrix} \end{bmatrix}. \quad (6)$$

Note that the system of kinematic differential equations is controllable if $v \neq 0$ and $\cos \lambda_s \neq 0$.

4.1. Standard approach

In the standard approach to determine controllability of a linear dynamical system as Equation (4), if the control input is restricted to a single variable, the controllability matrix

$$\mathbf{Q}_j = [\mathbf{b}_j, \mathbf{A}\mathbf{b}_j, \mathbf{A}^2\mathbf{b}_j, \dots, \mathbf{A}^{k-1}\mathbf{b}_j], \quad (7)$$

is formed. If this controllability matrix has a full row rank k , where k is the dimension of the system, which is equal to the number of state variables, then the system is fully controllable by

Table 1. Forward speed v_u at which the hybrid bicycle with the forward leaned rider with stretched arms on the handlebar from Figure 6(a) is uncontrollable by either steer torque control T_δ or upper body lean torque control T_θ together with the corresponding eigenvalue λ_u and right eigenvector coordinates $(\phi, \delta, \theta)_u$, with rear frame lean angle ϕ , steer angle δ and upper body lean angle θ together with the mode description; see also Figure 7 for the eigenvalue plot.

v_u (m/s)	λ_u (rad/s)	$(\phi, \delta, \theta)_u$ (rad)	Mode
Steer torque control, T_δ			
0.0091	-3.0150	(0.14, 0.56, -0.82)	Capsize
1.5482	-3.0150	(0.15, 0.69, -0.71)	Capsize
1.7656	7.8250	(0.15, 0.71, -0.69)	Lean1
4.5588	-7.8250	(0.06, -0.28, 0.96)	Caster
Upper body lean torque control, T_θ			
0.0067	3.0177	(0.14, 0.56, -0.82)	Weave
1.5033	-3.0233	(0.15, 0.69, -0.71)	Capsize

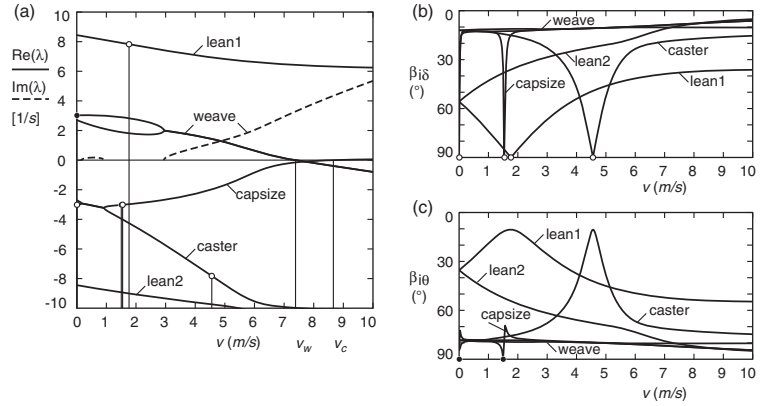


Figure 7. (a) Eigenvalues λ from the linearised stability analysis for the hybrid bicycle with the forward leaned rider with stretched arms on the handlebar from Figure 6(a), where the solid lines correspond to the real part of the eigenvalues and the dashed line corresponds to the imaginary part of the eigenvalues, in the forward speed range of $0 \text{ m/s} < v < 10 \text{ m/s}$, together with forward speeds for which the bicycle is uncontrollable by either steer torque (open circle) or upper body lean torque (black filled circle) alone. (b) Modal controllability β_δ (8) for steer control torque T_δ for this bicycle model. (c) Modal controllability β_θ (8) for an upper body control lean torque T_θ for this bicycle model.

input j , $j = \delta$ or $j = \theta$, alone. Here, we determine the speeds for which rank deficiency occurs by setting the determinant of $\mathbf{Q}_j(v)$ equal to zero and solving the resulting equation in v . The solutions are the forward speeds for which the system is uncontrollable with respect to the considered control input, which we call v_u . The corresponding eigenvector, \mathbf{v}_u^* , spans the null space of the transpose of the corresponding controllability matrix, $\mathbf{v}_u^* \in \text{null}(\mathbf{Q}_j^T(v_u))$. Since this is also an eigenvector of the system matrix $\mathbf{A}^T(v_u)$, the corresponding eigenvalue λ_u can be found from the definition $\mathbf{A}^T \mathbf{v}_u^* = \lambda_u \mathbf{v}_u^*$. The corresponding right eigenvector \mathbf{v}_u satisfies $\mathbf{A} \mathbf{v}_u = \lambda_u \mathbf{v}_u$ and gives the uncontrollable mode of the system. This procedure has been applied to the two bicycle-rider models and the results are presented in Table 1 and Figure 7 and in Table 2 and Figure 8.

For the hybrid bicycle with the forward leaned rider with stretched arms on the handlebar, controlled by steer torque control, we find four uncontrollable forward speeds, see Table 1

Table 2. As Table 1, but now for the city bicycle with an upright rider and flexed arms on the handlebar from Figure 6(b), see also Figure 8 for the eigenvalue plot.

v_u (m/s)	λ_u (rad/s)	$(\phi, \delta, \theta)_u$ (rad)	Mode
Steer torque control, T_δ			
0.0133	-2.8980	(0.16, 0.47, -0.87)	Caster
0.8271	6.5895	(0.14, 0.44, -0.89)	Lean1
1.0177	-2.8980	(0.14, 0.43, -0.89)	Caster
4.1381	-6.5895	(0.01, -0.26, 0.97)	Lean2
Upper body lean torque control, T_θ			
0.2695	2.9017	(0.16, 0.46, -0.87)	Capsize
1.2375	-2.9125	(0.13, 0.42, -0.90)	Caster

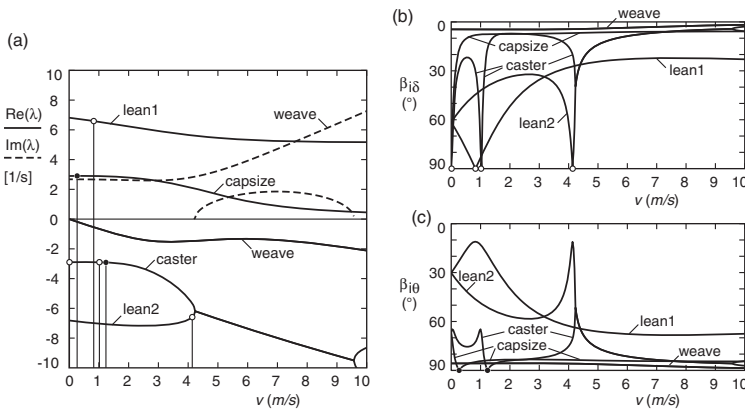


Figure 8. (a) Eigenvalues λ from the linearised stability analysis for the city bicycle with an upright rider and flexed arms on the handlebar from Figure 6(b), where the solid lines correspond to the real parts of the eigenvalues and the dashed line corresponds to the imaginary part of the eigenvalues, in the forward speed range of $0 \text{ m/s} < v < 10 \text{ m/s}$, together with forward speeds for which the bicycle is uncontrollable by either steer torque (open circle) or upper body lean torque (black filled circle) alone. (b) Modal controllability $\beta_{i\delta}$ (8) for steer control torque T_δ for this bicycle model. (c) Modal controllability $\beta_{i\theta}$ (8) for an upper body control lean torque T_θ for this bicycle model.

and Figure 7(a). However, only the one at 1.7656 m/s concerns an unstable mode, an upper body lean mode. This mode can be stabilised by placing a spring and a damper in parallel between the lower and upper body. For a spring stiffness of 100 N m/rad and a damping coefficient of 10 N m s/rad, the lean modes become stable and oscillatory, whereas the other modes change. The uncontrollability shifts to a much lower speed and corresponds to a weaver mode. If we consider only upper body lean torque control, then there are two uncontrollable forward speeds, but again only one, now at 0.0067 m/s, concerns an unstable mode. This mode is the forerunner to the oscillatory weaver mode, but since the speed is almost zero, this is again of no concern to the practical control of the bicycle. Adding a spring and damper acting in parallel with the control torque has no influence on the controllability. We conclude that this bicycle-rider configuration is fully controllable by either steer torque control or upper body lean torque control.

For the city bicycle with an upright rider and flexed arms on the handlebar we first find that the eigenvalue structure differs considerably from that of the hybrid bicycle with rider configuration. Whereas the hybrid bicycle had a stable forward speed range, between 7.4 and 8.7 m/s, the city bicycle configuration is always unstable. Although the weaver mode is now

always stable, there is a capsized mode which is always unstable. For steer torque control on the city bicycle configuration (see Table 2 and Figure 8(a)), we find again four forward speeds for which the bicycle is uncontrollable, where only the one at 0.8271 m/s concerns an unstable mode. As with the hybrid bicycle, this is again an upper body lean mode that can be stabilised by adding a spring and a damper between the lower and the upper body; again, this shifts the uncontrollability to a much lower speed for the weave mode. For upper body lean control we have two uncontrollable speeds, where only the one at 0.2695 m/s concerns an unstable capsized mode. But since this is at a very low speed, one can say that, from a practical point of view, this configuration is also fully controllable by either steer torque control or upper body lean torque.

4.2. Modal controllability

The standard approach as described above results in a discrete set of velocities for which the bicycle is uncontrollable. It does not tell us anything about the ease or difficulty with which the bicycle is controlled in the neighbourhood of these speeds at which controllability is lost. To investigate that, we will follow a somewhat different approach and look at the modal controllability.

A measure for modal controllability has been proposed by Hamdan and Nayfeh [11]. They measure modal controllability by the angle β_{ij} between the left eigenvector \mathbf{v}_i^* from $\mathbf{A}^T \mathbf{v}_i^* = \lambda_i \mathbf{v}_i^*$, and the control input vector \mathbf{b}_j , as in

$$\cos \beta_{ij} = \frac{\mathbf{v}_i^{*T} \mathbf{b}_j}{\|\mathbf{v}_i^*\| \|\mathbf{b}_j\|}. \quad (8)$$

They argue that, if the two vectors are orthogonal, then \mathbf{v}_i^* is in the left null-space of \mathbf{b}_j and the i th eigenmode is uncontrollable from the j th input. If the angle is not a right angle but nearly so, then again this indicates that the i th eigenmode is not easily controlled from the j th input. This modal controllability is applied to the two bicycle–rider models from Figure 6.

For steer torque control on the hybrid bicycle with the forward leaned rider with stretched arms on the handlebar, the modal controllability $\beta_{i\delta}$ is shown in Figure 7(b). Note that the vertical scale for the modal controllability angle β_{ij} runs from down 90° (uncontrollable) to up 0° (well controllable). Clearly, the unstable weave mode is well controllable. We also see two sharp dips in the capsized mode controllability near the uncontrollable speeds. It is interesting to see that the uncontrollability is so local, but since this capsized mode is still a stable mode, it is of no practical concern. What we call the caster mode shows a broad dip around the uncontrollable forward speed of 4.6 m/s, which seems paradoxical, because we use steer torque control, but note that there is still some steer amplitude in the corresponding eigenvector $(\phi, \delta, \theta)_u = (0.06, -0.28, 0.96)$ (Table 1). As expected, the unstable upper body lean mode (lean1) is marginally controllable by steer torque control and shows a wide dip around the uncontrollable speed of 1.8 m/s. The modal controllability for upper body lean torque control on this bicycle–rider model is shown in Figure 7(c). Here, we see that the modal controllability of the unstable weave mode is close to 90° and therefore hard to control by lateral upper body motions. The same holds for the capsized mode, with a notable small rise of the modal controllability just above the speed for which the mode is uncontrollable. The caster mode also shows marginal controllability. The unstable upper body lean mode (lean1) is well controllable, which we would expect, but its modal controllability levels off at higher speeds. Note that the modal controllability for the lean torque input is almost the complement of the one for the steer torque input, meaning that the two inputs taken together make the system well controllable.

The modal controllability of the city bicycle with the upright rider and flexed arms on the handlebar for steer torque control is shown in Figure 8(b). The unstable capsize mode and the stable weave mode are well controllable. In the stable caster and lean2 modes, we see sharp dips around the uncontrollable speeds and here again the unstable upper body lean is marginally controllable by this steer torque control. The modal controllability for upper body lean torque control on this bicycle–rider model is shown in Figure 8(c). The same trends as in the hybrid bicycle are present, meaning that the unstable mode, here the capsize mode, is hard to control by upper body lean motions. It is interesting to see that the overall structure of the modal controllability is about the same as in the hybrid bicycle, although the structure of the eigenvalues with respect to forward speed is completely different.

We conclude that for both bicycle–rider combinations the controllability of the unstable modes is very good for steer torque control and marginal for upper body lean motions. The uncontrollable speeds, which are present, are of no real concern since they are either at stable modes which are not practically important for the overall desired motion or at very low forward speeds for which human control is difficult because of the relatively large positive real parts of the unstable eigenvalues.

5. Conclusions

Adding a passive upper body to the three degrees of freedom Whipple model of an uncontrolled bicycle, without adding any extra degrees of freedom, can change the open-loop dynamics of the system. In the case of a forward leaned rider with stretched arms and hands on the handlebar, there is little change. However, an upright rider position with flexed arms and hands on the handlebar changes the open-loop dynamics drastically and ruins the self-stability of the system.

The unstable modes of both bicycle–rider combinations have very good modal controllability for steer torque control but are marginally controllable by lateral upper body motions. This indicates that most control actions for lateral balance on a bicycle are performed by steer control only and not by lateral upper body motions.

Future work is directed towards the comparison of the control effort of the human rider in both postures.

Acknowledgement

Thanks to Jason Moore for measuring the bicycles and riders during his Fulbright granted year (2008/2009) at TU Delft and thanks to Batavus (Accell Group) for supplying the bicycles.

References

- [1] K.J. Åström, R.E. Klein, and A. Lennartsson, *Bicycle dynamics and control*, IEEE Control Syst. Mag. 25(4) (2005), pp. 26–47.
- [2] J.P. Meijaard, J.M. Papadopoulos, A. Ruina, and A.L. Schwab, *Linearized dynamics equations for the balance and steer of a bicycle: a benchmark and review*, Proc. Roy. Soc. A 463 (2007), pp. 1955–1982.
- [3] R.S. Sharp, *On the stability and control of the bicycle*, Appl. Mech. Rev. 61 (2008), pp. 060803-1–24.
- [4] F.J.W. Whipple, *The stability of the motion of a bicycle*, Quart. J. Pure Appl. Math. 30 (1899), pp. 312–348.
- [5] J.D.G. Kooijman, J. Moore, and A.L. Schwab, *Some observations on human control of a bicycle*, in *11th mini Conference on Vehicle System Dynamics, Identification and Anomalies (VSDIA2008)*, Budapest, Hungary, I. Zobory, ed., Budapest University of Technology and Economics, 2008, pp. 65–72.
- [6] J.K. Moore, J.D.G. Kooijman, and A.L. Schwab, *Rider motion identification during normal bicycling by means of principal component analysis*, in *MULTIBODY DYNAMICS 2009, ECCOMAS Thematic Conference, 29 June–2 July 2009*, K. Arczewski, J. Frączek and M. Wojtyra, eds., Warsaw, Poland, 2009.

- [7] M. Nagai, *Analysis of rider and single-track-vehicle system; its application to computer-controlled bicycles*, Automatica 19(6) (1983), pp. 737–740.
- [8] K.A. Seffen, G.T. Parks, and P.J. Clarkson, *Observations on the controllability of motion of two-wheelers*, Proc. Inst. Mech. Eng. 1 J. Syst. Control Eng. 215(2) (2001) pp. 143–156.
- [9] R.S. Sharp, *The stability and control of motorcycles*, J. Mech. Eng. Sci. 13(5) (1971), pp. 316–329.
- [10] B. Friedland, *Controllability index based on conditioning number*, J. Dyn. Syst. Meas. Control 97(4) (1975), pp. 444–445.
- [11] A.M.A. Hamdan and A.H. Nayfeh, *Measures of modal controllability and observability for first- and second-order linear systems*, J. Guidance Control Dyn. 12(3) (1989), pp. 421–428.
- [12] J.D.G. Kooijman, A.L. Schwab, and J.P. Meijaard, *Experimental validation of a model of an uncontrolled bicycle*, Multibody Syst. Dyn. 19 (2008), pp. 115–132.
- [13] J.K. Moore, M. Hubbard, J.D.G. Kooijman, and A.L. Schwab, *A method for estimating physical properties of a combined bicycle and rider*, Proceedings of the ASME 2009 International Design Engineering Technical Conferences & Computers and Information in Engineering Conference, DETC2009, 30 August–2 September, San Diego, CA, 2009.
- [14] J.B. Jonker and J.P. Meijaard, *SPACAR - Computer program for dynamic analysis of flexible spatial mechanisms and manipulators*, in *Multibody Systems Handbook*, W. Schiehlen, ed., Springer, Berlin, Germany, 1990, pp. 123–143.
- [15] A.L. Schwab and J.P. Meijaard, *Dynamics of flexible multibody systems having rolling contact: Application of the wheel element to the dynamics of road vehicles*, Veh. Syst. Dyn. (Suppl.) 33 (2000), pp. 338–349.
- [16] A.L. Schwab and J.P. Meijaard, *Dynamics of flexible multibody systems with non-holonomic constraints: A finite element approach*, Multibody Syst. Dyn. 10(1) (2003), pp. 107–123.

Appendix 1. Measured bicycle and rider data

This appendix summarises the measured geometric and mass data of the bicycles and rider used, measured according to [13]. The first bicycle, Figure 1(a), can be characterised as a hybrid bicycle. The second bicycle, Figure 1(b), is a standard Dutch city bicycle (see Figure A1).

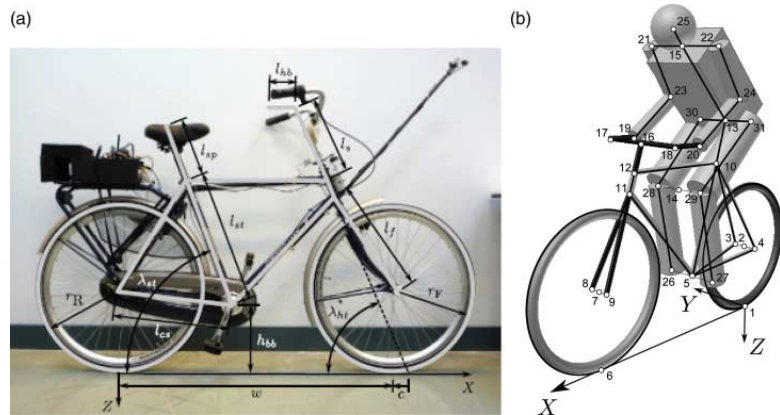


Figure A1. (a) Definition of the geometric parameters of the bicycle and (b) rider model with skeleton points, from [13].

Table A1. Bicycle geometric dimensions for the hybrid bicycle and the city bicycle according to Figure A1(a).

Parameter	Symbol	Value for hybrid bicycle	Value for city bicycle
Bottom bracket height	h_{bb}	0.290 m	0.295 m
Chain stay length	l_{cs}	0.445 m	0.460 m
Fork length	l_f	0.455 m	0.455 m
Front hub width	w_{fh}	0.100 m	0.100 m
Handlebar length	l_{hb}	−0.090 m	0.190 m
Rear hub width	w_{rh}	0.130 m	0.130 m
Seat post length	l_{sp}	0.195 m	0.240 m
Seat tube angle	λ_{st}	75.0°	68.5°
Seat tube length	l_{st}	0.480 m	0.530 m
Stem length	l_s	0.190 m	0.250 m
Wheel base	w	See Table A2	
Trail	c	See Table A2	
Head tube angle	$\lambda_{ht} = 90^\circ - \lambda_s$	See Table A2	
Rear wheel radius	r_R	See Table A2	
Front wheel radius	r_F	See Table A2	

Table A2. Parameters for the hybrid bicycle and the city bicycle for the bicycle model from Figure 2.

Parameter	Symbol	Value for Hybrid Bicycle	Value for City Bicycle
Wheel base	w	1.037 m	1.121 m
Trail	c	0.0563 m	0.0686 m
Steer axis tilt	λ_s	16.9°	22.9°
Gravity	g	9.81 N/kg	9.81 N/kg
Forward speed	v	various m/s	various m/s
Rear wheel R			
Radius	r_R	0.338 m	0.341 m
Mass	m_R	3.96 kg	3.11 kg
Inertia	(I_{Rxx}, I_{Ryy})	(0.0916, 0.1545) kg m ²	(0.0884, 0.1525) kg m ²
Rear Body and frame assembly B			
Centre of mass	(x_B, z_B)	(0.3263, −0.4826) m	(0.2760, −0.5378) m
Mass	m_B	7.22 kg	9.86 kg
Inertia	$\begin{bmatrix} I_{Bxx} & 0 & I_{Bxz} \\ 0 & I_{Byy} & 0 \\ I_{Bxz} & 0 & I_{Bzz} \end{bmatrix}$	$\begin{bmatrix} 0.37287 & 0 & 0.03835 \\ 0 & 0.71704 & 0 \\ 0.03835 & 0 & 0.45473 \end{bmatrix}$ kg m ²	$\begin{bmatrix} 0.52714 & 0 & 0.11442 \\ 0 & 1.31682 & 0 \\ 0.11442 & 0 & 0.75920 \end{bmatrix}$ kg m ²
Front Handlebar and fork assembly H			
Centre of mass	(x_H, z_H)	(0.9107, −0.7303) m	(0.8669, −0.7482) m
Mass	m_H	3.04 kg	3.22 kg
Inertia	$\begin{bmatrix} I_{Hxx} & 0 & I_{Hxz} \\ 0 & I_{Hyy} & 0 \\ I_{Hxz} & 0 & I_{Hzz} \end{bmatrix}$	$\begin{bmatrix} 0.17684 & 0 & 0.02734 \\ 0 & 0.14437 & 0 \\ 0.02734 & 0 & 0.04464 \end{bmatrix}$ kg m ²	$\begin{bmatrix} 0.25338 & 0 & -0.07205 \\ 0 & 0.24610 & 0 \\ -0.07205 & 0 & 0.09558 \end{bmatrix}$ kg m ²
Front wheel F			
Radius	r_F	0.340 m	0.344 m
Mass	m_F	3.334 kg	2.02 kg
Inertia	(I_{Fxx}, I_{Fyy})	(0.09387, 0.15686) kg m ²	(0.09041, 0.14939) kg m ²

Table A3. Anthropomorphic data for Rider A according to Figure A1(b).

Parameter	Symbol	Rider A
Chest circumference	c_{ch}	0.94 m
Forward lean angle	λ_{fl}	63.9° (on hybrid bicycle) 82.9° (on city bicycle)
Head circumference	c_h	0.58 m
Hip joint to hip joint	l_{hh}	0.26 m
Lower arm circumference	c_{la}	0.23 m
Lower arm length	l_{la}	0.33 m
Lower leg circumference	c_{ll}	0.38 m
Lower leg length	l_{ll}	0.46 m
Shoulder to shoulder	l_{ss}	0.44 m
Torso length	l_{to}	0.48 m
Upper arm circumference	c_{ua}	0.30 m
Upper arm length	l_{ua}	0.28 m
Upper leg circumference	c_{ul}	0.50 m
Upper leg length	l_{ul}	0.46 m
Rider mass	m_{Br}	72.0 kg
Head mass	m_h	0.068 m_{Br}
Lower arm mass	m_{la}	0.022 m_{Br}
Lower leg mass	m_{ll}	0.061 m_{Br}
Torso mass	m_{to}	0.510 m_{Br}
Upper arm mass	m_{ua}	0.028 m_{Br}
Upper leg mass	m_{ul}	0.100 m_{Br}

Table A4. Skeleton points code according to Figure A1.

```

%% Matlab code for Skeleton Grid Points see Figure A1a
%% Adapted Table 10 from MooreHubbardKooijmanSchwab2009
r1 = [0 0 0];
r2 = [0 0 -rR];
r3 = r2 + [0 wrh/2 0];
r4 = r2 + [0 -wrh/2 0];
r5 = [sqrt(lcs^2-(rR-hbb)^2) 0 -hbb];
r6 = [w 0 0];
r7 = r6 + [0 0 -rF];
r8 = r7 + [0 wfh/2 0];
r9 = r7 + [0 -wfh/2 0];
r10 = r5 + [-lst*cos(last) 0 -lst*sin(last)];
% calculate f0
f0 = rF*cos(laht)-c*sin(laht);
r11 = r7 + [-f0*sin(laht)-sqrt(lf^2-f0^2)*cos(laht)...
    f0*cos(laht)-sqrt(lf^2-f0^2)*sin(laht)];
r12 = [r11(1)-(r11(3)-r10(3))/tan(laht) 0 r10(3)];
r13 = r10 + [-lsp*cos(last) 0 -lsp*sin(last)];
% determine mid knee angle and mid knee position
a1 = atan2((r5(1)-r13(1)), (r5(3)-r13(3)));
l1 = sqrt((r5(1)-r13(1))^2+(r5(3)-r13(3))^2);
a2 = acos((l1^2+lul^2-l1l^2)/(2*l1*lul));
%
r14 = r13 + [lul*sin(a1+a2) 0 lul*cos(a1+a2)];
r15 = r13 + [lto*cos(lafl) 0 -lto*sin(lafl)];
r16 = r12 + [-ls*cos(laht) 0 -ls*sin(laht)];
r17 = r16 + [0 lss/2 0];
r18 = r16 + [0 -lss/2 0];
r19 = r17 + [-lhb 0 0];
r20 = r18 + [-lhb 0 0];
r21 = r15 + [0 lss/2 0];
r22 = r15 + [0 -lss/2 0];
% determine left elbow position
a1 = atan2((r19(1)-r21(1)), (r19(3)-r21(3)));

```

Table A4. Continued

```
l1 = sqrt((r19(1)-r21(1))^2+(r19(3)-r21(3))^2);
a2 = acos((l1^2+lua^2-lla^2)/(2*l1*lua));
%
r23 = r21 + [lua*sin(a1-a2) 0 lua*cos(a1-a2)];
r24 = r23 + [0 -lss 0];
r25 = r15 + [ch/(2*pi)*cos(laf1) 0 -ch/(2*pi)*sin(laf1)];
r26 = r5 + [0 lhh/2 0];
r27 = r5 + [0 -lhh/2 0];
r28 = r14 + [0 lhh/2 0];
r29 = r14 + [0 -lhh/2 0];
r30 = r13 + [0 lhh/2 0];
r31 = r13 + [0 -lhh/2 0];
```

Kooijman, J. D. G. and Schwab A. L. (2009). Experimental validation of the lateral dynamics of a bicycle on a treadmill. In *Proceedings of the ASME 2009 International Design Engineering Technical Conferences & Computers and Information in Engineering Conference*, DETC2009-86965, DETC2009, Aug 30 – Sep 2, 2009, San Diego, CA.

DETC2009-86965

EXPERIMENTAL VALIDATION OF THE LATERAL DYNAMICS OF A BICYCLE ON A TREADMILL

J. D. G. Kooijman & A. L. Schwab

Laboratory for Engineering Mechanics
Delft University of Technology
Mekelweg 2, NL 2628 CD Delft, The Netherlands
Phone: +31-15-2782701, Fax: +31-15-2782150
email: jodikooijman@gmail.com
email: a.l.schwab@tudelft.nl

ABSTRACT

In this paper, an experimental validation of the lateral dynamics of a bicycle running on a treadmill is presented. From a theoretical point of view, bicycling straight ahead on a treadmill with constant belt velocity should be identical to bicycling on flat level ground with constant forward speed. However, two major differences remain: first, stiffnesses of the contact of the tire with the belt compared to the contact on flat level ground; second, the belt velocity is fixed with respect to the world, irrespective of the change in heading of the bicycle on the treadmill. The admissibility of these two differences is checked by comparing experimental results with numerical simulation results.

The numerical simulations are performed on a three-degree-of-freedom benchmarked bicycle model [1]. For the validation we consider the linearized equations of motion for small perturbations of the upright steady forward motion. This model has been validated experimentally in a previous work [2].

The experimental system consists of an instrumented bicycle without a rider on a large treadmill. Sensors are present for measuring the roll rate, yaw rate, steering angle, and rear wheel rotation. Measurements are recorded for the case in which the laterally perturbed bicycle coasts freely on the treadmill. From these measured data, eigenvalues are extracted by means of curve fitting. These eigenvalues are then compared with the results from the linearized equations of motion of the model. As a result,

the model appeared to be accurate within the normal bicycling speed range, and in particular the transition from stable to unstable weave motion was very well predicted.

Keywords: Bicycle dynamics, experiments, instrumentation, treadmill, multibody dynamics, non-holonomic constraints.

1 Introduction

One of the characteristics of a bicycle is that it is highly unstable at low speed but easy to stabilize at moderate to high speed. Some bicycles can even show self-stability in the normal bicycling speed range. After the invention of the bicycle, more than 100 years ago [3], there has been a sudden revival in the research on the dynamics and control of a bicycle [1,4,5]. Results on the open loop stability are well established now [1], but little is known on how the rider controls the mostly unstable bicycle and what handling qualities are.

Recently a research program has been started at Delft University of Technology to investigate experimentally rider control during normal bicycling, model this behaviour and try to define the concept of handling qualities for bicycles. Instead of doing the experiments on the open road, there is the wish to execute the experiments in a more controlled environment. A large treadmill is such a controlled environment where one can look at rider control during normal straight-ahead bicycling or for small lat-



Figure 1. Large treadmill, courtesy of the faculty of Human Movement Sciences, Free University of Amsterdam, together with TUDelft instrumented bicycle.

eral motions like lane change manoeuvres. But how close is this to bicycling on the open road?

One of the big problems with bicycling on a treadmill is the conflicting information which the rider gets. Although he is bicycling with respect to the moving belt he remains stationary with respect to the surrounding world. This is very confusing in the beginning. However, we now know from experience that after some time, riders can easily adapt to this awkward situation.

There remains the question of how good the treadmill mimics bicycling on flat level ground from a purely mechanical point of view. From a theoretical point of view, bicycling straight ahead on a treadmill with constant velocity should be identical to bicycling straight ahead with constant forward speed on flat level ground. However, there remain two problems. First, the different stiffness of the contact of the tire with the belt, and second, that the direction of the forward velocity is fixed with respect to the world irrespective of the change in heading of the bicycle.

This paper investigates the validity of bicycling on a treadmill by comparing the lateral motions of an instrumented riderless bicycle [2] with results from a three-degree-of-freedom benchmarked bicycle model [1], which has been experimentally validated in [2]. The experimental system consists of an instrumented bicycle without rider on a large treadmill, see Figure 1. On the bicycle, sensors are present for measuring the roll rate, yaw rate, steering angle, and rear wheel rotation, see Figure 2. Trainer wheels prevent the complete fall of the bicycle for unstable conditions. Measurements are recorded for the case in which the bicycle coasts freely on the treadmill surface after some small lateral perturbation which initiates the lateral motion. From these measured data, eigenvalues are extracted by means of curve fit-

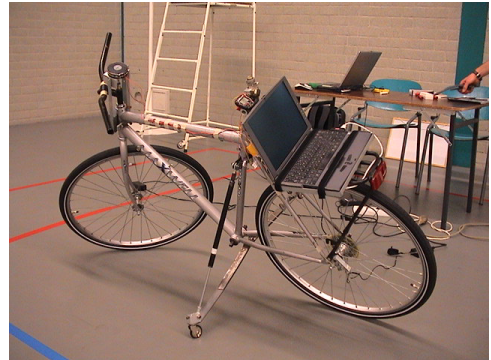


Figure 2. Instrumented bicycle from [2], with all the measurement equipment installed. Sensors are present for measuring the roll rate, yaw rate, steering angle, and rear wheel rotation. Data are collected via a USB-connected data acquisition unit on the laptop computer, mounted on the rear rack.

ting. These eigenvalues are then compared with the results from the linearized equations of motion of the model.

The organization of the paper is as follows. After this introduction, the treadmill, instrumented bicycle, and linearized equations of motion are described. Then the test procedure and a comparison of the experimental and numerical results are presented and discussed. The paper ends with some conclusions.

2 Treadmill and Instrumented Bicycle

The treadmill, see Figure 1, has a usable belt surface of 3×5 m which can be inclined from -5 to 15 deg, and a regulated maximum speed of 35 km/h. An emergency stop can stop the belt within 1 sec. The surface of the treadmill belt is of the ordinary rubber-like structure with moderate roughness. The treadmill is manufactured by Forcelink B.V., The Netherlands, and stationed at the faculty of Human Movement Sciences, Free University of Amsterdam.

The instrumented bicycle, see Figure 2, used in the test is fully described in [2]. It is a standard city-bicycle where all the superfluous parts of the bicycle are removed. Sensors are present for measuring the roll rate, yaw rate, steering angle and rear wheel rotation. The data are collected on a laptop computer mounted on the rear rack. Trainer wheels prevent the complete fall of the bicycle for unstable conditions.

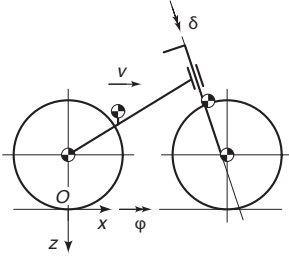


Figure 3. The bicycle model: four rigid bodies (rear wheel, rear frame, front handlebar assembly, front wheel) connected by three revolute joints (rear hub, steering axis, front hub), together with the coordinate system, and the degrees of freedom.

3 Linearized equations of motion for the bicycle model

The bicycle model used is the so-called Whipple [6] model which recently has been benchmarked [1]. The model, see Figure 3, consists of four rigid bodies connected by revolute joints. The contact between the knife-edge wheels and the flat level surface is modelled by holonomic constraints in the normal direction and by non-holonomic constraints in the longitudinal and lateral direction. In the absence of a rider (or with a rider rigidly attached to the rear frame) we assume no-hands operation. The resulting non-holonomic mechanical model has three velocity degrees of freedom: forward speed v , lean rate $\dot{\phi}$ and steering rate $\dot{\delta}$.

For the comparison we consider the linearized equations of motion for small perturbations of the upright steady forward motion, which are fully described in [1]. They are expressed in terms of small changes in the lateral degrees of freedom (the rear frame roll angle, ϕ , and the steering angle, δ) from the upright straight ahead configuration $(\phi, \delta) = (0, 0)$, at a forward speed v , and have the form

$$\mathbf{M}\ddot{\mathbf{q}} + v\mathbf{C}_1\dot{\mathbf{q}} + [\mathbf{K}_0 + v^2\mathbf{K}_2]\mathbf{q} = \mathbf{f}, \quad (1)$$

where the time-varying variables are $\mathbf{q} = [\phi, \delta]^T$ and the lean and steering torques $\mathbf{f} = [T_\phi, T_\delta]^T$. The coefficients in this equation are: a constant symmetric mass matrix, \mathbf{M} , a damping-like (there is no real damping) matrix, $v\mathbf{C}_1$, which is linear in the forward speed v , and a stiffness matrix which is the sum of a constant symmetric part, \mathbf{K}_0 , and a part, $v^2\mathbf{K}_2$, which is quadratic in the forward speed. The forces on the right-hand side, \mathbf{f} , are the applied forces which are energetically dual to the degrees of freedom \mathbf{q} .

The entries in the constant coefficient matrices \mathbf{M} , \mathbf{C}_1 , \mathbf{K}_0 , and \mathbf{K}_2 can be calculated from a non-minimal set of 25 bicycle

parameters as described in [1]. The procedure and measured values of these parameters for the instrumented bicycle can be found in [2]. From these measured parameters the coefficient matrices of the linearized equations of motion are calculated as:

$$\mathbf{M} = \begin{bmatrix} 7.98981, & 0.89569 \\ 0.89569, & 0.29857 \end{bmatrix}, \quad \mathbf{C}_1 = \begin{bmatrix} 0 & 7.17025 \\ -0.59389, & 1.32610 \end{bmatrix},$$

$$\mathbf{K}_0 = \begin{bmatrix} -109.91168, & -13.45745 \\ -13.45745, & -4.82272 \end{bmatrix}, \quad \mathbf{K}_2 = \begin{bmatrix} 0 & 11.19798 \\ 0 & 1.42200 \end{bmatrix}. \quad (2)$$

Then, with these coefficient matrices the characteristic equation,

$$\det(\mathbf{M}\lambda^2 + v\mathbf{C}_1\lambda + \mathbf{K}_0 + v^2\mathbf{K}_2) = 0, \quad (3)$$

can be formed and the eigenvalues, λ , can be calculated. These eigenvalues, in the forward speed range of $0 \leq v \leq 10$ m/s, are presented by the continuous lines in Figure 6. In principle there are up to four eigenmodes, where oscillatory eigenmodes come in pairs. Two are significant and are traditionally called the *capsize mode* and *weave mode*. The capsize mode corresponds to a real eigenvalue with eigenvector dominated by lean: when unstable, the bicycle just falls over like a capsizing ship. The weave mode is an oscillatory motion in which the bicycle sways about the headed direction. The third remaining eigenmode is the overall stable *castering mode* which corresponds to a large negative real eigenvalue with eigenvector dominated by steering.

4 Experimental Procedure and Results

Measurements were recorded for the case in which the laterally perturbed bicycle coasted freely on the treadmill. From these measured data eigenvalues were extracted by means of curve fitting. These eigenvalues were then compared with the results from the linearized equations of motion of the model. As a result, the model appeared to be fairly accurate for the normal bicycling speed range.

4.1 Expected motions

Looking at the eigenvalue plot, Figure 6, the following bicycle motions during the experiments can be expected. At low speed the motion of the free-coasting laterally-perturbed bicycle will be dominated by the unstable weave motion. Both the capsize and the castering modes are very stable here and any initial transient will quickly die out. The time frame for measurement will be short due to the unstable nature of the weave motion. Then in the stable speed range, again the motion will be dominated by the oscillatory weave motion. The moderately stable/unstable capsize motion will only give a small offset in the lean rate. Here, the measurement window will be large since the oscillatory weave motion is stable.

4.2 Test procedure

The experiments were carried out on the large treadmill of the faculty of Human Movement Sciences at the Free University of Amsterdam. The 3×5 m usable belt surface has a rubber-like structure with moderate roughness.

A total of 88 runs were carried out within a belt speed range of 10 to 30 km/h (2.8 to 8.3 m/s). In each run the bicycle was first put manually in the vertical equilibrium position and given some time for the wheels to speed up and get into the steady upright motion for the given belt speed. The bicycle was released and caught before the fall.

To measure the dynamic response of the bicycle at different speeds and to calculate the corresponding motion eigenvalues, the bicycle had to show some lateral dynamics. At speeds below the stable speed range no external excitation was required. Due to small imperfect or non perfect initial conditions the bicycle always started to weave about its general heading and this motion was measured. The time window for measuring was short due to the unstable motion.

For runs in the stable speed range the bicycle set itself in an upright position and showed no dynamic behaviour unless it was given a lateral excitation. This excitation was accomplished by applying a lateral impulse to the bicycle by simply hitting the bicycle's rear frame by hand in the lateral direction at approximately the insertion of the saddle pillar with the down tube. A side effect of this perturbation was that after the stable weave oscillation had died-out, the bicycle was heading in a slightly different direction and slowly running off the belt.

4.3 Stored data

The frequency of the weave of motion is low, of the order of 1 Hz (see Figure 6) and therefore only a low sample rate was needed here. However, the measurement of the forward speed by means of the 10 magnet ring needed a higher sampling rate. The first tests were measured with a 100 Hz sample frequency. Then to ensure no aliasing in the speedometer signal would take, 500 Hz was used. Unfortunately higher sampling frequencies gave a very erratic steering angle potentiometer signal at the recorder. The recorded data for each run were stored in a text file.

Every run was also recorded on video. Examples of these recordings can be found at [7]. This turned out to be essential for the processing of the run data and helped to identify nonstandard measurements, the quality of the launch, etc. It was thus possible to compare the recorded data afterwards with the video images and to extract the relevant data for the calculation of the eigenvalues from each file.

4.4 Data analysis

For each run the raw data were transferred to Matlab and at first inspected visually. A plot of the raw data for run 1202 is

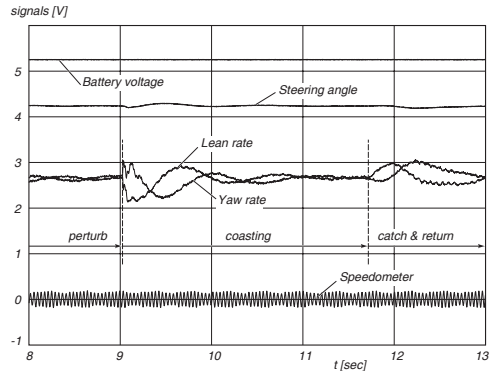


Figure 4. The raw measured data from run 1202. The signals from top to bottom are: battery voltage, steering angle, lean rate, yaw rate, and speedometer. The forward speed is around 5.5 m/s, which is clearly within the stable speed range (see Figure 6). Note the three different motion regimes: perturb, coasting, and catch & return.

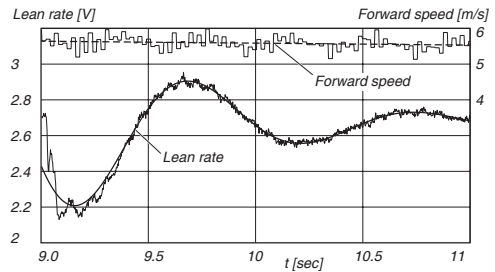


Figure 5. Least-squares curve fit of the oscillatory stable lean rate time history (solid smooth curve) to the measured lean rate (ragged line) for run 1202, together with the measured forward speed (staircase line) and linear regression of the forward speed (dashed line). Note the slight decrease in forward speed (from 5.6 to 5.5 m/s) during the measurement. The extracted weave eigenvalue within the time window of $9.4 \leq t \leq 11.0$ sec is $\lambda_{\text{weave}} = -1.32 \pm 5.96i$ 1/s.

shown in Figure 4. In the figure the signals from top to bottom are: battery voltage, steering angle, lean rate, yaw rate, and speedometer. These graphs were used, together with the videos of the runs, to locate the time window in which the bicycle coasted freely for each run. Once manually located, a curve fit of the time histories of the eigenmotions was performed on the lean rate data to extract the measured eigenvalues, see Figure 5.

Above a forward speed of 0.1 m/s there is in principle a sum of three eigenmodes to be fitted: the casting mode, the capsize mode and the oscillatory weave mode, see Figure 6. The casting mode is highly damped and will vanish quickly from the transient signal. The capsize mode is also reasonably damped below the weave speed and is mildly unstable above the capsize speed resulting here in a small and slow lean-rate offset. Initially we tried to fit the sum of the capsize mode and the oscillatory weave mode to the lean rate data but it turned out that the contribution of the capsize mode was very small. This resulted into almost random values for the capsize eigenvalue, which can be explained as follows. Below the weave speed, the capsize mode is well damped and vanishes quickly, whereas the weave mode is unstable and will dominate the response. Above the weave speed, the capsize eigenvalue is small compared to the weave eigenvalue, in an absolute sense, and again the weave mode will dominate the response. Therefore only an exponentially damped or growing oscillatory weave motion was fitted to the data. The function to be fitted to the measured lean rate was taken as

$$\dot{\phi} = c_1 + e^{dt} [c_2 \cos(\omega t) + c_3 \sin(\omega t)], \quad (4)$$

with the weave frequency $\omega = \text{Im}(\lambda_{\text{weave}})$, the weave damping $d = \text{Re}(\lambda_{\text{weave}})$ and the three constants: c_1 for the offset, c_2 for the cosine amplitude and c_3 for the sine amplitude. Since the weave frequency and damping appear in a non-linear way in the function a non-linear least-squares fitting method was used (Matlab's `fminsearch`) to extract the eigenvalues.

The speedometer signal, see Figure 4, was an oscillatory signal with a frequency of ten times the rear wheel rotation frequency. The signal was converted to a forward speed by counting the time between successive zero crossings. As each crossing represents a 1/20th of a complete rear wheel rotation an average speed for that portion could be calculated; this is the staircase line in Figure 5. As the forward speed during the coasting section of the measurements slowly decreased due rolling resistance, a speed range was assigned to the calculated λ 's instead of one specific speed. This speed range was calculated by looking at the linear regression of the speed for the chosen time window, see Figure 5.

Finally, for all runs, in Figure 6, the measured eigenvalues were plotted on top of the calculated eigenvalues where horizontal bars are used to indicate the forward speed variation during the measurements.

4.5 Discussion

At speeds above 3 m/s, the predicted weave frequency and damping by the model were forecasted accurately. The transition from the unstable to the stable region around the weave speed is accurately described by the model.

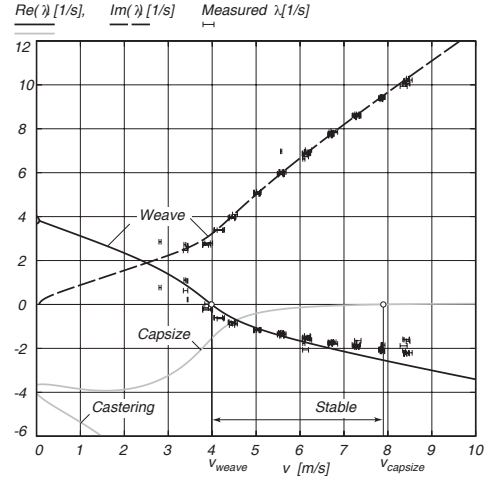


Figure 6. Measured eigenvalues λ (horizontal bars) and calculated eigenvalues λ (continuous lines) for the instrumented bicycle on the treadmill, from Figures 1 and 2, in the forward speed range of $0 \leq v \leq 10$ m/s. For the measured values only the weave motion is considered. The lengths of the horizontal bars indicate the forward speed range during the measurement. For the calculated values the solid lines correspond to the real part of the eigenvalues and the dashed line corresponds to the imaginary part of the eigenvalues. The zero crossings of the real part of the eigenvalues are for the weave motion at the weave speed $v_{\text{weave}} \approx 4.0$ m/s and for the capsize motion at capsize speed $v_{\text{capsize}} \approx 7.9$ m/s. The speed range for asymptotic stability of the instrumented bicycle is $v_{\text{weave}} < v < v_{\text{capsize}}$.

In the unstable speed region, in particular below 3 m/s, it turned out to be very difficult to measure the motion of the bicycle. The time window for measurement was very short compared with the period of the weave motion. Therefore, trying to fit only a part of a harmonic function to the measured data turned out to be very difficult and the results showed considerable spread.

The yaw rate signal was of the same quality as the lean rate signal, but the steering angle signal turned out to be too small and too erratic, due to noise in the potentiometer, to use.

5 Conclusions

The experimental results show a good agreement with the results obtained by a linearized analysis on a three-degree-of-freedom dynamic model of an uncontrolled bicycle. The transi-

tion from stable to unstable speeds is also well predicted. This shows that the tire-belt compliance and tire-belt slip, and the small changes in bicycle heading relative to the belt velocity are not important for the lateral dynamics of the bicycle on a treadmill.

Therefore we conclude that riding a bicycle on a treadmill with constant belt velocity is dynamically equivalent to riding a bicycle on flat level ground around the straight ahead direction with constant speed.

REFERENCES

- [1] Meijaard, J. P., Papadopoulos, J. M., Ruina, A., and Schwab, A. L., 2007. "Linearized dynamics equations for the balance and steer of a bicycle: a benchmark and review". *Proceedings of the Royal Society A*, **463**, p. 19551982.
- [2] Kooijman, J. D. G., Schwab, A. L., and Meijaard, J. P., 2008. "Experimental validation of a model of an uncontrolled bicycle". *Multibody System Dynamics*, **19**, pp. 115–132.
- [3] Herlihy, D. V., 2004. *Bicycle: the history*. Yale University Press, New Haven, CT.
- [4] Åström, K. J., Klein, R. E., and Lennartsson, A., 2005. "Bicycle dynamics and control". *IEEE Control Systems Magazine*, **25**(4), pp. 26–47.
- [5] Sharp, R. S., 2008. "On the stability and control of the bicycle". *Applied Mechanics Reviews*, **61**, November, 24 pp.
- [6] Whipple, F. J. W., 1899. "The stability of the motion of a bicycle". *Quarterly Journal of Pure and Applied Mathematics*, **30**, pp. 312 – 348.
- [7] <http://bicycle.tudelft.nl/schwab/Bicycle/index.htm>.

Kooijman, J. D. G., Meijaard, J. P., Papadopoulos, J. M., Ruina, A., and Schwab, A. L. (2011). A bicycle can be self-stable without gyroscopic or caster effects. *Science*, 332 (6027) : 339–342. Author generated pre-print.

A bicycle can be self-stable without gyroscopic or caster effects

J. D. G. Kooijman¹, J. P. Meijaard², Jim M. Papadopoulos³, Andy Ruina^{4*}, A. L. Schwab¹

A riderless bicycle can automatically steer itself so as to recover from falls. The common view is that this self-steering is caused by gyroscopic precession of the front wheel, or by the wheel contact trailing like a caster behind the steer axis. We show that neither effect is necessary for self-stability. Using linearized stability calculations as a guide, we built a bicycle with extra counter-rotating wheels (canceling the wheel spin angular momentum) and with its front-wheel ground-contact forward of the steer axis (making the trailing distance negative). When laterally disturbed from rolling straight this bicycle automatically recovers to upright travel. Our results show that various design variables, like the front mass location and the steer axis tilt, contribute to stability in complex interacting ways.

A bicycle and rider in forward motion balance by steering towards a fall, which brings the wheels back under the rider (1) (also see Ch. S1-2). Normally riders turn the handlebars with their hands to steer for balance. With hands off the handlebars, body leaning relative to the bicycle frame can also cause appropriate steering. Amazingly, many moving bicycles with no rider can steer themselves so as to balance; likewise with a rigid rider whose hands are off the handlebars. For example, in 1876 Spencer (2, 3) noted that one could ride a bicycle while lying on the seat with hands off, and the film *Jour de fête* by Jacques Tati, 1949, features a riderless bicycle self-balancing for long distances. Suspecting that bicycle rideability with rider control is correlated with self-stability of the passive bicycle, or at least not too much self-instability, much theoretical research has focused on this bicycle self-stability.

The first analytic predictions of bicycle self-stability were presented independently by French mathematician Emmanuel Carvallo (4) (1897) and Cambridge undergraduate Francis Whipple (3, 5) (1899). In their models, and in this paper, a bicycle is defined as a three-dimensional mechanism (Fig. 1A) made up of four rigid objects (the rear frame with rider body B, the handlebar assembly H, and two rolling wheels R and F) connected by three hinges. The more complete Whipple version has 25 geometry and mass parameters. Assuming small lean and steer angles, linear and angular momentum balance, as constrained by the hinges and

rolling contact, lead to a pair of coupled second-order linear differential equations for leaning and steering (6) (see also Ch. S3). Solutions of these equations show that after small perturbations the motions of a bicycle may exponentially decay in time to upright straight-ahead motion (asymptotic stability). This stability typically can occur at forward speeds v near to \sqrt{gL} , where g is gravity and L is a characteristic length (about 1m for a modern bicycle). Limitations in the model include assumed linearity and the neglect of motions associated with tire and frame deformation, tire slip, and play and friction in the hinges. Nonetheless, modern experiments have demonstrated the accuracy of the Whipple model for a real bicycle without a rider (7).

The simple bicycle model above is energy-conserving. Thus the asymptotic stability of a bicycle, that the lean and steer angles exponentially decay to zero after a perturbation, is jarring to those familiar with Hamiltonian dynamics. But because of the rolling (non-holonomic) contact of the bicycle wheels, the bicycle, although energy conserving, is not Hamiltonian and it is possible for a subset of variables to have exponential stability in time (6, 8). There is no contradiction between exponential decay and energy conservation because for a bicycle the energy lost from decaying steering and leaning motions goes to increase the forward speed. Unresolved, however, is the cause of bicycle self-stability. In some sense, perhaps, a self-stable bicycle is something like a system with control, albeit self-imposed.

Rider-controlled stability of bicycles is indeed related to their self-stability. Experiments like those of Jones (9) and R. Klein (10) show that special experimental bicycles that are difficult for a person to ride, either with hands on or off, tend not to be self-stable. Both no-hands control (using body bending) and bicycle self-stability depend on 'cross terms' in which leaning causes steering or vice versa. The central question about what causes self-stability is thus reduced to: what causes the appropriate coupling between leaning and steering? The most often discussed of the coupling effects are those due to front-wheel gyroscopic torque and to caster effects from the front wheel trailing behind the steer axis. Trail (or 'caster trail') is the distance c that the ground contact point trails behind the intersection of the steering axis with the ground (see Fig. 1A).

There is near universal acceptance that either spin angular momentum (gyroscopic torque) or trail, or both, are necessary for bicycle stability (3). These two effects are discussed below, in order, and then considered more critically. Active steering of a bicycle front wheel causes a gyroscopic torque on an upright frame and rider. Because the front wheel is relatively light compared to the more massive bicycle and rider, the effect of this gyroscopic torque on the lean is generally small (11) (see also Ch. S1). However, coupling the other way, i.e., the effect of active bicycle leaning on hands-free steering, is non-negligible. For example, when the bicycle has a lean rate to the right, the front axle also has a lean rate

*To whom correspondence should be addressed. E-mail: ruina@cornell.edu.¹Delft University of Technology, Delft, The Netherlands, ²University of Twente, Enschede, The Netherlands, ³UW-Stout, Menomonie, WI 54751, USA, ⁴Cornell University, Ithaca, NY 14853, USA.

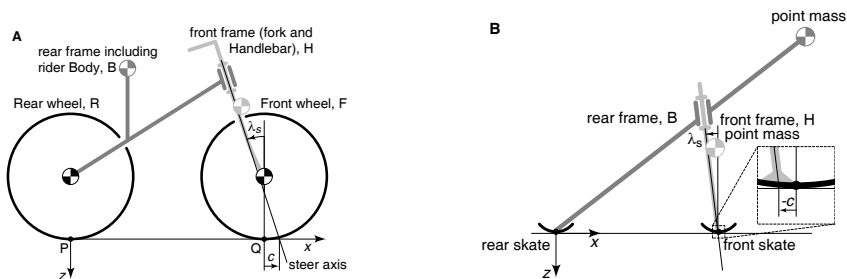


Figure 1: (A) The bicycle model consists of two interconnected frames B and H connected to two wheels R and F. The model has a total of 25 geometry and mass-distribution parameters. Central here are the rotary inertia I_{xy} of the front wheel, the steer axis angle ('rake') λ_s , and the trail distance c (positive if contact is behind the steer axis). Depending on the parameter values, as well as gravity g and forward speed v , this bicycle can be self-stable or not. (B) A theoretical two-mass-skate (TMS) bicycle is a special case described with only 9 free parameters (8 + trail). The wheels function effectively as ice-skates. The two frames each have a single point mass and no mass moments of inertia. A heavy point mass on the rear frame at the rear skate ground contact point can prevent the bicycle from tipping over frontward; because it has no effect on the linearized dynamics it is not shown. Even with negative trail ($c < 0$, see inset) this non-gyroscopic bicycle can be self-stable.

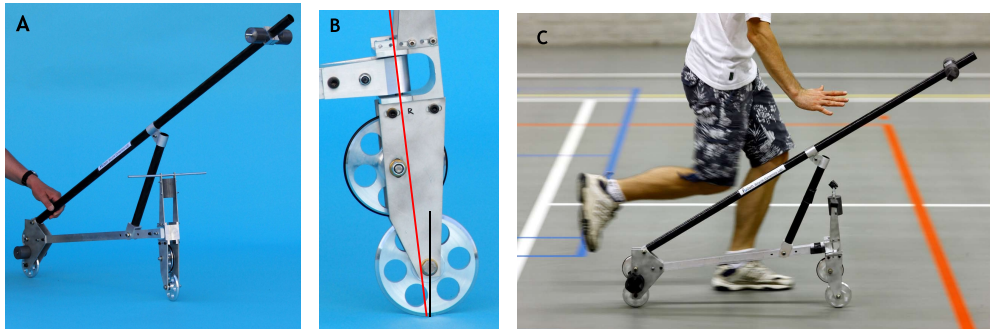


Figure 2: Realization of the model from Fig. 1B. (A) The experimental two-mass-skate (TMS) bicycle. (B) Front assembly. A counter-rotating wheel cancels the spin angular momentum. The ground contact is slightly ahead of the intersection of the long steer axis line with the ground, showing a small negative trail (Video S3). (C) Self-stable experimental TMS bicycle rolling and balancing (photo C by Sam Rentmeester/FMAX).

to the right, and the spinning wheel exerts a clockwise (looking down) reactive torque carried, at least in part, by the handlebar assembly. This reaction torque tends to turn the handlebars rightward. Thus the common explanation of no-hands rider control: to steer to the right, the rider bends her upper body to the left, tilting the bicycle and wheels rightward (5). The bicycle handlebars, considered as freely rotating on the steer axis and forced by the gyroscopic front wheel, thus initially turn rightward. Such leaning-induced steering can be used for rider control of balance. Likewise, this gyroscopic coupling also contributes to a forward-moving passive bicycle self-steering toward a fall (12).

The most thorough discussion of the necessity of gyroscopic coupling of leaning to steering for bicycle self-stability is in the bicycle chapter of the fourth volume of the gyroscope treatise by Klein and Sommerfeld (11) (K&S). They took the example bicycle parameters from Whipple and eliminated just the spin angular momentum of the wheels. Using their own linearized dynamic stability analysis of the Whipple model, K&S concluded that "... in the absence of gyroscopic actions, the speed range of complete stability would vanish" (11) and make what appears to be a strong general claim about bicycles:

"The gyroscopic action, in spite of its smallness, is necessary for self-stability." (p. 866 (11))

They emphasized that the gyroscopic torque does not apply corrective lean torques to a bicycle directly, as others seem to have thought (13). Rather, leaning causes, through the gyroscopic torque, steering, which in turn causes the righting accelerations: "The proper stabilizing force, which overwhelms the force of gravity, is the centrifugal force, and the gyroscopic action plays the role of a trigger." (11)

In Jones's famous search for an unrideable bicycle (URB) (9), he added a counter-rotating disk to the handlebar assembly, canceling the gyroscopic self-steering torque of the front wheel. He could still (barely) ride such a non-gyro bicycle no-hands. Jones rightly deduced that the gyroscopic effect discussed in K&S was not the only coupling between leaning and steering. Jones emphasized the importance of the front-wheel ground contact being behind the steering axis (i.e., positive trail, $c > 0$,

Fig. 1A). Even though the front forks of modern bicycles are typically bent forward slightly, with the wheel-center forward of the steering axis, all modern bicycles still have positive trail (typically from 2 - 10 cm) because of the steering axis tilt, $\lambda_s > 0$. When Jones modified his bicycle by placing the front-wheel ground contact in front of the steer axis (negative trail, $c < 0$) he could not ride no-hands.

In Jones's view a bicycle wheel is, in part, like a caster wheel on a shopping cart, where the wheel trails behind a vertical pivot axis. If a modern bicycle is rolled forward by guiding the rear frame in a straight line while it is held rigidly upright, the front wheel will quickly self-center like a shopping-cart caster. Jones noted "The bicycle has only geometrical caster [trail] stability to provide its self-centering". Jones's main focus was a second trail effect: the vertical ground contact force on the front wheel ground contact point exerts a steering torque on a leaned bicycle even when the bicycle is steered straight. Jones calculated the steer torque caused by lean as a derivative of a static potential energy, neglecting the weight of the front assembly. If a typical modern bicycle is firmly held by the rear frame, leaned to the right, and pressed down hard, then the vertical ground contact forces on the front wheel cause a rightward steering torque on the handlebars. The Jones torque can be felt on a normal bicycle by riding in a straight line and bending your upper body to the left, leaning the bicycle to the right: to maintain a straight path the hands must fight the Jones torque and apply a leftwards torque to the handlebars. According to Jones, this torque causes steering toward a fall only when the trail is positive. When the trail is zero, Jones's theory predicts no self-correcting steer torque. Jones seems to conclude that no-hands control authority (the ability to cause steering by body bending) and self-stability both depend on positive trail. A mixture of the two mechanisms Jones discusses certainly suggests that trail is a key part of bicycle stability.

Following K&S and Jones, it has become common belief that steering is stable because the front wheel ground contact drags behind the steering axis, and leaning is stable because some mixture of gyroscopic torques and trail cause an uncontrolled bicycle to steer in the direction of a fall (3).

Are gyroscopic terms or positive trail, together

or separately, really either necessary or sufficient for bicycle self-stability? Following Carvalho, Whipple, K&S and others since (see history in (6)) we start with the linearized equations of motion. Using the numerical values from the benchmark example in (6) and setting the gyroscopic terms to zero we find here that self-stability is lost (Ch. S6.1, similar to the result of K&S for the Whipple parameters). However, we also found bicycle designs that are self-stable without gyroscopic terms.

The conflict with K&S is partly resolved by noting sign errors in their key stability term (3). Despite their calculation errors, the Whipple bicycle, with Whipple's example parameters, does indeed lose self-stability when the gyro terms are set to zero. But with their incorrect expressions, K&S could make slightly more general claims that are not valid when the sign errors are corrected (3). Whatever generality K&S intended (their wording is ambiguous), their result does not apply to bicycles in general.

Similarly Jones's simplified static energy calculation seems incomplete in the context of a dynamical system, like the Whipple and Carvalho models. Jones's static energy calculation only calculates (incompletely) one term, $K_{0\delta\phi}$, of the full dynamics equations (3, 6). In a full dynamic analysis $K_{0\delta\phi}$ does not predict the steering of a falling bicycle (3). For example, that term can be non-zero for a bicycle that falls with no self-corrective steering at all. And, just as for the gyroscopic term, we can find designs with zero or negative trail that we predict are self-stable (Ch. S6.2).

In contrast to the conventional claims above for the necessity of gyroscopic terms and trail, we have found no rigorous reasoning that demands either. To understand better what is needed for self-stability, we eliminated as many bicycle parameters as possible (14). Most centrally, we eliminated the gyroscopic terms and set the trail to zero ($c = 0$). We also reduced the mass distribution to just two point masses: one for the rear frame B and one for the steering assembly H (Fig. 1B). With these theoretical parameters the wheels having no net spin angular momentum, are mechanically equivalent to skates. These simplifications reduce the number of parameters from Whipple's 25 to a more manageable 8.

Stability analysis of this theoretical two-mass-

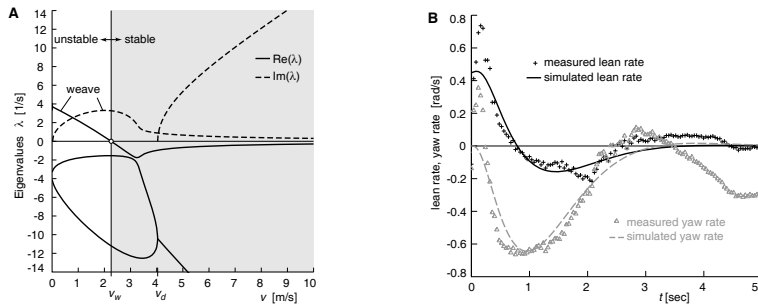


Figure 3: (A) Stability plot for the experimental TMS stable bicycle. Solutions of the differential equations are exponential functions of time. Stability corresponds to all such solutions having exponential decay (rather than exponential growth). Such decay only occurs if all four of the eigenvalues λ_i (which are generally complex numbers) have negative real parts. The plot shows calculated eigenvalues as a function of forward speed v . For $v > 2.3$ m/s (the shaded region) the real parts (solid lines) of all eigenvalues are negative (below the horizontal axis) and the bicycle is self-stable. (B) Transient motion after a disturbance for the experimental TMS bicycle. Measured and predicted lean and yaw (heading) rates of the rear frame are shown. The predicted motions show the theoretical (oscillatory) exponential decay. Not visible in these plots, but visible in high-speed video (Video S4), is a 20 Hz shimmy that is not predicted by the low-dimensional linearized model (Ch. S14-15).

skate (TMS) bicycle model (Ch. S7), confirmed by numerical solution of the governing differential equations (Fig. 3B), shows that neither gyroscopic terms nor positive trail are needed for self-stability (Routh-Hurwitz (15) analysis shows that all eigenvalues of the theoretical TMS bicycle can have negative real parts at some forward speeds, Fig. 3A).

We used the stable theoretical TMS bicycle parameters as a basis for building an experimental TMS bicycle (Fig. 2A, Ch. S8-9). We used small wheels to minimize the spin angular momentum. To further reduce the gyroscopic terms, following Jones, we added counter-spinning disks that rotate backward relative to the lower wheels (Fig. 2B, video S2). The experimental TMS bicycle was built to have a slightly negative trail ($c = -4$ mm < 0 , Video S3). While the experimental TMS bicycle looks like a folding scooter, it is still a bicycle (two wheels, two frames, three hinges).

Because all physical objects have distributed mass, the measured parameters of the experimental TMS bicycle were necessarily slightly different from those of the theoretical design, which was based on point masses. Using measured parameters, we calculate the stability plot of Fig. 3A (Ch. S7-8). For rolling speeds greater than 2.3 m/s all eigenvalues have negative real parts (implying self-stability).

After an initial forward push, the coasting experimental TMS bicycle (Fig. 2C) would remain upright before it slowed down to about 2 m/s (Video S1, Ch S10-11). As it slowed down below 2 m/s the bicycle would begin to fall. In a perturbation experiment, the stable coasting bicycle ($v > 2.3$ m/s) was hit sideways on the frame, causing a jump in the lean rate, followed by a recovery to straight-ahead upright rolling.

The lean and yaw rates were measured (telemetered). A data set is compared to theory in Fig. 3B (Video S4). One difference between experiment and theory is lateral wheel slip at the initial perturbation, which caused an initial jump in the measured yaw rate (triangles in the first 0.25 s of Fig. 3B). The theoretical model assumed no slip. High-speed video (Video S4) also shows a 20 Hz shimmy, which is due, at least in part, to unmodeled steering axis play (Ch. S11). Nonetheless, after the slipping period, even with the shimmy, the data reasonably track the

low-dimensional linear model's predictions.

Both the theoretical analysis and physical experiment show that neither gyroscopic torques nor trail are necessary for bicycle self-stability. Nor are they sufficient. Many bicycle designs with gyroscopic front wheels and positive trail are unstable at every forward speed (Ch. S6.3). Also, all known bicycle and motorcycle designs lose self-stability at high speeds *because* of gyroscopic terms (e.g. (6)). In contrast the TMS bicycle does not have gyroscopic terms and is predicted to maintain stability at high speeds.

With no gyroscopic torque and no trail, why does our experimental TMS bicycle turn in the direction of a fall? A general bicycle is complicated, with various terms that can cause the needed coupling of leaning to steering. Only some of these terms depend on positive trail or on positive spin angular momentum in the front wheel. In the theoretical and experimental TMS designs, the front assembly mass is forward of the steering axis and lower than the rear-frame mass. When the TMS bicycle falls, the lower steering-mass would, on its own, fall faster than the higher frame-mass for the same reason that a short pencil balanced on end (an inverted pendulum) falls faster than a tall broomstick (a slower inverted pendulum). Because the frames are hinged together, the tendency for the front steering-assembly mass to fall faster causes steering in the fall direction. The importance of front assembly mass for Jones-like static torques has been noted before (8, 16, 17).

Why does this bicycle steer the proper amounts at the proper times to assure self-stability? We have found no simple physical explanation equivalent to the mathematical statement that all eigenvalues must have negative real parts (Ch. S4).

For example, turning toward a fall is not sufficient to guarantee self-stability. For various candidate simple sufficient conditions X for stability, we have found designs that have X but that are not self-stable. For example, we have found bicycles with gyroscopic wheels and positive trail that are not stable at any speed (Ch. S6.3). We also have found no simple necessary conditions for self-stability. Besides the design with no gyroscope and negative trail we have found other counter-examples to common lore. We have found a bicycle that is self-stable with

rear-wheel steering (Ch. S6.7). We also found an alternative theoretical TMS design that has, in addition to no-gyro and negative trail, also a negative head angle ($\lambda_s < 0$, Ch. S6.6).

Are there any simply described design features that are universally needed for bicycle self-stability? Within the domain of our linearized equations, here is one simple necessary condition we have found (Ch. S5):

To hold a self-stable bicycle in a right steady turn requires a left torque on the handlebars.

Equivalently, if the hands are suddenly released from holding a self-stable bicycle in a steady turn to the right, the immediate first motion of the handlebars will be a turn further to the right. This is a rigorous version of the more general as-yet-unproved claim that a stable bicycle must turn toward a fall.

Another simple necessary condition for self-stability is that at least one factor coupling lean to steer must be present (at least one of $M_{\delta\phi}$, $C_{\delta\phi}$, or $K_{\delta\phi}$) must be non-zero, Ch. S3). These coupling terms arise from combinations of trail, spin momentum, steer axis tilt, and center of mass locations and products of inertia of the front and rear assemblies.

Although we showed that neither front-wheel spin angular momentum nor trail are necessary for self-stability, we do not deny that both are often important contributors. But other parameters are also important, especially the front-assembly mass distribution, and all the parameters interact in complex ways. As a rule we have found that almost any self-stable bicycle can be made unstable by mis-adjusting only the trail, or only the front-wheel gyro, or only the front-assembly center-of-mass position. Conversely many unstable bicycles can be made stable by appropriately adjusting any one of these three design variables, sometimes in an unusual way. These results hint that the evolutionary, and generally incremental, process that has led to common present bicycle designs might not yet have explored potentially useful regions in design space.

1. W. J. M. Rankine, *The Engineer* **28**, 79,129,153,175 and 29:2 (1870) (1869).
2. C. Spencer, *The modern bicycle* (Frederick Warne and Co., London, 1876). (pp. 23–24).
3. J. P. Meijaard, J. P. Papadopoulos, A. Ruina, A. L. Schwab, <http://arxiv.org> (2011).
4. E. Carvallo, *Théorie du mouvement du monocycle et de la bicyclette*. (Gauthier-Villars, Paris, France, 1899). (Submitted in 1897 for the Prix Fournerey, awarded shared second place in 1898.).
5. F. J. W. Whipple, *Quarterly Journal of Pure and Applied Mathematics* **30**, 312 (1899).
6. J. P. Meijaard, J. M. Papadopoulos, A. Ruina, A. L. Schwab, *Proceedings of the Royal Society A* **463**, 1955 (2007).
7. J. D. G. Kooijman, A. L. Schwab, J. P. Meijaard, *Multibody System Dynamics* **19**, 115 (2008).
8. J. I. Neimark, N. A. Fufaev, *Dynamics of non-holonomic systems*. (Providence, RI: American Mathematical Society., 1972). (Transl. from the Russian edition, Nauka, Moscow, 1967.).
9. D. E. H. Jones, *Physics Today* **23**, 34 (1970). (reprinted in September 2006).
10. K. J. Åström, R. E. Klein, A. Lennartsson, *IEEE Control Systems Magazine* **25**(4), 26 (2005).
11. F. Klein, A. Sommerfeld, *Über die Theorie des Kreisels* (Teubner, Leipzig, 1910). Ch IX §8, Stabilität des Fahrrads, by F. Noether, pp. 863–884.
12. J. A. Griffiths, *Proceedings of the Institution of Mechanical Engineers* **37**, 128 (1886). (p. 162–188 discussion by C. Vernon Boys).
13. W. Thomson, *Popular Lectures and Addresses* (Macmillan and co., 1889). (pp.142–146, Kelvin's lecture of March 4, 1881).
14. J. M. Papadopoulos, Bicycle steering dynamics and self-stability: a summary report on work in progress (1987). Cornell Bicycle Research Project.
15. E. J. Routh, *Proceedings of the London Mathematical Society* **1**, 97 (1873).
16. R. N. Collins, A mathematical analysis of the stability of two wheeled vehicles, Phd, University of Wisconsin, Madison (1963).
17. C. Chateau, *La Nature: Revue des sciences et de leurs applications aux arts et à l'industrie* pp. 353–355 (1892).
18. R. S. Hand helped with the theory and experiments, A. Dressel with the eigenvalue analysis, J. van Frankenhuyzen with designing the experimental machine and J. Moore with conducting the experiments. The manuscript was improved by comments from M. Broide, M. Cook, A. Dressel, J. Guckenheimer, R. Klein, D. Limebeer, C. Miller, J. Moore, R. Pohl, L. Schaffer and D. van Nouhuys. The research was initially supported by an NSF PYI award to A.R. The original theory was mostly by J.M.P. with later refinement by A.L.S.. J.P.M. found the error in K&S. Experiments mostly by J.D.G.K. and A.L.S. Writing mostly by A.R. and A.L.S.

Supporting Online Material Chapters S1–11 include details of the theory, design, construction and testing. Videos S1–4 show the experimental TMS bicycle in motion and some experimental details.

Acknowledgements

Even though performing a PhD may be an individual process, getting to the finish is always a joint effort. I have been fortunate enough to have had the support of a large team helping me along the way who I would therefore like to thank. Firstly I would like express my gratitude to the TU Delft faculty of Mechanical, Maritime and Materials Engineering (3mE) and the Precision and Microsystems Engineering (PME) department as the project would not have even been able to start without their financial support.

Thereafter I would like to thank my daily supervisor and co-promotor Arend Schwab, for his support, ideas, patience and setting of hard deadlines in order to get me to write this thesis. And my promotor, Prof. Daniel Rixen, for taking me onboard and always giving good insightful feedback on the work.

Next I must give a big thanks to Jason Moore, who visited us for a year and was such a boost to the whole bicycle lab project. Jason, I had a great year working together with you, building machines, performing experiments, discussing general bicycling aspects, learning Californian “hippy” (as you call them) customs, and being introduced to so many different social concepts.

I am also grateful for the support I received from people from outside the TU Delft: Rob van Regenmortel of Batavus, who kindly supported us with some of their beautiful bicycles for the experiments; And the Vrije Universiteit Amsterdam's faculty of Human Movement Sciences and in particular Knoek van Soest for enabling us to perform experiments on their treadmill, and Richard Casius for all his help with performing the experiments collecting the motion capture data.

Getting the experimental work done would have been far more difficult without the support of the PME staff and in particular the practical hands of Harry and Patrick, and the organizing by Rob. I also would like to thank to Corinne and Birgit for sorting all our administration stuff again every time. Without Jos van Driel's help on the measurement equipment and his thorough re-soldering of just about everything that I had previously

and unsuccessfully tried connect to one and other, I would probably still be trying to get my first test setup working. Building the TMS bicycle also became a lot easier thanks to the excellent practical advice given by Jan van Frankenhuyzen.

My time in the lab would have been a lot less fun without all my lab partners with whom I performed many experiments, and had numerous lunch time discussions at the PME village square. Danique, Eric-Jan, Peter (thanks also for the great cover artwork depicting the 3D plot of the eigenvalues of the TMS bicycle!), Antonie, Hugo, Nick, Gideon, Kazuto, Antonio and (Lord) Kelvin, Thank you all.

On a more personal note I would like to thank all my family and friends¹ for their “gezelligheid”, support and interest in what I was doing over the years. Without the positive support of Miriam ter Brake I would never have even started this project. Without enormous support of Thom van Beek, my partner in crime at Fietsenmakers Product Developers, and definitely the best friend anyone could ever wish for, I wonder if I would ever have gotten to the finish at all. Thom thanks for being there every time, and not only for staying till the wee hours of the morning to get the issues solved, but also for always saying what you think and meaning what you say.

Last but in no way least: Pap en Mam, bedankt dat jullie in mij hebben geloofd en voor alle onvoorwaardelijke steun tijdens de ‘ups’ en ‘downs’ die ik doorgemaakt heb!

*Jodi
Zoetermeer, August 2012*

¹You know who you are.

Johannes Dionisius Gerardus (Jodi) Kooijman was born in Dubai, in the United Arab Emirates on the 9th of February 1978. He would live there until 1996 when he passed his A-Level exams at Dubai College with A grades in the subjects: maths, physics, chemistry and further maths.

Understanding and enjoying the control and engineering of vehicles would turn out to play an important role in Jodi's life. From a young age he loved to ride bicycles, skateboards, motorcycles and karts. He followed his father's footsteps driving karts from the age of five and racing them from the age of eleven. His control skills rapidly improved once he started competing in races and became the United Arab Emirates karting champion in five consecutive seasons between 1991 and 1995. In 1996 he received his car racing license and he participated in the Formula Ford Benelux series in 1997.

Jodi's single track vehicle (bicycle and motorcycle) control skill development started on a small BMX bicycle at the age of three. As he had worked hard at school and learnt to write in two languages (Dutch and English, but to the dismay of his teachers, he often did this both illegibly and in the same sentence) Jodi was rewarded with his first motorbike at the age of 6. The following decade many hundreds of hours would be spent out in the desert attempting to understand and get to grips with (too often in an unsuccessful manner) the handling and flight dynamics of motorcycles. These skills would turn out to be very beneficial when he rediscovered the joys of riding a bicycle as a student in the Netherlands, and in particular once he was introduced to the mountain bike sport. Mountain biking initially started out as a small hobby but soon turned into his new racing passion. He twice became WTOS (Wij Trainen Ons Suf) club champion, participated at national level and in 2004 participated in the UCI Mountain Bike Marathon World Championships. Furthermore due to his cycling ability Jodi was invited to pilot the WASUB Human Powered Submarine in 2005 with which he set an (unofficial) world record in the 100m sprint at the 8th International Human Powered Submarine Race in Bethesda, USA.

Jodi's natural interest in vehicle engineering had grown during his teen years as a result of the thousands of hours of work that he performed to repair and prepare his

own kart and motor bike as well as the karts of many other Dubai Kart Club members. In 1995 he interned at the Kuka Kart factory team in Germany and was lead mechanic for the team at the Intercontinental A European Championships where a 3rd place was achieved. In 1996, Jodi wanted to learn more about the engineering of vehicles in general and therefore moved to the Netherlands to study Mechanical Engineering at the Delft University of Technology. Before graduating for his Master's degree in the field of Vehicle Technology in 2006, he worked part-time at TNO Weg Transport for four years as part of the Dutch Accident Research Team performing data collection and carrying out road accident research analysis.

During 2002 and 2003 Jodi worked full-time at the DUT Formula Student Racing Team, where he was responsible for the development of the suspension geometry of the vehicle during the first year, and for the complete race car as technical director of the team during the second year. He has remained committed to the Formula Student project ever since as a technical supervisor for the DUT Formula Student Racing Team.

A random email from a friend introduced Jodi to the bicycle stability research conducted at the TU Delft, which lead to his Master's thesis project entitled "Experimental Validation of a Model for the Motion of an Uncontrolled Bicycle". After graduating in 2006 Jodi continued with the research work as part of this PhD, however funding ran out in April 2007. He then worked as a racing-driver coach until further funding was arranged and he was able to continue with the PhD from November 2007 onwards.

In 2011, together with Thom van Beek, a friend and colleague from the DUT Formula Student Racing Team, Jodi started the engineering based product development firm: Fietsenmakers Product Developers.